Neuronal networks which underlie Impaired Awareness of Hypoglycaemia

A thesis submitted to the University of Manchester for the degree of Doctor of Philosophy in the Faculty of Biology, Medicine and Health

Adhithya Sankar

Faculty of Biology, Medicine and Health
School of Medical Sciences

2022

Contents

Word count: 66426

List of Figures

List of Tables

List of Abbreviations

2-DG	2-Deoxy-D-glucose
3V	Third ventricle
4-OHT	4-Hydroxytamoxifen
AAV	Adeno-associated virus
AgRP	Agouti-related peptide
ANOVA	Analysis of variance
AP	Area postrema
AR	Acute restraint stress
ARC	Arcuate nucleus of the hypothalamus
AUC	Area under curve
BNST	Bed nucleus of the stria terminalis
CA	Catecholaminergic
CeA	Central nucleus of the amygdala
CCK	Cholecystokinin
ChR2	Channel rhodopsin 2
CNO	Clozapine-N-oxide
CNS	Central nervous system
Cre	Cre-recombinase
CRH	Corticotrophin-releasing hormone
CRHR1	Corticotrophin-releasing hormone receptor 1
DAB	Diaminobenzidine
DMH	Dorsomedial hypothalamic nucleus
DMSO	Dimethyl sulphoxide
DMX	Dorsal motor nucleus of the vagus
dNTP	Deoxyribonucleotide triphosphate
EDTA	Ethylenediaminetetraacetic acid
ELISA	Enzyme-linked immunosorbent assay
eYFP	Enhanced yellow fluorescent protein
FG	Fluoro-Gold
GABA	γ-aminobutyric acid
Gad2	Glutamic acid decarboxylase 2
GE	Glucose-excited neurons
GFP	Green fluorescent protein
GI	Glucose-inhibited neurons
GLUT	Glutamatergic
HED	High energy diet
hM3Dq	Stimulatory designer receptor
ICV	Intracerebroventricular

IHC	Immunohistochemistry
IML	Intermediolateral nucleus of the spinal cord
i.p.	Intraperitoneal
LC	Locus coeruleus
LH	Lateral hypothalamus
Lox(P)	Locus of X-over P1
LS	Lateral septal nucleus
mPFC	Medial prefrontal cortex
MPO	Medial preoptic area
NA	Noradrenaline
NAc	Nucleus accumbens
NTS	Nucleus of the solitary tract
OXT	Oxytocin
PACAP	Pituitary adenylate cyclase activating peptide
PAG	Periaqueductal grey
PB	Phosphate buffer
PB-T	Phosphate buffer with triton X-100
PBN	Parabrachial nucleus
PBS	Phosphate buffered saline
PCR	Polymerase chain reaction
PFA	Paraformaldehyde
PFC	Prefrontal cortex
PVH	Paraventricular hypothalamus
PVT	Paraventricular thalamic nucleus
RH	Repeated hypoglycaemia
RPa	Raphé pallidus
RR	Repeated restraint stress
rVLM	rostral ventrolateral medulla
s.c.	Subcutaneous
SEM	Standard error of the mean
SH	Single hypoglycaemia
SR	Single restraint stress
TAE	Tris-acetate-EDTA buffer
TH	Tyrosine hydroxylase
TR	Tail restraint
VGlut2	Vesicular glutamate transporter 2
VMH	Ventromedial hypothalamus
VTA	Ventral tegmental area
WT	Wild type

Abstract

Neuronal networks with underlie Impaired Awareness of Hypoglycaemia

The counter-regulatory response (CRR) to hypoglycaemia requires behavioural, endocrine, and autonomic responses. The latter is important clinically, because sympathoadrenal activation produces symptoms, leading to hypoglycaemia awareness and corrective behaviours. A reduction in the efficacy of sympathoadrenal activation leads to impaired awareness of hypoglycaemia (IAH), a common condition which affects patients with insulin-treated diabetes and carries significant morbidity and mortality. These deficits are precipitated by repeated hypoglycaemia (RH), which can be experimentally modelled to gain mechanistic insights into IAH. The neurobiology which underlies this condition was investigated in this thesis using a mouse model of IAH.

IAH possesses the hallmarks of habituation, which were recapitulated in our mouse model. This includes a replicable decrease in the response of the sympathoadrenal system to RH, response recovery in the absence of RH and response dishabituation with a heterotypic stimulus. We postulated that specific neuronal networks regulate habituation following RH, but in the context of diabetes and insulin therapy, this culminates in IAH.

By using neuronal markers of acute activation and *in vivo* fibre photometry, corticotrophin-releasing hormone (CRH) neurons in the paraventricular nucleus of the hypothalamus (PVH) were identified as rapidly activated following acute stress, including hypoglycaemia and 2-DG-induced glucoprivation. In addition, the chemogenetic manipulation of CRH neurons in the medial parvocellular dorsal division of the PVH (CRH^{mpdPVH}) confirmed that they are necessary for the full activation of the sympathoadrenal system following hypoglycaemia. Furthermore, neuronal tracing experiments indicated that CRH^{mpdPVH} neurons connect with output elements of the sympathoadrenal system, through direct and indirect pathways involving CRH receptor-expressing neurons.

Using *in vivo* fibre photometry, I also found that CRH^{mpdPVH} neuronal activity habituated to the repeated homotypic stress of RH, but not to heterotypic stress, indicating regulation of stress responsivity by networks which encode stress familiarity. We postulated that these networks included neurons within the posterior paraventricular nucleus of the thalamus (pPVT), as RH was found to induce an increase in FosB, a marker of neuronal adaptation, in both the PVH and pPVT.

Finally, using a genetically targeted ablation strategy, I demonstrated that glutamatergic pPVT neurons are necessary for the RH-induced habituation of the sympathoadrenal response. Furthermore, using monosynaptic silencing and neuronal tracing techniques, I demonstrated that the pPVT drives an inhibitory forebrain circuit, via the ventral bed nucleus of the stria terminalis (vBNST), which is functionally significant to sympathoadrenal response habituation.

Combined, these findings localise RH-induced habituation to specific integrative neuronal networks, involving pPVT and CRH^{mpdPVH} neurons. This circuit may be responsible for reduced sympathoadrenal activation following RH and potentially for the development of IAH.

Declaration

The author declares that no portion of the work referred to in the thesis has been submitted in support of an application for another degree, or qualification, of this or any other university or other institute of learning.

Adhithya Sankar

January 2022

Copyright

i. The author of this thesis (including any appendices and/or schedules to this thesis) owns certain copyright or related rights in it (the “Copyright”) and s/he has given the University of Manchester certain rights to use such Copyright, including for administrative purposes.

ii. Copies of this thesis, either in full or in extracts and whether in hard or electronic copy, may be made only in accordance with the Copyright, Designs and Patents Act 1988 (as amended) and regulations issued under it or, where appropriate, in accordance with licensing agreements which the University has from time to time. This page must form part of any such copies made.

iii. The ownership of certain Copyright, patents, designs, trademarks and other intellectual property (the “Intellectual Property”) and any reproductions of copyright works in the thesis, for example graphs and tables (“Reproductions”), which may be described in this thesis, may not be owned by the author and may be owned by third parties. Such Intellectual Property and Reproductions cannot and must not be made available for use without the prior written permission of the owner(s) of the relevant Intellectual Property and/or Reproductions.

iv. Further information on the conditions under which disclosure, publication and commercialisation of this thesis, the Copyright and any Intellectual Property and/or Reproductions described in it may take place is available in the University IP Policy (see http://documents.manchester.ac.uk/DocuInfo.aspx?DocID=24420), in any relevant Thesis restriction declarations deposited in the University Library, the University Library’s regulations (see http://www.library.manchester.ac.uk/about/regulations/) and in the University’s policy on Presentation of Theses.

Acknowledgement

First, I must thank my family. I am very grateful to my wife Shalini for her love and support throughout this challenging period. You always patiently listened to my theories and your endless enthusiasm for my results has spurred me on, even when the data was not great! I would also like to express my gratitude to my parents for their enduring support and encouragement to fulfil my potential. I think I am getting closer to achieving that! This PhD is your success as much as mine and I hope to continue to make you proud. Thank you also to my grandparents, my in-laws and to my extended family for their blessings and well wishes throughout my PhD.

This work would not be possible without the help of many people behind the scenes: the 4Ward North Award and Wellcome Trust for funding this research, the staff in the BSF and the FBMH. I would also like to thank my colleagues, mentors and supervisors at the Luckman Lab. I want to give a special thank you to Tansi for her mentorship and supervision from my early MRes placements and well into my PhD. I was lucky to have such a patient and skilled person to train me in the ways of mouse whispering (though you will always retain that title)! The work outlined in this PhD would not be possible without your direction and the painstaking preliminary studies that you undertook. Thank you.

To the present and past members of the Luckman and D'Agostino Labs: Amy, Rosie, Court, Nic, Claire, Chris, Isa, Mehdi, Jenna and Peppe, thank you very much for your assistance, training and friendship. I want to give a special mention to Amy, Claire and Nic for always having answers to questions and going out of your way to help me. Thank you also to Mehdi for your help with the photometry work and apparent ability to "read the matrix" with MATLAB!

I would like to extend a big thank you to Prof Simon Luckman, who I feel lucky to have had as my supervisor for both my MRes and PhD. Thank you for providing me with the freedom to see where the science takes us with this project (within reason). I have greatly appreciated your mentorship and learning from how you approach scientific questions. I have thoroughly enjoyed working in your lab.

Recent events in my family have emphasised how little we still know about the human body, its complexity and unfortunately, susceptibility to unforeseen illnesses. Better understanding through research is the only solution.

It is the stories of people, like my own mother-in-law Savithri, which will always remind me of why I pursue a career in research.

I dedicate this thesis to them.

Chapter 1

Introduction

1.1 Hypoglycaemia

Hypoglycaemia is described classically by Whipple's triad: symptoms consistent with hypoglycaemia, a low plasma glucose concentration, and relief of those symptoms when the plasma glucose concentration is raised (Whipple, 1938). In the clinical setting, hypoglycaemia is defined as a plasma glucose concertation of <3.9 mmol/l in adults, though more detailed definitions are also available (**Table 1.1**).

Table 1.1: Hypoglycaemia Definitions

Classification of Hypoglycaemia	Glucose concentration (mmol/l)	Clinical features
Hypoglycaemia	<3.9	May be symptomatic or asymptomatic†
Severe hypoglycaemia	<3.9*	Requirement of assistance of another person to actively administer carbohydrate, glucagons, or other resuscitative actions
Probable symptomatic hypoglycaemia	-	Presence of typical hypoglycaemia symptoms but absence of glucose concentration measurement
Pseudo-hypoglycaemia	>3.9	Presence of typical hypoglycaemia symptoms but a glucose concentration >3.9 mmol/l. Often seen in patients with diabetes and poor glycaemic control

† Autonomic symptoms include palpitations, tremor, hunger, and sweating. Neuroglycopenic symptoms include behavioural changes, difficulty thinking, confusion, seizure, coma, and even death.

* Severe hypoglycaemia is defined by clinical features and not a defined glucose concentration. Neurological recovery attributable to the restoration of plasma glucose to normal is considered sufficient evidence that the event was induced by a low plasma glucose concentration (Seaquist et al., 2013).

Hypoglycaemia is uncommon in the absence of disease. However, in patients with diabetes, changes in physiology and the action of medications alter glucose homeostasis, increasing glucose fluctuations and the likelihood of hypoglycaemia (**Figure 1.1**).

In type 1 diabetes, pancreatic beta cell destruction is the primary pathophysiological process, resulting in the complete reliance on insulin replacement (McCrimmon, 2017). Beta cells continuously sense and adjust insulin release depending on blood glucose, importantly inhibiting insulin release during hypoglycaemia. Although there have been advances in glucose-monitoring technologies, insulin formulations and delivery systems,

all currently available treatment options fail to truly replicate the function of the beta cell. For all patients with type 1 diabetes, and a proportion of patients with type 2 diabetes, insulin is delivered into the systemic circulation via subcutaneous injection or infusion. Although the delivery of insulin into peripheral tissue allows ease of self-administration, much larger insulin doses are required to be administered peripherally in order for sufficient insulin to reach the hepatic portal vein and inhibit hepatic glucose production (Beall et al., 2012). Either way, systemic hyperinsulinaemia can often lead to excess glucose uptake into tissues, with subsequent hypoglycaemia.

Additionally, the disturbance to the pancreatic islet in type 1 diabetes, also affects alpha cells and, consequently, glucagon secretion. This defect is thought to arise from a loss of intra-islet signalling. Specifically, the autoimmune process causes islet-specific sympathetic nerve loss, which impairs the autonomic input to the alpha cell. This sympathetic islet neuropathy occurs early in the disease and impairs glucagon release (Mundinger et al., 2003). Interestingly, nearly all patients with type 1 diabetes lose the ability to secrete glucagon within 5 years of diagnosis (Mokan et al., 1994). The loss of glucagon, a key counter-regulatory hormone, leads to further risk of hypoglycaemia and a further reliance on sympathoadrenal responses to correct hypoglycaemia – a system which we know is itself impaired in many patients.

Combined, the profound deficits in glucose regulation and the inadequacies of current insulin treatments, explain why patients with type 1 diabetes experience, on average, two symptomatic episodes of hypoglycaemia and up to four asymptomatic episodes a week (Frier et al., 2016, Henriksen et al., 2018). Consequently, patients with diabetes (particularly type 1) are at a far higher risk of repeated hypoglycaemia (RH) events and, as I will discuss, impaired awareness of hypoglycaemia (IAH).

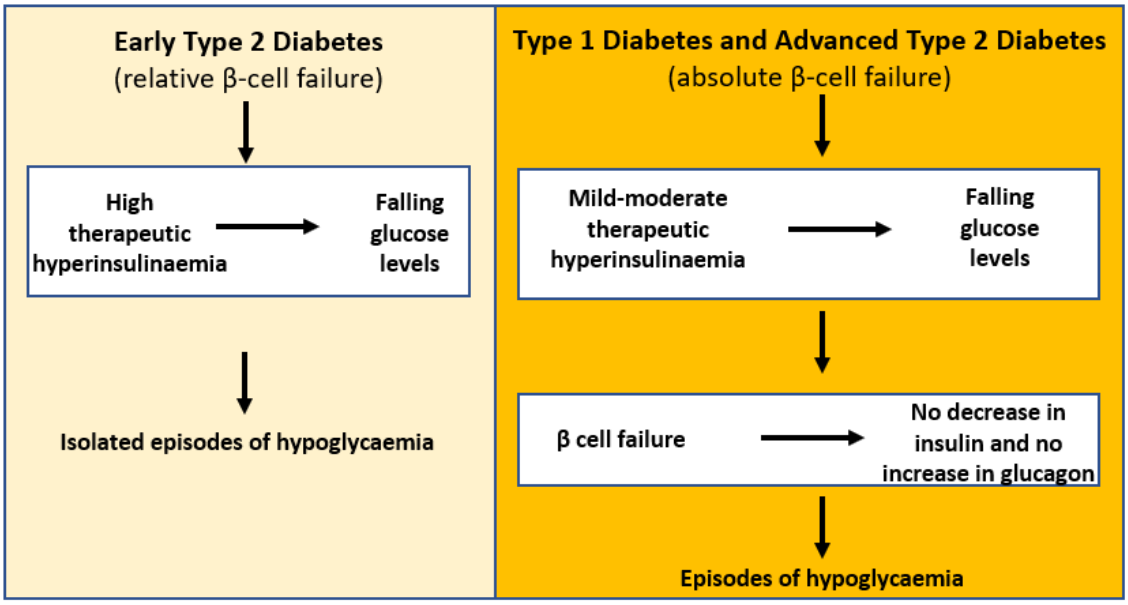

Figure 1.1: Pathophysiological mechanisms precipitating hypoglycaemia in diabetes

Hypoglycaemia is less common in patients with early type 2 diabetes and requires high therapeutic hyperinsulinaemia to occur. Less marked insulin excess (mild-moderate therapeutic hyperinsulinaemia) causes more frequent hypoglycaemia in patients with type 1 diabetes and advanced type 2 diabetes (Cryer, 2013).

1.2 Hypoglycaemia morbidity and mortality

Intensive glycaemic control has documented benefits to microvascular and macrovascular complications, but also increases the risk of severe hypoglycaemia (Diabetes et al., 1993).

Hypoglycaemia has multiple acute and chronic consequences to health and activities of daily living. Mild (self-treated) hypoglycaemia, which is frequently experienced by patients with type 1 diabetes, are distressing and negatively impacts cognitive performance (Beall et al., 2012). Even when the hypoglycaemia is short-lived, it can interfere with balance, coordination and vision, precipitating falls and injury (Frier, 2014a). Recently, studies into the chronic effects of repeated mild hypoglycaemia, show an increased risk of cardiovascular disease (Luk et al., 2016).

Severe hypoglycaemia, requiring the assistance of another person in order to achieve recovery, has all-together more profound effects (ADA, 2005). It impacts employment and excludes sufferers from working in areas which may put the public at risk. Everyday essential activities, such as driving, are restricted in individuals with repeated severe hypoglycaemia.

Acute severe hypoglycaemia can, at its worst, cause coma, seizures, strokes and sudden death (Graveling and Frier, 2009). Chronic severe hypoglycaemia impacts multiple organ systems, most notably the cardiovascular system and the brain.

1.2.1 Cardiovascular effects

Cardiovascular disease is the predominant cause of death in patients with diabetes (Frier et al., 2011). Three prominent trials investigating the reduction of cardiovascular disease risk with glucose lowering, ACCORD (Action to Control Cardiovascular Risk in Diabetes), ADVACE (Action in Diabetes and Vascular Disease: Preterax and Diamicron MR Controlled Evaluation) and VADT (Veterans Affairs Diabetes Trial), all showed excess severe hypoglycaemia with intensive treatment in type 2 diabetes (Frier et al., 2011). The ACCORD trial importantly found an association between symptomatic severe hypoglycaemia and increased mortality (Frier et al., 2011). Though the ACCORD investigators concluded a causative relationship could not be drawn, the effects of hypoglycaemia on the cardiovascular system are multiple, directly causing morbidity and mortality (Frier et al., 2011, Seaquist et al., 2012).

Severe hypoglycaemia provokes an augmented cardiac workload, which is mediated by repeated sympathoadrenal system activation (Wright and Frier, 2008). In people without cardiovascular disease, this increased workload is unlikely to be of great significance. However, chronic sympathoadrenal system activation, particularly in patients with diabetes and pre-existing cardiovascular disease, has been shown to precipitate myocardial infarction and heart failure (Wright and Frier, 2008). It is also likely that hypoglycaemia directly leads to an increase in myocardial ischaemia. Indeed, in patients with insulin-treated diabetes, ischaemic symptoms and ischaemic electrocardiogram changes were noted during hypoglycaemia but not during hyperglycaemia (Desouza et al., 2003).

Also notable is the risk of cardiac arrhythmias in patients with severe hypoglycaemia. Acute hypoglycaemia affects cardiac electrophysiology, delaying cardiac repolarisation and predisposing to dangerous arrhythmias of the heart (Heller, 2002). With the aid of continuous glucose monitoring and electrocardiographic (ECG) recording, investigators have identified a causative link between hypoglycaemia and abnormal cardiac rhythms (Stahn et al., 2014). This effect was more prominent during the night, when life-threatening brady-arrhythmias were more common (Stahn et al., 2014, Frier, 2014a). Electrophysiological changes following hypoglycaemia have been linked to sudden death in young adults with type 1 diabetes. Of concern is that several epidemiological studies have confirmed an increased risk of sudden unexpected deaths in diabetic populations compared with non-diabetic populations (Skrivarhaug et al., 2006, Tu et al.,

2008). Interestingly, in individuals with type 1 diabetes and RH, cardiac repolarisation abnormalities during experimental hypoglycaemia were reduced compared with individuals without prior severe hypoglycaemia (Lee et al., 2004). This raises the suggestion that RH in a person with impaired CRR and longstanding diabetes may lead to cardiac adaptations which confer protection.

Hypoglycaemia is also thought to have direct effects on the endothelial lining of blood vessels and on coagulation through the release of peptides such as endothelin (Wright and Frier, 2008). As a result, endothelial cells and small blood vessel flow are affected, culminating in an increase in microvascular disease (Wright and Frier, 2008). There is also evidence to support RH-induced atherogenesis to microvasculature (Giménez et al., 2011).

1.2.2 Neurological Effects

During hypoglycaemia, cognitive function is threatened as neuroglycopenia deprives the brain of its main fuel source. This manifests as a reduction in most domains of cognitive function, but particularly attention, reaction time, multitasking and performance of complex processes (Inkster and Frier, 2012, Zammitt et al., 2008). Following glucose-raising treatments, recovery of function following an acute hypoglycaemic episode often exceeds 60 minutes. Interestingly, the cognitive performance following a single hypoglycaemic (SH) episode was affected to a lesser extent in patients with IAH, compared with hypoglycaemia aware patients (Zammitt et al., 2008). This could again suggest a form of cerebral adaptation to hypoglycaemia, though this adaptation ultimately limits recognition of hypoglycaemia.

Following SH, electroencephalography (EEG) recordings in adolescents with type 1 diabetes have shown epileptiform activity and theta wave changes which persist even after recovery (Bjorgaas et al., 1998). Following repeated severe hypoglycaemia, altered brain electrical activity can persist for weeks and in some cases become permanent (Frier, 2014a). Repeated severe hypoglycaemia also alters cerebral blood flow and is likely to explain the increased incidence of transient ischaemic attacks and hemiplegia, particularly in elderly people with type 1 diabetes (Frier, 2014a). Brain imaging studies using magnetic resonance imaging have confirmed that repeated severe hypoglycaemia induces permanent changes to cerebral blood flow, which persist during normoglycaemia in patients with type 1 diabetes (Kennan et al., 2005). In a similar way to EEG findings, these changes are more prominent in patients with IAH, which may also represent a form of adaptive response to repeated neuroglycopenia (Kennan et al., 2005).

Studies into the effects of repeated severe hypoglycaemia on the developing mind also show interesting findings. Children under the age of 5 with type 1 diabetes and repeated severe hypoglycaemia, were found to have poorer cognitive performance (Asvold et al., 2010). There is evidence that this effect translates to lower scores of intelligence and executive function in adulthood (Ly et al., 2011). This susceptibility of the developing brain to neuroglycopenia is not seen in individuals diagnosed with type 1 diabetes in young adulthood and middle age (Ly et al., 2011). Indeed, the landmark DCCT (Diabetes control and complications trial) showed over a 20-year follow-up, that no differences were found in cognitive function between intensive and standard treatment groups, despite a higher frequency of severe hypoglycaemia with intensive treatment (Jacobson et al., 2007). As age increases further, there is evidence that ageing brains once again become more susceptible to the effects of hypoglycaemia. This may lead to cognitive impairment in elderly individuals with type 1 diabetes who experience severe hypoglycaemia and could also promote the development of dementia (Biessels, 2014). Thus, hypoglycaemia leads to age-specific changes in the brain that are exacerbated when these episodes are repeated, such as seen in individuals with diabetes and IAH (Biessels, 2014).

The multiple short- and long-term effects of hypoglycaemia highlight the burden of this condition on the everyday life of patients with diabetes. IAH further increases the risk of the serious consequences of insulin-treated diabetes.

1.3 The normal counter-regulatory response to hypoglycaemia

Ensuring a continuous supply of glucose to the tissues of the body, is a core physiological priority of any organism. As such, whole-body homeostatic mechanisms exist to sense, organise and respond to changes in blood glucose to ensure survival.

Glucose homeostasis is primarily maintained through the coordination of the liver, muscle, adipose tissue, adrenal gland, pancreas and brain, forming a glucose-regulatory network. The brain and in particular, the hypothalamus, plays a crucial role in the coordination of multiple effector systems to maintain euglycemia. Signals from peripheral organs relating to glucose status are continuously relayed to the brain. Peripheral feedback is processed within central neuronal networks, which possess sensory, integrative, pre-motor and motor elements, culminating in appropriate effector responses.

Any fall in blood glucose initiates a counter-regulatory response (CRR). This engages central and peripheral glucose-regulatory networks leading to changes in hormone levels (inhibition or release) and behaviour (symptom awareness and food ingestion) which

restore the blood glucose to normal levels (**Figure 1.2**). As a result, hypoglycaemia is rare in the absence of an underlying disease (Reya et al., 2001).

1.3.1 Counter-regulatory response thresholds

The CRR is a stepwise process involving autonomic, neuroendocrine and behavioural components with initiation of specific responses at defined thresholds (**Figure 1.3A**). The first response is triggered when the blood glucose falls below 4.5 mmol/l and involves inhibition of endogenous insulin secretion. This reduces glucose uptake by non-neuronal tissues and for most individuals is sufficient to maintain their blood glucose in the normal range. However, if the blood glucose falls below 3.8 mmol/l, the glucose-regulatory network in the central nervous system initiates a hormonal CRR (Williams and Pickup, 2004, Fanelli et al., 1994). This includes glucagon release from pancreatic alpha cells and adrenaline release from the adrenal gland chromaffin cells (Williams and Pickup, 2004). This is followed by hypoglycaemia autonomic symptoms (**Figure 1.3B**), which are a vital response for individuals with diabetes. Autonomic symptoms primarily arise from sympathoadrenal system activity and develop at a glucose level of 3.3 mmol/l (McAulay et al., 2001). They lead to awareness and a prompt behavioural response from the individual (carbohydrate ingestion or to seek assistance), before cognitive dysfunction and neuroglycopenia occurs at 3.0 mmol/l. Thus, individuals who retain symptom awareness of hypoglycaemia can act before cerebral dysfunction occurs.

Unfortunately, in around 25% of patients with type 1 diabetes, this stepwise CRR becomes dysfunctional. These individuals have reduced perception of hypoglycaemia-related autonomic symptoms and are termed as having IAH. This condition reflects unknown changes in the counter-regulatory network which consequently lead to a diminished hypoglycaemia CRR. As a result patients with IAH have a significantly increased risk of severe hypoglycaemia, which affects health and employment (Geddes et al., 2008).

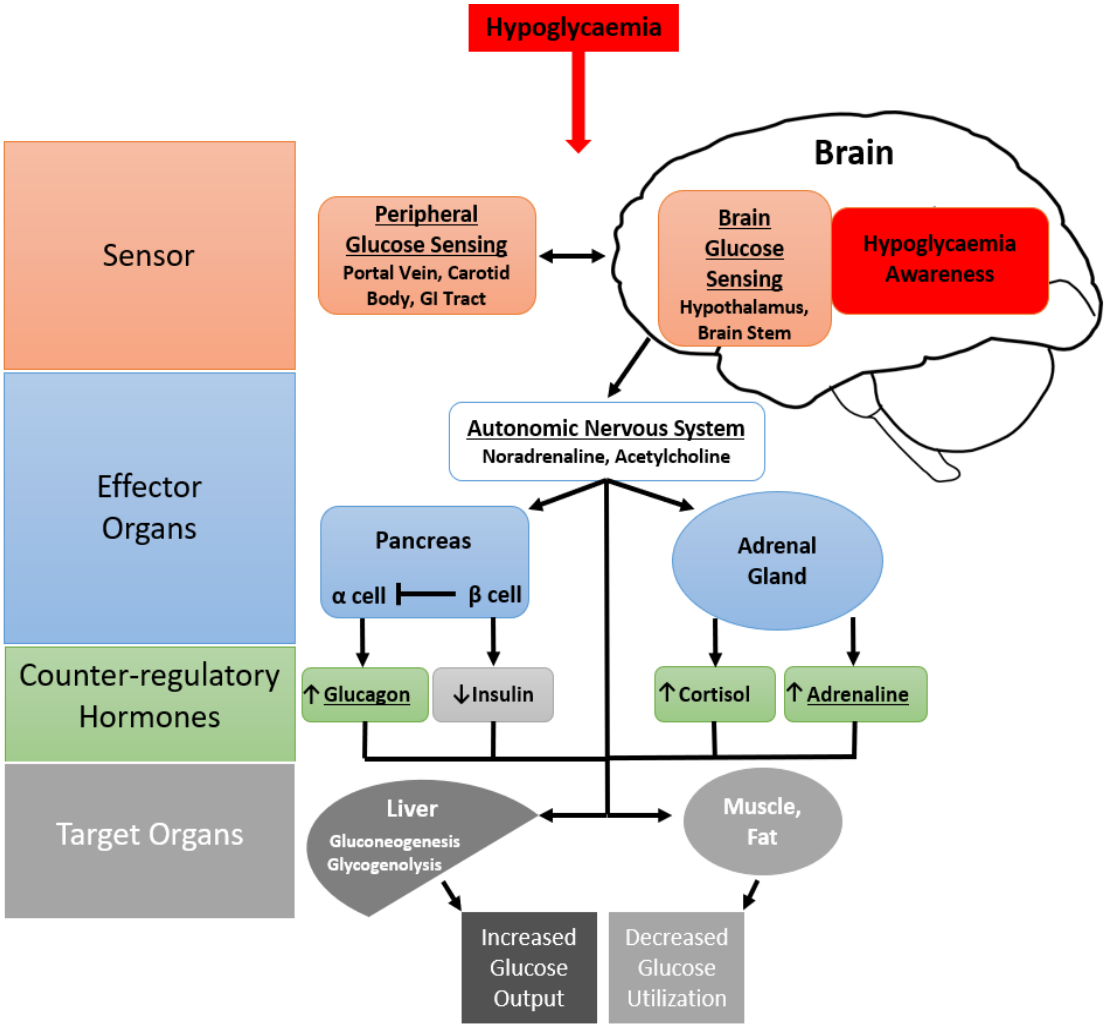

Figure 1.2: The whole-body hypoglycaemia counter-regulatory network

Hypoglycaemia is sensed by cells in the brain and the periphery and a co-ordinated response is generated by the counter-regulatory network. The brain is undoubtedly key to regulating this complex network. Autonomic nervous system outflow from the brain is crucial in initiating appropriate neuroendocrine responses, as well as behaviours.

A

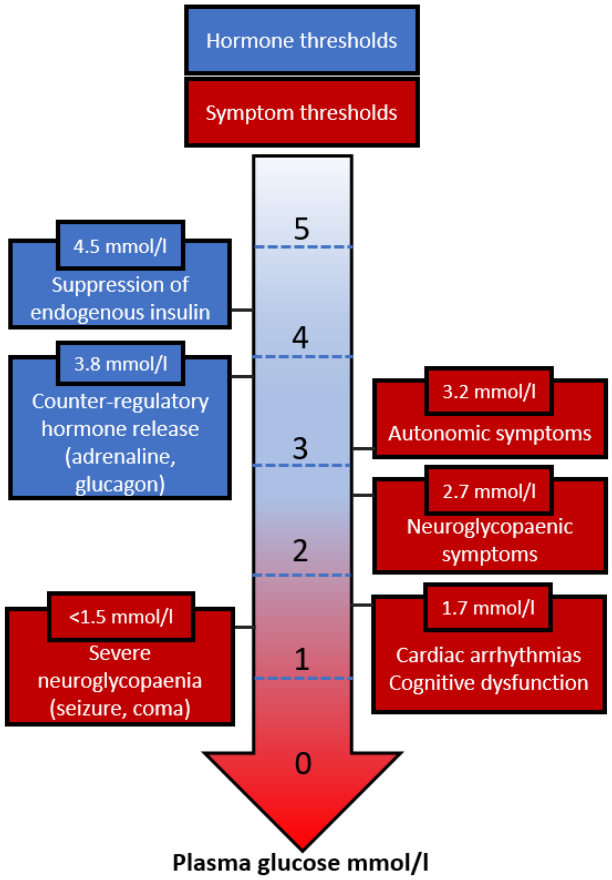

B

Autonomic	Neuroglycopaenia	Malaise
Sweating Palpitations Shaking/tremor Hunger	Confusion Drowsiness Speech difficulty Incoordination Odd behaviour	Headache Nausea

Figure 1.3: Counter-regulatory response thresholds and corresponding symptoms

A: The stepwise hypoglycaemia counter-regulatory response (CRR) showing hormone (blue) and symptom (red) glucose thresholds.
B: Corresponding autonomic and neuroglycopenic symptoms.

1.4 Impaired awareness of hypoglycaemia (IAH)

IAH is a common condition, with an estimated prevalence of between 25-50% in patients with type 1 diabetes and 10% in patients with type 2 diabetes (Pramming et al., 1991, Schopman et al., 2010). It is defined as 'a diminished ability to perceive the onset of acute hypoglycaemia' (Frier, 2014b). Individuals with IAH have a six-fold increased risk of severe hypoglycaemia, leading to significant morbidity and mortality (Geddes et al., 2008). IAH is distressing for patients and family members, placing a significant psychosocial burden on those affected (Lawton et al., 2014). It is also one of the main barriers for patients with diabetes in achieving optimal glycaemic control, leading to increased risk of microvascular and macrovascular complications (Iqbal and Heller, 2018). What is particularly worrying is that incidence rates of IAH have not improved and therapeutic options remain suboptimal (Geddes et al., 2008).

1.4.1 Management of IAH

Early identification of IAH is vital and can be accomplished through a careful clinical history and the use of validated questionnaires (e.g., Gold, Clarke, HypoCOMPaSS) (Gold et al., 1994, Clarke et al., 1995, Speight et al., 2016). Subsequent therapeutic options for individuals diagnosed with IAH are summarised in **Figure 1.4.** Until recently, the mainstay of treatment was the meticulous avoidance of hypoglycaemia, achieved by relaxing insulin therapy, often to the detriment of glycaemic control (Fanelli et al., 1993, Cranston et al., 1994). A more pragmatic approach, focusing on individualised treatment targets, patient preference and local resources is currently recommended (Farrell and McCrimmon, 2021).

Despite improvements in the individualised care for patients with type 1 diabetes and IAH, there is no therapy, except pancreatic transplantation, which completely restores awareness (Choudhary et al., 2015). Pancreatic and islet cell transplantation carry the potential for insulin independence and to be free from hypoglycaemia. However, this treatment is impractical for most patients with IAH due to costs, availability, immunosuppressant therapy and procedural risks.

Advances in insulin delivery systems such as the insulin pump and glucose monitoring devices are having dramatic effects on the management of patients with type 1 diabetes and IAH (Choudhary and Amiel, 2018). There is also promising evidence that structured diabetes education and behavioural-psychological programmes may restore awareness, without compromising glycaemic control or placing additional risks on patients (Choudhary and Amiel, 2018, Farrell and McCrimmon, 2021).

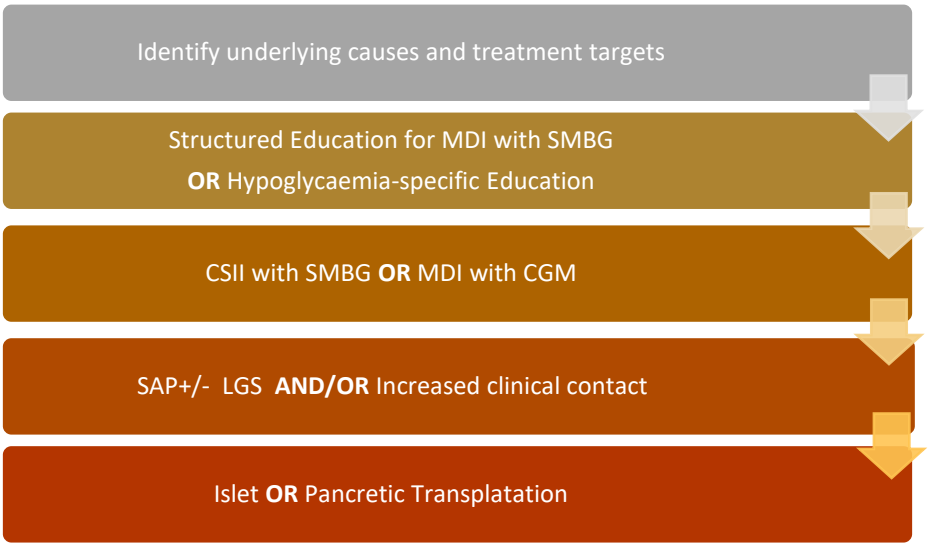

Figure 1.4: Treatment approach for patients with severe hypoglycaemia and IAH

Tiered algorithm for the treatment of IAH, with the aim of achieving optimal glucose control and limiting hypoglycaemia (Choudhary et al., 2015, Farrell and McCrimmon, 2021).

MDI: multiple daily injections; SMBG: self-monitoring blood glucose; CSII: continuous subcutaneous insulin infusion; CGM: continuous glucose monitoring; SAP: sensor augmented pump; LGS: low glucose suspend.

1.4.2 Pathophysiology of IAH

IAH reflects impairments in the hypoglycaemia CRR and particularly the sympathoadrenal response. Early studies identified that patients with longer duration of type 1 diabetes and insulin treatment, exhibited a reduced sympathoadrenal response to hypoglycaemia (Bolli et al., 1983). This was followed by the observation that intense glucose lowering therapy in patients with type 1 diabetes, lowered the glucose level at which the hormonal CRR was initiated with subsequent experimental hypoglycaemia (Amiel et al., 1988). However, the most important finding was that previous (antecedent) exposure to hypoglycaemia was itself the cause for reduced symptom awareness and CRR to subsequent hypoglycaemia (Heller and Cryer, 1991). This breakthrough by Heller and Cryer, identified that even a single prior episode of hypoglycaemia reduced neuroendocrine and symptom responses to subsequent experimental hypoglycaemia in non-diabetic humans (Heller and Cryer, 1991). This finding was subsequently shown to hold true for patients with type 1 diabetes and accurately reproduces the clinical phenotype of IAH (Dagogo-Jack et al., 1993). Thus, longer duration of diabetes, but more crucially RH, causes impaired hypoglycaemia CRR (both in terms of magnitude and altered thresholds) and IAH follows. The vicious cycle which occurs is shown in **Figure 1.5**.

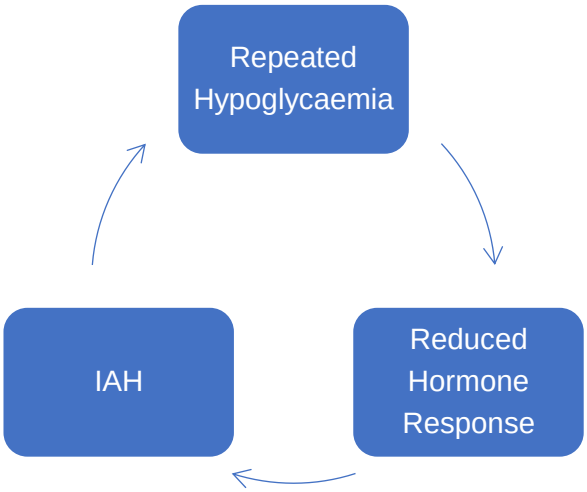

Figure 1.5: The vicious cycle of IAH and RH

Cryer termed these observations Hypoglycaemia-Associated Autonomic Failure (HAAF) and included IAH and impaired hypoglycaemia CRR as components of HAAF (Cryer, 2013). However, HAAF only provides a description of the physiological responses to RH and does not explain why this phenomenon develops. Additionally, it has been argued that HAAF does not fully capture the clinical presentation of IAH, in which a spectrum of CRR impairments exists and complete 'failure' of autonomic responses does not occur (McCrimmon, 2017). Therefore, in this thesis I will refer to the clinical condition of IAH and the underlying impaired sympathoadrenal CRR.

Despite an understanding that IAH is the most significant cause of severe hypoglycaemia in patients with insulin-treated diabetes, finer mechanistic details are not yet known. One way to rectify this is by using experimental RH in humans and animals, creating useful disease models.

1.5 Modelling RH and IAH

Following the seminal work which identified that a single antecedent hypoglycaemic episode diminishes sympathoadrenal and symptom responses to subsequent hypoglycaemia, human and animal studies have adapted this experimental design in a number of ways to more fully investigate IAH (Rattarasarn et al., 1994, Lingenfelser et al., 1993, Dagogo-Jack et al., 1993). A more detailed review of experimental models of RH and difficulties in the translation of experimental paradigms across species was published by me during my PhD (Sankar et al., 2020). Here, I will summarise the key insights which have informed investigators in this field and our own experimental approach.

1.5.1 Human studies

In addition to the direct relevance of human studies to understanding IAH, symptom awareness scores can be measured and monitored in response to treatments (Dagogo-Jack et al., 1993, Lingenfelser et al., 1993). This ability separates human from animal studies, as direct measures of hypoglycaemia symptom awareness have proven difficult to measure in animals.

As IAH and the impaired CRR to RH is a spectrum, it is difficult to define a biochemical threshold at which the condition is successfully reproduced. However, there is a consensus that impaired sympathoadrenal and glucagon responses correspond to loss of symptom awareness in IAH (McCrimmon, 2017, Sankar et al., 2020).

RH leads to consistent attenuation of glucagon release to subsequent hypoglycaemia in patients with diabetes and healthy volunteers (Cryer, 2004). However, glucagon release ceases (through a separate mechanism) within 5 years of diagnosis, in most patients with type 1 diabetes. (Mundinger et al., 2003). Therefore, many patients with type 1 diabetes develop an attenuated glucagon release, often before IAH arises.

Plasma cortisol also increases following experimental SH, but whether this changes with RH remains unclear in humans. In one study, tightening of glycaemic control with insulin treatment (causing iatrogenic hypoglycaemia) in patients with type 2 diabetes blunted the cortisol response to subsequent hypoglycaemia (Korzon-Burakowska et al., 1998). However, these findings have not been replicated consistently in other studies. Hypothalamo-pituitary-adrenal (HPA) axis activation typically occurs as the blood glucose falls to < 3.7 mmol/l; however, the effects of cortisol on blood glucose are delayed. Cortisol-deficient patients only begin to display reductions in plasma glucose (compared with controls) 2.5 hrs after insulin-induced hypoglycaemia (Boyle and Cryer, 1991). Also, HPA-axis activation does not contribute to hypoglycaemia-symptom awareness. Therefore, it can be argued that its measurement is also of lesser relevance. As such, plasma adrenaline measurement is generally considered to be the best proxy for the impaired CRR in the experimental modelling of RH and IAH (McNeilly and McCrimmon, 2018).

It is interesting that studies in diabetic humans and healthy volunteers both report a reduction in adrenaline of between 40-50% following RH (Beall et al., 2012, Senthilkumaran et al., 2016). This suggests that the fundamental glucose-regulatory network changes which follow RH, seem less dependent on the pathophysiology of diabetes, but rather network adaptations to the repeated stress of hypoglycaemia.

1.5.2 Animal studies

A large variation in RH protocols and experimental approaches exits in animals studies (Sankar et al., 2020). This includes differences in species, strains, insulin dosage, mode of administration, injection timing and frequency. Unsurprisingly this has led to some difficulties in the interpretation of results. Here, I will outline important learning points from experimental protocols of RH from studies in rats and mice.

Many rodent studies examining CRR impairment have utilised repeated injections of 2-deoxyglucose (2-DG), a potent glucoprivic stimulus. Indeed, in experiments where 2-DG is injected into the hypothalamus following RH, a significant suppression of the CRR occurs (Borg et al., 1999). However, the effect of RH with insulin and repeated 2-DG-induced glucoprivation, are not consistent in all aspects. In rats, RH with insulin does not attenuate the feeding response to subsequent hypoglycaemia, whereas repeated 2-DG administration does (Sanders et al., 2006, Sanders and Ritter, 2000). As supraphysiological exogenous insulin administration is the primary cause of RH and subsequently IAH in patients with diabetes, it follows that protocols using insulin over 2-DG are more relatable to the disease.

A recent effective protocol in rats, involved intraperitoneal (i.p.) insulin-induced hypoglycaemia (0.75–1 units/kg, Novorapid) or volume-matched i.p. saline injections, three times weekly for 4 weeks. Importantly this protocol significantly attenuated adrenaline responses to subsequent hypoglycaemia (McNeilly et al., 2017, McNeilly et al., 2016). We can gather from other studies in rats that, despite differences in protocols, many groups have achieved attenuation of the sympathoadrenal response. Therefore, parameters such as route, fasting durations, hypoglycaemia duration and even the number of antecedent episodes, are less important. However, RH of extreme severity (causing seizures and unconsciousness) should be avoided, as this causes cell death and fundamentally alters brain function.

Despite the development of successful experimental models in rats, translation to the mouse has proven to be more difficult. Recently, Ma *et al.,* demonstrated diminished adrenaline levels (urinary not plasma) following a four-day protocol of repeated intraperitoneal insulin injection (Ma et al., 2018). Interestingly, the authors noted differences in glucose tolerance between neuropeptide Y (NPY) knock-out (KO) and wild-type (WT) mice, with NPY-KO mice requiring less than half the insulin dose administered to WT mice, to elicit hypoglycaemia (Ma et al., 2018). This highlights the potential difficulties in comparing results from different strains of mice, given that glucose homeostasis can be dramatically altered with manipulation of single genes – for instance, the complete knock-out of the NPY gene in the example above.

Although human studies have provided important insights into the hypoglycaemia CRR, animal studies are required to gain a more granular understanding of the pathophysiology of IAH. Developing a robust mouse model is of particular interest in neuroscience, as techniques using transgenic strains and recombinant techniques enable unprecedented appreciation of neural pathways, including those implicated in glucose homeostasis.

1.6 A glucose-regulatory network

When considering a complex system such as the glucose-regulatory network, it can be useful to apply sensory-motor integration principles to aid understanding (**Figure 1.6**) (Watts and Donovan, 2010). In this framework, glucose is the sensory signal which engages a glucose-regulatory network to control autonomic, neuroendocrine and behavioural motor responses, achieving a CRR. Though considerable overlap of function occurs in many parts of the nervous system, the organisation of the glucose-regulatory network can be separated into three main components:

1) Glucose sensing

Glucose-sensing elements detect changes in glucose and communicate this information by altering neuronal firing. Peripheral glucose sensors reside in the oral cavity, gut, portal-mesenteric vein (PMV) and carotid body. Central glucose-sensing neurons are primarily located in hypothalamus and hindbrain, however other brain regions also participate in glucose sensing (**Figure 1.7**) (Steinbusch et al., 2015, Watts and Donovan, 2010).

2) Integrative / pre-motor

Integrative networks receive direct projections from glucose sensors (peripheral and central). They are primarily located in the hypothalamus and hindbrain; however, forebrain regions also participate in this arm of the network (Thompson and Swanson, 2003, Watts and Donovan, 2010). Information from integrative networks is projected directly, or indirectly to pre-motor and motor neurons. Pre-motor or autonomic neurons are defined by their projections to autonomic pre-ganglionic or neuroendocrine motor neurons. These neurons tend to reside in more well-defined cell groups within the hypothalamus and hindbrain, respectively (Watts and Donovan, 2010, Saper, 2002).

3) Motor/output

Motor neurons receive inputs from pre-motor neurons (which often overlap with integrative neuronal populations). They directly control autonomic and neuroendocrine output and direct behaviours. Motor neurons reside within the hypothalamus, hindbrain

and autonomic ganglia. Projections from motor neurons enable an effective CRR, importantly through direct innervation of adrenal medulla chromaffin cells and, therefore, adrenaline release. Motor neurons also control pituitary and pancreatic islets (α and β cells) to direct hormone release (Donovan and Watts, 2014).

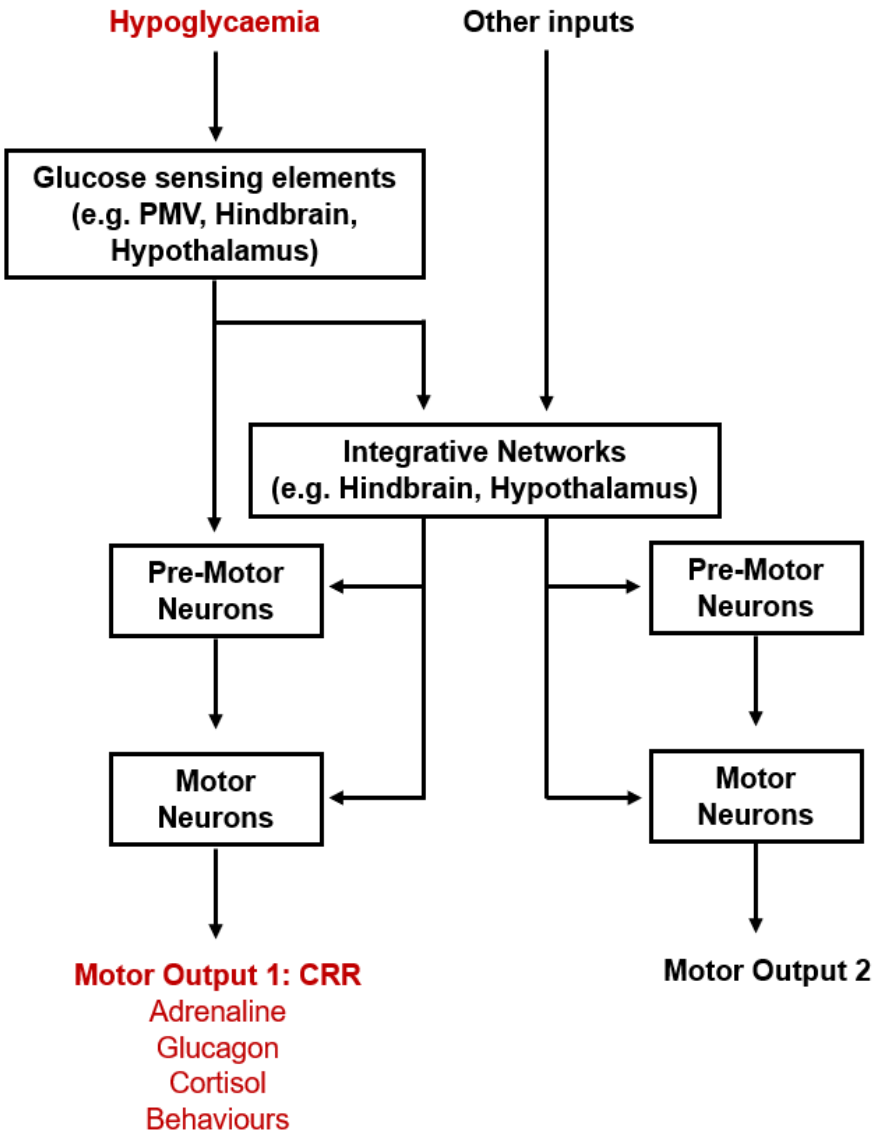

Figure 1.6: A sensory-motor integration framework for the glucose-regulatory network

Changes in blood glucose, in this case hypoglycaemia, are detected by peripheral and central glucose sensing elements that convey signals via neuronal pathways to activate specific networks and control the hypoglycaemia CRR. This signal may be able to drive motor neurons in a reflex manner or can undergo modulation by integrative networks (Fujita and Donovan, 2005). Integrative networks allow the hypoglycaemia signal to be integrated with other sensory information, fine-tuning the CRR. Integrative networks also provide a way for glucose sensing information to direct other motor outputs (e.g., food seeking behaviours) (Watts and Donovan, 2010, Fujita and Donovan, 2005).

1.7 Glucose sensing

1.7.1 Peripheral sensors

Peripheral glucose sensors are found in many locations. Gastrointestinal tract sensors are thought to detect elevations in blood glucose following food ingestion and can convey satiety signals via the vagus nerve (Teff, 2011). On the other hand, carotid body and PMV glucose sensors are thought to respond to both hyperglycaemia and hypoglycaemia, though the exact properties of carotid body sensors remain equivocal (Koyama et al., 2000, Donovan, 2002). The largest body of research into peripheral glucose sensors centres on the PMV. A series of local glucose infusion studies, demonstrated that normalising PMV glucose levels during systemic hypoglycaemia, led to suppression of the sympathoadrenal response (Donovan et al., 1991a, Donovan et al., 1991b). Subsequent denervation studies, involving PMV nerve supply destruction, led to marked impairment of the sympathoadrenal response to hypoglycaemia (Hevener et al., 2000, Perseghin et al., 1997). Also, superior mesenteric ganglionectomy, but not vagotomy, led to an impaired adrenaline response following hypoglycaemia, suggesting PMV glucose sensing is mediated by spinal rather than vagal afferents (Fujita and Donovan, 2005). Peripheral glucose signals from the PMV and other glucose sensors reach the brain via both the vagus nerve and spinal cord, allowing processing in neuronal networks (Watts and Donovan, 2010).

Given the importance of PMV sensors on the hypoglycaemia CRR, the question of dominance between central and peripheral sensors often arises. A convincing explanation was provided by Saberi *et al.,* who showed that PMV glucose sensors preside over slow-onset hypoglycaemia and have lesser influence over fast-onset hypoglycaemia (Saberi et al., 2008). Thus, rather than providing redundancy, central and peripheral sensors have complementary roles, with central sensors important during fast-onset hypoglycaemia, which is often the case in insulin-treated patients.

1.7.2 Central sensors

Central glucose-sensing neurons are distributed in many brain regions (**Figure 1.7**). They are intrinsically sensitive to physiological changes in the level of glucose in the extracellular space of the brain. These neurons are either directly 'glucose-excited' (GE), if their firing rate increases in response to rising glucose levels, or directly 'glucose-inhibited' (GI) if their firing rate falls (Marty et al., 2007).

The hypothalamus benefits from being adjacent to the third ventricle and median eminence, enabling continuous circulatory glucose sampling (Beall et al., 2012). Several hypothalamic locations have received attention with regards to glucose sensing,

including the ventromedial (VMH), arcuate (ARC), lateral (LH), dorsomedial (DMH), and paraventricular (PVH) nuclei. However, the VMH contains the highest concentration of both intrinsically GE and GI neurons in the brain (Routh et al., 2014). A series of classical experiments in rats found that VMH glucopenia triggers the CRR, whilst VMH lesions or local glucose perfusion block the CRR to peripheral hypoglycaemia (Borg et al., 1995, Borg et al., 1997, Borg et al., 1994). In mice, optogenetic stimulation following virus-mediated delivery of channel rhodopsin 2 to the majority of VMH neurons which express steroidogenic factor-1 (SF-1), induces hyperglycaemia and enhances the CRR (Meek et al., 2016). Also, the disruption of glutamate release from VMH SF-1 neurons attenuates recovery from insulin-induced hypoglycaemia (Tong et al., 2007). VMH GI neurons are activated in low glucose and use a mechanism which involves the energy sensing kinase, 5' AMP-activated protein kinase (AMPK), which triggers nitric oxide (NO) production by the neuronal NO synthase (nNOS) (Routh et al., 2014). Indeed, the disruption of NO signalling in VMH GI neurons leads to impaired CRR and recovery from hypoglycaemia. This suggest that nNOS is a critical mechanism which enables VMH neurons to detect hypoglycaemia and signal the CRR (Fioramonti et al., 2010, Routh et al., 2014).

VMH glucose-sensing is further modified through a variety of inputs, including from the amygdala, PVH and hindbrain (Beall et al., 2012). Retrograde tracing experiments have confirmed that VMH glucose-sensing neurons do not project directly to the pancreas or adrenal gland. Rather, they project to integrative regions, including the ARC, LH, DMH and the PVH, which only then connect with pre-motor autonomic regions (Canteras et al., 1994). Recently, VMH pituitary adenylate cyclase-activating peptide (PACAP) neurons, which are GI, were identified to project to a number of hypothalamic brain regions including the PVH and LH (Khodai et al., 2018). In addition to glucose-sensing properties, the VMH is believed to also participate in the integration of glucose-sensing information. Unlike other hypothalamic nuclei VMH neuron dendrites extend into neighbouring nuclei, including the DMH, ARC and LH, allowing glucose information from the wider hypothalamus to be received and possibly integrated (Watts and Donovan, 2010).

Within the hindbrain, the area postrema (AP), the nucleus of the tractus solitarius (NTS) and the dorsal motor nucleus of the vagus (DMX) have all been identified as having glucose-sensing cells (Balfour et al., 2006, Donovan and Watts, 2014). Less is known about glucose sensing properties in VLM neurons. It is possible that VLM catecholamine (CA) neurons possess intrinsic glucose-sensing capabilities, or there may be as yet unidentified neighbouring neuronal populations which convey this signal (Ritter et al., 2019).

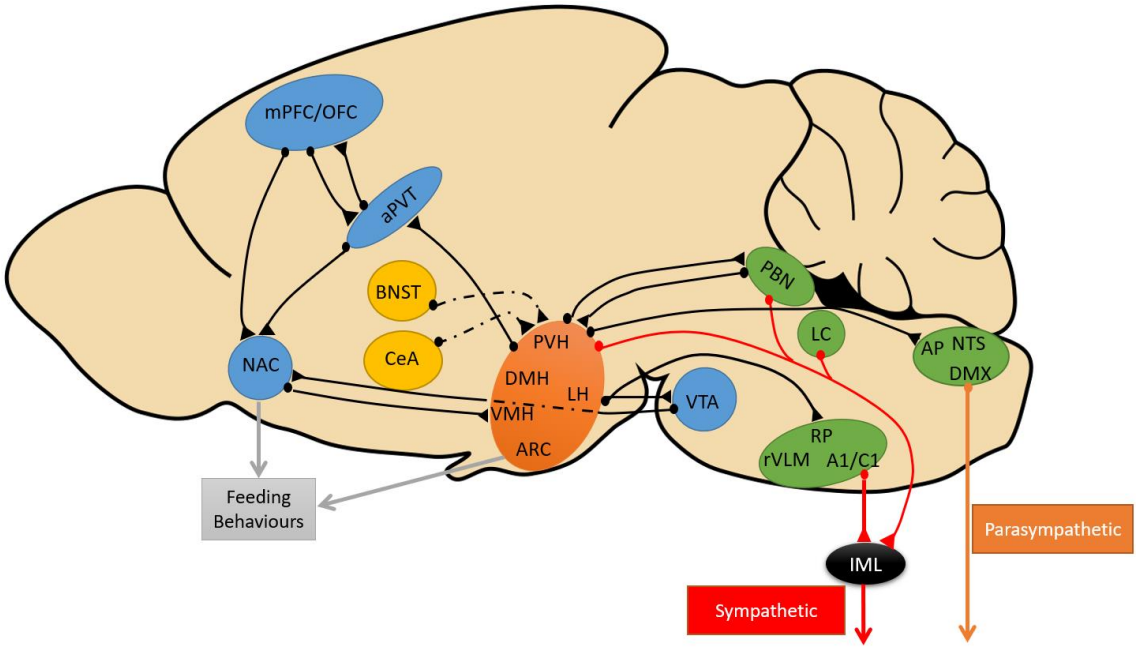

Figure 1.7: Glucose-regulatory regions in the central nervous system

Glucose sensing

Glucose-sensing neurons reside in multiple regions. In the hindbrain: area postrema (AP), the nucleus of the tractus solitarius (NTS), the dorsal motor nucleus of the vagus (DMX), basolateral medulla, the rostral ventrolateral medulla (rVLM), and the raphé pallidus (RP). They are also located in the locus coeruleus (LC) and the parabrachial nucleus (PBN). In the hypothalamus, the ventromedial (VMH), arcuate (ARC), lateral (LH), dorsomedial (DMH), and paraventricular (PVH) nuclei all contain abundant glucose-sensing cells.

Integrative/pre-motor

Within the hypothalamus, the DMH, VMH, ARC and LH are associated with integration of glucose sensory information. The LH has a complex projection pattern, with bidirectional connections to the VMH, ARC and PVH and hindbrain regions. Hindbrain integrative networks are poorly characterised, however, may involve the PBN, NTS and VLM.

Brain regions connected to the mesocorticolimbic system, including the ventral tegmental area (VTA), the nucleus accumbens (NAc), the medial prefrontal cortex (mPFC) and orbitofrontal cortex (OFC) also receive inputs from the hypothalamus and from the paraventricular nucleus of the thalamus (PVT). The NAc influences motor and behavioural responses to glucose variation. The bed nucleus of the stria terminalis (BNST) and central nucleus of the amygdala are involved in emotional processing of stressful stimuli and project to the PVH. These regions provide additional modulation and integration of sensory information.

Within the hindbrain pre-motor neurons are located within the NTS, LC, rVLM and RP. Interestingly the NTS contributes solely to parasympathetic autonomic outflow. In the hypothalamus, the PVH and LH are the primary pre-motor nuclei. PVH neurons receive inputs from ARC, LH, VMH and DMH neurons and can regulate both neuroendocrine and autonomic arms of the CRR. LH neurons project extensively to both hypothalamic and hindbrain regions.

Motor/output

Neuroendocrine motor neurons are predominantly located in the PVH, whilst autonomic motor neurons originate from the NTS, DMX and spinal intermediolateral cell column (IML). Sympathetic efferents (red) project to the periphery via the IML, whilst parasympathetic efferents (orange) originate in the NTS/DMX. Adapted from (Steinbusch et al., 2015, Watts and Donovan, 2010).

1.7.3 Neuronal intracellular glucose-sensing mechanisms

Glucose-sensing neurons employ a variety of intracellular mechanisms to sense extracellular glucose levels and alter neuronal firing. These intracellular mechanisms are diverse and differ between GI and GE neurons.

Neuronal firing depends on the function of ATP-dependent membrane ion channels such as the ATP-sensitive K^+ channel (K_{ATP}). During non-physiologically low extracellular glucose concentrations (typically <0.2mM), which can occur with insulin-induced hypoglycaemia, these K_{ATP} channels hyperpolarise/inhibit neurons (Burdakov et al., 2013). They therefore provide a non-specific protective role in both glucose-sensing and non-sensing neurons. Interestingly these channels demonstrate a secondary glucose-sensing response, which only occurs within the physiological range of glucose and, more specifically, in glucose-sensing cells (Burdakov et al., 2013). These GE cells, which include the pancreatic beta cells and GE neurons, contain additional components (e.g. glucokinase in the beta cell) which are postulated to enable a glucose-sensing response (Yang et al., 1999).

Glucokinase is suggested to have a role in cellular glucose-sensing, by controlling the rate of entry of glucose into the glycolytic pathway. Importantly, glucokinase is critical to producing glucose-6-phosphate and, therefore, ATP-dependent activity of membrane ion channels (Beall et al., 2012). However, it must be noted that glucokinase is present in non-sensing cells, suggesting that this rate-limiting function, primarily regulates cellular glucose metabolism and energy needs (Park et al., 2015).

Further evidence for the importance of the K_{ATP} channel in glucose-sensing and the hypoglycaemia CRR has been shown by examining the type 1 sulphonylurea receptor (SUR1). SUR1 is a component of the K_{ATP} channel and is expressed in the majority of GE and a proportion of GI neurons. Inhibition of SUR1-specific K_{ATP} activity in the VMH impairs the CRR and systemic application of SUR1-specific K_{ATP} channel activators potentiates the CRR (Evans et al., 2004a, Fan et al., 2008, McCrimmon et al., 2005). Also, in the LH, glucose-induced excitation of melanin-concentrating hormone (MCH) expressing neurons, has been shown to be mediated via the glucose dependent closure of SUR1 K_{ATP} channels (Kong et al., 2010).

In contrast to MCH neurons, orexin (ORX) neurons in the LH are GI. These cells utilise background K^+ currents to bring about glucose-induced hyperpolarisation and a reduction in neuronal firing (Burdakov et al., 2013). These glucose-stimulated K^+ currents have been identified in several glucose-inhibited cell types in both vertebrates and invertebrates; however how this channel precisely functions is unclear (Burdakov and Lesage, 2010). Despite the strong evidence for glucose-stimulated K^+ currents, other

mechanisms have also been suggested to control glucose-sensing in other GI cell types. These include Cl^- channel activation and K_{ATP} channel depolarization block (Burdakov and Lesage, 2010). Further experimentation is still required to resolve this debate.

The energy-sensing kinase, AMPK is another component of intra-neuronal glucose-sensing. Again, the precise molecular mechanism of AMPK in glucose-sensing is unclear. However, the pharmacological activation of AMPK in VMH neurons augments the CRR to insulin-induced hypoglycaemia, whilst suppression correspondingly reduces this response (Fan et al., 2009, McCrimmon et al., 2008).

1.7.4 Glucose-sensing machinery dysfunction and IAH

There is evidence that RH alters glucose-sensing elements within the glucose-regulatory network. Song and Routh showed in rats, that RH reduces the glucose-sensing threshold of GI neurons in the VMH (Song and Routh, 2006). Also, RH exposure in the hypothalamus but not the hindbrain, causes VMH GE neurons to hyperpolarise (Sanders et al., 2007, Kang et al., 2008).

It can be postulated that RH may induce adaptive shifts in glucose-sensing machinery. Indeed, RH increases the activity of neuronal glucokinase, which may enable an increased cellular capacity for glucose metabolism and ATP generation (Osundiji et al., 2011). This adaption to RH may result in modulation of K_{ATP} channels, altering thresholds for glucose-sensing neuron activation (Osundiji et al., 2011). Interestingly, K_{ATP} channel activation with diazoxide associates with an improvement in CRR to SH in patients with type 1 diabetes (George et al., 2015).

Adaptation of other glucose-sensing components to RH may also be relevant. AMPK activation or inhibition leads to corresponding changes to the CRR to hypoglycaemia (McCrimmon et al., 2006a). Following RH, VMH AMPK activation enhances the previously defective CRR to subsequent hypoglycaemia in rats with and without type 1 diabetes (Fan et al., 2009, McCrimmon et al., 2006a). These findings have been corroborated by studies in NTS GLUT2, glucose-sensing neurons, where electrophysiological evidence demonstrated excitability when the neurons were exposed to an AMPK activator (Lamy et al., 2014). Though the exact route by which AMPK activity regulates the glucose-sensing neuron response is unclear, it may be due to phosphorylation of key receptors which lead to enhanced neuronal depolarisation (Beall et al., 2012). AMPK phosphorylates the cystic fibrosis transmembrane conductance regulator (CFTR), which is important for GI neuron excitability (Murphy et al., 2009). AMPK also phosphorylates NMDA, $GABA_B$ and Kv2.1 receptors, which are all important

in synaptic transmission in glucose-sensing neurons (Kuramoto et al., 2007, Ikematsu et al., 2011).

1.8 Motor/output

The glucose-regulatory system corrects a fall in blood glucose through neuroendocrine, autonomic (the sympathoadrenal system being most important in relation to IAH) and behavioural outputs. The anatomy and circuitry of key counter-regulatory systems are discussed in this section.

1.8.1 Neuroendocrine system

The neuroendocrine system is coordinated by the hypothalamus. Through direct control of the pituitary, the hypothalamus exerts control on diverse homeostatic pathways. Hypothalamic neuroendocrine neurons can be considered as motor neurons, due to their ability to direct the secretory function of multiple endocrine effectors (Watts, 2015). Hypothalamic neuroendocrine motor neurons are heterogenous but can be characterised by their neuropeptide phenotype. Notable examples in the PVH include corticotrophin-releasing hormone (CRH), oxytocin (OXT) and arginine vasopressin (AVP). In the ARC, growth hormone-releasing hormone (GHRH) neurons may also participate in the hypoglycaemia CRR (Stanley et al., 2013).

Following stressors, including hypoglycaemia, CRH motor neurons engage the hypothalamic-pituitary-adrenal (HPA) axis, a vital pathway which culminates in adrenal cortisol release. Several studies have examined the importance of cortisol in the CRR. Cortisol augments glucose production, decreases glucose utilisation and accelerates lipolysis; though, these glucose raising effects tend to be delayed (Bolli et al., 1983, De Feo et al., 1989). ARC GHRH neurons and growth hormone (GH) release increases following hypoglycaemia (Stanley et al., 2013). GHRH deficiency worsens hypoglycaemia and impairs recovery in humans and rodents, through reducing hepatic glucose production and increasing glucose utilisation (De Feo et al., 1989) (Stanley et al., 2013). However, in a similar way to cortisol, the effect is delayed (De Feo et al., 1989). AVP neurons in the PVH are activated by hypoglycaemia and 2-DG-induced glucoprivation. Activation of AVP neurons increases AVP secretion, which directly stimulates glucagon and elevation of blood glucose. Interestingly this activation is driven by VLM catecholaminergic (CA) neurons (Kim et al., 2021). In humans, hypoglycaemia increases circulating AVP, which stimulates glucagon release. However, this system becomes impaired in patients with type 1 diabetes (Kim et al., 2021). Less is known about OXT neuron involvement in the hypoglycaemia CRR, however circulating oxytocin

is increased during an insulin tolerance test (ITT) (Coiro et al., 1988). Neuroendocrine systems have not yet been shown to have a significant contribution to hypoglycaemia symptoms.

1.8.2 Sympathoadrenal system

The autonomic response to hypoglycaemia is initiated by motor neurons in the hindbrain, spinal cord and autonomic ganglia. The parasympathetic output from the hindbrain originates from motor neurons in the NTS and DMX and, passing via the vagus nerve, exerts control on pancreatic islet function. Parasympathetic activation stimulates insulin release and, though it leads to modest glucagon secretion, its role in the hypoglycaemia CRR is limited (Ahrén and Taborsky, 1986, Thorens, 2010).

On the other hand, the sympathetic nervous system and in particular, the sympathoadrenal response, is critical to the hypoglycaemia CRR. The sympathoadrenal system includes sympathetic neural and adrenomedullary arms. Hindbrain pre-motor neurons in the LC, RP and importantly VLM engage spinal sympathetic preganglionic motor neurons (SPNs) in the intermediolateral nucleus of the spinal cord (IML) (Kumagai et al., 2012). Several classical tracing studies have identified PVH and LH pre-motor neuronal projections to SPNs (Luiten et al., 1985, Verberne et al., 2014). These pathways were further shown to be involved in the control of pancreatic islet and chromaffin cell function (Kerman et al., 2007, Jansen et al., 1997).

From the IML, preganglionic and postganglionic autonomic nerves innervate the pancreas and adrenal gland, controlling glucagon and insulin, and adrenaline release, respectively. Adrenaline is released from the adrenal chromaffin cell, and together with sympathetic neural noradrenaline, rapidly raises blood glucose. This is achieved through direct stimulation of hepatic glucose production, inhibition of insulin and stimulation of glucagon release. Hypoglycaemia-induced autonomic symptoms are an equally potent result of sympathoadrenal system activation (**Figure 1.3B**). An increase in circulating adrenaline can initiate autonomic symptoms, through actions on adrenergic receptors (DeRosa and Cryer, 2004). However, Cryer *et al.,* convincingly showed that sympathetic neural, rather than adrenomedullary adrenaline was the primary driver for autonomic symptoms in hypoglycaemia (DeRosa and Cryer, 2004). Sympathetic neural activity is more difficult to measure, whereas circulating adrenaline is readily sampled and acts as a good proxy of the sympathoadrenal response (Sankar et al., 2020).

1.8.3 Peripheral output dysfunction

Only a small number of investigations have examined the direct impact of RH on peripheral systems involved in the hypoglycaemia CRR. These studies mainly concentrate on the adrenal sympathetic nerve and adrenal gland.

Sivitz *et al.,* showed that RH reduced adrenaline release, however did not reduce adrenal sympathetic nervous activity in rats (Sivitz et al., 2001). When compared with SH, adrenal nerve activity following RH was increased at baseline with an attenuated rise in activity to subsequent hypoglycaemia (a non-significant reduction in adrenal nerve responsiveness when expressed as a percentage increase) (Sivitz et al., 2001). Therefore, the acute responsiveness of the adrenal sympathetic nerve may become refractory with RH, leading to an attenuation in corresponding adrenaline release. An alternative explanation could be that chronic adrenal sympathetic activation leads to desensitisation of the adrenal tissue and consequently reduced adrenaline release (Sivitz et al., 2001).

More recently, Ma *et al*. studied the effect of RH on mouse adrenal chromaffin cells (Ma et al., 2018b). They showed impaired chromaffin cell secretion and a corresponding reduction in tyrosine hydroxylase (TH) immunoreactivity following RH. However, neuropeptide Y (NPY) immunoreactivity was elevated. Interestingly, in NPY knock-out mice, TH immunoreactivity and adrenaline responses were not reduced following RH. Therefore, NPY release in the adrenal gland could provide an independent mechanism by which RH induces diminished adrenaline secretion (Seaquist, 2018, Ma et al., 2018b).

As I have outlined, RH impairs the sympathoadrenal response, precipitating IAH and risk of severe hypoglycaemia. Despite this knowledge and a large body of research examining central determinants of the impaired sympathoadrenal response to RH, little remains known about changes at the level of SPNs, autonomic nerves or adrenal gland.

1.8.4 Behavioural output

The behavioural responses of arousal, such as seeking and ingesting carbohydrates, are crucial components of the hypoglycaemia CRR. Though behaviours occur rapidly, they require the integration of multiple networks. Hypoglycaemia, leads to autonomic activation, generating signals which lead to defined behaviours. In addition to the glucose raising effects, sympathoadrenal activation produces a variety of visceral phenomena (increase in heart rate, tremor, sweating, etc.) which are detected and communicated to the brain via spinal and vagal afferents (Chen et al., 2021). These ascending signals pass via the NTS and lateral PBN to thalamic and cortical regions (Craig, 2002, Garfield et al., 2014). It is here that perception of autonomic symptoms (**Figure 1.3B**), which are

vital for hypoglycaemia detection in patients with type 1 diabetes, occurs. Within the cortex, the cingulate (cortex) is involved in monitoring the body's internal state and imaging studies suggest it plays an important role in hypoglycaemia symptom perception or awareness (Hurst et al., 2012, Amiel, 2009).

Appropriate arousal is necessary to recognise and interpret signals relating to hypoglycaemia and initiate behaviours (Routh et al., 2014). The LC is a major noradrenergic (NA) nucleus, which regulates arousal following autonomic activation and is responsive to hypoglycaemia (Morilak et al., 1987). The LC-NA system achieves this through connections with forebrain, thalamic, hypothalamic and hindbrain regions, and via functional interactions with the orexin system (hypothalamic peptides which also promote arousal) (Samuels and Szabadi, 2008, Carter et al., 2013). Interestingly, Otlivanchik *et al.,* used a novel behavioural model for IAH, the aversive salience of hypoglycaemia, to demonstrate the importance of arousal-promoting orexin neurons in the perifornical hypothalamus (PFH) (Otlivanchik et al., 2016). The PFH and LH have been implicated in catecholaminergic (CA) VLM circuits, which may enable the orexin system to coordinate arousal with feeding behaviour following hypoglycaemia (Li et al., 2015).

Hypoglycaemia-induced hunger and feeding behaviours may be mediated by hindbrain circuits centred on the NTS and VLM. NTS CA neurons project densely to ARC agouti-related protein (AgRP) neurons and have been shown to be functionally important for glucoprivic feeding induced by 2-DG (Aklan et al., 2020). In addition, activation of specific clusters of VLM CA neurons which project to the LH, PFH and posterior paraventricular nucleus of the thalamus (pPVT), lead to an increase in glucoprivic feeding following 2-DG (Sofia Beas et al., 2020, Li et al., 2018).

The PVT influences arousal, motivated feeding, reward seeking and aversion (Do-Monte et al., 2017, Labouebe et al., 2016, Bhatnagar et al., 2002). The PVT receives substantial inputs from feeding-related hypothalamic regions, including the LH and ARC, and cortical regions linked with decision making (Lee et al., 2015). The PVT, in turn, innervates the nucleus accumbens (NAc), medial prefrontal cortex, amygdala and the bed nucleus of the stria terminalis (BNST) (Parsons et al., 2006). These anatomical connections suggest that the PVT integrates feeding-related information from hypothalamic nuclei and signals the mesocorticolimbic system to seek food (Kirouac, 2015, Parsons et al., 2006).

1.9 Integrative and pre-motor networks

There is significant overlap in the neuroanatomy and projection patterns of integrative and pre-motor network (Jansen et al., 1997, Kerman et al., 2003, Kerman et al., 2007). Hindbrain integrative networks are poorly understood but are likely include CA neurons in NTS and the lateral PBN, influencing feeding and autonomic CRR respectively (Aklan et al., 2020, Garfield et al., 2014). In the hypothalamus, the DMH, VMH, LH and ARC all contain sensing and integrative networks. VMH and LH connections have been explored in previous sections, however the ARC merits further discussion.

The ARC is an important metabolic centre and houses neuropeptide Y (NPY) and proopiomelanocortin (POMC) neurons, which have opposing effects on appetite and food intake (Wang et al., 2004). A variety of central and peripheral metabolic signals reach the ARC, which itself has glucose-sensing elements (Wang et al., 2004). ARC NPY neuronal projections to the hypothalamus, hindbrain and spinal cord, favour anabolic processes and energy conservation (Kuperman et al., 2016). In addition, ARC and DMH projections to the PVH influence autonomic and neuroendocrine responses to hypoglycaemia (Evans et al., 2004b). Other integrative regions, including the PVT, CeA and BNST, will be discussed in greater detail in Chapters 3 and 7.

Pre-motor networks provide an additional site of modulation (Watts and Donovan, 2010). Only a limited number of hindbrain regions contain pre-motor neurons. It should be noted that whilst some hindbrain pre-motor neurons selectively engage the autonomic parasympathetic system, others care capable of initiating sympathetic and parasympathetic activation (Jansen et al., 1997, Buijs et al., 2001). In the hindbrain, the VLM is a crucial to the hypoglycaemia sympathoadrenal response and merits discussion.

The VLM contains integrative and pre-motor networks sufficient to independently elevate blood glucose following hypoglycaemia or glucoprivation (Ritter et al., 2019). This was first demonstrated in decerebrate rats (in which neural connections between the forebrain and hindbrain were severed), which continued to maintain a CRR to glucoprivation (DiRocco and Grill, 1979). This was followed by a series of classical cannula mapping experiments, where glucoprivic agents were injected into specific hindbrain regions, demonstrating that activating medullary CA neuron groups leads to increased blood glucose, cortisol, glucagon and food intake (Andrew et al., 2007). Subsequently, hindbrain cFos induction in response to glucoprivation, was found to be most prevalent in CA neurons in the VLM (Ritter et al., 1998). A more detailed chemogenetic study in rats identified that activation of both rostral C1 (C1r) and middle C1 (C1m) neurons, but not the A1/C1 overlap region, leads to an increase in blood glucose. This was supplemented by a corresponding increase in cFos expression in the

adrenal medulla and IML only in rats transfected at both the C1r and C1m. On the other hand, food intake and cortisol release require activation of C1m and A1/C1 regions (Li et al., 2018). Similarly in rats exposed to insulin-induced SH, rVLM C1 neurons displayed an increase cFos, which is attenuated with RH (Kakall et al., 2019). Relatively few studies have examined the role of the rVLM in mice. However, Zhao *et al.* used virus-mediated chemogenetic and tracing approaches to show that stimulation of rVLM CA neurons rapidly increases blood glucose and corresponding adrenaline release. This was subsequently shown to be mediated by descending projections from rVLM CA neurons to the spinal cord IML (Zhao et al., 2017). VLM CA neuron groups and main projection patterns are shown in **Figure 1.8**. It is interesting and important to note that rVLM CA neurons also project to the LH and PVH, where they stimulate additional glucoprivic effects, such as arousal and cortisol secretion (Ritter et al., 2019). This reinforces the idea that hindbrain and hypothalamic networks combine to enable a more nuanced CRR to glucoprivation and hypoglycaemia.

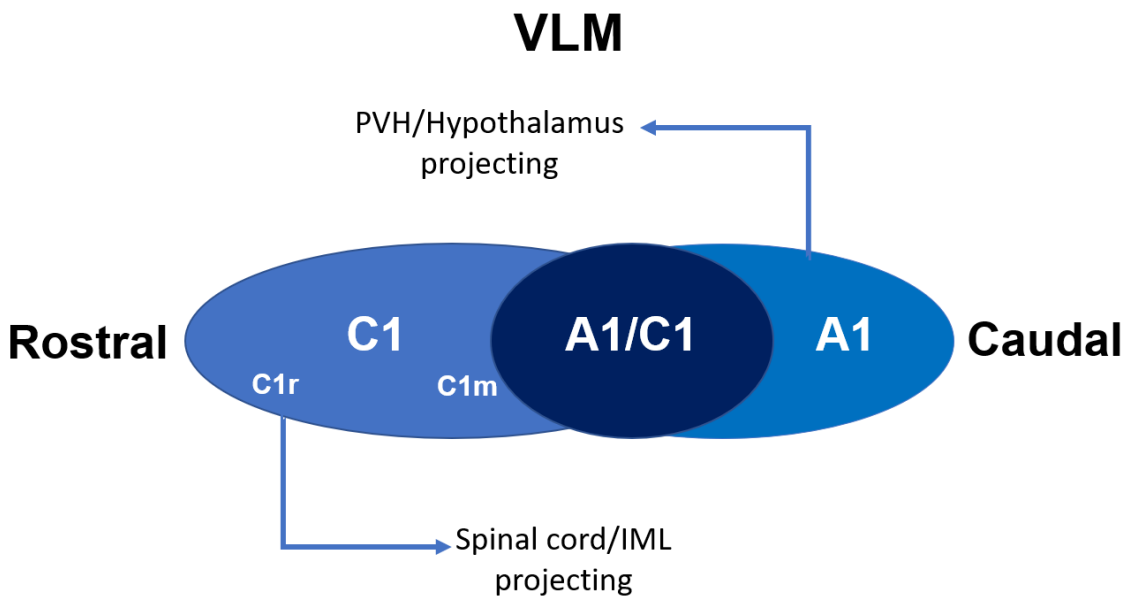

Figure 1.8: Subdivisions and main projections of VLM CA neuron groups

VLM CA neuron groups termed "A" or "C" are composed of noradrenaline or adrenaline expressing neurons, respectively. The A1/C1 group refers to the area of overlap of caudal A1 and rostral C1 neuron groups and contains a mixed noradrenaline/adrenaline population of CA neurons. The terms C1r and C1m are applied to separate the rostral and middle areas of C1, respectively. Hypoglycaemia and glucoprivation leads to an increase in activity in C1 neurons with corresponding initiation of CRR and signalling of adrenaline release via projection to the spinal cord/IML. On the other hand, A1 neurons are involved in hypoglycaemia/glucoprivation-induced feeding and arousal, mediated by projections to the PVH and wider hypothalamus (Ritter et al., 2019, Zhao et al., 2017).

Hypothalamic pre-motor neurons project to the hindbrain and spinal cord to regulate autonomic function, or to the posterior pituitary and median eminence for neuroendocrine function. The PVH is an important region for hypoglycaemia counter regulation, but also in the wider response to both physiological and psychological stressors. Within the glucose sensory-motor integration framework, it is primarily considered to be a pre-motor/autonomic element. However, neurons which possess sensory, integrative and motor functions are all present within the PVH (Jiang et al., 2018, Donovan and Watts, 2014).

The PVH receives glucose-sensory information from multiple hypothalamic nuclei including VMH PACAP neurons, as well as from the hindbrain (Canteras et al., 1994, Fuzesi et al., 2007, Khodai et al., 2018). Therefore, signals communicating hypoglycaemia are relayed to the PVH to signal autonomic and neuroendocrine responses. Indeed, PACAP of unknown origin, acting via the PVH, induces hepatic glucose production (Kalsbeek et al., 2004). Also, the PVH has direct connections to the sympathetic nervous system. Both anterograde and retrograde tracing studies have shown that the PVH projects directly to sympathetic preganglionic neurons and

sympathetic pre-motor neurons, thus establishing a direct pathway for PVH control of sympathoadrenal outflow (Shafton et al., 1998, Luiten et al., 1985). More recently, a PVH to ventrolateral medulla (VLM) excitatory pathway has been identified which then projects via the spinal cord to the adrenal gland (Zhao et al., 2017). Optogenetic activation of this circuit resulted in sympathoadrenal activation and hyperglycaemia (Zhao et al., 2017). Also, a study in neuron-specific insulin receptor knockout mice, found a direct correlation between reduced adrenaline response following hypoglycaemia and reduced induction of the early transcriptional marker, nuclear cFos protein in the PVH (Diggs-Andrews et al., 2010). This study also identified the importance of insulin and leptin in modulating glucose sensing and the CRR through neurons in the PVH (Diggs-Andrews et al., 2010).

The PVH can be subdivided in many ways though, in terms of projection patterns relevant to the hypoglycaemia CRR, they can be divided into two groups:

1) **Median eminence and posterior pituitary projecting**
   These include parvocellular (small size) neurons which secrete corticotrophin-releasing hormone (CRH), arginine vasopressin (AVP), thyrotrophin-releasing hormone (TRH) and somatostatin (SST); or magnocellular (large size) neurons which secrete oxytocin (OXT) or AVP (Aguilera and Liu, 2012).
2) **Hindbrain and spinal cord projecting**
   Diverse populations of parvocellular neurons which secrete or express AVP, OXT SST, CRH, CRHR1, dopamine (DA), angiotensin II, MC4R and others (Nunn et al., 2011, Qin et al., 2018).

This subdivision is heavily based on detailed anatomical and tracing studies in rats, however the mouse PVH has notable differences (Simmons and Swanson, 2008, Feetham et al., 2018). For example, parvocellular and magnocellular neuronal populations are more difficult to differentiate in the mouse PVH. In addition, there is a difference in the anatomical location of neuronal populations, notably CRH neurons (Biag et al., 2012). A summary of PVH subdivisions and our current understanding of projection patterns in the mouse brain is summarised in **Figure 1.9**.

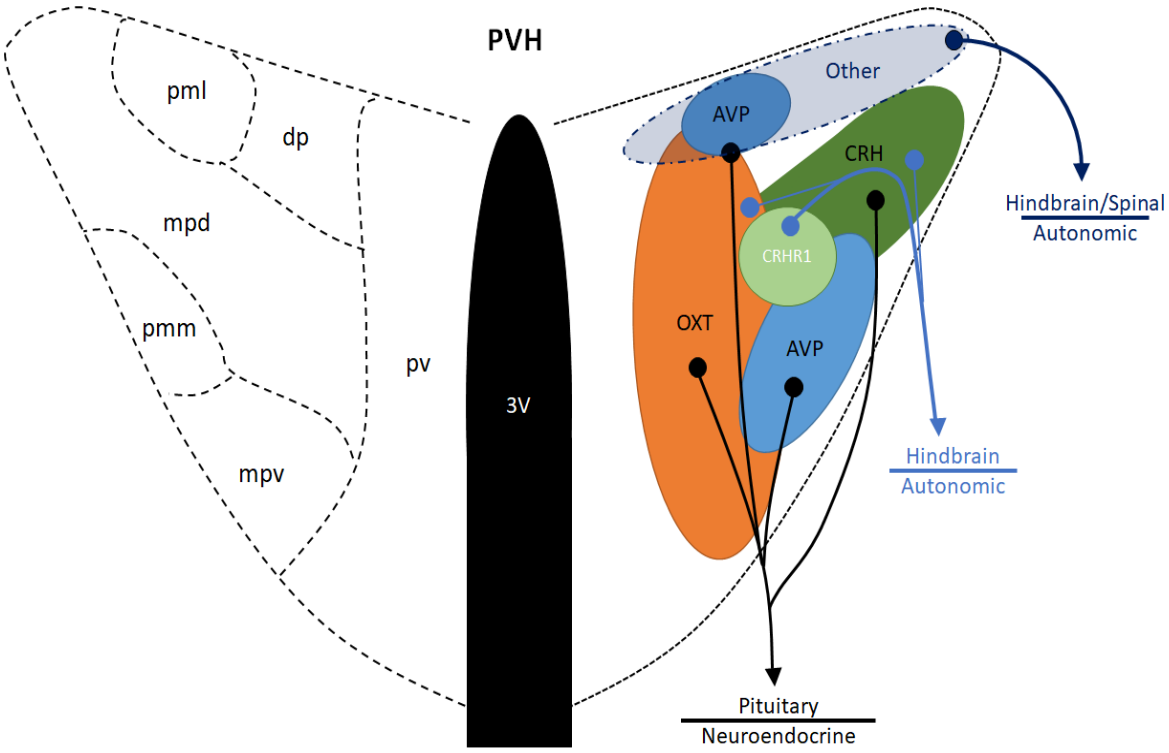

Figure 1.9: Subdivision of the PVH in the mouse brain

PVH neurons can be subdivided anatomically based on neuron size, neuropeptide release and projection pattern (though co-expression of neuropeptides and receptors occurs). Neuroendocrine neurons project to the median eminence or posterior pituitary, are generally located more medially and primarily express OXT, AVP, CRH and TRH. Hindbrain (VLM and NTS)-projecting autonomic neurons do not follow a specific distribution pattern but are generally located more laterally in the PVH and have been found to express OXT, CRH and recently CRHR1. Hindbrain- and spinal-projecting autonomic neurons are generally located in the dorsal PVH. These neurons are generally parvocellular and express a wide range of neuropeptides and receptors, including but not limited to AVP, OXT SST, CRH, CRHR1, dopamine (DA), angiotensin II and melanocortin 4 receptor (MC4R).

3V: 3rd ventricle; **pml**: posterior magnocellular lateral zone; **mpd:** medial parvocellular dorsal division **mpv:** medial periventricular; **pmm:** posterior magnocellular medial zone; **pv:** periventricular zone; **dp:** dorsal parvicellular.

Within the PVH, CRH neurons have a prominent role in organising the HPA axis and, as is increasingly apparent, the sympathoadrenal response to hypoglycaemia (Kuperman et al., 2016, Jiang et al., 2018, McCrimmon et al., 2006b). These neurons will be discussed in much greater detail in Chapters 3, 5 and 6.

Potential mechanisms to explain RH-related network changes at the level of integrative and pre-motor networks will now be discussed. However, it must be recognised that that some mechanisms may be indiscriminate and affect the entire glucose-regulatory network.

1.9.1 Altered neurotransmission

Gamma-aminobutyric acid (GABA) is the major inhibitory neurotransmitter in the CNS. Antagonism of $GABA_A$ receptors in the VMH amplifies the CRR whilst stimulation of these receptors reduces the CRR (Chan et al., 2006). In the VMH of rats, acute hypoglycaemia decreases GABA levels, but with RH, the levels are maintained (Chan et al., 2008). Similarly, in a magnetic resonance spectroscopy study in healthy humans, acute hypoglycaemia led to a reduction in GABA concentration in the hypothalamus (Moheet et al., 2014a). Interestingly, akin to findings in RH, diabetic rat models display elevated basal GABA levels in the VMH, which are associated with an increased expression of GAD65 protein which is a GABA-synthesizing enzyme (Chan et al., 2011). Despite these observations, the precise circuitry of GABAergic neurons is unclear. We are aware that large numbers of GABAergic neurons are present in the ARC and many investigators have also observed that they surround VMH and PVH glutamatergic neurons (Ovesjo et al., 2001, Tong et al., 2007, Vong et al., 2011). GABAergic neurons synapse with glutamatergic (SF-1) neurons in the VMH and this connection is important in generating a normal CRR to acute hypoglycaemia (Kamitakahara et al., 2016). Also, brain derived neurotrophic factor (BDNF) is key to maintaining these inhibitory GABAergic inputs on SF1 neurons (Kamitakahara et al., 2016). Exploring the consequences of BDNF suppression following RH on GABA signalling, may be of interest considering its potential role as a neuromodulator (Pezet et al., 2002, Rao et al., 2016).

Monoamine neurotransmitters, particularly serotonin and noradrenaline are important within glucose-regulatory circuits. Systemic and central delivery of serotonin receptor agonists increases circulating adrenaline in a dose-dependent manner (Sanders et al., 2008). In rats, sertraline – a selective serotonin reuptake inhibitor (SSRI), caused an enhanced hormonal CRR following hypoglycaemia and prevented a diminished response following RH (Sanders et al., 2008). Significantly, these findings were replicated in humans with type 1 diabetes and in healthy volunteers (Briscoe et al., 2008a, Briscoe et al., 2008b). It is possible that this effect is mediated through hindbrain serotonin neurons, which connect via the IML to SPNs innervating the adrenal gland (Strack et al., 1989). These findings are tempered by case studies reporting that some patients treated with SSRIs experience an increased hypoglycaemia frequency and, in fact, develop IAH (Sawka et al., 2001).

Noradrenaline (NA) and TH activity both increase following central and systemic hypoglycaemia. Whilst hypothalamic injection of NA increases blood glucose and promotes food intake (Chafetz et al., 1986). The raphé nuclei, through connections with the LC and possibly hypothalamus, seems to be particularly important in regulating

autonomic output, motor activity and hunger following hypoglycaemia (Belfort-DeAguiar et al., 2018).

Though the focus of this thesis is on neuronal networks, the potential role of glial cells, including astrocytes, in modulating neurotransmission must be acknowledged. Astrocytes release gliotransmitters, including glutamate, D-serine and ATP, which have a modulatory effect on synapses (Harada et al., 2016). Astrocytic dysfunction following RH, which has recently been shown in cell culture, may also contribute to neuronal dysfunction in IAH (Gao et al., 2021).

1.9.2 Signalling molecules and pathways

Endogenous opioids, together with opioid receptors have a role in stress signalling during hypoglycaemia (Caprio et al., 1991). Opioid receptor pre-treatment with intravenous morphine attenuates adrenaline and symptom response to hypoglycaemia in healthy human volunteers (Carey et al., 2017). Whilst, naloxone, an opioid receptor antagonist, amplifies both adrenaline and corticosterone responses to hypoglycaemia in healthy volunteers and patients with type 1 diabetes (Caprio et al., 1991). Also, opioid blockade during antecedent hypoglycaemia improves adrenaline responses to subsequent hypoglycaemia in patients with type 1 diabetes. The investigators suggested that the endogenous opioid system exerts an inhibitory influence on CRR and may, with recurrent stimulation, lead to pronounced negative feedback on catecholamine release (Vele et al., 2011).

Other signalling molecules and pathways, including cortisol, dehydroepiandrostenedione (DHEA), β_2 adrenergic and serotonergic pathways, have been investigated on a smaller scale (McNeilly and McCrimmon, 2018). More recently there has been evidence that the normal pro- and anti-inflammatory cytokine release which follows stressors such as SH, becomes modified with prior RH and also type 1 diabetes (McNeilly et al., 2016).

If altered extracellular signals play a role in the development of impaired CRR and IAH, this may be by modulating neuronal firing in the glucose-regulatory network, perhaps via neurotransmitter release altering K_{ATP} channel activity or actions on astrocytes (McNeilly and McCrimmon, 2018).

1.9.3 Altered fuel usage and transport

The alternative fuel use theory posits that RH leads to a switch from glucose to lactate metabolism or increased reliance on glycogen (Herzog et al., 2013). This followed observations in humans and rodents that brain glycogen content reduces following SH and a compensatory increase in glycogen storage follows RH (Beall et al., 2012, Tesfaye

et al., 2011, Herzog et al., 2008). This finding was not unique to humans and has been shown in mouse and rat models of RH. Others have used repeated 2-DG to show an elevation in hypothalamic glycogen levels and correlated this with delayed AMPK activation (Alquier et al., 2007). Increases in glycogen storage may be facilitated by changes in glucose/fuel transport in neurons and astrocytes. Some studies in rodents show increased glucose transport through the blood-brain barrier following RH and prolonged hypoglycaemia (Boyle et al., 1995, Rooijackers et al., 2016). However, these findings are not consistent, and others have reported a decrease in neuronal glucose metabolism after RH (Jiang et al., 2009). In addition, brain glycogen stores are comparatively small and the CRR following hypoglycaemia remains defective even when brain glycogen levels recover (Herzog et al., 2008a). More recent investigations in patients with type 1 diabetes and IAH, have failed to show increased brain glycogen stores or glucose metabolism. Therefore, correlation with findings in patients with the disease is vital (Henry et al., 2010, Öz et al., 2017).

1.9.4 Habituation

Habituation refers to ‘a reduction in the psychological, behavioural or physiological response to a stimulus because of repeated or prolonged exposure’ (Thompson and Spencer, 1966, McCrimmon, 2017). Recently neuronal adaptations to RH have been convincingly described as habituation (McCrimmon, 2017). In this description, RH poses a significant cellular stress, which initiates general cellular and neuronal adaptations to enable survival (**Figure 1.10**). When this adaptation becomes generalised to a whole neuronal population or network, this may lead to a habituation of a response. In this case, following RH, habituation of the CRR occurs to subsequent hypoglycaemia. This adaptation becomes detrimental when, combined with the insult of diabetes and insulin treatment, it leads to IAH.

Whether habituation of the CRR to RH results from whole-network adaptations, or changes at specific loci, will be the subject of further investigation in this thesis.

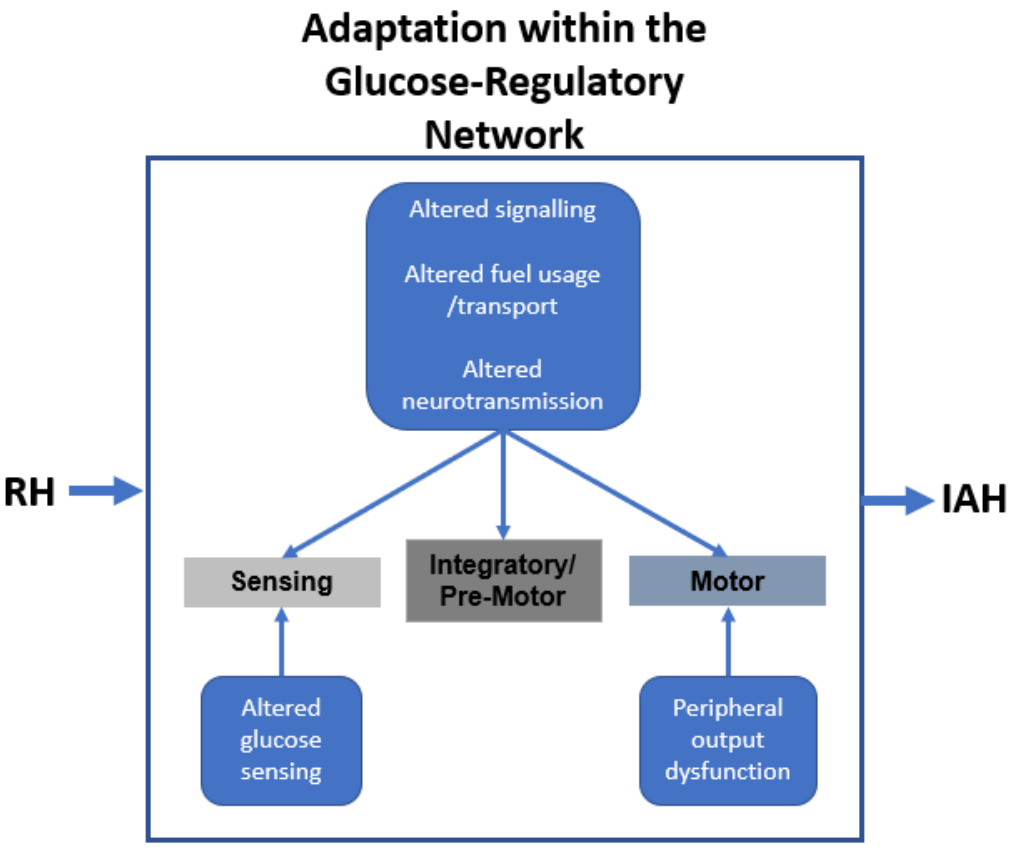

Figure 1.10: A theorised framework for loci-specific adaptations to RH leading to IAH

Using the sensory-motor integration framework and current proposed mechanisms for IAH, we can postulate that, following RH, specific mechanisms converge on sensing, integrative/pre-motor and motor components of the glucose-regulatory network. These adaptive changes, lead to IAH and may represent habituation.

1.10 Aims

The broad aim of this doctoral research is to demonstrate that specific neuronal networks involved in the hypoglycaemia CRR become disrupted following RH, explaining the development of IAH.

This is achieved through the development of a mouse model of RH and impaired CRR, which I outline in Chapter 3. Chapter 3 also investigates the acute and chronic neuronal response to both SH and RH, in key hypoglycaemia-responsive brain regions. This provides a basis for further interrogation of specific neuronal circuits and populations in subsequent chapters. In Chapter 4, I assess whether the mouse model of IAH and impaired CRR shows key hallmarks of habituation, providing a mechanistic understanding of adaptations to RH. In Chapters 5 and 6, I investigate the *in vivo* response of CRH^{PVH} neurons to stress, focusing on SH and RH (Chapter 5), followed by their functional significance to the hypoglycaemia CRR (Chapter 6). Finally in Chapter 7, I question the role of the pPVT and vBNST in the habituation of the CRR to RH and identify pathways which enable anatomical and functional integration with the wider glucose-regulatory network.

1.11 Objectives

Specific objectives for each study are described in the corresponding experimental chapter, however key objectives include:

- Characterise and validate a mouse model of RH and impaired CRR.
- Investigate the acute and chronic neuronal response to SH and RH within the glucose-regulatory network using cellular markers.
- Assess whether RH leads to classical features of habituation in the mouse model of IAH.
- Using fibre photometry, characterise the real-time *in vivo* response of PVH^{CRH} neurons to physiological stressors including SH, and identify alterations to neuronal activity to RH.
- Investigate the functional significance of PVH^{CRH} neurons to the hypoglycaemia CRR using chemogenetic modalities and understand the circuits which mediate these effects using neuronal tracing techniques .
- Explore the functional roles of the pPVT and vBNST in the habituation of the CRR to RH and establish key connections with the glucose-regulatory network using neuronal tracing techniques.

Chapter 2

General Methods

2.1 *In vivo* methods

2.1.1 Animals

All procedures and experiments on mice were performed in accordance with the Animal (Scientific Procedures) Act 1986 (UK) and approved by the University of Manchester Animal Welfare and Ethics Review Board. Experiments were performed either with adult male C57Bl/6J mice (Charles River, UK) or adult transgenic mice (bred in house, University of Manchester). Mice were aged between 8-16 weeks at the start of all experiments. Mice were housed in the animal unit and maintained in standardised conditions, with 12h:12h light/dark cycle and constant environment of 21 ± 2°C and 45 ± 10% humidity. Standard diet (Special Diet Services; Witham, UK) and sterile pouch water were available *ad libitum.* Mice were group housed (2-5 per cage) with littermates to minimise stress. All animals were handled daily for two weeks prior to the start of experiments.

2.1.1.1 ROSA26-eYFP reporter mouse

The ROSA26-eYFP mouse (B6.129X1-*Gt (ROSA)26Sortm1 (EYFP)Cos*/J; JAX strain #006148; C57Bl/6J background) is a transgenic reporter line which expresses enhanced Yellow Fluorescent Protein (eYFP) in a Cre-recombinase-dependent manner (Taniguchi et al., 2011, Srinivas et al., 2001). The ROSA26-eYFP line was maintained in-house as a homozygous colony.

2.1.1.2 *Crh*-cre mouse

The *Crh*-cre mouse (B6(Cg)-Crh<tm1(cre)Zjh>J; JAX strain #012704; C57BL/6J background) is a knock-in line which expresses Cre recombinase under the control of the endogenous promoter/enhancer elements of the corticotrophin releasing hormone (*Crh)* locus (Taniguchi et al., 2011, Wamsteeker Cusulin et al., 2013). When crossed with the ROSA26-eYFP reporter mouse, Cre-mediated recombination results in eYFP expression in CRH neurons, producing *Crh*-cre::eYFP offspring. The *Crh*-cre mouse was maintained in-house as a hemizygous colony.

2.1.1.3 *VGlut2*-cre mouse

The *VGlut2*-IRES-cre mouse (*Slc17a6tm2 (cre)Lowl*; Jax strain #016963; mixed C57BL/6;FVB/N;129S6 genetic background) is a knock-in line which expresses Cre-recombinase under the control of the endogenous vesicular glutamate transporter 2 (*VGlut2*) promoter. This line was crossed with the ROSA26-eYFP reporter mouse to

produce *VGlut2*-cre::eYFP offspring. The *VGlut2*-cre mouse was maintained in-house as a hemizygous colony.

2.1.1.4 *Gad2*-cre mouse

The *Gad2*-cre mouse (*Gad2tm2 (cre)Zjh*; Jax strain #010802; C57BL/6J background) is a knock-in line which expresses Cre recombinase under the control of the glutamic acid decarboxylase 2 (*Gad2*) promoter. Here, the IRES-linked Cre-recombinase gene was inserted in the 3' UTR of the *Gad2* locus, resulting in Cre-recombinase expression directed to *Gad2* positive neurons: the γ-aminobutyric acid (GABA)ergic population of neurons (GAD_{65}). The *Gad2*-IRES-cre mouse was maintained in-house as a hemizygous colony.

2.1.1.5 *Gad2*-GFP mouse

The *Gad2*-GFP mouse (C57BL/6J background) is a transgenic reporter line produced by Szabo Gabor at the Institute of Experimental Medicine in Budapest, Hungary (López-Bendito et al., 2004). In this line, the Green Fluorescent Protein (GFP) gene is fused to the *Gad2* gene driving the expression of GFP to the GABAergic population of GAD_{65} neurons. The *Gad2*-GFP mouse was maintained in-house as a hemizygous colony.

2.1.2 Drugs

All drugs were obtained from commercial suppliers and certified to be pyrogen and pathogen free. Drugs used in experiments were administrated via subcutaneous (s.c.) or intraperitoneal (i.p.) injection. Subcutaneous and intraperitoneal injections were administered at 4 ml/kg (body weight) using 29 G insulin syringes. Unless, stated otherwise, drugs were diluted in sterile saline (0.9% w/v NaCl: Braun; Melsungen, Germany). Control injections involved volume matched saline injections by the appropriate route.

Insulin: Insulin (insulin human: Sigma-Aldrich; Saint Louis, MO, USA) was first dissolved in 0.01 M HCl (Sigma-Aldrich) and then diluted in 0.9% NaCl. A final concentration of 1.75 units/kg (U/kg) was administered via the s.c. route between shoulder blades to induced hypoglycaemia.

Clozapine-N-oxide: CNO (1 mg/kg: Tocris; Bristol, UK) was dissolved and diluted in 0.9% saline, then administered via the i.p. route.

4-Hydroxytamoxifen: 4-OHT (10 mg/kg: Sigma-Aldrich) was first dissolved in DMSO, diluted in a solution containing 0.9% NaCl and 2% Tween 80 (Sigma-Aldrich) and administered via the i.p. route.

2-Deoxy-D-glucose: 2-DG (500 mg/kg: Sigma-Aldrich) was dissolved and diluted in 0.9% saline, then administered via the i.p. route.

2.1.3 Stereotaxic surgery

2.1.3.1 Site-specific parenchymal injections

Animals were injected unilaterally or bilaterally with adeno-associated virus (AAV) or tracer into specific brain nuclei for all studies outlined in this thesis . All surgeries were conducted under anaesthesia with isoflurane (Abbot Abbvie Ltd; Maidenhead, UK). For induction of anaesthesia 3% isoflurane in oxygen (1500 ml/min) was used. After induction, fur was removed from the surgical area. Depth of anaesthesia was checked by loss of the foot-pinch reflex and by respiratory rate/pattern. The skull was immobilised in a stereotaxic frame using ear and incisor bars, followed by application of iodine solution to the exposed skin. Throughout the procedure, mice were monitored for correct depth of anaesthesia and maintained at 1-2% isoflurane in oxygen (1000 ml/min). A 1 cm incision was made along the midline of the cranium, exposing the skull. Holes for these injections were drilled at the at relevant co-ordinates for each brain region being targeted (Paxinos and Franklin, 1997).

Injections were made with a nanoinjector (Nanoinject II Automatic Nonolitre Injector: Drummond Scientific Company; Broomall, PA, USA). Prior to injection, the pipette was loaded with AAV, tracer or control. Where possible (when a theatre assistant was available) the operator was blinded to the injection contents to limit any potential bias relating to the surgical procedure. Stereotaxic co-ordinates, AAV or tracer construct details and injection parameters are outlined in **Table 2.1** and **Table 2.2**. Animals received intramuscular buprenorphine (0.03 mg/kg Vetergesic®: Reckitt Benckiser Healthcare; Hull, UK) for analgesia and 1 ml warm, sterile, 0.9% NaCl (for rehydration), After injection, the wound was closed with sutures (6/0 Mersilk: Ethicon Inc; New Jersey, USA) and swabbed with iodine. Animals were allowed to recover for 2-3 weeks following surgery, to enable recovery and viral transfection.

2.1.3.2 Optic fibre implantation

Optic fibre implantation, to enable *in vivo* fibre photometry, was performed immediately after AAV injection, during the same surgical procedure. An optic fibre (fibre core of 400 µm; length if 5 mm, numerical aperture (NA) of 0.66, 1.25 mmØ metal ferrule: Doric

Lenses; Quebec, Canada) was implanted unilaterally over the PVH, according to stereotaxic co-ordinates. The optic fibre was fixed externally to the skull with acrylic dental cement (Simplex Rapid Powder: Kemdent; Swindon, UK / Methyl methacrylate: Metrodent; Huddersfield, UK) and cured with ultraviolet light applied for 30 seconds. Wound closure around the optic fibre was achieved using sutures and tissue adhesive (Vetbond: 3M Animal care products; St Paul, USA). The same analgesia, hydration and recovery steps were taken.

Table 2.1: Co-ordinates and volumes for site-specific injections in brain nuclei

Site	Rostral-Caudal (mm)*	Midline-Lateral (mm)	Dorsal - Ventral (mm)	Injection Volumes
NAc	+1.5	±1.4	-4.5	3 x 9nl injection of retrograde tracer
vBNST	+0.2	±0.7	-4.7	3 x 42nl injection of AAV 3 x 9nl injection of retrograde tracer
CeA	-1.4	±2.6	-5.2	3 x 9nl injection of retrograde tracer
PVH (mpd region)	-0.8	±0.3	-5.0	3 x 49nl injection of AAV (hM4Di which was injected at 3 x 32nl) 3 x 32nl of anterograde tracer 3 x 9nl injection of retrograde tracer
aPVT	-0.5	0	-3.2	3 x 9nl injection of retrograde tracer
pPVT	-2.2	0	-3.0	3 x 27nl injection of AAV 3 x 9nl injection of retrograde tracer
rVLM	-6.7	±1.3	-6.2	3 x 9nl injection of retrograde tracer

*Co-ordinates are relative to bregma

mpd: medial parvocellular dorsal division

2.1.4 AAVs and Tracers

All AAV constructs and tracers used are outlined in **Table 2.2**. AAV are fused with either mCherry (red fluorescent protein) or eGFP (green fluorescent protein) reporters, allowing visualisation of the transduced neurons. When coupled with the Cre-lox system, the targeted injection of AAVs enables genetic access to a specific neuronal population (**Figure 2.1**). Flanking the AAV construct with a flip excision (FLEX) switch permits the Cre-dependent expression of the transgene. The FLEX system is sometimes also referred to as DIO (Double-floxed Inverse Orientation).

AAVs/tracers were aliquoted and frozen at -80°C on arrival. Fresh aliquots were de-frosted and kept on ice for each day.

Table 2.2: Summary of AAVs used in experiments

AAV		
Construct	Source	Viral Titre* (particles/µl)
hM3Dq-mCherry AAV8-hSyn-DIO-hM3D(Gq)-mCherry	Addgene (#44361) Batch: v85852	2.1 x10^{13}
hM4Di-mCherry AAV8-hSyn-DIO-hM4D(Gi)-mCherry	Addgene (#44362) Batch: v6048	1.9 x 10^{12}
Caspase AAV5-flex-taCasp3-TEVp	UNC Vector Core Batch: AV576DE	1.5 x 10^{12}
Tetanus Toxin AAVDJ-CMV-DIO-eGFP-2A-TeNT	Stanford (AAV-71) Batch: 4816	1.8 x 10^{12}
GCaMP AAV1-hSyn-FLEX-jGCaMP7s-WPRE	Addgene (104491) Batch: v93729	8.5 x 10^{12}
mCherry AAV5-hSyn-DIO-mCherry	Addgene (#50459) Batch:v61605	7.3 x 10^{12}
Anterograde Tracing: ChR2 AAV8-EF1a-DIO-hChR2(H134R)-mCherry-WPRE-HGHpA	Addgene (#20297) Batch: v13093	1.9 x 10^{13}

*Values represent the tire used in experiments. In most cases AAVs were used undiluted, however for AAVs which inhibit or lesion neurons, 1:2 or 1:3 dilution with 0.9% saline was performed before use. This limited non-specific transfection and toxic effects of a high titre. The hM4Di-mCherry virus tire was initially tested at 5.0 x10^{12} and found to produce non-specific transfection. This was improved when diluted to 1.9 x 10^{12}.

Addgene; Watertown, MA, USA
University of North Carolina (UNC) Vector Core; Chapel Hill, NC, USA
Stanford University; Stanford, CA, USA

hSyn: human synapsin promoter

TEVp: tobacco etch virus protease

CMV: cytomegalovirus promotor

WPRE: woodchuck hepatitis post-transcriptional regulatory element

HGHpA: human growth hormone polyA

EF1a: elongation factor 1-alpha 1

2.1.4.1 DREADDs

The designer receptors exclusively activated by designer drugs (DREADDs) allow targeted activation or inhibition of a specific neuronal subtype when coupled with the Cre-lox system (**Figure 2.1**). Flanking the DREADD construct with a flip excision (FLEX) switch permits the Cre-dependent expression of the DREADD. Systemic administration of CNO, the synthetic ligand for DREADDs, enables the selective control of DREADD-expressing neurons (Urban and Roth, 2015). Activation of DREADDs which contain a modified human M3 muscarinic (hM3) receptor (hM3Dq) leads to calcium release, depolarisation and neuronal firing (Urban and Roth, 2015). Whilst, activation of DREADDs which contain a modified form of the human M4 muscarinic (hM4) receptor (hM4Di), in-turn activates inwardly rectifying potassium channels, silencing neuronal firing (Armbruster et al., 2007).

2.1.4.2 Caspase

Caspases are a family of protease enzymes that are involved in programmed cell death. By using AAVs, which contain a caspase 3 construct flanked with a FLEX switch, Cre-dependent autonomous apoptosis can be achieved. This allows Cre-dependent lesioning of specific neuronal populations, whilst minimizing toxicity to adjacent non-Cre cells (Yang et al., 2013).

2.1.4.3 Tetanus Toxin

Tetanus neurotoxin (TeNT) constructs provide an approach to achieve the long-term disruption of presynaptic transmission by cleaving SNARE proteins, which are involved in neurotransmitter release (Han et al., 2017). Similarly, AAV constructs containing TeNT flanked with a FLEX switch, allow Cre-dependent transduction. Cre+ neurons will therefore be presynaptically silenced, but otherwise intact (Zingg et al., 2020).

2.1.4.4 GCaMP

GCaMP is a genetically encoded calcium indicator (GECI) which is fusion of green fluorescent protein (GFP) and calmodulin (CAM). Escalations in intracellular Ca^{2+} which precede neuronal firing, lead to enhanced fluorescence emission in neurons expressing GCaMP constructs. This emission fluorescence acts as proxy of neuronal activity and can be recorded using fibre photometry. Injecting AAVs packaged with Cre-dependent GCaMP constructs enables the activity of a defined neuronal population to be measured (Chen et al., 2013).

2.1.4.5 Reporter Virus

AAV constructs which enable Cre-dependent mCherry labelling of specific neuronal population was used for visualisation and as controls in experiments.

2.1.4.6 Anterograde tracing

Anterograde tracing studies involved the delivery of Cre-dependent AAVs packaged with constructs containing channel rhodopsin 2 (ChR2) fused with a fluorescent reporter protein (e.g., mCherry). ChR2 is a membrane-bound ion channel which is incorporated into the whole cell membrane, enabling tracing of neuronal fibres, including axonal projections (Atasoy et al., 2008).

2.1.4.7 Retrograde tracing with Fluoro-Gold

Hydroxystilbamidine (Fluoro-Gold™) is a fluorescent, inorganic compound which is taken up by nerve terminals and retrogradely transported to cell bodies in vesicles, accumulating in the cytoplasm and labelling neurons in a reliable and long-lasting manner (Saleeba et al., 2019). Fluoro-Gold was reconstituted in distilled water and a 4% solution injected.

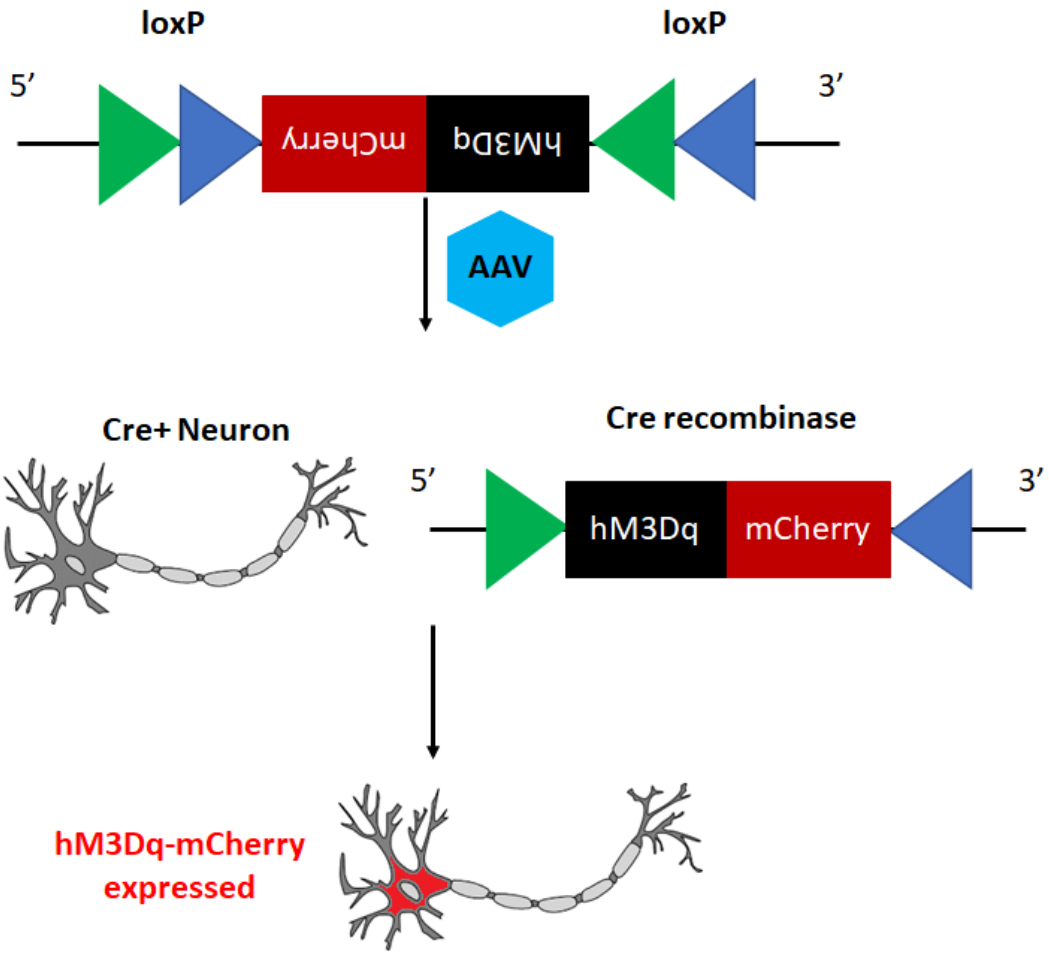

Figure 2.1: The Cre-lox system and control of site-specific recombination

The Cre-lox system enables cell-specific expression of proteins, allowing control and manipulation of cellular function. AAVs are engineered to contain an artificial protein construct (e.g., hM3Dq-mCherry) within its genome. In this example, the DNA sequence of the hM3Dq-mCherry construct is inserted in the viral genome in the incorrect orientation and flanked by two loxP sites in opposing orientations. LoxP sites are the site of action of the enzyme Cre-recombinase. Injection of the AAV into the brain leads to transduction of cells in the vicinity. However, in cells containing Cre-recombinase (achieved by using Cre-driver lines), the hM3Dq-mCherry construct is inverted into the correct orientation, enabling transcription.

2.1.5 Insulin-induced hypoglycaemia

All animals were handled daily for two weeks prior to the start of experiments. Prior to receiving insulin, animals were fasted for 3 hours to minimise baseline glucose variability. Blood glucose levels were measured via tail-tip sampling (Accuchek Glucose Meter: Roche Diagnostics Ltd; Burgess Hill, UK). After the baseline blood glucose was measured, insulin (1.75U/kg, s.c.) was injected and blood glucose levels were measured every 30 minutes, for 120 minutes. At each time point, two blood glucose readings were taken. A third reading was taken where measurements were >10% apart. After the final measurement at 120 minutes, food was returned.

2.1.5.1 Repeated hypoglycaemia

The repeated hypoglycaemia protocol will be discussed in detail in Chapter 3. Briefly, the same protocol was used as above for each episode of insulin-induced hypoglycaemia. Hypoglycaemia episodes occurred three times a week for four weeks (total of 12 episodes). In most experiments, saline and SH groups were included and received s.c. volume-matched 0.9% NaCl. On the final day, insulin (RH and SH groups) or volume-matched saline (saline group) was administered, and blood sampled for counter-regulatory hormone measurement.

2.1.6 Blood sampling

In general, baseline (pre-stimulus) and 30-minute blood samples were collected. This was performed tail-tip sampling. Following clipping of the tail-tip, the tail was gently massaged to stimulate blood flow, and 80-100 µl of blood was collected in a glass capillary tube, prior to transfer to 1.5ml Eppendorf tube. Blood samples were centrifuged at 10,000 rpm for 20 minutes at 4^{o}C to spin out blood cells. Subsequently, 40 µl of the plasma fraction was transferred to Eppendorf tubes containing 10µl of 1mM ethylenediaminetetraacetic acid (EDTA: Sigma-Aldrich) and 5 µl sodium metabisulphite (Sigma-Aldrich). This was to prevent catecholamine degradation. Samples were immediately frozen on dry ice and transferred to the -80^{o}C freezer for storage.

2.1.7 Tissue Fixation

Animals were deeply anaesthetised using 4% isoflurane in oxygen (1500ml/min) until the reflex response to a toe pinch stimulus was absent. The heart was exposed and a butterfly needle connected to the perfusion pump was inserted into the left ventricle. The right atrium was cut to enable outflow of blood and an isotonic solution containing heparinised saline (10,000 units/l heparin in 0.9% NaCl: Fisher Scientific; Loughborough, UK) was perfused using a peristaltic pump set to a flow rate between 10-15ml/min. The tissues were then fixed *in situ* by switching the solution to 4% paraformaldehyde (PFA: Sigma-Aldrich) in 0.1M phosphate buffer (PB; 95mM Na2HPO4 and 24mM NaH2PO4 in distilled water; both sourced from Sigma-Aldrich) until full contraction of limbs had occurred, from which point perfusion was carried out for a further 5 minutes. Brains were dissected and post fixed overnight in 4% PFA in 0.1M PB, then placed in 30% sucrose/0.1M PB solution (Fisher Scientific) at 4°C to dehydrate the tissue. Brains were then frozen on dry ice and stored at -80°C prior to cutting.

2.2 *Ex vivo* methods

2.2.1 Sectioning of frozen tissue

Fixed and frozen brains were cut into 30 µm coronal sections on a freezing, sledge microtome (Series 8000: Bright Instruments Ltd; Luton, UK). Sections were divided into four sets meaning each set contained a section every 120 µm and placed into a cryoprotectant solution (20% glycerol (Fisher Scientific), 30% ethylene glycol (Sigma-Aldrich), 23mM Na_2HPO_4 and 3mM NaH_2PO_4 in distilled water) enabling long-term storage at -20°C.

2.2.2 Immunohistochemistry (IHC)

All IHC was performed by following a general protocol, with relevant antibodies (**Table 2.3**) used depending on the cellular visualisation required. In all protocols, sections were first washed thoroughly in PB-T (0.2% v/v Triton X-100 (Sigma-Aldrich) in 0.1M PB). All washing and incubation steps involved gentle agitation of multi-well plates containing free-floating brain sections.

For protocols with peroxidase amplification, sections were then incubated in a peroxidase blocking solution (20% v/v methanol (Fisher Scientific) and 1.5% v/v hydrogen peroxide (Sigma-Aldrich) in 0.1M PB-T), which inhibits endogenous peroxidase activity.

Sections were then incubated in a blocking buffer composed of 10% normal serum in PB-T. The serum used for each IHC protocol was from the same species that the secondary antibody was derived in to reduce non-specific staining. Sections were then incubated overnight at 4°C in the relevant primary antibody in a solution of 1% normal serum in PB-T.

The following day, sections were washed thoroughly in 0.1M PB. They were then incubated for two hours at room temperature in the appropriate secondary antibody in a solution with 5% normal serum in 0.1M PB. In most experiments a fluorophore-linked secondary antibody was used to enable strong fluorescent labelling of cells. After a final set of washes in 0.1M PB and distilled water, sections were mounted onto slides and left overnight to dry.

Prior to imaging, a mountant, such as Prolong Gold (Invitrogen; Carlsbad, CA, USA) was applied and a coverslip placed over the slide. In all studies, involving the visualisation and quantification of CRH- or VGlut2-positive cells, a chicken anti-GFP antibody, which also binds to eYFP was used.

2.2.2.1 Streptavidin-based IHC

Streptavidin-biotin signalling was used to amplify a weak IHC signal. This was used to enhance the signal of neuronal cFos. The same steps were performed on the first day of the protocol as above. At the secondary antibody step, sections were instead incubated for two hours in a biotinylated secondary antibody. Sections were then washed thoroughly in 0.1M PB. This was followed by a final one-hour incubation at room temperature in a streptavidin-conjugated fluorophore-linked antibody in 0.1M PB (**Table 2.3**). Sections were then washed and mounted as above.

2.2.2.2 Peroxidase-based diaminobenzidine (DAB) IHC

This method was used where further amplification of the signal was required, for example with the FosB antibody. The same steps were performed on the first day of the protocol as above. At the secondary antibody step, sections were incubated for two hours in a biotinylated secondary antibody. Sections were then washed thoroughly in 0.1M PB. They were then incubated for one hour in a solution containing streptavidin-conjugated horseradish peroxidase (HRP) (GE Healthcare; Little Chalfont, UK) in 0.1M PB. Sections were then washed thoroughly in 0.1M PB. Next the sections were incubated in a diaminobenzidine (DAB) solution (Vector Laboratories; Peterborough, UK). Where nuclear staining was desired (e.g., FosB) nickel was added to the DAB solution, to give black staining. The reaction was constantly visualised to determine the strength of the

staining. When the desired strength of labelling was achieved, the reaction was ended by washing in 0.1M PB and then distilled water. Sections were then mounted with DPX (Fisher Scientific), a xylene-based mountant.

Where dual staining with DAB was required, to give nuclear and cytoplasmic staining, nuclear staining with a DAB-nickel solution was performed first. Sections were then incubated with a different primary antibody and biotinylated secondary antibody, following the same steps as above. Sections were again incubated in a streptavidin-conjugated HRP solution and then washed thoroughly in 0.1M PB. Next, sections were incubated in a DAB solution without nickel, which produces brown staining. The reaction was again ended by washing in 0.1M PB and then distilled water. Sections were then mounted as above.

Table 2.3: Antibodies used for IHC

Primary antibodies		
Antibody	**Origin**	**Concentration**
Guinea Pig anti-AVP	T-5048 (PenLabs)	1:1000
Rabbit anti-c-Fos	ab10839 (AbCam)	1:1000
Rabbit anti-FosB	SC 7203 (Santa Cruz)	1:500
Goat anti-ChAT	AB144P (Millipore)	1:1000
Goat anti-CHR1	ab59023 (AbCam)	1:250
Rabbit anti-dsRed	632496 Clontech	1:2500
Goat anti-dsRed	33353 Sata cruz	1:1000
Chicken anit-GFP	13970 (Cell Signalling)	1:1000
Guinea pig anti-Oxytocin	AB1542 (Millipore)	1:1000
Sheep anti-TH	AB1542 (Millipore)	1:1000
Secondary Antibodies		
Donkey anti-chicken^{ALEXA488}	703-545-155 (Jackson)	1:1000
Donkey anti-rabbit^{ALEXA594}	711-585-132 (Jackson	1:1000
Donkey anti-goat^{ALEXA594}	705-585-147 (Jackson)	1:1000
Donkey anti-sheep^{ALEXA594}	A11016 (Invitrogen)	1:1000
Donkey anti-sheep^{ALEXA488}	A11015 (Invitrogen)	1:1000
Goat anti-guinea pig^{ALEXA594}	A11076 (Invitrogen)	1:1000
Donkey anti-rabbit^{BIOTIN}	711-065-152 (Jackson)	1:1000
Streptavidin^{ALEXA594}	016-580-084 (Jackson)	1:1000
Streptavidin^{ALEXA488}	016-540-084 (Jackson)	1:1000
Streptavidin^{AMCA350}	016-150-084 (Jackson)	1:1000

Clontech; Mountain View, CA, USA
Invitrogen; Carlsbad, CA USA
Jackson ImmunoResearch Inc; West Grove, PA, USA
PenLabs; Shanghai, China
Santa Cruz Biotechnology; Heidelberg, Germany

2.2.2.3 Microscopy and image acquisition

Fluorescence microscopy was carried on a Zeiss Axioimager.D2 upright microscope (Zeiss; Oberkochen, Genmany) using a 5x / 10x / 20x EC Plan-neofluar objective and captured using a Coolsnap HQ2 camera (Photometrics; Tucson, AZ, USA) through Micromanager software v1.4.23. Specific band pass filter sets for DAPI, FITC and Texas Red were used to prevent bleed through from one channel to the next. Where better z-axis resolution was required, microscopy was also performed using a Leica TCS SP8 AOBS inverted confocal (Leica; Wetzlar, Germany) using a 20x / 40x Plan Fluotar objective. Images were collected using hybrid detectors configured for DAPI, FITC and Texas Red, using a laser set at 10% power. Images for sections labelled with DAB were acquired using a Olympus BX63 upright microscope (Olympus; Southend-on-Sea, UK) using a 20x / 0.75 UApo/340 objective) and captured and white-balanced using an DP80 camera through CellSens Dimension v1.16. Standardised settings for image capture for all sections in a specific experiment were used. Images were processed and analysed using Fiji/ImageJ *(*https://fiji.sc/).

2.2.2.4 Quantification of labelled neurons

Quantification of labelled neurons was carried out manually in captured images using a manual cell counter plug-in within Fiji/ImageJ. Anatomical boundaries of specific brain regions were established with close co-ordination with the mouse brain atlas (Paxinos and Franklin, 1997). Neurons within a brain region were only counted if a clear contrast between the labelled cell body and the background tissue could be identified. Neurons which met this criterion were manually selected and a coloured number overlayed preventing duplication of neurons in counts. For multi-channel images, labelled neurons were manually selected across each channel using different coloured number overlays. Neurons which were manually selected across all channels, were identified by the overlap of coloured number overlays, indicating dual- or triple-labelling. All counts were performed by me, except for Chapter 3, where I was assisted by Dr Alessia Costa. However, an identical manual quantification method was used by Dr Costa. All investigators were blinded to the treatment groups until all counts had been performed for each experiment.

2.2.3 Genotyping

Ear punches were collected from transgenic mice to determine the genotype. Genotyping was carried out in-house for all Ce-recombinase lines. The *Gad2*-GFP mice were genotyped by Transnetyx (automated genotyping service; Cordova, TN, USA) and GFP-positive mice donated by the D'Agostino Lab for experiments.

2.2.3.1 DNA Extraction

Ear punches were incubated at 95°C in a lysis buffer solution (0.25% v/v 10M NaOH, 0.04% v/v 0.5M EDTA, in distilled water) for 45 minutes, cooled on ice, then neutralised with 0.63% w/v Trizma hydrochloride (Sigma-Aldrich), in distilled water.

2.2.3.2 PCR

Polymerase chain reaction (PCR) was used to amplify target alleles (Cre) using specific primers (**Table 2.4**). The PCR reaction mixtures used are outlined in **Table 2.5**, but all contained standard master mix components (5x buffer, distilled water, MgCl2, dNTPs, GoTaq Hot Start Polymerase (all Promega; Madison, WI, USA) along with the relevant primers and were prepared on ice. Master mix of 22.5µl was combined with 2.5µl DNA and mixed in individual PCR tubes. PCR reactions were performed using a AB Veriti 96 Well Thermal Cycler (Applied Biosystems, Life Technologies; CA, USA). The Cre PCR parameters are shown in **Table 2.6**.

2.2.3.3 Gel electrophoresis

A 1.5% agarose (Bioline; London, UK) gel was melted in 1x tris-acetate-EDTA (TAE) buffer (24.2% w/v Trizma hydrochloride, 5.71% v/v glacial acetic acid, 1% v/v 0.5M EDTA, in distilled water) by warming to 60 C in a microwave and 0.005% SYBR safe stain (Invitrogen, Carlsbad, CA USA) added to visualise bands. PCR product and Hyperladder IV marker (Bioline) was loaded and gels were run in 1x TAE buffer at 70V for 45 minutes. Bands were visualised using a UV transilluminator.

Table 2.4: PCR primers for Cre genotyping

PCR Reaction	Primer	Sequence	Band Size
Cre*	Control F	GGT CAG CCT AAT TAG CTC TGT	650 bp
	Control R	GAT CTC CAG CTC CTC CTC TGT C	
	Target F	GCC CTG GAA GGG ATT TTT GAA GCA	259 bp
	Target R	ATG GCT AAT CGC CAT CTT CCA GCA	

*All Cre-recombinase lines were genotyped using the same protocol. Cre-positive mice were identified by presence of control and target bands.

Table 2.5: Genotyping PCR master mix

Reagent	Cre*
5x buffer	5µl
$MgCl_2$	2µl
dNTPs	0.5µl
GoTaq	0.125µl
H20	12.37µl
Primers	Target F & R: 0.75µl each Control F & R: 0.5µl each
DNA	2.5µl

*All Cre-recombinase lines were genotyped using the same protocol.

Table 2.6: Genotyping PCR cycling parameters

Cycling step	Cre*	
Polymerase activation	95°C, 2mins	
Denaturation	95°C, 30s	32 x
Annealing	62°C, 60s	
Extension	72°C, 60s	
Final extension	72°C, 5mins	
Hold	4°C	

*All Cre-recombinase lines were genotyped using the same protocol.

2.3 Enzyme-linked immunosorbent assay (ELISA)

Adrenaline (DEE5100: Demeditec Diagnostics GmbH; Kiel, Germany), glucagon (10-1281-01: Mercodia; Uppsala, Sweden) and corticosterone (ADI-900-097: Enzo Life Sciences; Exeter, UK) ELISA kits were used to measure plasma hormone levels. For most of the experiments in this thesis, a single hormone was measured due to limits on the minimum ELISA kit sample volume (10 µl), unless otherwise specified. ELISAs were performed by me in all experiments, except for the pilot studies in Chapter 3, which were performed by Dr Tansi Khodai. Investigators were blinded to treatment groups until the ELISA had been performed.

Samples were first defrosted and allowed to reach room temperature. Standards, controls and samples were then loaded in duplicates (10µl per well) onto the microtiter plate. The protocol for each assay is outlined below.

In all three assays, the microtiter plate was read using 405nm light by a microplate reader (Biotek Synergy HT; NorthStar Scientific, Leeds, UK). Sample concentrations were determined by comparing optical density/absorbance values with a standard curve prepared with known standard concentrations.

2.3.1 Adrenaline

The Demeditec adrenaline kit is a competitive ELISA which measures the concentration of an antigen by detection of signal interference. First, standards, controls and samples were pipetted into wells in a microtiter plate. They then underwent extraction, acylation and enzymatic conversion steps. Standards, control and samples were then incubated in adrenaline antiserum, which contained rabbit anti-adrenaline antibody. A further wash was performed to remove free antigen and free antigen-antibody complexes. This was followed by an incubation with an anti-rabbit IgG-peroxidase conjugate. A further wash step was then performed. This was followed by incubation with 3,3',5,5'-tetramethylbenzidine (TMB) as a substrate. This enabled the antibody bound to the pre-coated reference antigen to be detected. The reaction was stopped at the specified timepoint with a stop solution and the optical density of the microtiter plate was read.

2.3.2 Glucagon

The Mercodia glucagon ELISA kit is based on the direct sandwich technique, in which two monoclonal antibodies are directed against separate epitopes on the glucagon molecule. Standards, control and samples were pipetted into wells in a microtiter plate. This was followed by an incubation step with an enzyme conjugate solution which contained peroxidase-conjugated anti-glucagon antibodies. During incubation, glucagon in the sample reacts with the peroxidase-conjugated anti-glucagon antibodies and anti-glucagon antibodies bound to the microplate wells. A subsequent washing step removed unbound enzyme-labelled antibody. The bound conjugate was detected with the addition of a TMB substrate. The reaction was stopped at a specified time point with a stop solution and the optical density of the microtiter plate was read.

2.3.3 Corticosterone

The Enzo life corticosterone ELISA uses the competitive assay technique. Samples were first diluted (1:40) in a steroid displacement reagent solution, which contained PBS and ELISA buffer (provided in-kit). Standards, control and samples were then pipetted into wells in a microtiter plate and then incubated simultaneously with solutions containing sheep polyclonal antibody to corticosterone and alkaline phosphatase conjugated to corticosterone. This was followed by a wash step to remove excess reagents. The next step involved incubation with a substrate containing p-nitrophenyl phosphate, which detects alkaline phosphatase. The enzyme reaction was stopped at a specified time point with a stop solution and the optical density of the microtiter plate was read

2.4 Statistical analysis

All graphs and statistical analysis were performed using GraphPad Prism (version 9.2.0: GraphPad Software, Inc; La Jolla, CA, USA). Data is presented as mean ± standard error of the mean (SEM). The statistical tests that were used will be stated for each dataset.

2.4.1 Area under the curve (AUC)

The AUC was calculated in GraphPad Prism to provide a means of measuring cumulative glucose excursions during hypoglycaemia (Chapter 3) and the calcium dynamics within CRH^{PVH} neurons (Chapter 4). Within Prism, a fitted curve is identified as a series of connected XY data points. Prism then computes the AUC using the trapezoidal method, where the area of the trapezoid under each connecting series of XY points is converted to an equivalent rectangle. The AUC being the sum of areas of all the rectangles. AUC calculations were performed on complete datasets, as missing values have a significant impact on calculations.

Chapter 3

Characterising a mouse model of IAH

3.1 Introduction

3.1.1 Modelling IAH using experimental RH

An important hallmark of IAH is the presence of an impaired hypoglycaemia CRR following RH, a finding which was first demonstrated in the absence of diabetes and then confirmed in patients with type 1 diabetes (Heller and Cryer, 1991, Dagogo-Jack et al., 1993). This principle has been employed to good effect by many investigators over the preceding three decades, leading to a large variety of IAH disease models, and important mechanistic insights (Sankar et al., 2020, McNeilly and McCrimmon, 2018). In animals, studies have mainly measured RH-induced impairments to the sympathoadrenal or glucagon response, as a surrogate for IAH. However, in a smaller number of studies, behavioural responses, focusing on RH-related food intake, or conditioned placed preference/avoidance have been employed (Otlivanchik et al., 2016, Sanders et al., 2006). Both approaches have merits and aim to model different, but equally important arms of the hypoglycaemia CRR. Therefore, questions remain on how best to model IAH in animals. Added to these questions are the common challenges faced when disease models are developed or translated across species (Sankar et al., 2020). Yet, there are many advantages in trying to achieve a successful animal model of IAH. Principally, the use of transgenic animal strains, particularly murine Cre-recombinase lines, enables powerful routes of enquiry into disease mechanisms. Therefore, characterising a robust disease model for IAH, which can take advantage of transgenic mouse lines, is an important goal of this doctoral research.

3.1.2 Developing an IAH model

Our lab has focused on developing a IAH model in mice which uses experimental RH and demonstrates impairments to counter-regulatory hormone release to subsequent hypoglycaemia. These investigations had begun prior to my doctoral thesis and involved the testing of 5-day, and 2-day experimental RH protocols. These experiments were led by Dr Tansi Khodai, with assistance from Dr Nic Nunn. I assisted in investigating the 2-day RH protocol. To give some context to the development of our mouse model of IAH, I have included these initial investigations in this section. They will be briefly outlined and discussed in this section. These data are provided with the permission of Dr Khodai and Dr Nunn and are unpublished.

5-day experimental RH protocol

A 5-day experimental RH protocol was adapted from methods published in rats (Chan et al., 2013, Orban et al., 2015, Osundiji et al., 2011). Male C57Bl/6J mice (n = 6 per group) were randomised to saline, SH or RH groups. RH mice received once daily s.c. insulin

(1.75 U/kg) for 4 days, whilst saline and SH groups received volume matched s.c. saline. On the day 5 (test day), SH and RH groups also received an injection of insulin and saline animals a final injection of saline. In addition, corticosterone and glucagon levels were measured at baseline (0 min) and 30 min after injection, via saphenous vein sampling. We aimed to perform blood glucose sampling for 120 mins following every injection. However, on day 2, 2 animals in the RH and SH group, respectively, demonstrated significant stress behaviours (e.g., jumping, biting, aggression) necessitating termination of glucose measurements at 90 min. These animals were still included in the experiment, as the overall aim was to assess hormone responses to subsequent insulin or saline injection on the final day. As a result, blood glucose profiles are shown for 90 min after injection in **Figure 3.1B-C**. On the test day, one animal in the SH group was mis-injected and did not display a reduction in blood glucose level at 30 min, therefore this animal was excluded from subsequent analyses. The protocol, glucose and counter-regulatory hormone results are summarised in **Figure 3.1**.

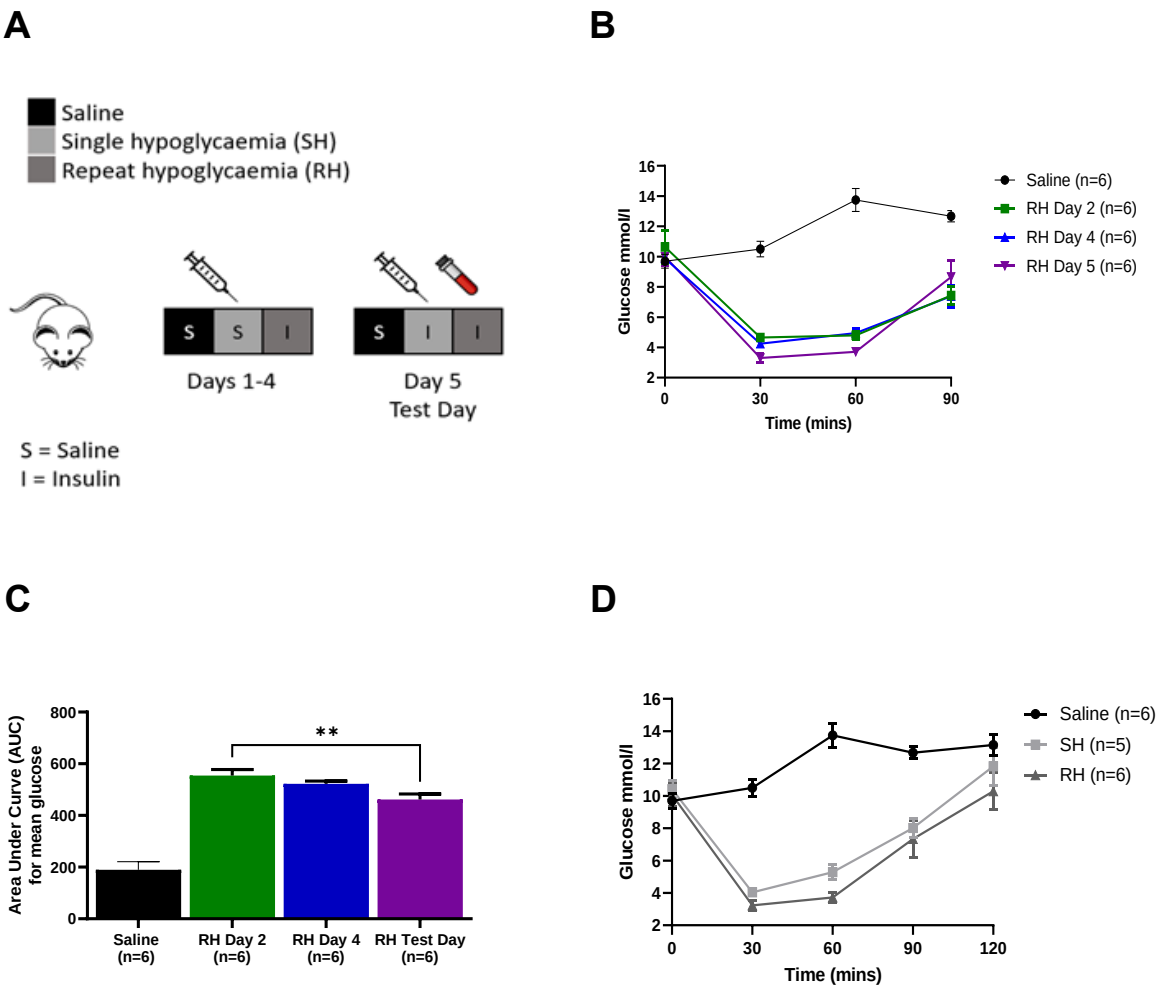

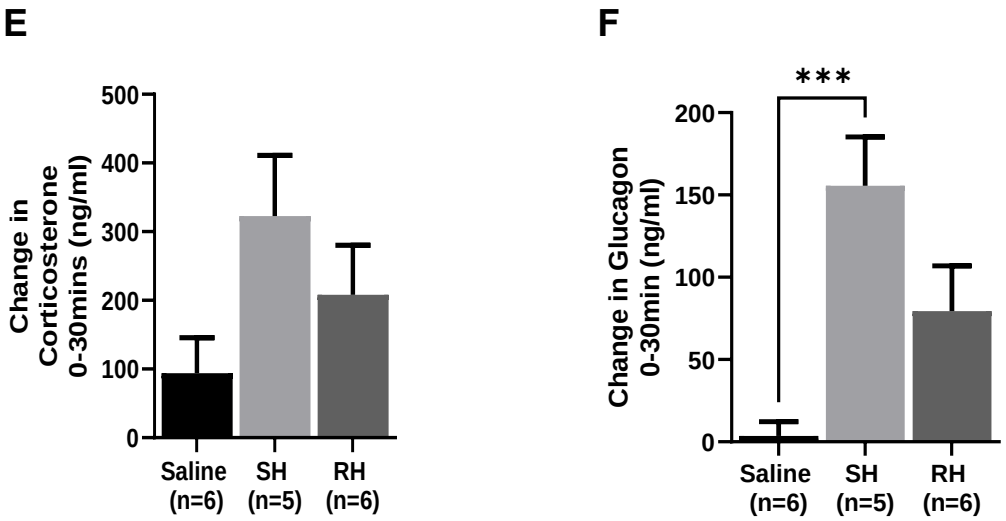

Figure 3.1: Glucose and counter-regulatory hormone responses following a 5-Day RH protocol

A: Study protocol**.**
B: Mean blood glucose profile for the 90 min following injection, in RH exposed mice (days 2,4,5) and saline mice (day 5).
C: Area under the curve (AUC) of glucose levels for RH mice (days 2, 4, 5) and saline mice (day 5). AUC was significantly decreased in RH mice by day 5, when compared with day 2 (**p<0.01; repeated measures two-way ANOVA with Dunnett's *post hoc* tests).
D: Mean glucose profile for the 120 min following injection on day 5 (test day).
E: Change in corticosterone release (0-30 min) following injection in saline, SH and RH mice on day 5.
F: Change in glucagon release (0-30 min) following injection in saline, SH and RH mice on day 5, showing a significant increase in glucagon release with SH, when compared with saline (*** p<0.001; one-way ANOVA with Tukey's *post hoc* test), but no significant difference when compared with RH.
Data presented as mean ± SEM. n=5/6 per group.

In this experiment, RH over 5 days led to a progressive change in the glucose profile (**Figure 3.1B**). This corresponded with a significant reduction in AUC on day 5, when compared with day 1 (**Figure 3.1C**), which suggests a delay in hypoglycaemia recovery. On day 5, despite receiving the same insulin dose, RH mice reached a lower glucose nadir when compared with SH mice (3.2 ± 0.8 versus 4.0 ± 0.2 mmol/l; **Figure 3.1D**). Despite this, corticosterone and glucagon release following insulin injection, was not significantly reduced in RH mice, versus SH mice (**Figure 3.1E-F**). At this stage, the adrenaline assay had not yet been optimised, so this could not be measured.

In conclusion, in our hands, a 5-day RH protocol demonstrated progressive reductions in glucose nadir (30mins post-injection) and hypoglycaemia recovery. However, RH failed to attenuate significantly measured corticosterone or glucagon responses to subsequent hypoglycaemia. It is possible that the adrenaline response may have provided a more sensitive measure, however this was not available.

2-day experimental RH protocol

Several short RH protocols, over 1-2 days, have enabled investigators to model IAH in humans and rodents (Dagogo-Jack et al., 1993, Al-Noori et al., 2008b, Sanders et al., 2006, Figlewicz et al., 2002, Evans et al., 2001). Therefore, we also tested a 2-day experimental RH protocol. Male C57Bl/6J mice (n = 5-6 per group) were randomised to receive saline, SH or RH. RH mice received two s.c. insulin (1.75U/kg) injections on day 1 and in parallel, saline and SH groups received volume matched s.c. saline. On day 1 blood glucose levels were only checked at baseline and 30 min after injection to limit blood sampling related stress. On the test day (day 2), SH and RH groups received a final injection of insulin and saline animals a final injection of saline. On day 2, adrenaline, corticosterone and glucagon levels were measured at baseline (0 min) and at 30 min after injection, via saphenous vein sampling. A full glucose profile was only conducted on day 2, to limit stress. Blood glucose sampling was terminated at 90 min as 2 animals in the saline group and 1 animal in the SH group were displaying significant stress behaviours (e.g., jumping, biting, aggression). These animals were still included in this experiment as hormone measurements were taken at earlier timepoints, prior to the onset of stress behaviours. The protocol, glucose profile and hormone results are summarised in **Figure 3.2**.

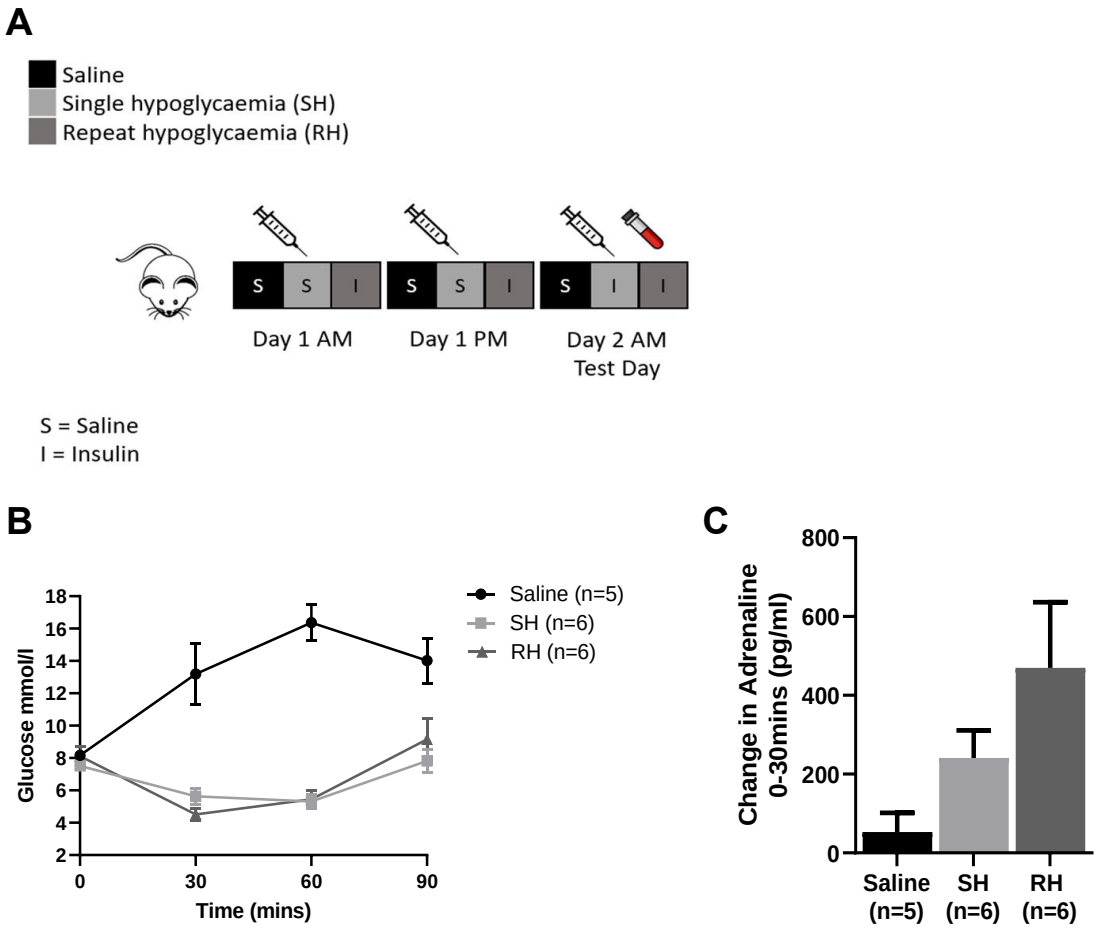

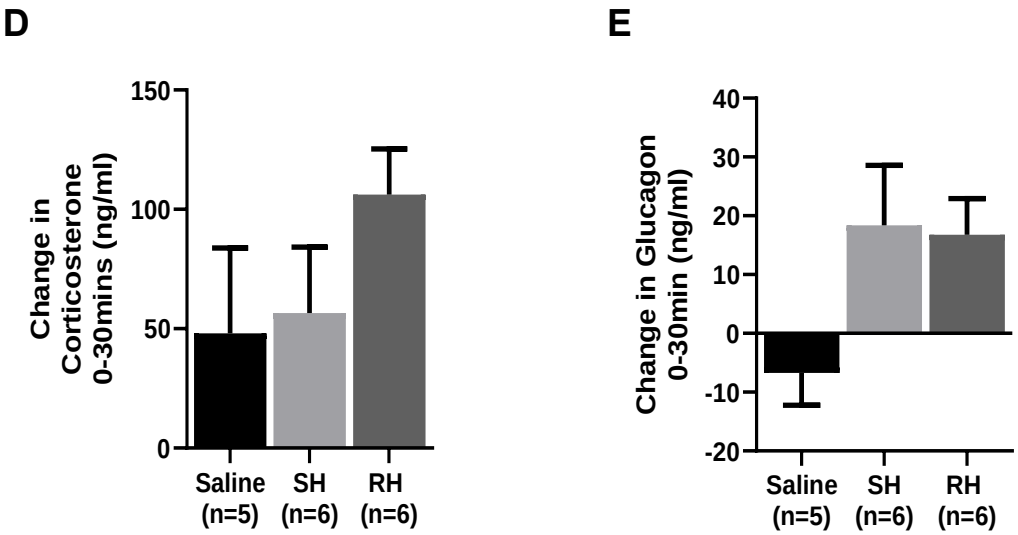

Figure 3.2: Glucose and counter-regulatory hormone responses following a 2-day RH protocol

A: Study protocol**.**
B: Mean blood glucose profile for the 90 min following injection, in saline, SH and RH mice on day 2 (test day).
C: Change in adrenaline release (0-30 min) following injection in saline, SH and RH mice on day 2.
D: Change in corticosterone release (0-30 min) following injection in saline, SH and RH groups on day 2.
E: Change in glucagon release (0-30 min) following injection in saline, SH and RH groups on day 2.
Data presented as mean ± SEM. n=5/6 per group.

In this experiment, RH on day 1 (two episodes) was followed by measurement of counter-regulatory hormones to a subsequent episode of hypoglycaemia on day 2. Measurements were only taken on day 2 and were heavily affected by animal stress. On day 2, RH mice reached a lower glucose nadir (30 min after injection) when compared with SH mice (4.3 ± 0.9 versus 5.3 ± 0.9 mmol/l; **Figure 3.2B**). However, all mice receiving SH and two mice receiving RH did not reach the glucose (hypoglycaemia) threshold which is normally required for counter-regulatory hormone release (<3.9 mmol/l). As a result, hormone levels on day 2 were difficult to interpret. Following injection on day 2, there was a non-significant trend towards increased adrenaline and corticosterone levels in RH mice, when compared with SH mice (**Figure 3.2C-D**). Glucagon release was very variable within groups. The mean change in glucagon was similar for SH and RH mice and not statistically different when compared with saline mice (**Figure 3.2E**).

One interpretation of these data is that animal stress was the major driver for hormone release in this experiment. Blood glucose levels climbed steeply following injection in the saline group, suggesting that s.c. injection, coupled with blood sampling, were significant stressors (**Figure 3.2B**). SH mice did not reach the necessary glucose (hypoglycaemia)

threshold for counter-regulatory hormone release; however, some RH mice did. This finding, combined with injection and blood sampling stress, may explain the trend towards elevated adrenaline and corticosterone in the RH group. Therefore, a firm conclusion relating to a 2-day RH protocol is not possible from these data. However, it may be that in mice, short RH protocols do not enable sufficient time for habituation to animal handling, injection and blood sampling stress. This poses a challenge when trying to isolate hypoglycaemia-specific changes in counter-regulatory hormone release.

3.1.3 Investigation of neuronal activity using a 4-week RH protocol

Rodent and, increasingly, transgenic mouse models have provided a valuable insight into functions of the central glucose-regulatory network, and adaptations which follow RH. A common approach has been to use neuronal activity markers, to quantify neuronal responses to acute and repeated stressors, such as SH and RH (Sanders and Ritter, 2000, Al-Noori et al., 2008b, Paranjape and Briski, 2005). These markers include early (cFos) and late (FosB) regulatory transcription factors, whose induction convey the kinetics of neuronal activity (Morgan and Curran, 1991). Importantly, these activity markers can be related to changes in effector function following chemogenetic or optogenetic manipulations, e.g., adrenal adrenaline release, hepatic glucose production and behaviours (Sanders et al., 2006, Meek et al., 2016, Khodai et al., 2018, Zhao et al., 2017). The normal pattern of neuronal cFos induction to SH or acute glucoprivation with 2-DG is highly reproducible (Sanders and Ritter, 2000). Only a small number of studies have examined the expression of neuronal FosB, following SH and RH (Al-Noori et al., 2008b, Paranjape and Briski, 2005, Sanders and Ritter, 2000, Bayne et al., 2020). Interestingly, these studies suggest that RH alters the expression of activity markers to subsequent hypoglycaemia or 2-DG, in specific neuronal populations, including within the PVH. The PVH, which displays high levels of neuronal cFos following SH, is heterogenous and contains important pre-motor glucose-regulatory elements (Evans et al., 2001, Watts and Donovan, 2010). In rats, RH attenuates PVH neuronal cFos, but increases FosB to subsequent hypoglycaemia (Al-Noori et al., 2008b). Interestingly, PVH FosB was only expressed in CRH neurons (Al-Noori et al., 2008b). Despite these important insights, the pattern of neuronal cFos and FosB induction following RH, has not been characterised in mice. Transgenic Cre-reporter strains provide a useful tool with which we can characterise cFos an FosB expression, in specific populations, including CRH^{PVH} neurons. This approach provided a basis for subsequent studies to manipulate specific neuronal populations and demonstrate their involvement in the CRR.

3.1.4 Objectives

1) Characterise a mouse model of IAH using experimental RH

The ability to model IAH relies on several factors; principally the experimental RH protocol used. Our experience with shorter (2- and 5-day) experimental RH protocols proved inconclusive but highlighted the importance of mitigating other sources of stress. We also postulated that increasing the number of episodes of RH, may improve our ability to successfully model IAH. To this end, we investigated a 4-week experimental RH protocol which was adapted from studies in rats (McNeilly et al., 2017). This protocol focused on demonstrating impairments to the sympathoadrenal response to provide an experimental model of IAH. This was achieved by measuring impairments to circulating adrenaline levels following RH.

2) Identify the responsiveness of specific central neuronal populations to SH and RH

Although, previous work in rats has identified neuronal populations which display altered makers of neuronal activity after RH, this has not been characterised in mice. By using our experimental RH protocol, which is outlined in the first section of this Chapter, we investigated the pattern of cFos and FosB in identifiable brain regions.

3) Characterise the anatomical distribution and identity of hypoglycaemia responsive PVH neurons

The PVH is an important glucose-regulatory region, which has a complex structure and displays a high level of neuronal activity following SH. However, the exact location and phenotypic identity of hypoglycaemia-responsive PVH neurons remains unclear. We elected to address these questions, by investigating the anatomical distribution and neuropeptide identity of hypoglycaemia-responsive PVH neurons, by measuring cFos expression.

4) Characterise the neuro-anatomical distribution of hypoglycaemia responsive CRH^{PVH} neurons

CRH neurons, represent an important stress-responsive neuronal population and in rats, occupy a distinct sub-region within the PVH (Aguilera and Liu, 2012). However, the distribution of hypoglycaemia-responsive CRH^{PVH} neurons remains poorly characterised in mice. To this end, we investigated the anatomical distribution of hypoglycaemia-responsive CRH^{PVH} neurons.

5) **Characterise the response of CRH^{PVH} neurons to both SH and RH using markers of acute and chronic neuronal activity**

In rats, PVH neurons display altered cFos and FosB induction to repeated stressors, including RH (Al-Noori et al., 2008b). It is not known whether this shift in neuronal marker expression is also exhibited in the mouse PVH, or if this pattern is specific to CRH^{PVH} neurons.

3.2 Methods

3.2.1 Animals

Adult, male mice aged 8-10 weeks old were used in experiments described in this Chapter. C57BL/6J mice (Charles River, UK), used to characterise the mouse model of IAH, were handled daily for 2 weeks and underwent experimental RH. Animals were then randomised to saline, SH or RH groups (n = 6 per group). No animals were excluded from the final analysis.

Data from pilot studies outlined in this Chapter were used in a power analysis to inform group sizes in the characterisation of a mouse model of IAH. This was based on performing a grouped analysis, where the treatment difference would be analysed using a one-way ANOVA with Tukey's *post hoc* (alpha = 0.05). A moderate effect size (0.50) indicated that an n = 5 per group was required to achieve a power of 80%.

The 4-week experimental RH protocol used to model IAH is described in Chapter 2 and pictorially in **Figure 3.3A**. Blood glucose measurement, blood sampling and hormone measurement methods are also outlined in the Chapter 2.

Crh-cre::eYFP (Chapter 2) aged 8-10 weeks old (n = 6 per group) were used for all studies in this chapter which investigated cFos and FosB expression in specific brain regions.

Adult male *VGlut2*-cre::eYFP (Chapter 2) were used to enable dual-label immunohistochemistry to identify *VGlut2*-cre::eYFP neurons alongside cFos. This line was only used to identify the proportion of SH-activated PVT neurons which were *VGlut2*-cre::eYFP positive.

3.2.2 Investigating cFos and FosB expression following RH

Crh-cre::eYFP mice were handled daily for 2 weeks before the 4-week RH protocol. Two hours after the final injection with s.c. insulin (SH and RH groups) or s.c. saline (saline groups), animals were perfused with fixative, enabling tissue fixation at peak cFos protein

expression. Immunohistochemistry methods are outlined in greater detail in Chapter 2. Briefly, visualisation of cFos or FosB was achieved using single-label immunohistochemistry and either fluorescent or peroxidase-dependent substrates. Dual-label immunohistochemistry was used in *Crh*-cre::eYFP (or *VGlut2*-cre::eYFP neurons in the PVT) mouse brain sections, using the anti-green fluorescent protein (GFP) antibody, with either anti-cFos or anti-FosB antibodies. To aid with the investigation of specific hypoglycaemia-responsive neuronal populations, relevant brain sections also were dual-labelled for either tyrosine hydroxylase (TH), oxytocin (OXT) or arginine vasopressin (AVP). For each animal, quantification of labelled neurons followed the same protocol, irrespective of investigator. The investigator was always blinded to the treatment group during counting. Forebrain regions were solely counted by me, whilst hindbrain counts, were permed by an independent investigator, Dr Alessia Costa. Neuronal counts were performed on a minimum of three brain sections (3-10 sections per region, depending on the rostro-cauda extent of the region and availability of intact brain sections) containing the region of interest and then averaged to provide a mean count/section. Where brain nuclei/regions were bilateral, the final value was a total for both nuclei. Animals which had less than three brain sections containing the specific region of interest were excluded and not included in group counts for that region. This accounts for variability in group numbers, however a minimum of n = 5 was available for all regions counted in this Chapter.

3.3 Results

3.3.1 Blood glucose response following RH

Adult male C57BL/6J mice were randomised to receive saline, SH or RH (n=6 per group) as shown in the experimental protocol diagram (**Figure 3.3A**). RH mice received repeated s.c. insulin three times a week for four weeks, resulting in hypoglycaemia which reached similar levels through the 4-week protocol (mean 30 min glucose of 4.3 ± 0.2 mmol/l). Data presented are at 30 min after insulin injection and averaged for each week in the protocol (**Figure 3.3B**). Glucose levels remain stable in the saline-treated mice during the 4-week protocol.

All mice recovered from hypoglycaemia within 120 min of insulin administration (**Figure 3.3C**). Importantly, in RH mice, recovery from hypoglycaemia progressively prolonged with successive episodes of hypoglycaemia (**Figure 3.3C**). This is likely to represent the evolving CRR deficits from the accumulation of RH episodes. The evolving CRR deficits are supported by the AUC for the glucose profile, which is shown for RH mice across the 4 weeks and on the final test day (**Figure 3.3D**). The AUC was significantly different for RH mice from week 3 onwards, when compared with week 1.

3.3.2 CRR hormone response to RH

On the test day, SH and RH groups were given a final injection of insulin. Glucose and hormone measurements were taken to quantify the hypoglycaemia CRR and possible impairment (**Figure 3.4**). Following the final injection, both SH and RH groups experienced a reduction in blood glucose to a nadir at 30 min after insulin injection (SH: 4.4 ± 0.2 mmol/l; RH: 3.8 ± 0.4 mmol/l; **Figure 3.4A**). Counter-regulatory hormones (adrenaline and glucagon) were measured by tail-tip blood sampling at baseline (0 min) and at 30 min after injection. Due to limits on the blood volume that could be sampled via the tail tip, glucagon was only measured at the 30 min time point. This also served to limit stress resulting from larger blood volume sampling. The change in adrenaline (0-30 min) was significantly elevated in both SH and RH mice versus saline. Importantly, the adrenaline response was significantly reduced in RH mice, versus SH mice (**Figure 3.4B**). This represented a 55.9% reduction in adrenaline release following the final episode of hypoglycaemia, in RH mice compared with SH mice.

Glucagon release was only measured at 30 min after injection. When compared with saline mice, SH mice displayed a significant elevation in glucagon release (**Figure 3.4C**). Glucagon release was reduced in RH mice compared with SH mice. However, glucagon levels in RH mice were not statistically different to saline and SH groups (**Figure 3.4C**).

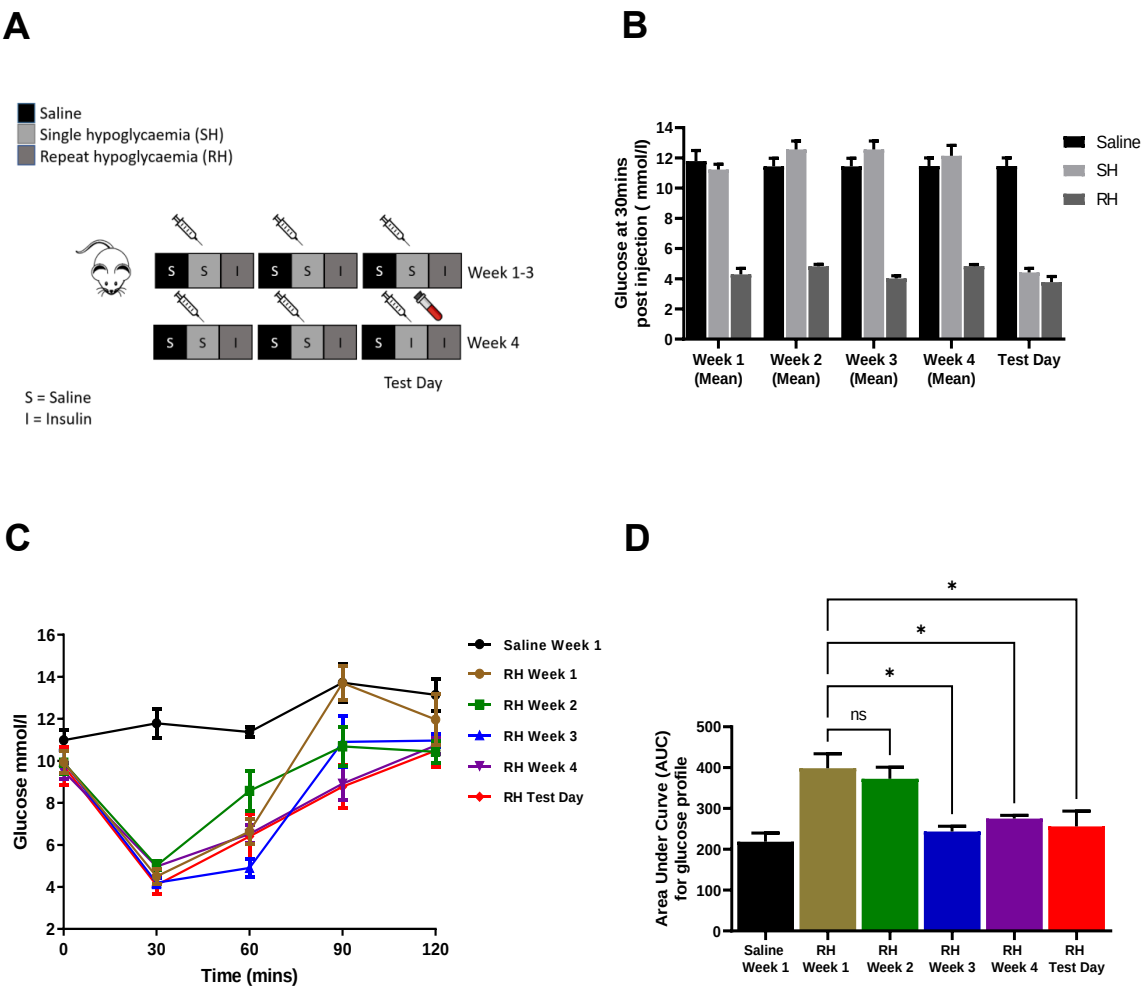

Figure 3.3: Glucose response following 4-week experimental RH protocol

A: Study protocol**.**
B: Mean weekly glucose nadir (30 min after injection) for saline, SH and RH mice across the 4-week experimental RH protocol.
C: Mean weekly blood glucose profile for the 120 min following injection in RH exposed mice (weeks 1-4 and test day) and saline mice (week 1).
D: Area under the curve (AUC) of glucose profiles for RH (weeks 1-4 and test day) and saline mice (week 1). AUC was significantly decreased in RH mice by week 3 when compared with week 1 (*p<0.05; repeated measures two-way ANOVA with Dunnett's *post hoc* test).
Data presented as mean ± SEM. n=6 per group.

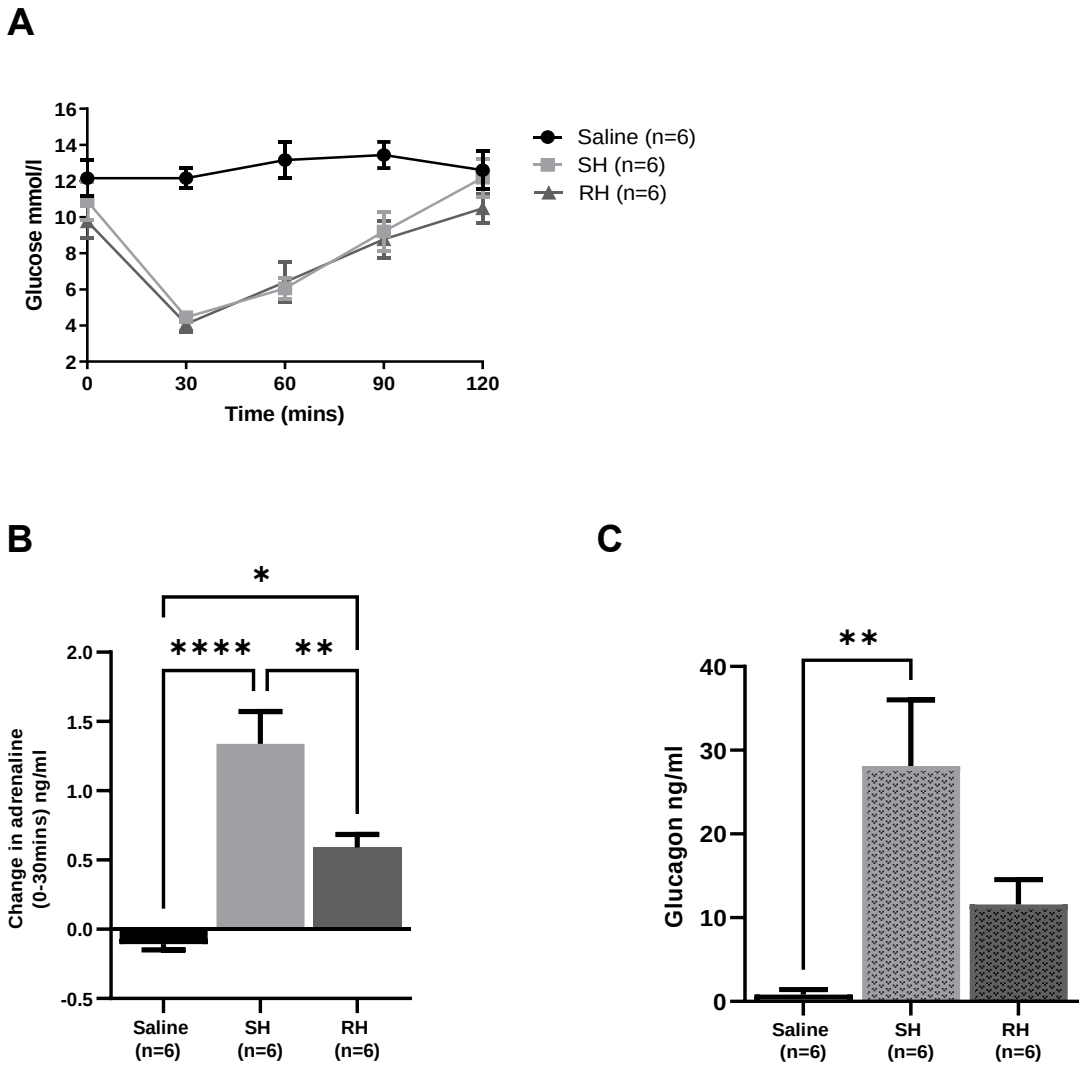

Figure 3.4: Glucose and counter-regulatory response on test day

A: Mean blood-glucose profile for the 120 min following injection, in saline, SH and RH mice on the test day.
B: Change in adrenaline release (0-30 min) following injection in saline, SH and RH mice. RH and SH led to an increase in adrenaline release when compared with saline. RH mice displayed a significant attenuation to the adrenaline response versus SH (**** p<0.0001, SH versus saline; *p<0.05, RH versus saline; **p<0.01, SH versus RH; one-way ANOVA with Tukey's *post hoc* test).
C: Glucagon levels (30 min after injection) in saline, SH and RH mice. Glucagon levels were significantly increased in SH mice compared with saline (**p<0.01; one-way ANOVA with Tukey's *post hoc* test) but not different on statistical testing with RH mice.
Data presented as mean ± SEM. n=6 per group.

3.3.3 Neuronal cFos response to SH and RH in specific brain regions

Hypoglycaemia induces neuronal activation in multiple brain regions. This leads to the expression of the acute activity marker, cFos. But, with repeated activation, there is induction of another regulatory protein, FosB. These activity markers can be quantified following SH and RH, providing an approach to assess key brain regions involved in hypoglycaemia counter regulation. We observed activation of areas of the brain, including those which we hypothesised are key to the CRR and to understanding the development of IAH. These regions are discussed in Chapter 1, and include forebrain (aBNST, CeA, PVH, PVT) and hindbrain (LC, NTS, VLM) regions. The VMH is a key glucose-sensing region, however, it has not been assessed in these experiments as our lab have previously observed that, unusually, cFos is not expressed following hypoglycaemia in the VMH of rodents (Dodd et al., 2010).

This study was conducted in a cohort of adult male *Crh*-cre::eYFP mice, which were allocated randomly to receive saline (n=5), SH (n=6) or RH (n=6). Animals then underwent the same 4-week experimental RH protocol that was characterised in the previous section. Following the final injection, animals were perfused with fixative and tissues were processed to enable immunohistochemistry. Subsequently, a quantitative assessment of cFos and FosB expression was performed.

The acute neural response following saline, SH and RH is shown using cFos immunohistochemistry (red) and neuronal counts for all brain regions of interest. This has been split into separate figures to aid visualisation (**Figures 3.5-3.8**). Following saline injection, a very low level of cFos expression was noted in all brain regions. Hypoglycaemia (SH and RH groups) led to an increase in neuronal cFos, signifying neuronal activation. This pattern was particularly true for the aBNST, PVH, VLM, NTS and DMX, where cFos was significantly higher following SH than saline (**Figures 3.5-3.8**). As predicted, the PVH showed a highly significant neuronal response after SH, when compared with saline. A lesser, non-significant rise in cFos was found in the CeA, PVT and LC following SH, when compared with saline. For the aBNST, this pattern was driven by cFos expression in the ventral (vBNST) and medial (mBNST) divisions.

Interestingly, with RH, neuronal cFos expression was altered in several brain regions. RH led to a significant attenuation in cFos-labelled neurons within the PVH, VLM and NTS, when compared with SH mice. There was also a trend to a reduction in cFos expressing neurons in the aBNST, LC and DMX. On the other hand, RH led to a non-significant increase in cFos in the PVT and a significant increase in cFos in the CeA, when compared with SH (**Figures 3.5C** and **Figure 3.6B**).

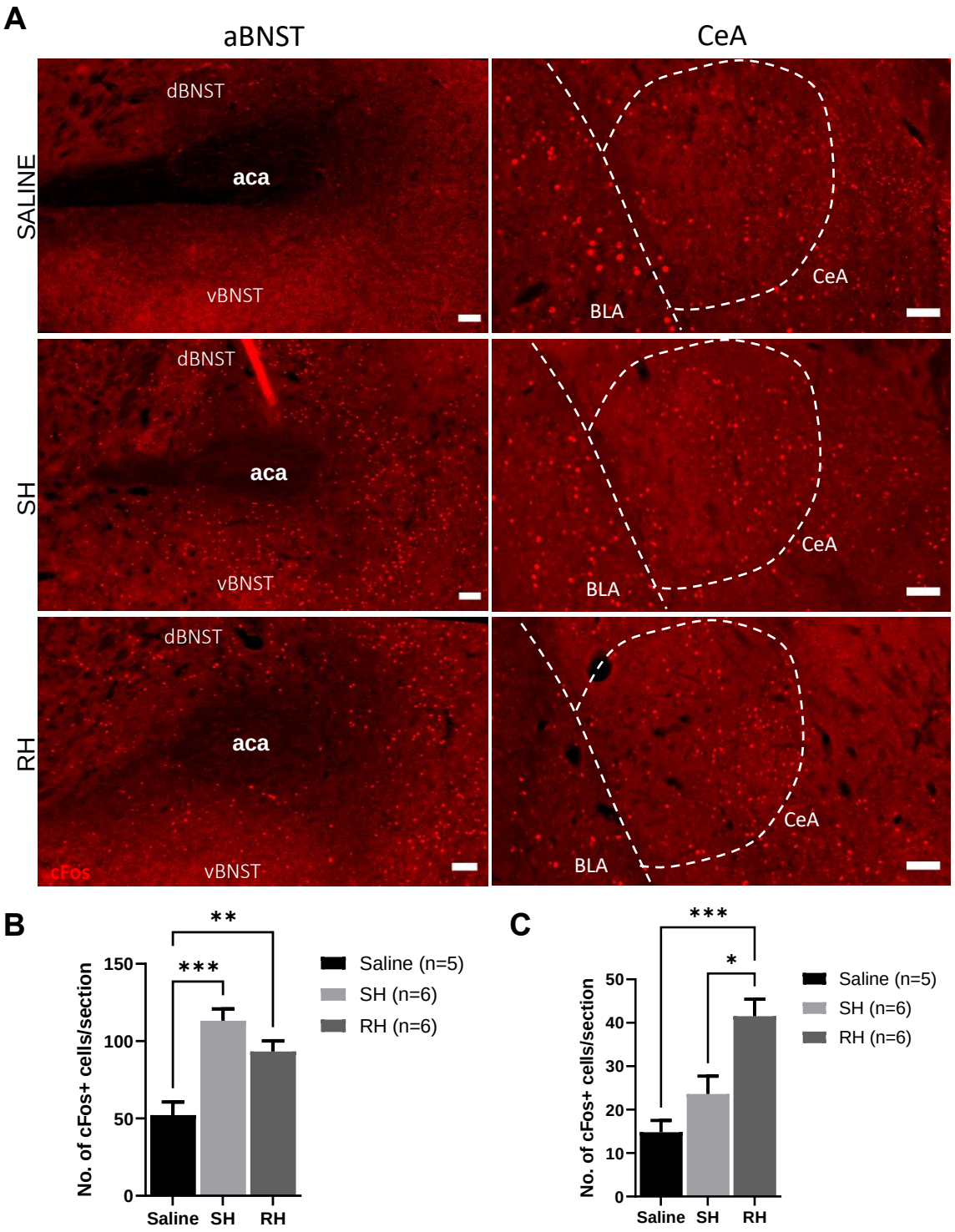

Figure 3.5: Acute neuronal response to SH and RH in the aBNST and CeA

A: Representative images of cFos-labelled neurons (red) in CeA and aBNST in saline, SH- and RH-treated mice. Scale bar represents 100 µm.
B: Number of cFos-labelled neurons in the aBNST, following saline, SH and RH. Neuronal cFos was significantly increased in SH and RH mice, when compared with saline (***p<0.001, **p<0.01, respectively; one-way ANOVA with Tukey's *post hoc* test).
C: Number of cFos-labelled neurons in the CeA, following saline, SH and RH. Neuronal cFos was significantly increased in RH mice, when compared with both saline and SH mice (***p<0.001, *p<0.05, respectively; one-way ANOVA with Tukey's *post hoc* test).
Data presented as mean ± SEM. n=5/6 animals per group. n = 3 -10 sections per animal, averaged.

dBNST: dorsal BNST; **vBNST**: ventral BNST; **aca**: anterior commissure; **BLA**: basolateral amygda**la**

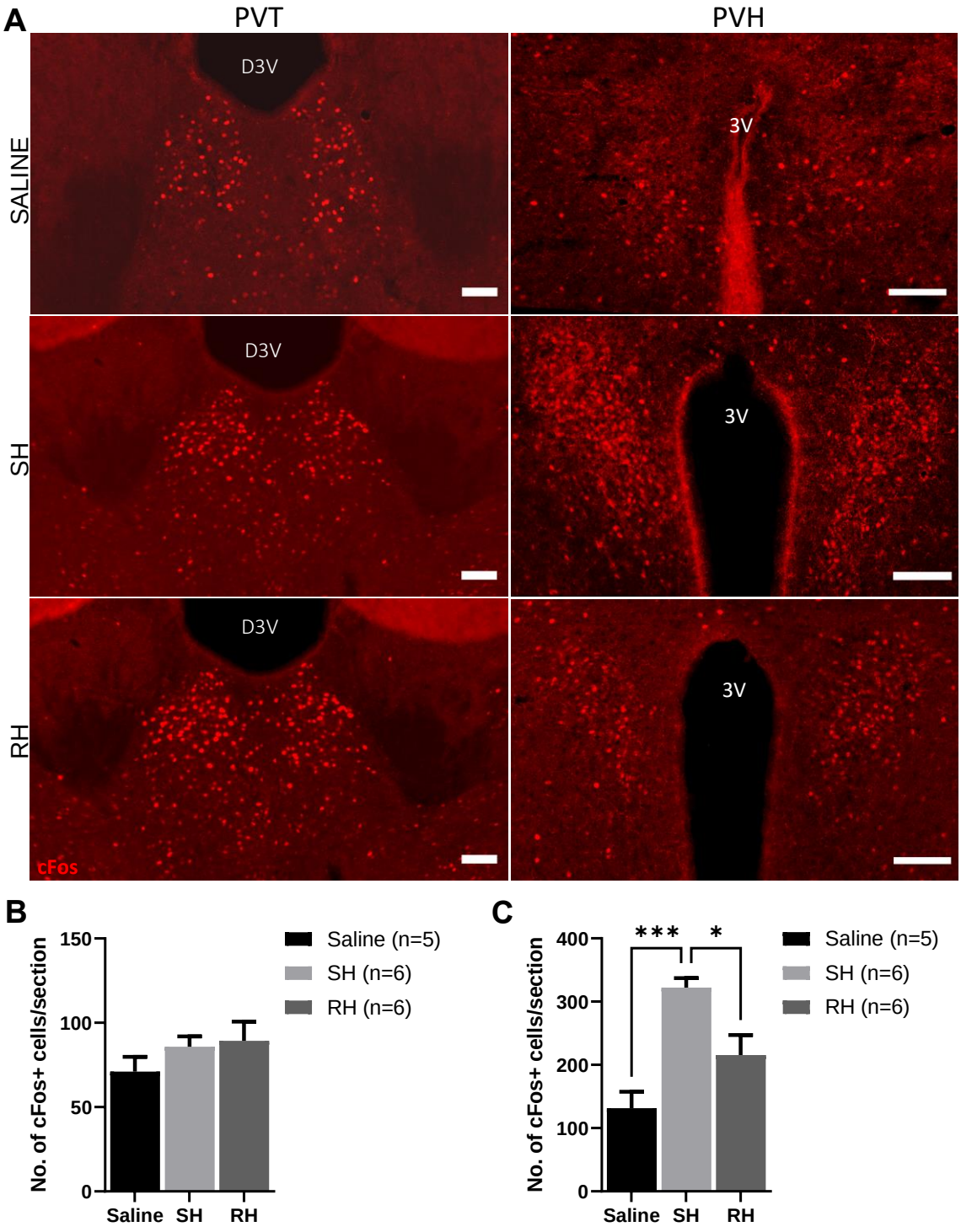

Figure 3.6: Acute neuronal response to SH and RH in the PVT and PVH

A: Representative images of cFos-labelled neurons in the PVT and PVH in saline, SH- and RH-treated mice. Scale bar represents 100 µm.
B: Number of cFos-labelled neurons in the PVT, following saline, SH and RH. Neuronal cFos was greater in SH mice, when compared with saline (non-significant). Similarly, RH mice displayed a small increase in cFos versus SH and saline mice (non-significant).
C: Number of cFos-labelled neurons in the PVH, following saline, SH and RH. Neuronal cFos was significantly increased in SH mice when compared with saline, whilst RH led to an reduction in cFos-labelled neurons, relative to SH (***p<0.001, SH versus saline; *p<0.05, SH versus RH; one-way ANOVA with Tukey's *post hoc* test).
Data presented as mean ± SEM. n=5/6 animals per group. n = 3 -10 sections per animal, averaged.

D3V: dorsal 3rd ventricle; **3V**: 3rd ventricle (ventral)

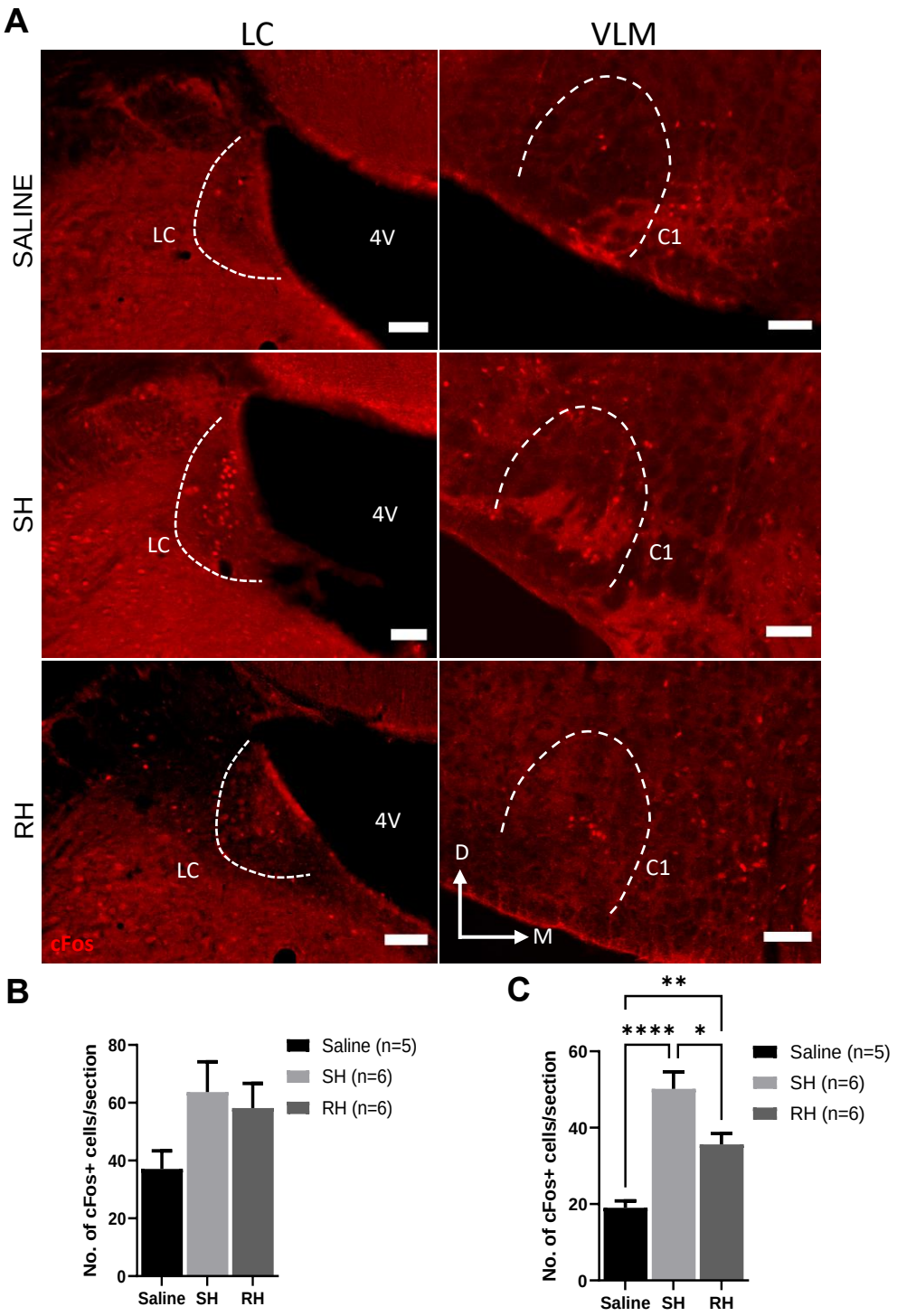

Figure 3.7: Acute neuronal response to SH and RH in the LC and VLM

A: Representative images of cFos-labelled neurons in LC and VLM in saline, SH- and RH-treated mice. Scale bar represents 100 µm.
B: Number of cFos-labelled neurons in the LC, following saline, SH and RH. Neuronal cFos was not significantly increased in SH and RH mice, when compared with saline. RH mice displayed similar cFos expression levels compared with SH mice.
C: Number of cFos-labelled neurons in the VLM, following saline, SH and RH. Neuronal cFos was significantly increased in SH and RH mice when compared with saline. In addition, RH mice displayed attenuated cFos, versus SH (****p<0.0001, SH versus saline; **p<0.01, RH versus saline; *p<0.05, SH versus RH; one-way ANOVA with Tukey's *post hoc* test)
Data presented as mean ± SEM. n=5/6 animals per group. n = 3 -10 sections per animal, averaged.

4V: 4th ventricle; BNST; **D**: dorsal; **M**: medial

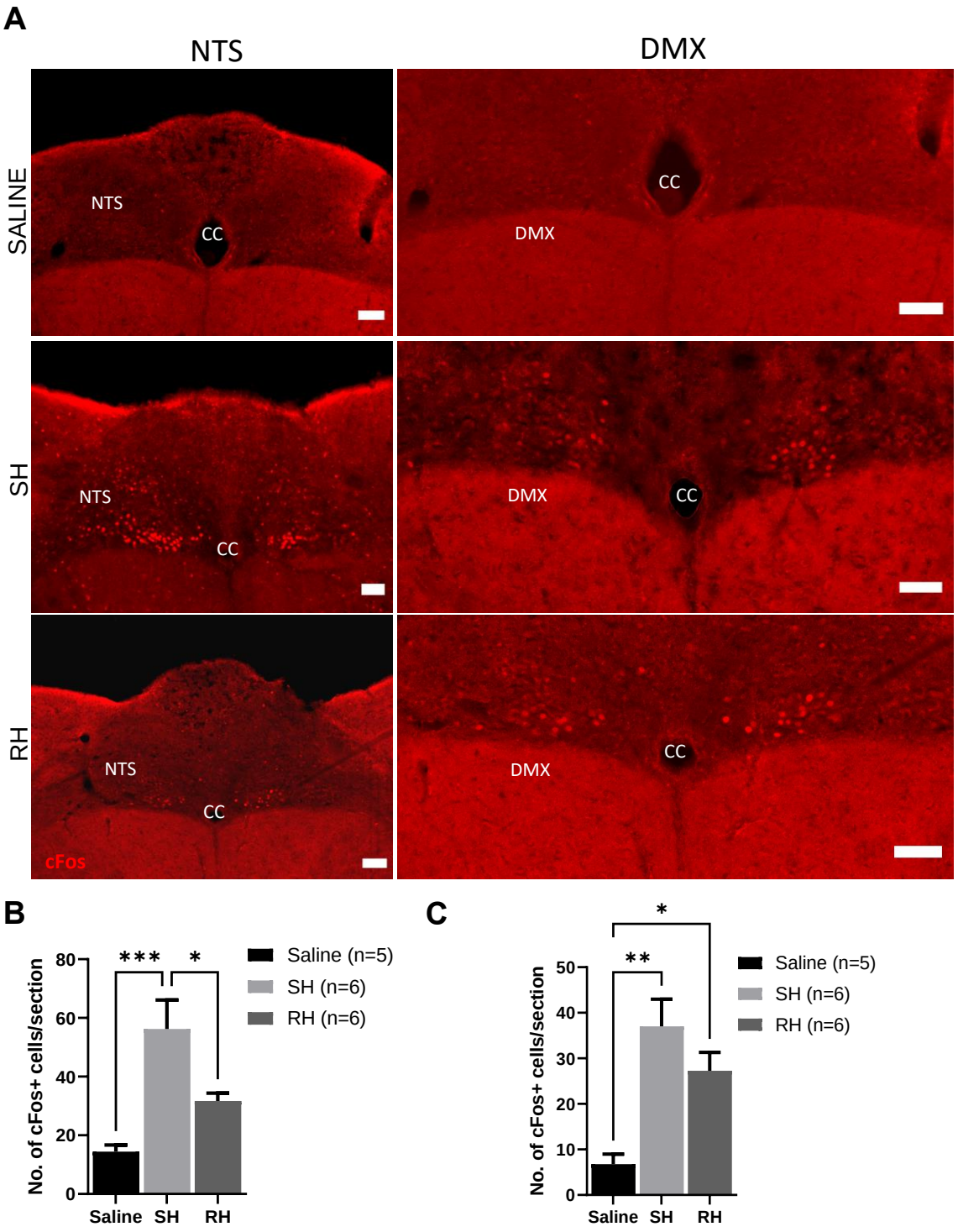

Figure 3.8: Acute neuronal response to SH and RH in the NTS and DMX

A: Representative images of cFos-labelled neurons in NTS and DMX in saline, SH- and RH-treated mice. Scale bar represents 100 µm.
B: Number of cFos-labelled neurons in the NTS, following saline, SH and RH. Neuronal cFos increased in SH mice, when compared with saline (***p<0.001). RH mice displayed a significant reduction in cFos relative to SH mice (*p<0.05; one-way ANOVA with Tukey's *post hoc* test).
C: Number of cFos-labelled neurons in the DMX, following saline, SH and RH. Neuronal cFos was significantly increased in SH and RH mice when compared with saline (**p<0.01, *p<0.05, respectively versus saline; one-way ANOVA with Tukey's *post hoc* test). RH led to fewer cFos-labelled neurons versus SH, however this was not significantly different.
Data presented as mean ± SEM. n=5/6 animals per group. n = 3 -10 sections per animal, averaged.

CC: central canal

These data confirm that brain regions of interest show an increase in neuronal cFos following hypoglycaemia, suggesting they are activated acutely. Interestingly, several brain regions display altered neuronal activation with prior RH. Following this initial experiment, a further investigation of the anatomical distribution and phenotype of specific neuronal populations was performed.

Hindbrain catecholaminergic (CA) neurons within the LC, NTS and VLM form important pre-motor and motor networks, modulating autonomic output from the brain (Donovan and Watts, 2014). CA neurons can be identified by labelling for tyrosine hydroxylase (TH), the rate-limiting enzyme for catecholamine synthesis. In the NTS and VLM, most CA neurons tend to be organised into well-defined adrenergic (termed “C”) or noradrenergic (termed “A”) cell groups (**Figure 3.9-3.10**). This organisation becomes less well-defined in the caudal NTS, where TH neurons are more widely dispersed (**Figure 3.10C**). By examining the colocalisation of cFos and TH using immunohistochemistry, it is evident that a high proportion of TH neurons are activated acutely by SH in the LC, NTS and VLM (**Figure 3.9A,C** and **Figure 3.10A,C**). SH leads to a statistically significant increase in activation of TH neurons in the LC, NTS and VLM, compared with saline, confirming that TH neurons in these regions respond to hypoglycaemia (**Figure 3.9-3.10**). For the LC, a greater number of cFos and TH dual-labelled cells were identified in more rostral LC sections (bregma -5.4mm, **Figure 3.9A-B**). TH neurons in the rostral LC were activated acutely by SH and showed reduced activation in RH mice, however this difference was not statistically significant.

In the VLM, TH neurons reside within CA cell groups (termed C1, C1/A1 and A1), which can be sub-divided based on their rostro-caudal location relative to bregma (**Figure 1.8** and **Figure 3.9D**). TH neurons within all VLM CA cell groups show a significant increase in cFos expression following SH, when compared with saline, signifying acute activation. Interestingly, following RH, only TH neurons in the C1 group showed attenuated cFos, when compared with SH (**Figure 3.9D**). These findings suggest that in the VLM, RH leads to differential effects on specific cell populations, which may reflect differences in connections or neuronal function, with respect to the CRR.

The NTS has a complex structure and TH neurons can be found both in defined cell groups, but also more caudally, surrounding the DMX and area postrema (AP) (**Figure 3.9A,C**). TH neurons throughout the rostro-caudal extent of the NTS, display increased cFos following SH, suggesting acute activation. However, only TH neurons in the C2 group show a statistically significant increase in activity, when compared with saline. With RH, TH neurons throughout the rostro-caudal extent of NTS, express significantly less cFos, versus SH, signifying reduced activation. Interestingly, only the C2 group, showed a corresponding cFos attenuation in RH mice (**Figure 3.10**).

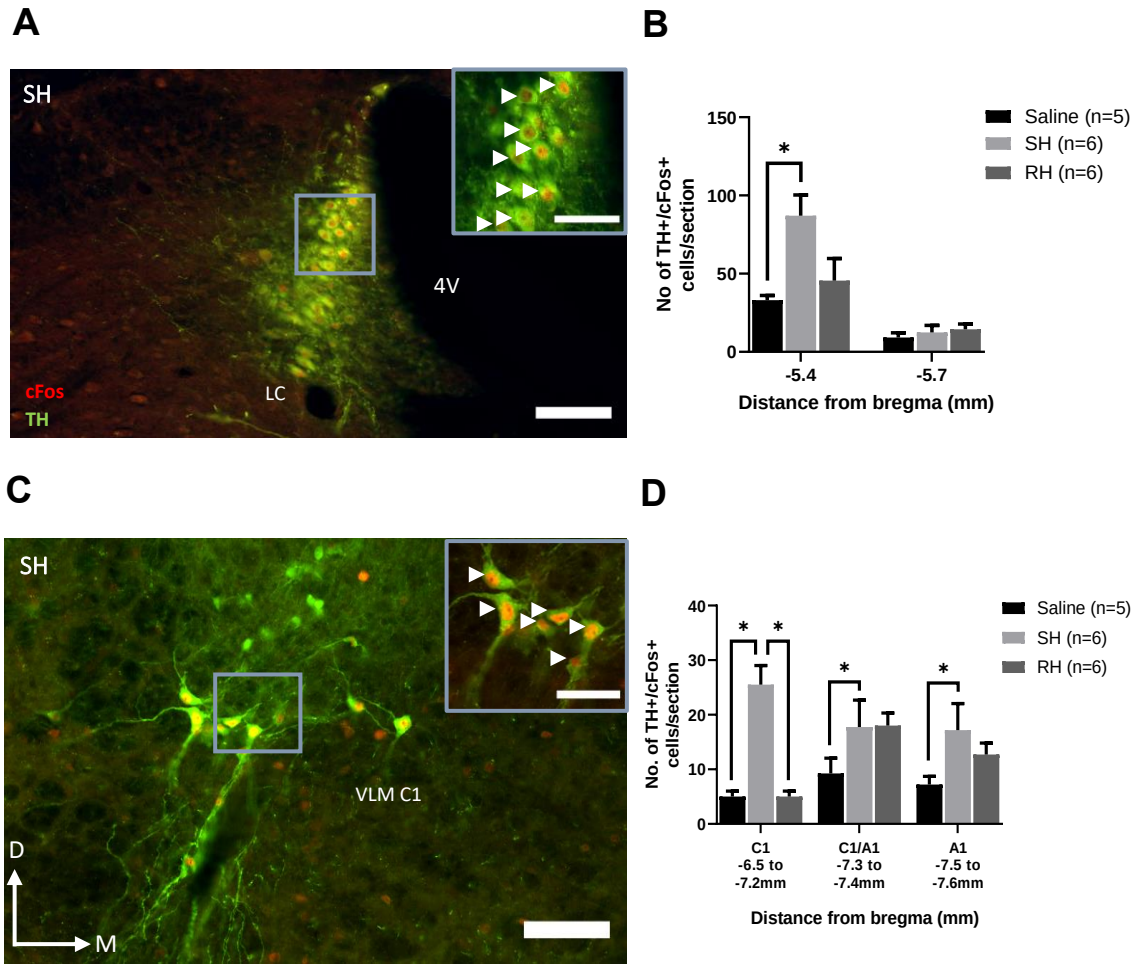

Figure 3.9: Hindbrain CA neuron response to saline, SH, RH in the LC and VLM

A: Representative image of TH+ (green) and cFos+ (red) neurons in the LC following SH. Main image scale bar represents 100 µm and magnified image scale bar represents 50 µm. Arrows mark TH+/cFos+ dual-labelled neurons.
B: Number of dual-labelled (TH+/cFos+) neurons in the LC, in saline, SH and RH mice. Neuronal cFos increased in the rostral LC in SH mice, when compared with saline (*p<0.05; one-way ANOVA with Tukey's *post hoc* test). RH mice displayed fewer activated (cFos+) TH neurons, compared with SH, but this was non-significant.
C: Representative image of TH+ and cFos+ neurons in the VLM (C1 group) following SH. Main image scale bar represents 100 µm and magnified image scale bar represents 50 µm. Arrows mark TH+/cFos+ dual-labelled neurons.
D: Number of dual-labelled (TH+/cFos+) neurons in the VLM, in saline, SH and RH mice. TH neuronal cFos increased at all bregma levels and corresponding CA cell groups in SH mice, when compared with saline. Following RH, only TH neurons in the VLM C1 group displayed attenuated cFos, when compared with SH (*p<0.05, SH versus saline; *p<0.05, SH versus RH; one-way ANOVA with Tukey's *post hoc* test).
Data presented as mean ± SEM. n=5/6 animals per group. n = 3 -10 sections per animal, averaged.

CC: central canal; **4V**: 4th ventricle; **D**: dorsal; **M**: medial

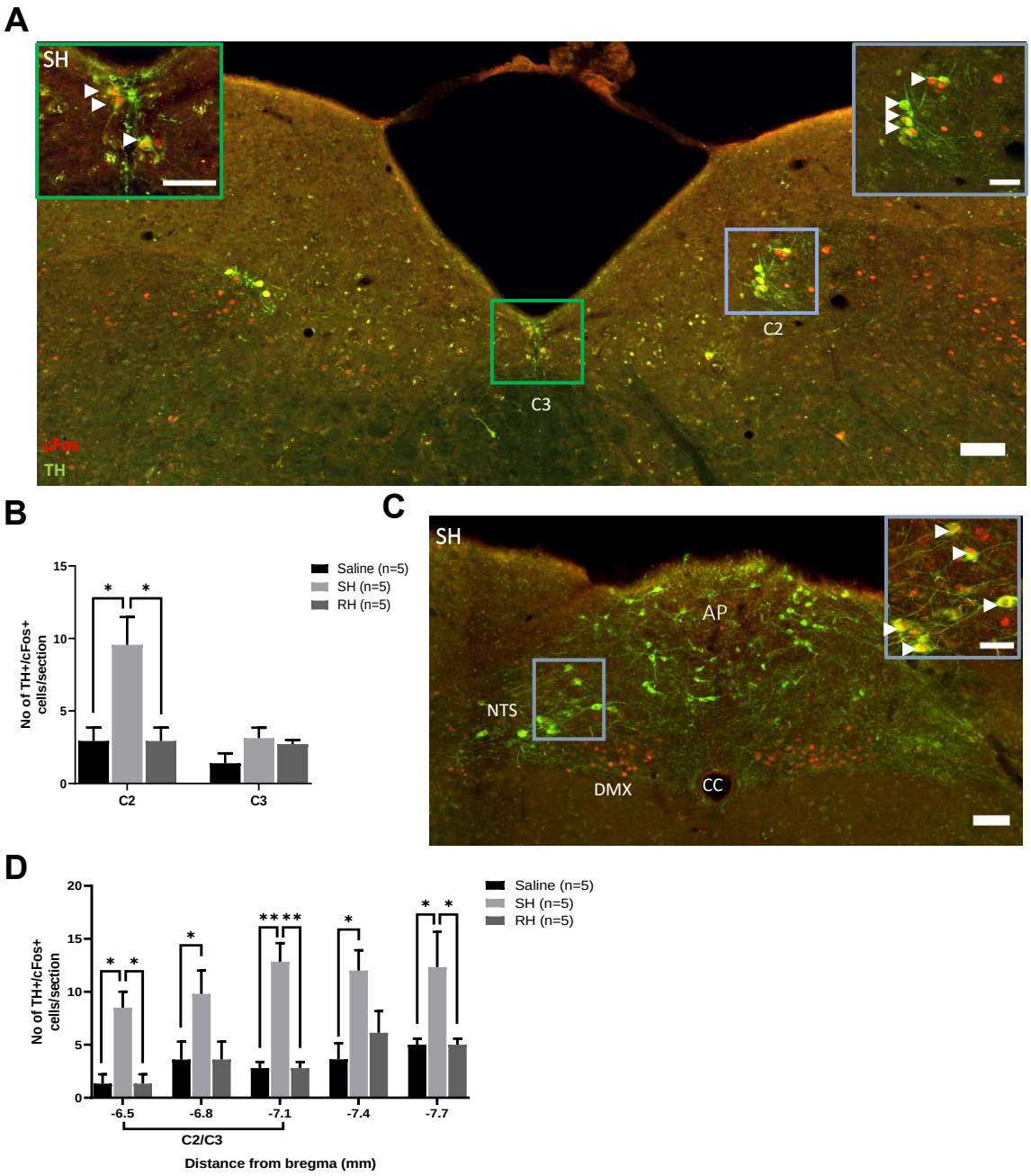

Figure 3.10: Hindbrain CA neuron response in NTS to saline, SH, RH in the NTS

A: Representative image of TH+ (green) and cFos+ (red) in the rostral NTS following SH. Main image scale bar represents 100 µm and magnified image scale bar represents 50 µm. Arrows mark TH+/cFos+ dual-labelled neurons.
B: Number of dual-labelled (TH+/cFos+) neurons in rostral NTS cell groups, in saline, SH and RH mice. Following SH, TH neuronal cFos only increased in the NTS C2 group, when compared with saline. Following RH, TH neurons in the C2 group also displayed a significant reduction in cFos relative to SH mice (*p<0.05; SH versus saline; *p<0.05, SH versus RH; one-way ANOVA with Tukey's *post hoc* test).
C: Representative image of TH+ and cFos+ in the caudal NTS following SH. Main image scale bar represents 100 µm and magnified image scale bar represents 50 µm. Arrows mark TH+/cFos+ dual-labelled neurons.
D: Number of dual-labelled (TH+/cFos+) neurons in the NTS, in saline, SH and RH mice. Following SH, TH neuronal cFos increased at rostral, middle, and caudal NTS bregma levels when compared with saline (*p<0.05, rostral and middle NTS; **p<0.01, middle NTS; one-way ANOVA with Tukey's *post hoc* test). Following RH, TH neurons at the same NTS bregma levels, displayed attenuated cFos, when compared to SH (*p<0.05, rostral and middle NTS; **p<0.01, middle NTS; one-way ANOVA with Tukey's *post hoc* test). Data presented as mean ± SEM. n=5/6 animals per group. n = 3 -10 sections per animal, averaged.

CC: central canal; **AP**: area postrema

3.3.4 Neuronal FosB response in specific brain regions

The neuronal expression of FosB was also examined in the same regions of interest. FosB expression increases following neuronal activation and remains elevated for several days. This provides a tool with which we can assess the neuronal response to repeated stimuli, like RH. To this end, the chronic neuronal response following saline, SH and RH was assessed using FosB immunohistochemistry. Dual-labelling for *Crh*-cre::eYFP neurons (DAB without nickel producing brown cytoplasmic staining) and FosB (DAB with nickel producing black nuclear staining) was conducted. For hindbrain regions, dual-labelling for TH (DAB without nickel) and FosB (DAB with nickel) was conducted. Representative images for FosB immunohistochemistry and neuronal counts are shown for all brain regions of interest, in saline, SH and RH mice (**Figures 3.11-3.14**).

In most brain regions, a low number of neurons expressed FosB following saline and SH, respectively (**Figures 3.11-3.14**). The exception being the DMX, which interestingly, did not express FosB in any of the treatment groups (**Figure 3.14C**). Unlike observations with cFos expression, following RH, neuronal FosB induction was more abundant in each region of interest, apart from the DMX. The increases were statistically significant in the aBNST, CeA, PVT, PVH and LC, demonstrating that repeated activation with RH induces high levels of neuronal FosB (**Figures 3.11-3.14**). For the aBNST, this pattern was driven by FosB labelling in the vBNST. Of all the brain regions assessed, the PVH displayed the highest number of FosB-labelled neurons (**Figure 3.12A,C**). Here, the number of FosB-labelled neurons was similar after saline and SH. However, after RH, there was a large increase in labelled neurons (**Figure 3.12A,C**). The PVT, which continued to demonstrate high levels of cFos with RH, also displayed elevated FosB following RH, when compared with SH (**Figure 3.11A,B**). Interestingly, the CeA displayed a significant increase in both cFos and FosB following RH, which was a unique response pattern.

In hindbrain regions, FosB almost exclusively colocalised with TH, which was not seen with cFos. The LC, which is the major noradrenergic nucleus in the brain, displayed a low level of FosB with saline and SH, but a large increase in FosB-labelled neurons on repeated stimulation with RH (**Figure 3.13A,B**). Only a small number of neurons in the NTS and VLM expressed FosB in saline, SH or RH groups (**Figure 3.13-3.14**). RH led to a small, non-significant increase in FosB, relative to SH and RH in the NTS and VLM. It is interesting that DMX neurons express cFos following all treatments, but do not express FosB at all.

Thus, important brain regions within the glucose-regulatory network, demonstrate unique patterns of cFos and FosB expression after RH. Knowledge of the identity of specific neuronal populations located in these regions of interest, may help to decipher this pattern.

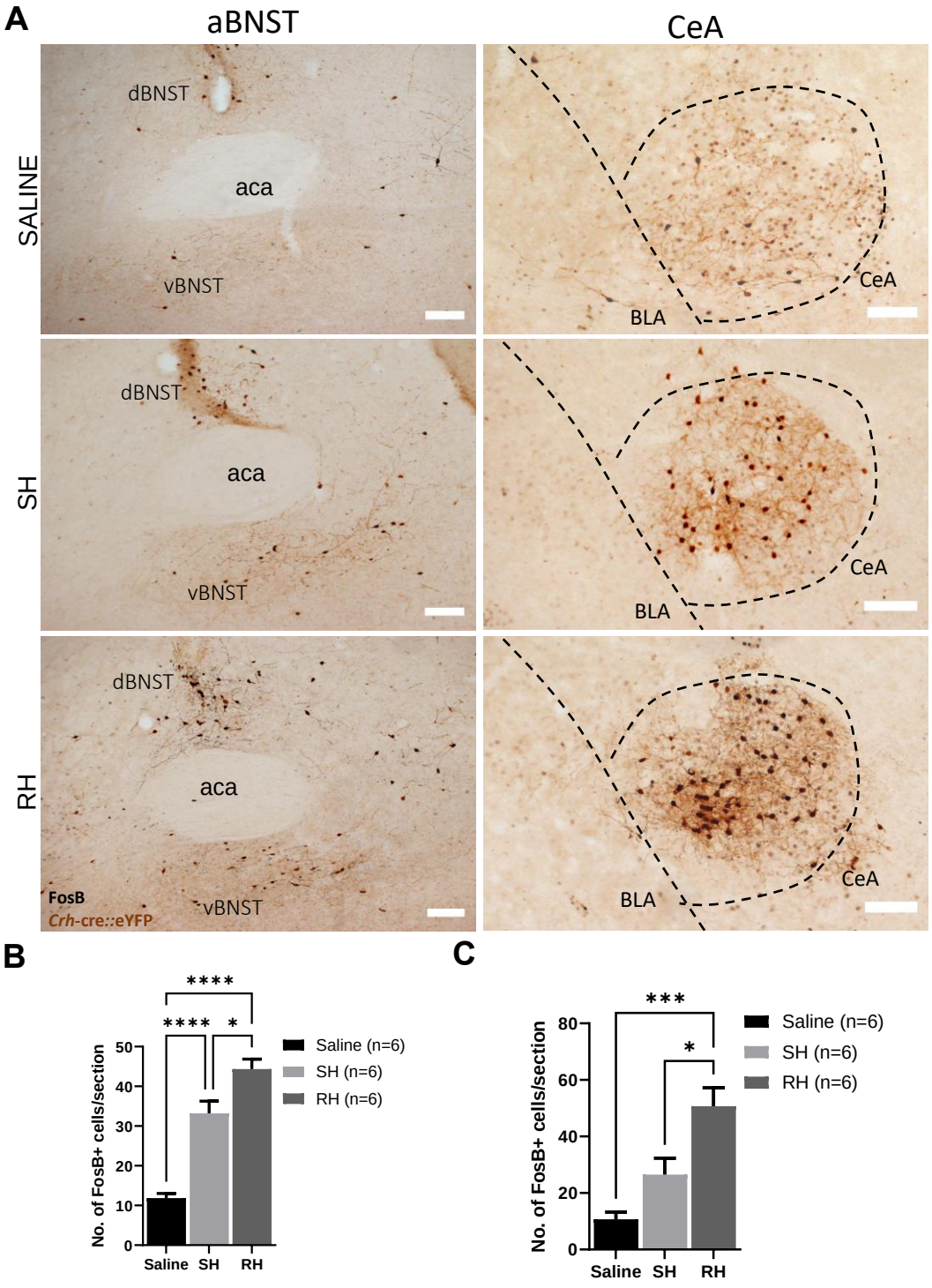

Figure 3.11: Neuronal FosB response to SH and RH in the aBNST and CeA

A: Representative images of FosB-labelled neurons (black) in CeA and aBNST in saline, SH- and RH-treated mice. Scale bar represents 100 µm.
B: Number of FosB-labelled neurons in the aBNST, following saline, SH and RH. Neuronal FosB was significantly increased in RH mice, when compared with saline and SH. (****p<0.0001, *p<0.05, RH versus saline and SH, respectively; one-way ANOVA with Tukey's *post hoc* test).
C: Number of FosB-labelled neurons in the CeA, following saline, SH and RH. Neuronal FosB was significantly increased in RH mice, when compared with both saline and SH mice (***p<0.001, *p<0.05, respectively; one-way ANOVA with Tukey's *post hoc* test).
Data presented as mean ± SEM. n=6 animals per group. n = 3 -10 sections per animal, averaged.

dBNST: dorsal BNST; **vBNST**: ventral BNST; **aca**: anterior commissure; **BLA**: basolateral amygda**la**

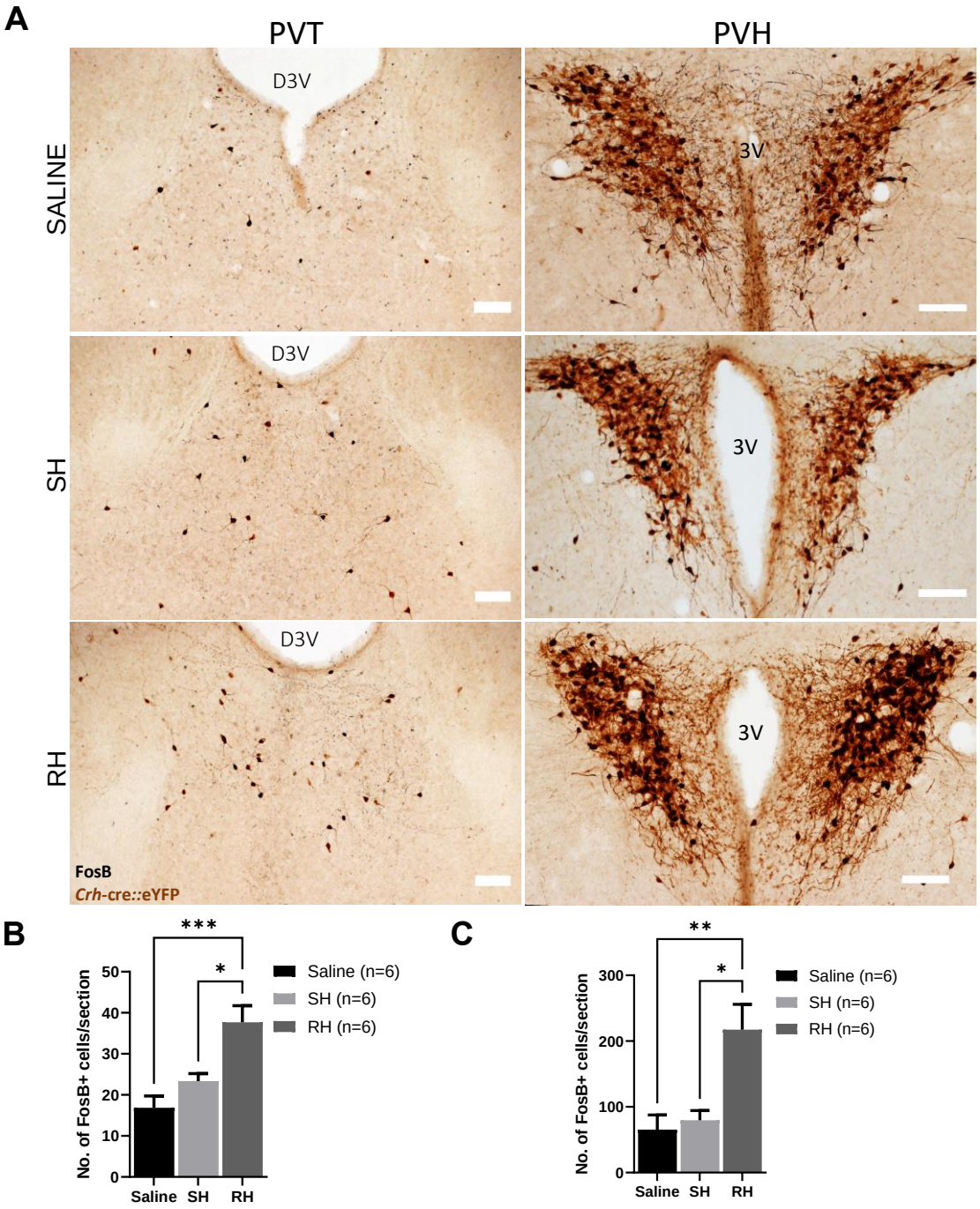

Figure 3.12: Neuronal FosB response to SH and RH in the PVT and PVH

A: Representative images of FosB-labelled neurons (black) in PVT and PVH in saline, SH- and RH-treated mice. Scale bar represents 100 µm.
B: Number of FosB-labelled neurons in the PVT, following saline, SH and RH. Neuronal FosB was significantly increased in RH mice, when compared with saline and SH (***p<0.001, *p<0.05, RH versus saline and SH, respectively; one-way ANOVA with Tukey's *post hoc* test).
C: Number of cFos-labelled neurons in the PVH, following saline, SH and RH. A high number of FosB-labelled neurons were present in the PVH. FosB-labelled neurons were significantly increased with RH, when compared with saline and SH (**p<0.01, *p<0.05, RH versus saline and SH, respectively; one-way ANOVA with Tukey's *post hoc* test).
Data presented as mean ± SEM. n=6 animals per group. n = 3 -10 sections per animal, averaged.

D3V: dorsal 3rd ventricle; **3V**: 3rd ventricle (ventral)

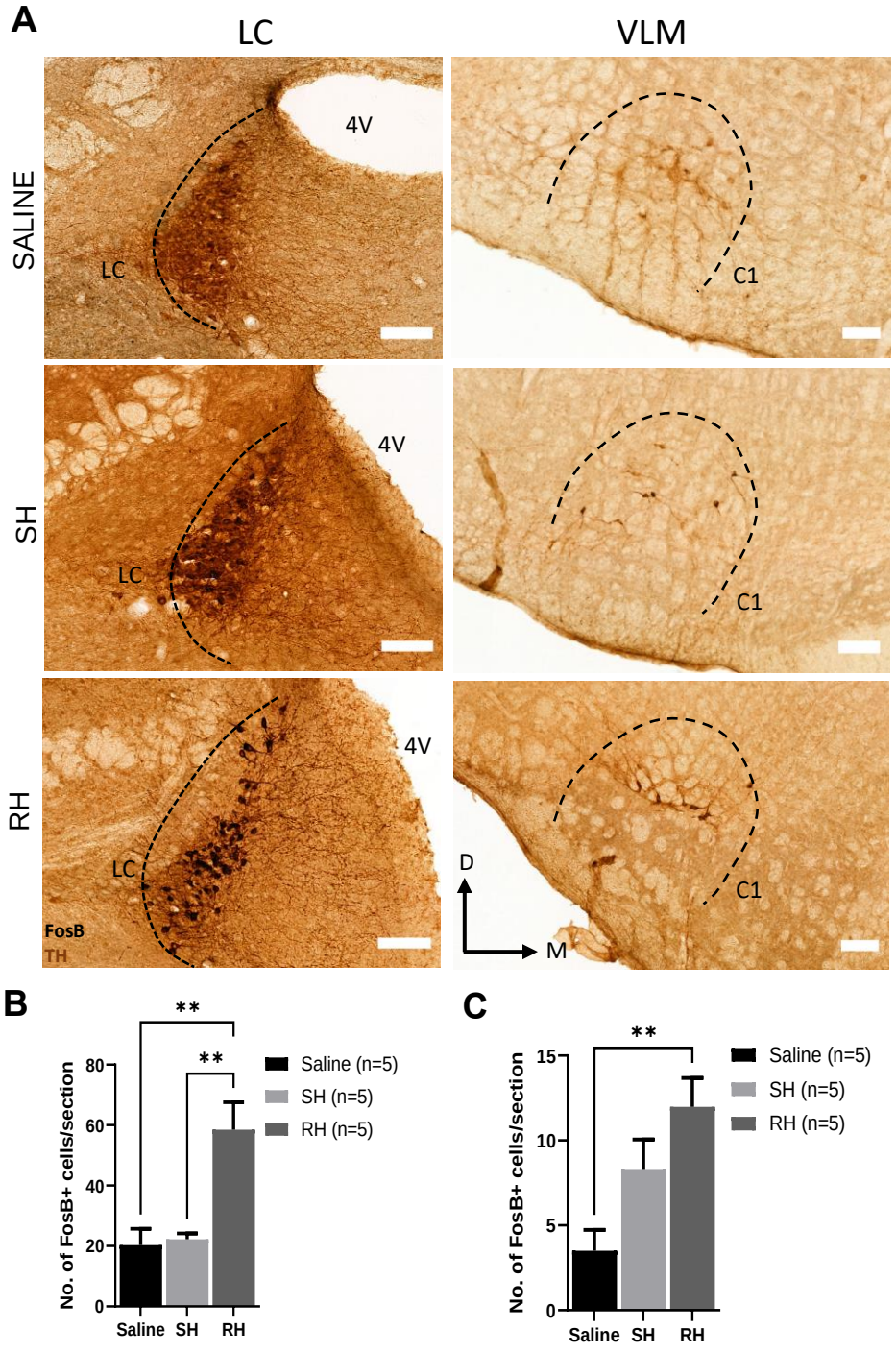

Figure 3.13: Neuronal FosB response to SH and RH in the LC and VLM

A: Representative images of FosB-labelled neurons (black) in LC and VLM in saline, SH- and RH-treated mice. Scale bar represents 100 µm. Most FosB-labelled neurons, colocalised with TH (brown).
B: Number of FosB-labelled neurons in the LC, following saline, SH and RH. FosB levels were significantly increased following RH, versus saline and SH (**p<0.01, SH versus saline; *p<0.05, SH versus RH; one-way ANOVA with Tukey's *post hoc* test).
C: Number of FosB-labelled neurons in the VLM, following saline, SH and RH. Only a small number of neurons expressed FosB and all were found within CA neuron cell groups. Neuronal FosB was significantly increased following RH, when compared with saline, but not SH (**p<0.01, RH versus saline; one-way ANOVA with Tukey's *post hoc* test).
Data presented as mean ± SEM. n=5 animals per group. n = 3 -10 sections per animal, averaged.

4V: 4th ventricle; BNST; **D**: dorsal; **M**: medial

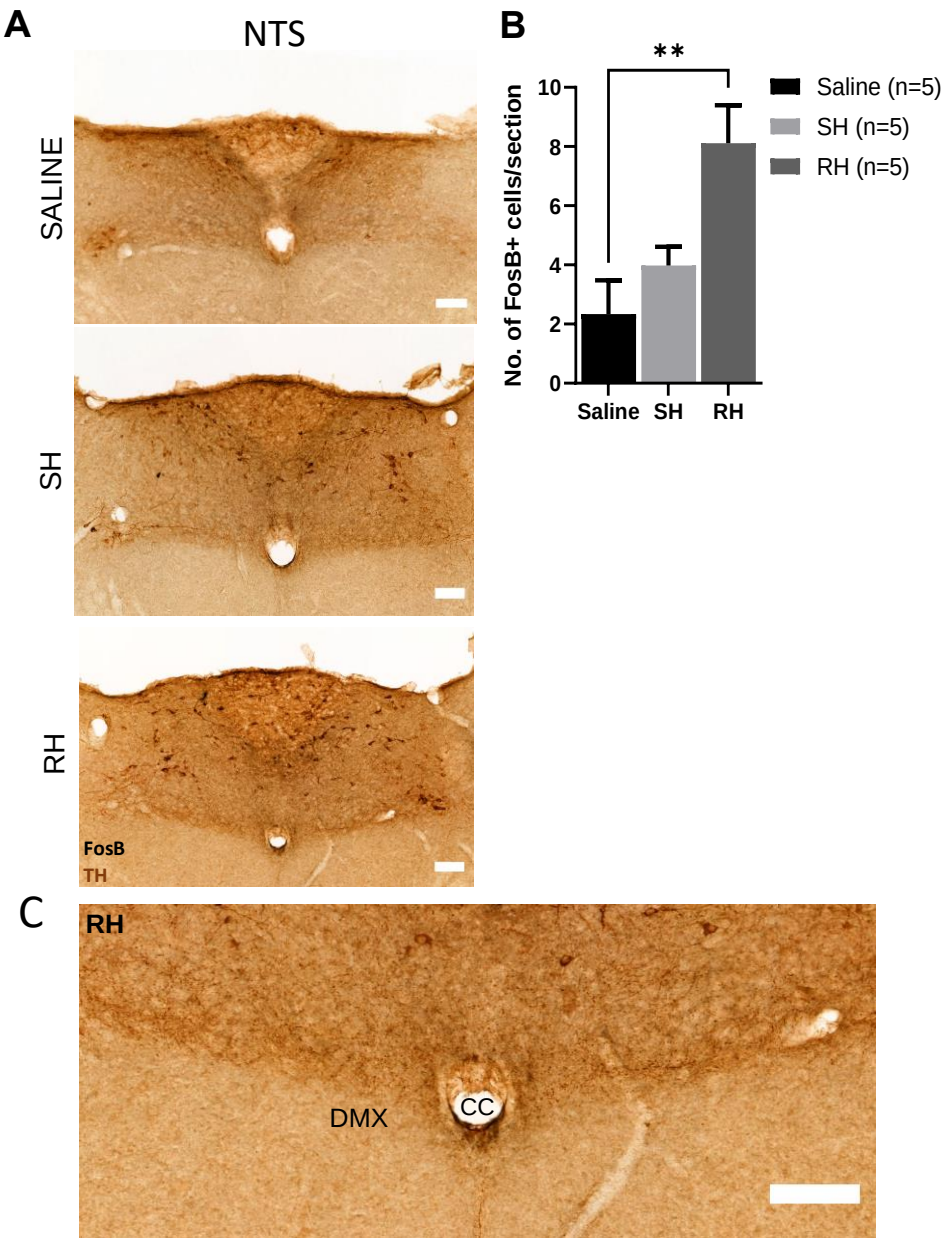

Figure 3.14: Neuronal FosB response to SH and RH in the NTS and DMX

A: Representative images of FosB**-**labelled neurons in the NTS in saline, SH- and RH-treated mice. Scale bar represents 100 µm.
B: Only a small number of neurons express FosB following saline, SH or RH. FosB expression was increased relative to saline, but not SH (**p<0.01, RH versus saline; one-way ANOVA with Tukey's *post hoc* test).
C: Neurons within the DMX did not display FosB in any of the groups. Representative image of DMX following RH, showing no FosB**-**labelled neurons. Scale bar represents 100 µm.
Data presented as mean ± SEM. n=5 animals per group. n = 3 -10 sections per animal, averaged.

CC: central canal

3.3.5 Characterising the response of PVT neurons to SH and RH

The PVT demonstrated a unique pattern of cFos and FosB expression, following SH and RH. Specifically, PVT neurons maintain high levels of cFos and FosB expression following both SH and RH. In light of these initial data and literature supporting persistent activation of PVT neurons following repeated stressors (Bhatnagar and Dallman, 1998), further characterisation of this brain region was performed. To this end, an anatomical analysis of PVT cFos and FosB expression, following SH and RH was conducted. The PVT is an elongated nucleus which has traditionally been divided rostro-caudally into anterior (aPVT), middle (mPVT) and posterior (pPVT) divisions (**Figure 3.15A**). First the phenotype of cFos expressing neurons in the different subregions of the pPVT was assessed. To achieve this, a separate cohort of adult male *VGlut2*-cre::eYFP (n=3) were exposed to SH and perfused with fixative. Brain sections containing the PVT were dual-labelled for *VGlut2*-cre::eYFP neurons (green) and cFos (red) using immunohistochemistry with fluorescent antibodies. This confirmed that throughout the rostro-caudal extent of the PVT, all cFos-labelled neurons colocalised with *VGlut2*-cre::eYFP (**Figure 3.15B**). Therefore, based on these data, SH-activated PVT neurons are glutamatergic in nature

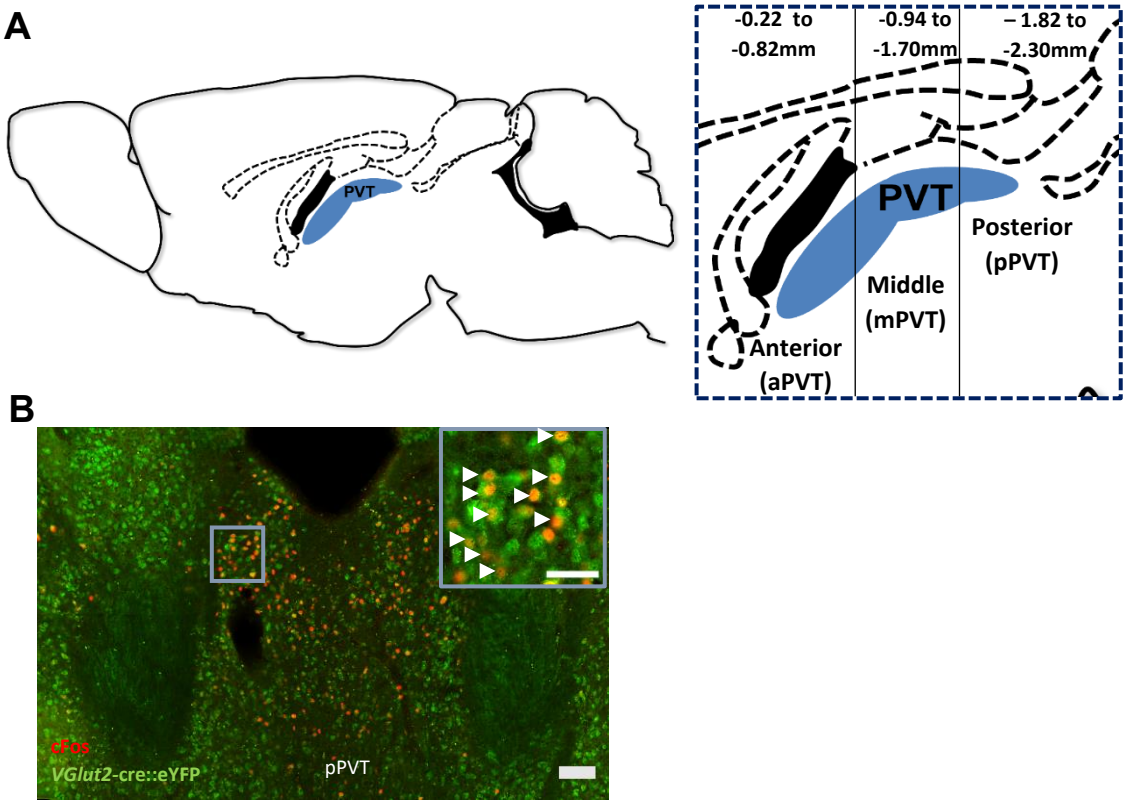

Figure 3.15: Anatomical analysis of PVT subdivisions and neuronal phenotype

A: Diagram to show rostro-caudal anatomical subdivisions of PVT along with distance from bregma in the mouse brain.
B: Representative images of cFos- and *VGlut2*-cre::eYFP-labelled neurons in the pPVT following RH, demonstrating all cFos-labelled neurons colocalised with *VGlut2*-cre::eYFP. Main image scale bar represents 100 µm, magnified image 50 µm. Arrows mark dual-labelled neurons.

Next, a quantitative assessment of cFos/FosB expression in saline, SH and RH groups was conducted for each of the PVT subdivisions (**Figure 3.16**). This was performed in brain sections which originated from the same cohort of *Crh*-cre::eYFP mice investigated earlier in this chapter. There was a high level of neuronal cFos in all PVT subdivisions following saline, SH and RH (**Figure 3.16A,B**). This was greatest in the aPVT and marginally less in the pPVT and mPVT. In contrast, a smaller number of PVT neurons expressed FosB following saline, SH and RH. Interestingly, FosB expression was greatest in the pPVT and to a lesser extent in the mPVT and aPVT, respectively. Importantly, following RH, the number of FosB-labelled neurons was significantly increased, only in the pPVT (**Figure 3.16A,C**). These data highlight neurons in the pPVT subdivision as an interesting area for further investigation.

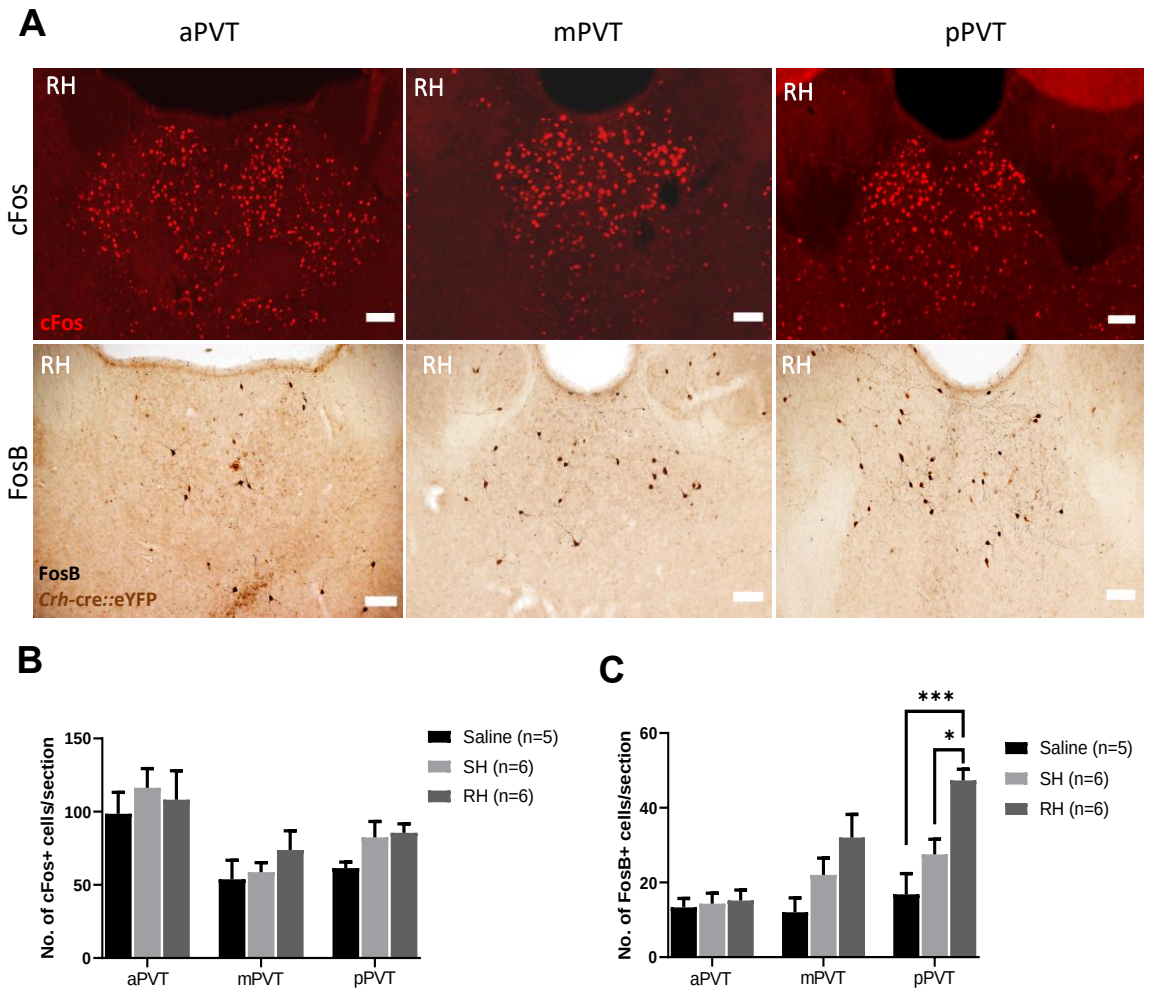

Figure 3.16: Acute and chronic neuronal response in PVT subdivisions

A: Representative images of cFos- and FosB-labelled neurons in the PVT subdivisions following RH. Scale bar represents 100 µm.
B: Number of cFos-labelled neurons in PVT subdivisions, following saline, SH and RH. Neuronal cFos was expressed at high levels in all PVT subdivisions and not changed by RH.
C: Number of FosB-labelled neurons in PVT subdivisions, following saline, SH and RH. Neuronal FosB was significantly increased following RH in the pPVT, when compared with saline and SH (***p<0.001, RH versus saline; *p<0.05, RH versus SH; one-way ANOVA with Tukey's *post hoc* test).
Data presented as mean ± SEM. n=5/6 animals per group. n = 3 -10 sections per animal, averaged.

3.3.6 Characterising the anatomical distribution and identity of SH-responsive PVH neurons

The PVH is of particular interest to this doctorial research project and was identified in this Chapter as displaying high levels of cFos and FosB following SH and RH, respectively. These data suggest that PVH neurons participate in the acute neuronal response to hypoglycaemia and, since they modulate the sympathoadrenal axis, are likely to have a significant role in the adrenaline CRR. However, the anatomical distribution of hypoglycaemia-activated PVH neurons and their phenotypic identity requires confirmation. The PVH, like the PVT, can be separated anatomically rostro-caudally, into anterior (aPVH), middle (mPVH) and posterior (pPVH) sub-regions (**Figure 3.17A**).

To this end, I assessed the distribution of cFos expressing neurons in PVH sub-regions, following saline, SH and RH (**Figure 3.17B,C**). Further subdivisions within the anterior, middle and posterior PVH in the mouse brain, have been proposed by investigators in the field (Biag et al., 2012). These anatomical subdivisions have utility in understanding the organisation of specific neuronal populations within the PVH and potentially their function (**Figure 3.17B**). Following SH, cFos expression was increased in anterior, middle and posterior PVH divisions, when compared with saline. However, this was only statistically significant in aPVH and mPVH sections. Though there was an attenuation in cFos levels following RH in all sub-regions, this also was only statistically significant in the mPVH (**Figure 3.17C**). This highlighted the importance of the mPVH sub-region, in the acute neuronal response to SH, and suggests that with RH, mPVH neurons become less responsive to hypoglycaemia.

The PVH, contains heterogenous populations of neurons, which are traditionally identified based on neuropeptide phenotypes (though overlap of populations does occur). As the mPVH had been identified as an interesting region for further investigation, I elected to explore the phenotype of SH-activated neurons within this sub-region. Sections containing the mPVH were identified in SH-exposed *Crh*-cre::eYFP mice. To ensure consistency, these sections originated from the same cohort of mice used in earlier studies in this Chapter. Dual-labelling for cFos along with either *Crh*-cre::eYFP (GFP), oxytocin (OXT) or arginine vasopressin (AVP) was performed using immunohistochemistry with fluorescent antibodies.

Representative images for dual-label immunohistochemistry are shown in **Figure 3.18**. As the *Crh*-cre::eYFP reporter line was used in this study, CRH neuron cell bodies and fibres were strongly labelled with a GFP antibody. CRH neurons were distributed more medially and dorsally within the mPVH (**Figure 3.18A**). When expressed as a percentage of cFos-labelled neurons, CRH neurons accounted for 81% of activated neurons

following SH (**Figure 3.18A**). There were fewer OXT-labelled neurons identified (**Figure**). These were magnocellular in nature and demonstrated strong cell body and fibre straining. Relative to CRH neurons, OXT neurons were distributed more medially and ventrally. Following SH, only 18% of cFos colocalised with OXT (**Figure 3.18B**). AVP labelling was not as strong as for OXT or CRH. However, both parvocellular and magnocellular AVP neurons were present. Consistent with the literature, AVP neurons cluster in two distinct PVH region, dorsally and ventro-laterally. Following SH, 15% of cFos-expressing neurons also contained AVP (**Figure 3.18C**). In summary, these data highlight that CRH neurons are the most abundant hypoglycaemia-responsive neuronal population in the mPVH. This prompted a further investigation into the anatomical distribution and neuronal response of CRH^{mPVH} neurons after saline, SH and RH.

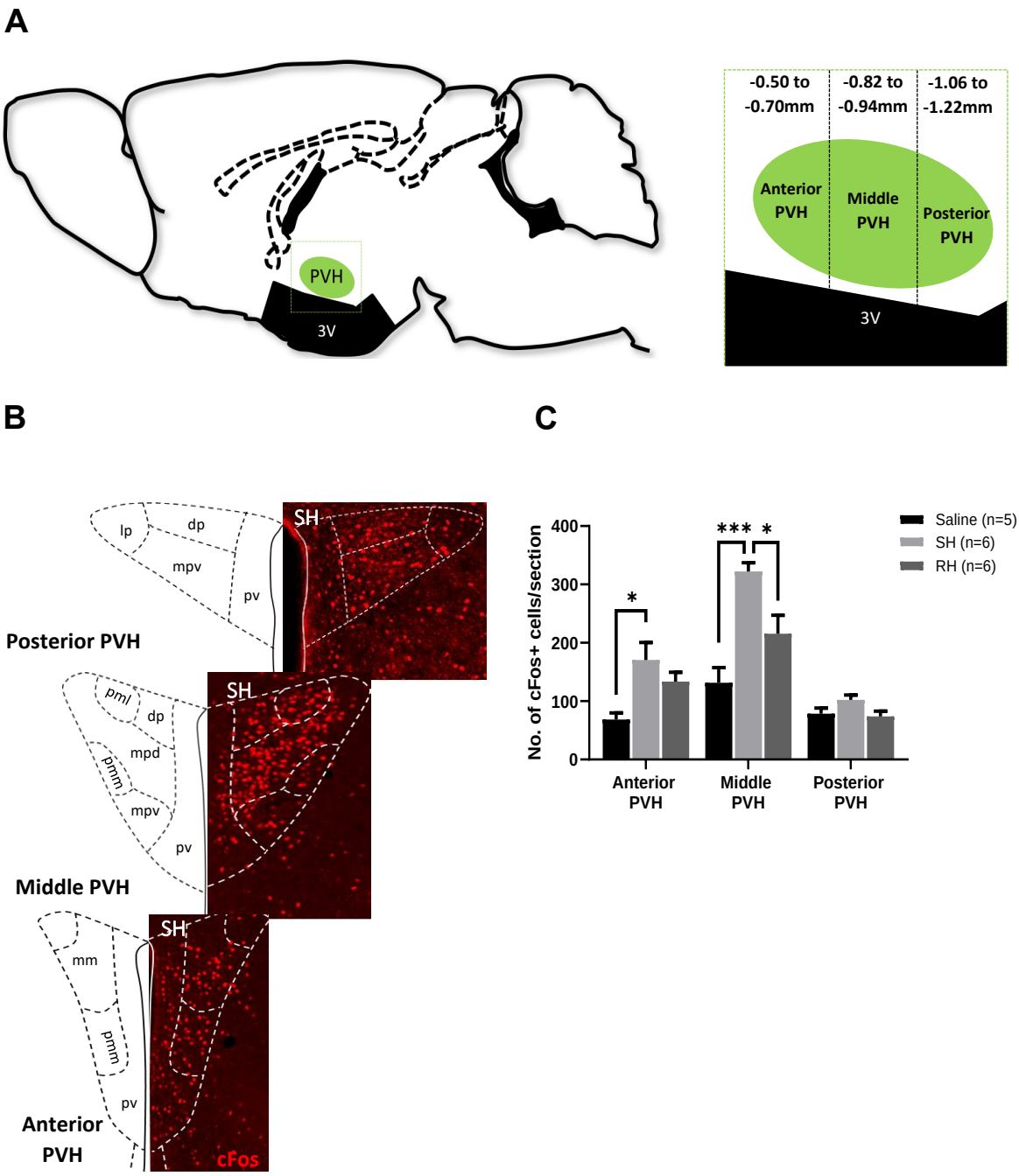

Figure 3.17: Neuronal cFos response within PVH sub-regions

A: Diagram to show rostro-caudal anatomical sub-regions in the PVH along with distance from bregma in the mouse brain.
B: Representative images of cFos-labelled neurons in PVH sub-regions following SH. An overlay of the aPVH, mPVH and pPVH sub-divisions is shown.
C: Number of cFos-labelled neurons in PVH sub-regions, following saline, SH and RH. Neuronal cFos was expressed at high levels in all PVH sub-regions following SH, when compared with saline (***p<0.001, mPVH; *p<0.05, aPVH; one-way ANOVA with Tukey's *post hoc* test). In RH mice, cFos induction was significantly reduced only in the mPVH (*p<0.05, RH versus SH; one-way ANOVA with Tukey's *post hoc* test).
Data presented as mean ± SEM. n=6 animals. n = 3-10 sections per animal, averaged.

pml: The posterior magnocellular lateral zone; **mpd:** medial parvocellular dorsal division **mpv:** medial periventricular; **pmm:** posterior magnocellular medial zone; **pv:** periventricular zone; **dp:** dorsal parvicellular

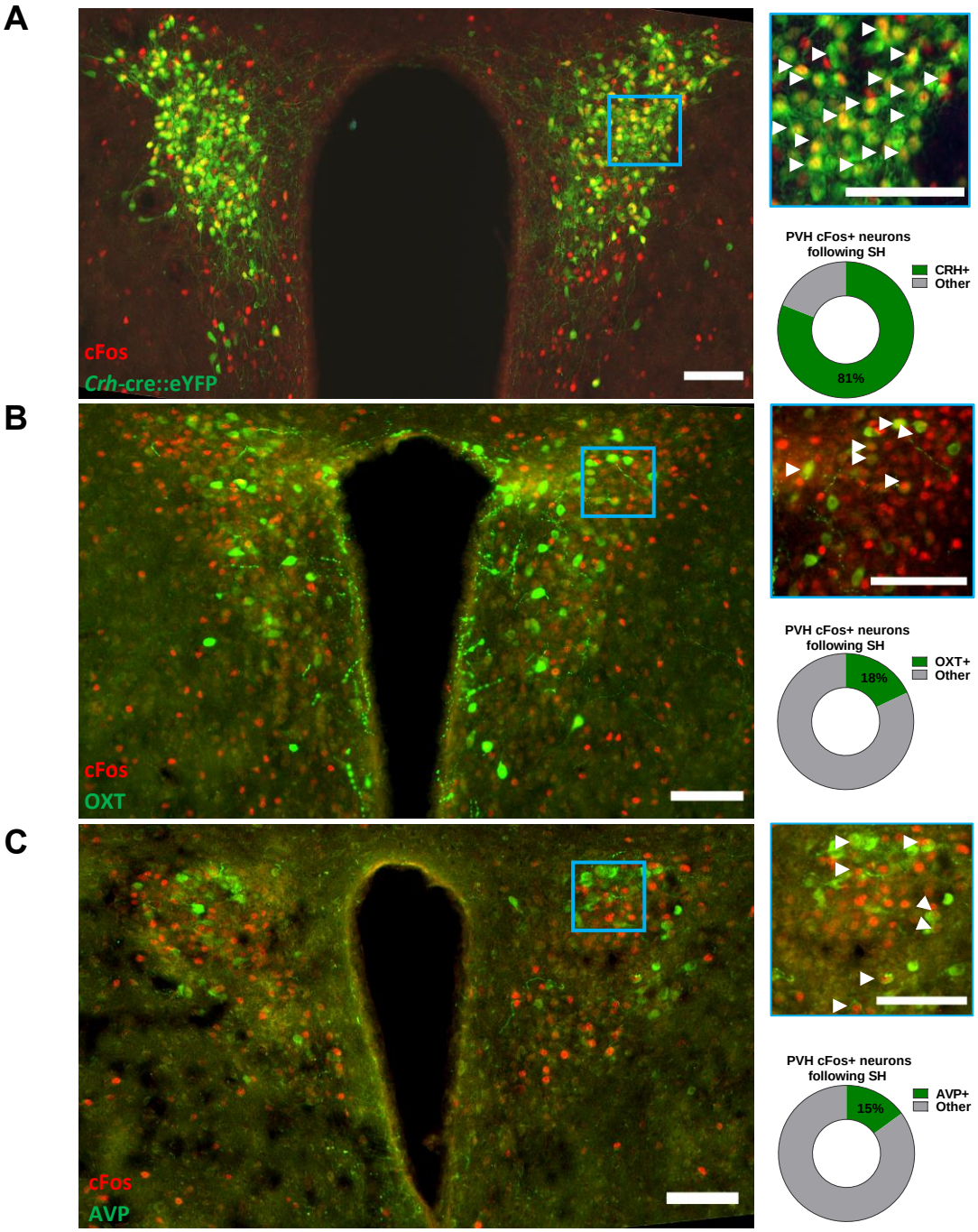

Figure 3.18: Neuropeptide phenotype of activated mPVH neurons following SH

A: Representative images of cFos- and *Crh*-cre::eYFP-labelled neurons in mPVH following SH. The plot adjacent to image shows 81% of cFos+ neurons colocalise *Crh*-cre::eYFP.
B: Representative images of cFos- and OXT-labelled neurons in mPVH following SH. Plot adjacent to image shows 18% of cFos+ neurons colocalise OXT.
C: Representative images of cFos- and AVP-labelled neurons in mPVH following SH. Plot adjacent to image shows 15% of cFos+ neurons colocalise AVP.
Main image scale bar represents 100 µm, magnified image 50 µm. Arrows mark dual-labelled neurons.
Data presented as mean ± SEM. n=4 animals. n = 3 sections per animal, averaged.

3.3.7 Neuro-anatomical distribution of CRH^{PVH} neurons

A large proportion of cFos-expressing neurons in the PVH colocalise with CRH neurons. Therefore, next I investigated the rostro-caudal distribution of CRH neurons in the PVH (**Figure 3.19**). This was again performed in the same cohort of *Crh*-cre::eYFP mice, through single-labelling of *Crh*-cre::eYFP neurons using GFP antibody. CRH neurons were identified throughout the rostro-caudal extent of the PVH, but the highest number was in the middle PVH (250 ± 14 CRH neurons/section) (**Figure 3.19B**).

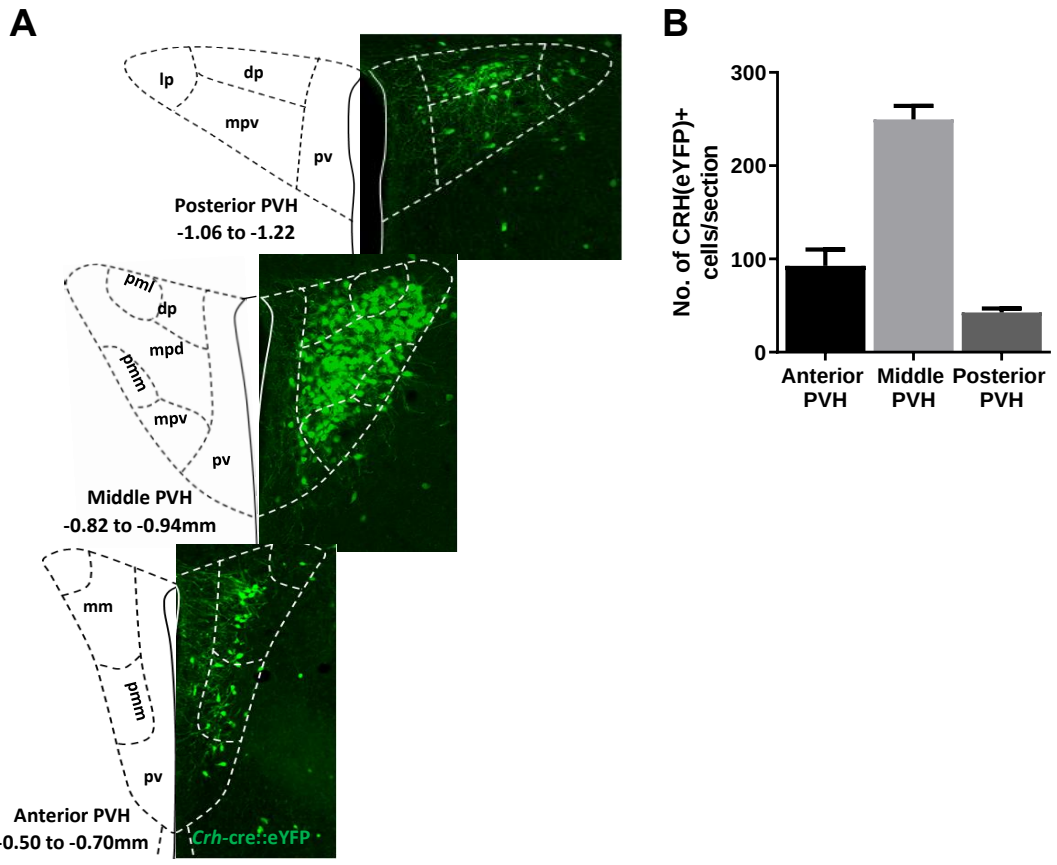

Figure 3.19: Distribution of CRH neurons within PVH sub-regions

A: Representative images of *Crh*-cre::eYFP neurons in the PVH sub-regions. An overlay of the aPVH, mPVH and pPVH sub-divisions is also shown.
B: Number of *Crh*-cre::eYFP-labelled neurons in PVH sub-regions, demonstrating that the mPVH contains the greatest number of neurons.
Data presented as mean ± SEM. n=6 animals. n = 3-10 sections per animal, averaged.

pml: The posterior magnocellular lateral zone; **mpd:** medial parvocellular dorsal division **mpv:** medial periventricular; **pmm:** posterior magnocellular medial zone; **pv:** periventricular zone; **dp:** dorsal parvicellular

3.3.8 Characterising cFos and FosB expression in CRH^{mpdPVH} neurons

The mPVH itself contains sub-divisions (**Figure 3.20A**) which are based on observations that different PVH neuronal populations show anatomical segregation (Biag et al., 2012). Our data revealed that the medial parvocellular dorsal division (mpd) of the PVH (**Figure 3.20B**) contained the greatest number of CRH neurons (142 ± 9 CRH neurons/section). Notably, all other sub-divisions contain markedly fewer CRH neurons. CRH^{mpdPVH} neurons are highly responsive to SH, with 73% expressing cFos (**Figure 3.20C,D**). Importantly, the percentage activation of CRH^{mpdPVH} neurons was attenuated in RH mice (**Figure 3.20D**).

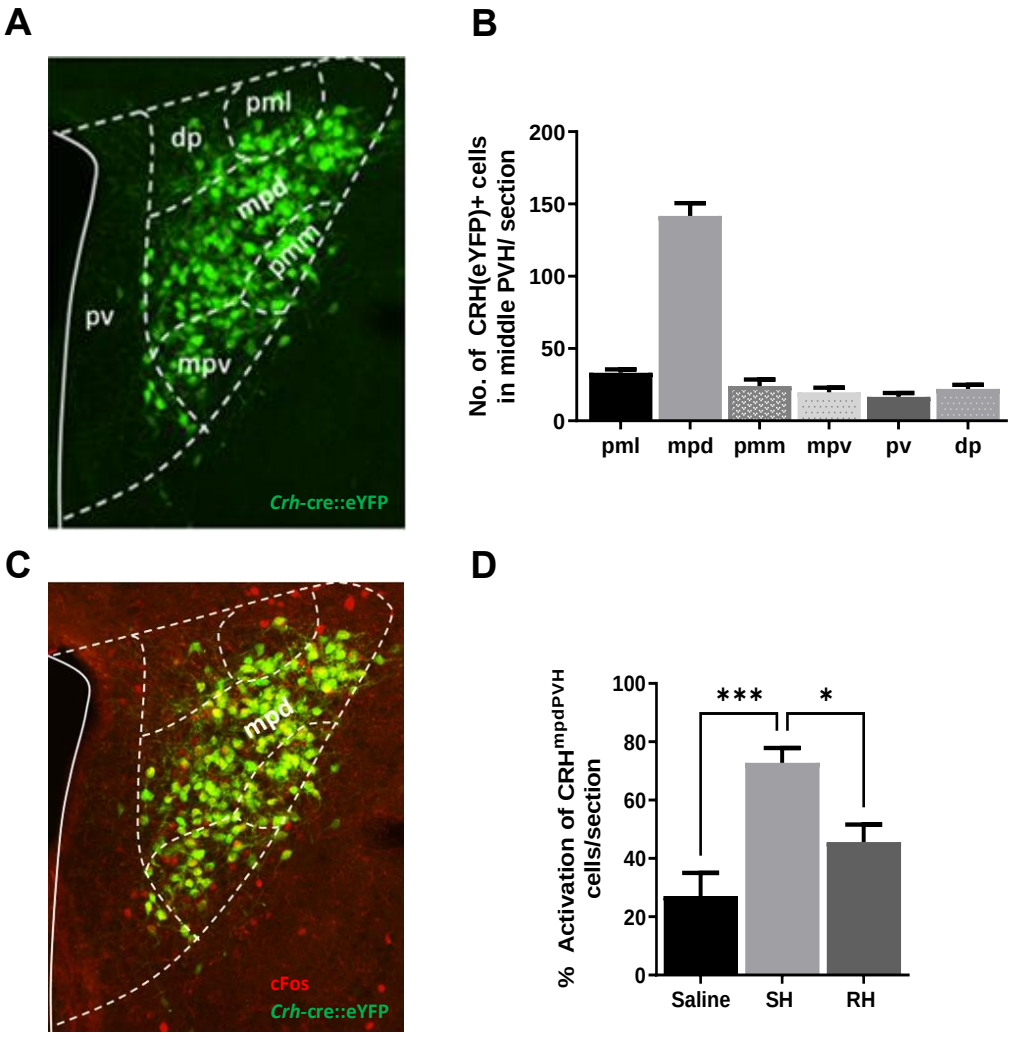

Figure 3.20: Distribution of SH-responsive CRH neurons within PVH sub-divisions

A: Representative image of *Crh*-cre*::*eYFP neurons in the mPVH.
B: Number of *Crh*-cre::eYFP-labelled neurons in mPVH sub-divisions, demonstrating that the mpdPVH subdivision contains the greatest number of *Crh*-cre::eYFP-labelled neurons.
C: Representative image of cFos and *Crh*-cre*::*eYFP neurons in the mPVH,
D: Percentage activation of CRH^{mpdPVH} neurons (cFos+/ *Crh*-cre::eYFP+ neurons), demonstrating a significant increase in activation following SH RH mice display reduced activation of CRH^{mpdPVH} neurons relative to SH (***p<0.001, SH versus saline; *p<0.05, SH versus RH; one-way ANOVA with Tukey's *post hoc* test).
Data presented as mean ± SEM. n= 5/6 animals/group. n = 3 sections per animal, averaged.

Similarly, colocalization of CRH^{mpdPVH} neurons with cFos was significantly increased following SH and this increase was attenuated following RH (**Figure 3.21A,C**). Repeated activation of CRH^{mpdPVH} neurons following RH was next assessed by the induction of FosB (**Figure 3.21B**). A low level of FosB was seen in CRH^{mpdPVH} neurons following saline and SH. However, with RH, FosB activity was significantly increased, when compared with saline and SH (**Figure 3.21D**). Interestingly, 86% of CRH^{mpdPVH} neurons express FosB following RH. This suggests that CRH^{mpdPVH} neurons are the predominant neuronal population within the PVH which expresses FosB following RH.

Taken together, the cFos and FosB data support the importance of CRH neurons and particularly those within the mpdPVH in neuronal responses to hypoglycaemia. These data suggest that CRH^{mpdPVH} neurons are the largest PVH neuronal population to become acutely activated by hypoglycaemia. Of significance, was the finding that the CRH^{mpdPVH} neuronal response is attenuated with prior RH, corresponding with an increase in FosB, a marker of neuronal adaptation (Al-Noori et al., 2008b).

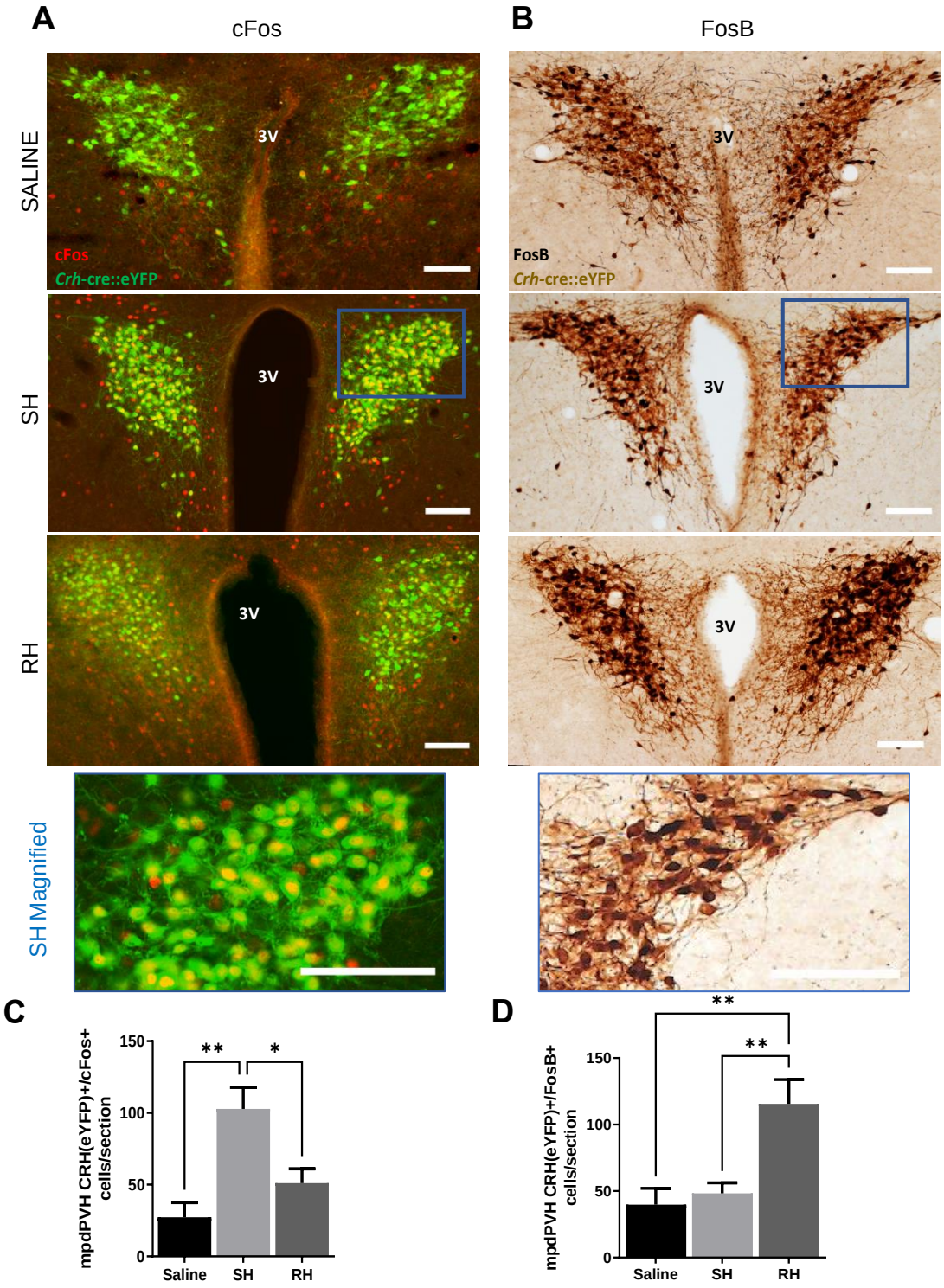

Figure 3.21 cFos and FosB expression in CRH^{mpdPVH} neurons, following saline, SH and RH

A: Representative images of dual-labelled cFos (red) and *Crh*-cre::eYFP (green) neurons (IHC with fluorescent antibodies), following saline, SH and RH.

B: Representative images of dual-labelled FosB (black) and *Crh*-cre::eYFP (brown) neurons (IHC with DAB), following saline, SH and RH.

C: Number of colocalised *Crh*-cre::eYFP and cFos neurons in the mpdPVH, showing attenuation in activated *Crh*-cre::eYFP neurons following RH (*p<0.05, RH versus SH; one-way ANOVA with Tukey's *post hoc* test).

D: Number of colocalised *Crh*-cre::eYFP and FosB neurons in the mpdPVH, showing a significant increase in labelled *Crh*-cre::eYFP neurons following RH (**p<0.01, RH versus SH; one-way ANOVA with Tukey's *post hoc* test).

Main image scale bar represents 100 µm, magnified image 50 µm.

Data presented as mean ± SEM. n=5/6 animals per group. n = 3-10 sections per animal, averaged.

3.4 Discussion

The focus of this Chapter has been, firstly, to characterise a mouse model of IAH using experimental RH and, secondly, using this model to investigate neuronal responses to acute and repeated stimulation in specific brain regions.

3.4.1 Characterising a mouse model of IAH

A variety of experimental protocols of RH been described in the literature, with varying degrees of success (Senthilkumaran et al., 2016, Sankar et al., 2020). In humans and rats, CRR impairment to RH has been commonly achieved using between 1 and 5 antecedent episodes (Flanagan et al., 2003, Evans et al., 2001, Al-Noori et al., 2008b). In our hands, a shorter 2-day experimental RH protocol resulted in elevated hormone release, when compared to SH. One interpretation for this is that with fewer antecedent hypoglycaemia episodes, mice display a sensitised response to a subsequent episode of hypoglycaemia. Whereas, adaptation or habituation of the response requires a greater frequency or number of antecedent episodes of hypoglycaemia. Consistent with this, following a 5-day RH protocol, the glucose response (AUC) was significantly attenuated by the final day **Figure 3.1**. Unfortunately, adrenaline measurement was not possible in this experiment, however, there was a trend towards attenuated glucagon and corticosterone release in the RH group. Protocols with a larger number or more frequent antecedent episodes of hypoglycaemia lead to more profound hypoglycaemia and CRR impairment (Powell et al., 1993, Moheet et al., 2014, Davis et al., 1997), though it is not clear whether the total number of episodes or the frequency of episodes is the prevailing driver for CRR impairment. To this end, we employed a longer, 4-week RH protocol, with a greater number of antecedent episodes of hypoglycaemia.

In this 4-week RH protocol, glucose responses in mice receiving RH were modified during the protocol. Specifically, recovery to baseline glucose levels took longer as the 4-week protocol proceeded, with corresponding reductions to the glucose profile AUC (**Figure 3.3D**). Similarly, in a 4-week RH protocol in rats, investigators noted that the insulin dosage needed to be reduced at week 3, to prevent the development of life-threatening hypoglycaemia (McNeilly et al., 2017). Longer protocols have the benefit of providing the opportunity for animals to habituate to other stressors associated with the protocol. Injection, blood sampling and handling of animals are all sources of stress, which may interfere with the detection of hypoglycaemia-specific changes (Balcombe et al., 2004). This may explain our own observation with short experimental RH protocols, and some of the variation reported in the literature.

The experimental end point in our model was the measurement of glucose and hormone responses to subsequent hypoglycaemia. We were particularly interested in identifying changes in the sympathoadrenal response, which is vital for the generation of autonomic symptoms to hypoglycaemia (Cryer, 2013). Though sympathoneural activation is more important in generating autonomic symptoms than the adrenomedullary system, both arms of the sympathoadrenal response increase in parallel during hypoglycaemia (DeRosa and Cryer, 2004). Therefore, adrenaline levels, which reflect adrenomedullary system activation, provide the most technically accessible and accurate measure of the sympathoadrenal response (McNeilly and McCrimmon, 2018). In the 4-week experimental protocol, RH led to a blood glucose nadir at 30 min of 3.8 ± 0.4 mmol/l, whereas this was 4.4 ± 0.2 mmol/l in SH mice (**Figure 3.4A**). Despite this apparent greater hypoglycaemic stimulus, analysis of adrenaline and glucagon responses revealed that both were attenuated following RH, compared with SH (**Figure 3.4B,C**). Importantly, the change in adrenaline (0-30 min) was significantly attenuated with RH compared with SH, representing a 56% reduction in release. Studies in humans and rats report reductions in adrenaline of 40-50% following RH (Senthilkumaran et al., 2016). As autonomic symptom measurement is technically challenging in animals, it is not possible to define a level of hormone impairment which might signify IAH. In addition, IAH is a spectrum in patients. Therefore, any level of CRR impairment could be of significance to sufferers if this translates to impaired autonomic symptoms.

Though glucagon responses were reduced, they were not significantly different following RH, when compared with SH. The difference may have become statistically significant with increased numbers of mice. However, this finding may be related, instead, to the segregation of patterns of hormone release dependent on the depth of antecedent hypoglycaemia. Davis *et al.,* reported that hypoglycaemia of 3.9 mmol/l during antecedent episodes, led to reduced plasma adrenaline and glucagon responses to subsequent hypoglycaemia. Whereas, with blood glucose levels of <3.3 mmol/l a more significant reduction in glucagon, adrenaline, noradrenaline and growth hormone occurred with subsequent hypoglycaemia (Davis et al., 1997). We can postulate that protocols which lead to deeper hypoglycaemia, may yield greater CRR impairments to both adrenaline and glucagon release. However, this would require increased insulin doses, which may be injurious to animals and not translate to the clinical condition.

It is also possible that, as central and peripheral networks controlling adrenaline and glucagon release are largely distinct, adaptation to RH will also differ between the two pathways. In support of this, is the finding that experimental RH protocols in humans and rodents consistently achieve impairment of adrenaline release, but this is much more inconsistent for glucagon (Sankar et al., 2020, Senthilkumaran et al., 2016).

By modelling a human condition in mice, we must acknowledge physiological differences in glucose homeostasis across species. Examples include a much higher basal metabolic rate and endogenous insulin production in mice, when compared with both humans and rats (Kleiber, 1947, Kowalski and Bruce, 2014). With respect to the endocrine CRR, glucose thresholds for glucagon secretion (<4 mmol/l), but not adrenaline, are conserved across species (Malmgren and Ahrén, 2015). Interestingly, in chronically cannulated mice, a blood glucose of < 4.4mmol/l was sufficient to increase adrenaline release, whereas in humans the reported threshold is 3.3-3.9 mmol/l (Jacobson et al., 2006, Schwartz et al., 1987). Reassuringly, sympathoadrenal response impairment, which we have taken as a defining hallmark of IAH, is observed following RH in humans, rats and mice. This suggests that animal models can provide a good representation of the human condition.

There are improvements that could be made to our mouse model of IAH. It is likely that using chronically cannulated mice, combined with a hypoglycaemic clamp would ensure precise hypoglycaemia thresholds are reached. This would likely reduce variability in glucose and hormone measurements. However, this is technically more challenging and may be less adaptable to the various methods used to understand neuronal circuitry, which is the main aim of this thesis. Another potential area of improvement, is in limiting stress related to handling, restraint, blood sampling and environment (Nonogaki, 2000). In our mouse model of IAH, all mice were habituated to handling and restraint stress by daily handling for 2 weeks prior to initiation of injections. In addition, all measurements were conducted in the same environment and at the same time of day. Despite this, further steps to limit stress may be possible.

Here, we have focused on an IAH model which demonstrates sympathoadrenal response impairment. However, animal models which measure hypoglycaemia symptoms or behaviours would be a compelling alternative. Interestingly, feeding responses to insulin-induced hypoglycaemia have proven to be a poor measure of hypoglycaemia-induced hunger and do not appear to be blunted with prior RH (Sanders et al., 2006). One approach in rodents was to develop a conditioned place preference (CPP) behavioural model of IAH. In this model, a CPP is first induced through an appetitive reward. This CPP is then blunted with the negative perception of SH, reversing the reward conditioning. Rats exposed to prior RH are no longer ‘aware’ of the negative valency of a subsequent hypoglycaemic episode and the CPP is preserved (Otlivanchik et al., 2016).

Ultimately findings from non-diabetic disease models must be demonstrated in a diabetic model to fully relate to the clinical condition. However, it is reassuring that significant

mechanistic insights have been gained through understanding how RH affects physiology in the non-diabetic state.

3.4.2 Neuronal cFos and FosB response within specific brain regions

Hypoglycaemia leads to an immediate and stereotyped neuronal response within the glucose-regulatory network, which can be detected with activity markers. However, it is not fully understood how repeated activation of neurons with RH, alters neuronal activity to subsequent hypoglycaemia (Verberne et al., 2014, Paranjape and Briski, 2005). This question was investigated in specific forebrain (CeA, BNST, PVT and PVH) and hindbrain regions (DMX, NTS, LC, VLM), which are important integrative and pre-motor regions within the glucose-regulatory network (Donovan and Watts, 2014, Watts and Donovan, 2010). These regions may form an interconnected neuronal network, which adapts following RH. We hypothesised that RH would lead to a reduction in acute activity markers, but increases in adaptive markers in specific brain regions. We were particularly interested in characterising the anatomical profile of CRH^{PVH} neurons, which are known to adapt to repeated stressors.

In this experiment, the expression of cFos and FosB was quantified following saline, SH or RH using the same 4-week RH protocol developed to model IAH. In this experiment, the induction of cFos identified neurons which are acutely activated to hypoglycaemia. Following saline, cFos was expressed at very low levels and its expression increased following SH in regions of interest. This was expected and has been well documented in the literature (Al-Noori et al., 2008b, Foster et al., 2016, Niimi et al., 1995, Meek et al., 2016, Paranjape and Briski, 2005). Interestingly, with RH, cFos induction was attenuated in the PVH, VLM, NTS and to a lesser extent the aBNST (**Figures 3.5C** and **Figure 3.6B**). RH, as well as repeated glucoprivation with 2-DG, has been shown previously to attenuate cFos within components of the glucose-regulatory network, including the PVH, NTS and VLM (Al-Noori et al., 2008b, Paranjape and Briski, 2005, Sanders and Ritter, 2000). Hindbrain cFos expression was found prominently in catecholaminergic (CA) neurons in the LC, NTS and VLM. Consistent with the literature, CA cell groups in the NTS (C2 group) and rVLM (C1 group) showed a significant attenuation in cFos expression following RH (Sanders and Ritter, 2000).

Strikingly, it was observed that RH augmented the acute neuronal response in the CeA to a subsequent episode of hypoglycaemia. This has not been shown previously in the literature. However, McNay *et al.* demonstrated that rats exposed to RH have elevated noradrenaline in the amygdala and display increased anxiety following subsequent hypoglycaemia (McNay, 2015). In the current experiment, the PVT was found to display

moderate levels of cFos following saline, SH and RH, with RH leading to the most significant number of activated neurons. This contrasts with findings in rats exposed to shorter, 4-5-day RH protocols (Paranjape and Briski, 2005, Al-Noori et al., 2008b). Here, I found cFos induction varied between PVT subregions, with substantially more cFos expressed in the aPVT compared to the pPVT. Interestingly, it is known that different sub-regions within the PVT have distinct functions and respond differently to the same acute stimulus. Indeed, separate investigators have shown differential behaviour (food consumption) contingent on whether the manipulation was to the aPVT or pPVT (Bhatnagar and Dallman, 1998, Do-Monte et al., 2017, Stratford and Wirtshafter, 2013).

The induction of neuronal FosB was also quantified in the same regions. FosB has a slower onset of expression, longer half-life and can identify cells which are either repeatedly activated or which display adaptation. For example, there is a large literature on the potential role for FosB in adaptations in the mesolimbic system during the development of drug dependence (Lobo et al., 2013, Kaplan et al., 2011, Nestler et al., 2001). FosB expression levels were low in saline and SH groups in all brain regions. When compared with SH, RH led to an increase in neuronal FosB in brain regions of interest, apart from the DMX. FosB has been studied infrequently in the context of hypoglycaemia. The only study of direct relevance was by Al-Noori *et al.,* which reported similar findings of raised FosB following RH in the rat PVH, VMH and DMH, when compared with SH (Al-Noori et al., 2008b). Also, only the pPVT was found to display increased FosB expression after RH, when compared with saline, but not SH (Al-Noori et al., 2008b). These findings match our own sub-region analysis of the PVT, identifying that pPVT neurons show adaptive changes to RH. The pattern of cFos and FosB expression following RH is interesting, as the PVT has a known role in modulating the neuroendocrine response to repeated stressors (e.g., restraint) (Bhatnagar et al., 2002, Al-Noori et al., 2008b). Also, inactivation of the PVT with lidocaine infusions in rats subjected to RH, prevents CRR impairment compared with SH (Al-Noori et al., 2008a). Similarly, in humans, positron emission tomography (PET) imaging studies show that the dorsal midline thalamus (the equivalent region to include the PVT) displays increased activity in patients with impaired CRR following RH, as compared with controls (Arbelaez et al., 2008, Arbelaez et al., 2012). The role of the PVT in responses to repeated stressors will be examined in greater detail in Chapter 7.

The acute and longer-term neuronal response in the CeA and BNST to RH has not been characterised before. In fact, the CeA has not previously received much attention relating to hypoglycaemia. However, in PET imaging studies, the amygdala was found to display attenuated labelled glucose uptake following hypoglycaemia in patients with IAH (Dunn et al., 2007). This, in effect, suggests altered activation to repeated stressors like RH.

Following non-hypoglycaemic stressors, such as chronic opioid and restraint stress, the CeA expresses increased FosB (Kaplan et al., 2011, Perrotti et al., 2004). Also, in rats exposed to chronic restraint stress, CeA cFos expression is increased following a novel stressor, compared with undisturbed rats experiencing the same novel stressor (Hoffman et al., 2014). Therefore, consistent with the experiments in this Chapter, CeA neurons appear to demonstrate increased activation, particularly in the setting of repeated stressors. The aBNST, like the CeA, has important roles in affective and behavioural processing of stressors. It is also well documented to participate in autonomic responses to stress and is involved in glucose counter regulation via VMH neurocircuits (Perrotti et al., 2004). In rats, the aBNST also expresses cFos following SH and to a lesser extent with RH (not significantly different), corroborating findings outlined in this Chapter (Paranjape and Briski, 2005).

Neurons in the PVH displayed the highest levels of cFos and FosB expression after SH and were investigated further. Analysis of PVH regions revealed that the middle PVH (mPVH, bregma -0.82 to -0.94 mm) contained the largest number of cFos-labelled neurons, suggesting this region is highly responsive to hypoglycaemia. Interestingly, we found that after SH, the majority (81%) of cFos-expressing mPVH neurons were contained CRH. Further anatomical characterisation of the mPVH, revealed that most CRH neurons are concentrated within the medial parvocellular dorsal division (mpd), which is corroborated by other investigators (Biag et al., 2012). Interestingly this anatomical distribution differs in rats (Aguilera and Liu, 2012). Following RH, CRH^{mpdPVH} neurons show reduced cFos expression, but an increase in FosB expression. The effect size was greater for FosB, with over 86% of CRH^{mpdPVH} showing adaptation with RH. Collectively, these results suggest a particularly important role for CRH^{mpdPVH} neurons in adaptations to RH. In Chapters 4 and 5, I will characterise the *in vivo* activity of CRH^{mpdPVH} neurons during hypoglycaemia and their functional significance to the hypoglycaemia CRR.

In agreement with my findings, Foster *et al.,* demonstrated that SH increases cFos expression in the PVH, whilst Evans *et al.,* identified a decrease in PVH cFos expression in rats following RH (Evans et al., 2001, Foster et al., 2016). Increased co-expression of CRH with cFos, has been noted previously in the PVH of rats (Al-Noori et al., 2008b). Additionally, PVH *Crh* mRNA synthesis is reduced by other repeated stressors, such as repeated restraint, such that subsequent exposure results in decreased *Crh* mRNA synthesis (Ma et al., 1997). We can, therefore, postulate that with RH, akin to other repeated stressors, CRH^{PVH} neurons become less active, which may in turn contribute to impairments in the hypoglycaemia CRR.

Responses to FosB were more consistent across brain regions, with increased expression following RH. The exception being the DMX, which expresses high levels of neuronal cFos, but no FosB in the conditions observed. This was a surprising finding and could be interpreted as a sign that DMX neurons might not adapt to RH. Alternatively, it could be that DMX neurons may not express FosB, instead relying on other regulatory or adaptive proteins. This is evidenced by the fact that a much smaller number of neurons in each of the brain regions assessed, express FosB. This may indicate that neuronal populations which express FosB are particularly important in understanding glucose-regulatory network changes which follow RH.

FosB accumulation may not only indicate neurons which are repeatedly activated, it may be of mechanistic significance in neuronal adaptations to repeated stressors, like RH. FosB, like other members of the Fos family of transcription factors, can regulate its own expression and drive gene transcription, important for neuronal function (Hoffman et al., 1993). FosB and its splice variant, ΔFosB, accumulate following a variety of repeated stimuli including opiates, antipsychotic drugs, psychological stress and restraint, potentially altering behaviours on re-exposure to the same stimuli (Lobo et al., 2013, Perrotti et al., 2004, Nestler et al., 2001). Interestingly, ΔFosB has also been shown to modulate synaptic properties, and its over expression decreases excitatory synaptic strength (Grueter et al., 2013). Indeed, neuronal plasticity - the ability for a neuron to change in form and function, can be characterised by changes in the expression of key transcription factors following a chronic or repeated stimulus (Corbett et al., 2017). We can postulate that RH leads to lower cFos expression, and in combination with FosB/ ΔFosB accumulation, alters neuronal function to a subsequent episode of hypoglycaemia.

3.5 Summary of results

- A 4-week experimental RH protocol in mice recapitulates the key feature of IAH – the impaired sympathoadrenal response.
- Multiple brain regions are acutely activated following SH, but display different patterns of activity following RH.
- Following RH, a small number of regions display an increase in a marker of repeated or adaptive neuronal activity, which may signify habituation.
- PVH neurons display a high level of acute activity following SH, and an adaptive marker following RH.
- The majority of SH-activated PVH neurons are located in the middle PVH region and 81% contain CRH.
- Most SH-activated CRH neurons are located within the mpdPVH region
- RH attenuates cFos in CRH^{mpdPVH} neurons and, concurrently, enhances FosB relative to SH.

3.6 Conclusion

Collectively, these data show that a 4-week experimental RH protocol adapted from rats, can be effectively applied in mice and provides a disease model for IAH. Also, this experimental RH protocol, replicates the pattern of neuronal responses to SH and RH reported in rats. However, my investigations have added a further layer of detail, by exploring specific neuronal populations within the glucose-regulatory network. The key finding was that RH attenuates the acute neural response but leads to enhanced adaptive neuronal changes. Importantly, these observation were not global and only present in specific neuronal loci. This was particularly true for CRH^{mpdPVH} neurons. CRH^{mpdPVH} neurons are believed to receive indirect connections from the PVT, an area identified to maintain high levels of activity following RH (Herman and Tasker, 2016). Important relay points between the PVT and PVH include the CeA and aBNST, which are both capable of regulating the activity of the PVH and importantly CRH neurons (Keifer et al., 2015). A neuronal circuit involving the above regions may be key to the CRR following SH and RH. However, more functional and connectivity studies are required to establish this. Adaptation of neurons within this network and possibly habituation is postulated to follow RH and will be investigations in Chapter 4.

Chapter 4

Does IAH have the characteristics of habituation?

4.1 Introduction

In Chapter 3, I provide evidence that neurons within the glucose-regulatory network show changes in neuronal markers (altered cFos and FosB induction) following RH, which we hypothesise signify neuronal adaptation.

Recently, the adaptation occurring in the glucose-regulatory network which follow RH, and which culminate in IAH, have been described as habituation. Habituation is a non-associative form of learning and refers to a reduction in the psychological, behavioural or physiological response to a stimulus as a result of repeated or prolonged exposure (Thompson and Spencer, 1966). Habituation, though often witnessed during non-threatening repeated stimuli, has also been observed to threatening stimuli. Examples across species include habituation of the defensive gill and siphon withdrawal response in the *Aplysia,* the predator escape response in several species and the nociception backwards escape response in *C.elegans* (Ardiel et al., 2016, Pinsker et al., 1970, Ardiel et al., 2017). This suggests that habituation can prove to be maladaptive in some scenarios, hindering survival of the organism. This may be true for patients with IAH, where habituation of the hypoglycaemia CRR becomes maladaptive and is detrimental to health. Habituation, in its most classical description, possesses nine defining features, which can be tested in the context of IAH (Thompson and Spencer, 1966, McCrimmon, 2017).

1) Repeated applications of a stimulus results in a decreased response

It can be seen that this feature holds true as antecedent RH impairs the CRR and symptoms to subsequent hypoglycaemia in humans (Heller and Cryer, 1991). I have replicated this observation to characterise a mouse model of IAH using experimental RH (Chapter 3).

2) If the habituating stimulus is withdrawn, the response spontaneously recovers over time

This has been demonstrated in patients with IAH, as strict avoidance of hypoglycaemia can recover the CRR and symptom awareness (Cranston et al., 1994, Fanelli et al., 1993). Hypoglycaemia avoidance, which is a cornerstone in the clinical management of patients with IAH, remains challenging despite advances in insulin formulations and technology (Choudhary and Amiel, 2018). Response recovery will be examined in this Chapter and in Chapter 5.

3) Following repeated habituation and then recovery, habituation becomes successively more rapid

This hallmark has also been described as the potentiation of habituation. Although direct evidence for this feature in patients with IAH is lacking, it suggests that recovered (previously habituated) neurons may retain a memory of prior hypoglycaemia, such that habituation returns more rapidly in the future. In Chapter 3, I showed evidence of changes in adaptive genes (FosB) following RH, pointing to cellular mechanisms which may allow quicker reinstatement of habituation following periods of recovery.

4) An increased frequency of stimulation produces more pronounced habituation

There is evidence from experiments in humans and rodents that increasing the frequency, as well as the total number of antecedent hypoglycaemic episodes, leads to greater impairments to the CRR (Powell et al., 1993, Moheet et al., 2014, Davis et al., 1997). In Chapter 3, I showed that in our mouse model of RH, there is a greater depth and duration of hypoglycaemia with successive antecedent hypoglycaemic episodes.

5) Weaker stimuli produce more rapid and/or pronounced habituation

The effect of antecedent hypoglycaemia depth on the development of IAH has not been directly studied in humans. In Chapter 3, I showed that even a mild RH stimulus is sufficient to impair the CRR, though this required a larger number of antecedent hypoglycaemia episodes. On the other hand, studies in rats show that increasing the depth of hypoglycaemia produces more widespread CRR hormone impairments (Davis et al., 1997). This suggests that deeper antecedent hypoglycaemia may precipitate IAH faster. Although the exact kinetics remain unclear, habituation of a response appears to vary depending not only on actual, but the perceived severity, alongside the nature of stimulus that is applied (Belda et al., 2015, Armario et al., 2004).

6) The effects of habituation may proceed beyond the zero level

This suggests that even if the habituated response is reduced to a minimal or zero level, the response remains habituated for as long as the stimulus is present. This feature has been shown to be true in rodents with profoundly suppressed CRR following RH (Powell et al., 1993).

7) Habituation to a given stimulus can become generalized to other stimuli

This feature has been indirectly explored in cross-tolerance experiments which show that prior moderate exercise exposure suppressed the CRR to subsequent hypoglycaemia (Galassetti et al., 2001). Similarly the catecholamine release following a cold pressor

test was reduced in patients with type 1 diabetes with presumed prior hypoglycaemia, compared with healthy volunteers (Kinsley et al., 1994).

8) Presentation of another, heterotypic stimulus results in recovery of the habituated response

Recently, high-intensity exercise and cold stress have been used as heterotypic, dishabituating stimulus in rats exposed to RH, restoring the CRR to subsequent hypoglycaemia (McNeilly et al., 2017, Vickneson et al., 2021). Also important, was a proof-of-concept study in patients with type 1 diabetes which also suggested that high-intensity exercise could improve CRR and symptom responses to subsequent hypoglycaemia (Farrell et al., 2020). Dishabituation, with an alternative heterotypic stimulus will also be examined in this chapter.

9) Habituation of the dishabituating stimulus

This feature has not yet been studied in the context of hypoglycaemia; however, it is of importance when considering the therapeutic application of dishabituation in patients with IAH. Although this is difficult to test, our investigations into alternative repeated stressors in this Chapter suggest that this is likely to be true.

4.1.1 Objectives

In this Chapter, I tested whether classical features of a habituation response (outlined above), are also observed in our mouse model of IAH. The features examined here are also of particular importance in establishing whether there is a specific locus of habituation within glucose-regulatory network (Chapters 5 and 7).

1) Repeated applications of a stimulus results in a decreased response

Our current understanding of mammalian stress habituation largely relies on studies which examine the HPA axis. The HPA axis undergoes habituation to a variety of physiological and psychological stimuli, demonstrating that repeated stressors of differing natures can still habituate (Herman, 2013). However, habituation of the sympathoadrenal response to various repeated stressors has not been characterised to the same level. We have shown that RH, leads to an impaired sympathoadrenal response in Chapter 3. We postulated that this impairment was not specific to hypoglycaemia and that other repeated stressors are also capable of habituating the sympathoadrenal response. To this end, we elected to use a repeated restraint stress protocol. Restraint stress consistently induces habituation of the HPA axis (Bhatnagar et al., 2002) and as we hypothesise the sympathoadrenal response too.

2) **Investigate spontaneous recovery of response on removal of the habituating stimulus**

Removal of the habituating stimulus leads to a 'reset' within the system, leading to response recovery. This has been shown in patients with type 1 diabetes and IAH (Fanelli et al., 1993, Cranston et al., 1994). However, this has not been directly shown in experimental models of IAH. Therefore, I elected to investigate in the mouse model of IAH, whether withdrawal of hypoglycaemia for a period of 4 weeks, leads to spontaneous recovery of the sympathoadrenal response to a subsequent hypoglycaemic episode.

3) **Investigate dishabituation of the RH-related impaired sympathoadrenal response**

A strong heterotypic stress is capable of dishabituation and normalisation of responses to the original homotypic stressor (e.g., hypoglycaemia). Also, the heterotypic stress usually leads to a potentiated response (facilitation) when compared to the homotypic stressor. These features have previously been shown in rodents and humans using cold stress and high-intensity exercise as the dishabituating stimulus (McNeilly et al., 2017b, Vickneson et al., 2021, Farrell et al., 2020). We hypothesise that other strong heterotypic stimuli may also be able to dishabituate the system, leading to recovery of the sympathoadrenal response. This was investigated in our mouse model of IAH, by using the heterotopic stimulus of acute restraint stress and measuring the sympathoadrenal response to a subsequent episode of hypoglycaemia.

4.2 Methods

4.2.1 Animals

All experiments in this Chapter were performed in 8-10-week-old adult male C57BL/6J mice (Charles River, UK). Animals were acclimatised to the holding room and handled daily for 2 weeks prior to each experiment. Group sizes for experiments 1 and 2 were guided by data generated in Chapter 3, which indicated n = 6 would provide sufficient power to detect meaningful differences. The group size for experiment 3 was guided by the literature, which indicated that larger group sizes would be necessary to identify the effect of a dishabituating stimulus on the sympathoadrenal response (McNeilly et al., 2017, Vickneson et al., 2021). Each individual experiment was performed in one cohort/batch of animals to control external factors which may lead to variability with multiple cohorts/batches of animals.

4.2.2 Experiment 1: Repeated applications of a stimulus results in a decreased response

To enable comparisons between the 4-week RH protocol and alternative repeated stressors, a 4-week repeated restraint (RR) protocol was utilised **Figure 4.1C**. Animals were randomised to no restraint (NR), single restraint (SR) and repeated restraint (RR) groups (n = 6 each group). RR group mice underwent restraint stress for 30 min in a clear-acrylic, head-first horizontal restrainer. To mimic the RH protocol, this was carried out three times a week for four weeks. NR and SR groups continued to be handled daily during this period but were otherwise not exposed to any other stimuli.

At the end of this 4-week protocol, RR and SR mice were exposed to 30 min of restraint stress, whilst NR group mice were handled. Adrenaline levels were measured prior to being placed in the restrainer (0 min) and at 30 min after restraint stress, enabling assessment of the sympathoadrenal response. The blood sampling, processing and analysis methods are outlined in detail in the Chapter 2 and apply for all experiments described in this Chapter.

4.2.3 Experiment 2: Response recovery on removal of the habituating stimulus

Animals were randomised to saline, SH and RH (n = 6 each group) and underwent the 4-week RH protocol as outlined in Chapter 2 and Chapter 3. On the final day of the 4-week RH protocol (Test 1), animals received a s.c. injection of insulin (1.75 U/kg) or volume-matched saline, depending on the group. Blood glucose levels were measured for 120 min following injection via tail tip sampling. Adrenaline levels were measured before injection (0 min) and 30 min after injection, enabling assessment of the sympathoadrenal response.

Following this, all mice were allowed to recover for 4 weeks. During this period all animals were handled daily but were not subject to any further episodes of hypoglycaemia, ensuring complete withdraw of the habituating stimulus. At the end of this recovery period, mice received a final s.c. injection of insulin (1.75 U/kg) or volume-matched saline, depending on the group (Test 2). Blood glucose and adrenaline levels were measured again as described before. The experimental design is summarised in **Figure 4.2A**.

4.2.4 Experiment 3: Dishabituation with acute restraint stress

Animals were randomised to saline, SH, RH and RH with acute restraint (RH+AR) groups (n = 11/12 each group). Subsequently all animals underwent the 4-week RH protocol as

outlined in Chapter 2. This protocol was slightly adapted to enable testing of the sympathoadrenal response on two test days, which were at the end of the 4-week RH protocol (**Figure 4.3A**).

Test 1 investigated response habituation to RH and facilitation of the response with restraint (RH+AR). During test 1, mice received a s.c. injection of insulin (1.75 U/kg) or volume-matched saline, depending on the group. In parallel, mice in the RH+AR group received 30 min restraint stress in a restrainer. Adrenaline levels were measured immediately before injection or restraint (0 min), and at 30 min after injection or restraint, enabling assessment of the sympathoadrenal response.

Test 2 investigated response dishabituation to the original homotypic stimulus (hypoglycaemia). During test 2, saline, RH and RH+AR treated mice, underwent a final s.c. injection of insulin (1.75 U/kg) or volume-matched saline, depending on the group. Adrenaline levels were again measured immediately before injection (0 min) and at 30 min after injection.

4.3 Results

4.3.1 Experiment 1: Repeated applications of a stimulus results in a decreased response

In Chapter 3, I demonstrated that a 4-week RH protocol in mice, significantly attenuates the sympathoadrenal response to a subsequent episode of hypoglycaemia (**Figure 4.1A,B**). Next, I investigated whether a different repeated stress could also attenuate the sympathoadrenal response. To parallel the 4-week RH protocol, mice were randomised to no restraint (NR), single restraint (SR) and repeated restraint (RR) groups (n = 6 each group) and underwent a 4-week RR protocol (**Figure 4.1C**). Restraint stress for 30 min led to a significant increase in adrenaline release in SR and RR mice, relative to mice receiving handling only (NR) (**Figure 4.1D**). Importantly, following a final episode of restraint stress, the adrenaline response was significantly attenuated in RR mice relative to SR (43.0% reduction in adrenaline release, following RR, relative to SR) (**Figure 4.1D**). Taken together, these data show that RH and RR are both independently capable of habituating the sympathoadrenal response to subsequent homotypic stress. This adds weight to the argument that it is the repetition of the stress, rather than the type of stress, which leads to habituation of the sympathoadrenal response.

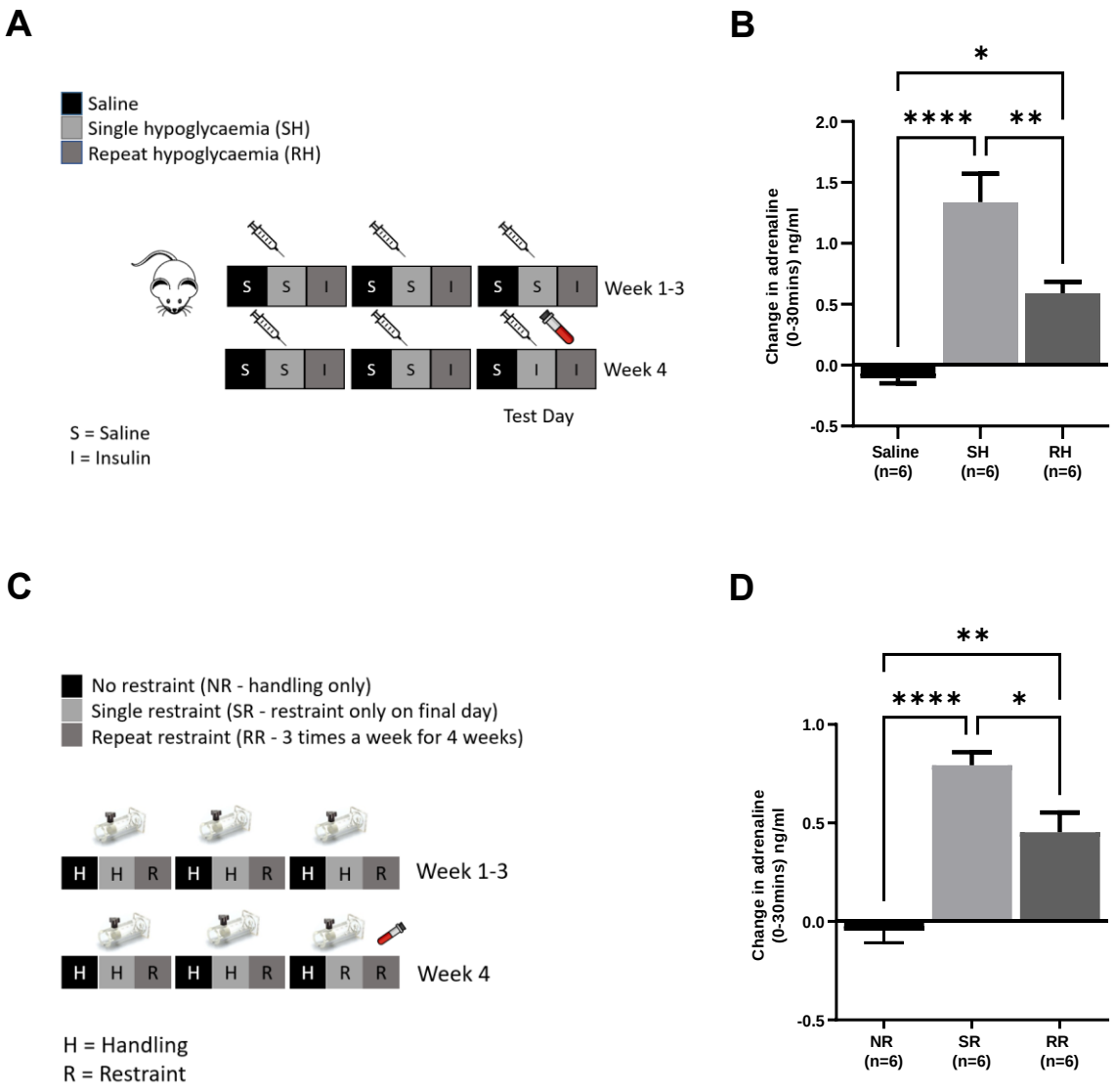

Figure 4.1: Different types of repeated stressors habituate the sympathoadrenal response

A: 4-week RH protocol.
B: Change in adrenaline release (0-30 min) following injection in saline, SH and RH mice. RH led to an increase in adrenaline release when compared with saline, but a significant attenuation in adrenaline release when compared with SH (*p<0.05, RH versus saline; **p<0.01, RH versus SH; one-way ANOVA with Tukey's *post hoc* test).
C: 4-week RR protocol.
D: Change in adrenaline (0-30 min) following a final episode of restraint, showing a significant increase in adrenaline release with SR and RR, compared with NR. In addition, RR mice displayed a significant attenuation in adrenaline release, compared with SR (****p<0.0001, SR versus NR; **p<0.01, RR versus NR; *p<0.05, RR versus SR; one-way ANOVA with Tukey's *post hoc* test).

4.3.2 Experiment 2: Response recovery on removal of the habituating stimulus

Next, I investigated whether withdrawal of the habituating stimulus of RH, for a period of 4 weeks, led to sympathoadrenal response recovery. This feature has been shown to hold true for patients with IAH, however, has not been directly tested in an animal model of RH. The experimental protocol is shown in **Figure 4.2A**.

Successive episodes of RH altered the glucose profile, slowing glucose recovery and normalisation (**Figure 4.2B**). During test 1, the glucose and adrenaline response to s.c. insulin or saline was measured. Insulin injection led to a fall in blood glucose at 30 min (SH: 4.5 $\pm$ 0.2 versus RH: 3.9 $\pm$ 0.1 mmol/l) and corresponding adrenaline release (**Figure 4.2C**). Importantly the adrenaline response was significantly attenuated in RH mice (43.4% reduction in adrenaline release to subsequent episode of hypoglycaemia, RH versus SH) signifying habituation of the sympathoadrenal response (**Figure 4.2D**).

After a 4-week recovery period, where animals were only handled, a final injection of s.c. insulin or saline was administered (test 2). During test 2, s.c. insulin again led to a reduction in blood glucose, reaching a similar nadir in both groups (SH: 4.5 $\pm$ 0.2, RH: 4.3 $\pm$ 0.5 mmol/l). Despite receiving the same s.c insulin dose, the glucose nadir in RH mice was increased, when compared with test 1. Both SH and RH groups demonstrated a robust adrenaline response to s.c. insulin, when compared with saline. Though the adrenaline response in RH mice was still reduced (23.1% reduction in adrenaline release to a subsequent episode of hypoglycaemia, RH versus SH) this was no longer statistically significant when compared with SH mice. Comparison of the adrenaline response in RH mice on test 1 and test 2, demonstrated adrenaline response recovery (77.8% increase from test 1 to test 2) (**Figure 4.2G**). These data confirm that withdrawal of the habituating stimulus of hypoglycaemia for 4 weeks leads to sympathoadrenal response recovery, fulfilling this hallmark of habituation.

A

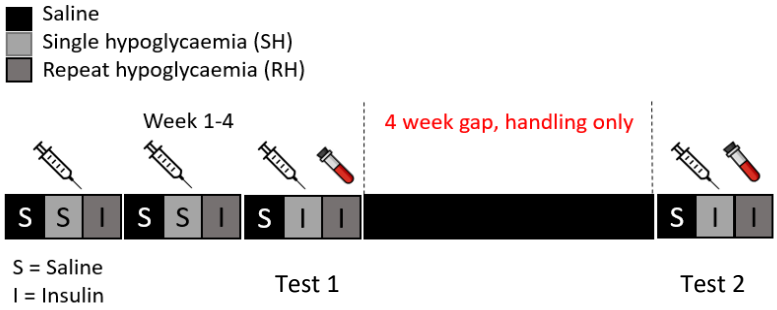
Saline
Single hypoglycaemia (SH)
Repeat hypoglycaemia (RH)
Week 1-4
4 week gap, handling only
S S I S S I S I I S I I
S = Saline
I = Insulin
Test 1
Test 2

B

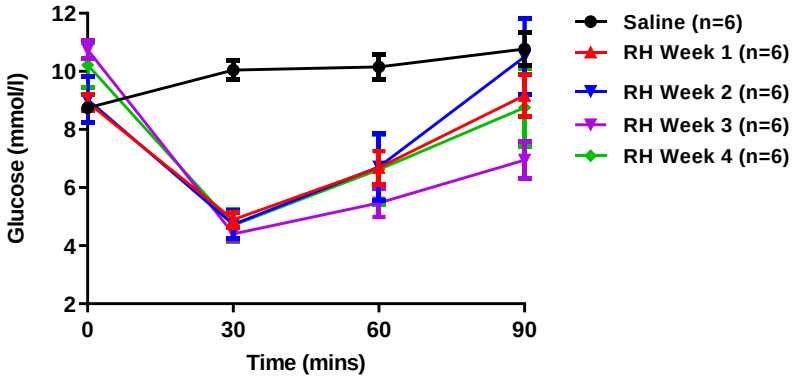
Glucose (mmol/l)
Time (mins)
Saline (n=6)
RH Week 1 (n=6)
RH Week 2 (n=6)
RH Week 3 (n=6)
RH Week 4 (n=6)

C

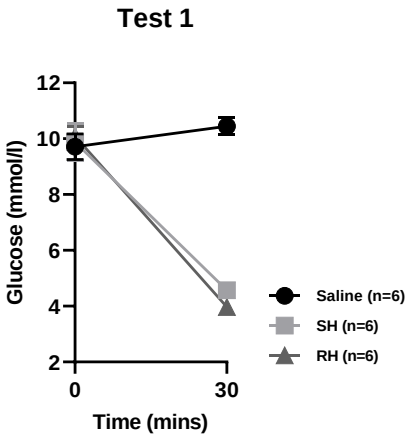
Test 1
Glucose (mmol/l)
Time (mins)
Saline (n=6)
SH (n=6)
RH (n=6)

D

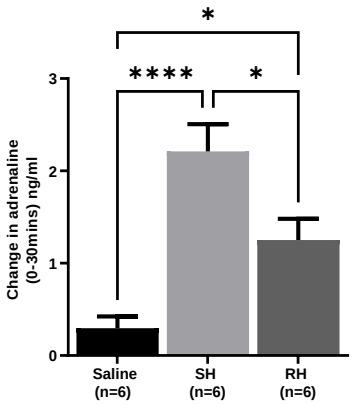
Test 1
Change in adrenaline (0-30mins) ng/ml
Saline (n=6)
SH (n=6)
RH (n=6)

E

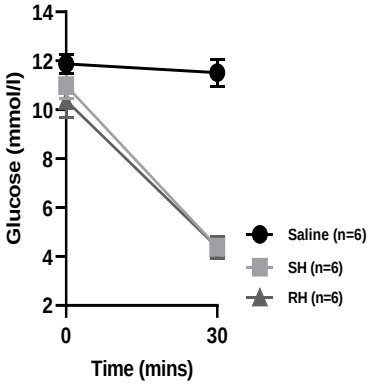
Test 2
Glucose (mmol/l)
Time (mins)
Saline (n=6)
SH (n=6)
RH (n=6)

F

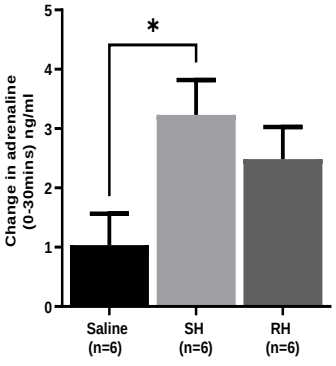
Test 2
Change in adrenaline (0-30mins) ng/ml
Saline (n=6)
SH (n=6)
RH (n=6)

G

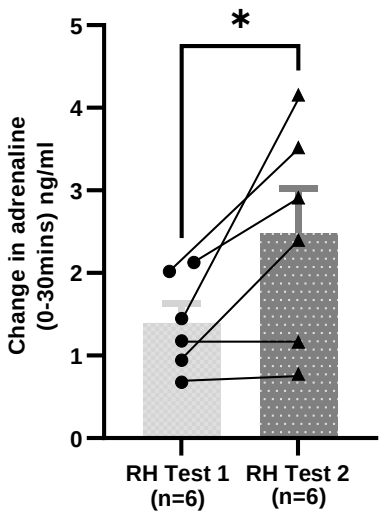

Figure 4.2: Spontaneous recovery of sympathoadrenal response on removal of the habituating stimulus

A: Study protocol**.**
B: Mean weekly blood glucose profile for the 90 mins following injection in RH exposed mice (weeks 1-4 and test day) and saline mice (week 1). RH mice displayed a shift in the glucose profile during the 4 weeks, leading to progressive delay in glucose recovery.
C: Test 1 glucose profiles at 0 and 30 min after s.c. insulin or saline injection. RH mice experienced a lower glucose nadir, compared with SH mice.
D: Test 1 adrenaline response (change in adrenaline 0-30 min after injection) following s.c. insulin or saline injection. SH and RH mice showed a significant increase in adrenaline release, when compared with saline However, the adrenaline response in RH mice was significantly reduced, when compared with SH (****p<0.0001, SH versus saline; *p<0.05, RH versus saline; *p<0.05, RH versus SH; one way-ANOVA with Tukey's *post hoc* test).
E: Test 2 glucose profile at 0 and 30 min after a final s.c. insulin or saline injection. RH and SH mice experienced similar glucose nadirs, after the 4-week recovery period, suggesting improvements in the CRR and defence against hypoglycaemia.
F: Test 2 adrenaline response (change in adrenaline 0-30 min after injection) following a final s.c. insulin or saline injection. SH mice again showed a significant increase in adrenaline release, when compared with saline. RH mice displayed reduced adrenaline release when compared with SH mice, however this was not significantly different (*p<0.05, SH versus saline; one-way ANOVA with Tukey's *post hoc* test).
G: Adrenaline response (change in adrenaline 0-30 min) during test 1 and after the 4-week recovery period on test 2 for each animal. A repeated measures repeated measures two-way ANOVA with Sidak's *post hoc* test demonstrated a significant effect of time (test 1 versus test 2) on adrenaline response in all groups (*p<0.05). However, only RH mice displayed a significant increase in adrenaline release to hypoglycaemia from test 1 to test 2, signifying recovery (*p<0.05*,* test 1 versus test 2; a paired t-test was used to identify differences in sympathoadrenal response within the same animal, separated by time in the RH group).

4.3.3 Experiment 3: Dishabituation with acute restraint stress

In experiment 1, I demonstrated that mice exposed to a single episode of restraint stress displayed a large increase in adrenaline level, commensurate with sympathoadrenal activation (**Figure 4.1D**). Therefore, I elected to use acute restraint stress (AR) as a heterotypic dishabituating stimulus in mice exposed to RH (**Figure 4.2A**).

Animals were randomised to saline, SH, RH or RH+AR groups (saline n=11, other groups n=12) and again underwent the 4-week RH protocol as outlined previously. RH and RH+AR groups received the same number of prior hypoglycaemia episodes. At the end of the 4-week RH protocol, the glucose and sympathoadrenal response was measured after s.c insulin or saline injection, or 30 mins of restraint stress (RH+AR) (test 1) (**Figure 4.3A**). During test 1, insulin injection led to a similar glucose nadir at 30 min in SH and RH mice (SH: 4.4 ± 0.1, RH: 4.2 ± 0.1 mmol/l) (**Figure 4.3B**). In parallel, glucose levels at 30 min were slightly increased following saline injection, but dramatically increased with AR (RH+AR: 20.7 ± 0.9 mmol/l) (**Figure 4.3B**). SH, RH and RH+AR groups all displayed a significant increase in adrenaline levels, when compared with saline. This occurred with an impaired adrenaline response in RH mice, when compared with SH mice, signifying habituation of the sympathoadrenal response (**Figure 4.3C**). However, the adrenaline response in RH+AR mice was comparable to SH mice. Interestingly, RH+AR led to increase in adrenaline release, relative to RH mice, suggesting facilitation of the response (**Figure 4.3C**).

The next day (test 2), saline, RH and RH+AR groups underwent a final episode of s.c insulin or saline, and the sympathoadrenal response was measured once more. During test 2, the blood glucose nadir was comparable between RH and RH+AR groups (RH: 3.9 ± 0.2, RH+AR: 4.2 ± 0.2 mmol/l) (**Figure 4.3D**). RH and RH+AR groups both displayed a significant increase in adrenaline, when compared with saline (**Figure 4.3E**). Importantly, the corresponding adrenaline response was significantly elevated in RH+AR mice, when compared with RH exposed mice (58.3% increase in adrenaline release in RH+AR mice, relative to RH mice), demonstrating dishabituation of the response (**Figure 4.3E**).

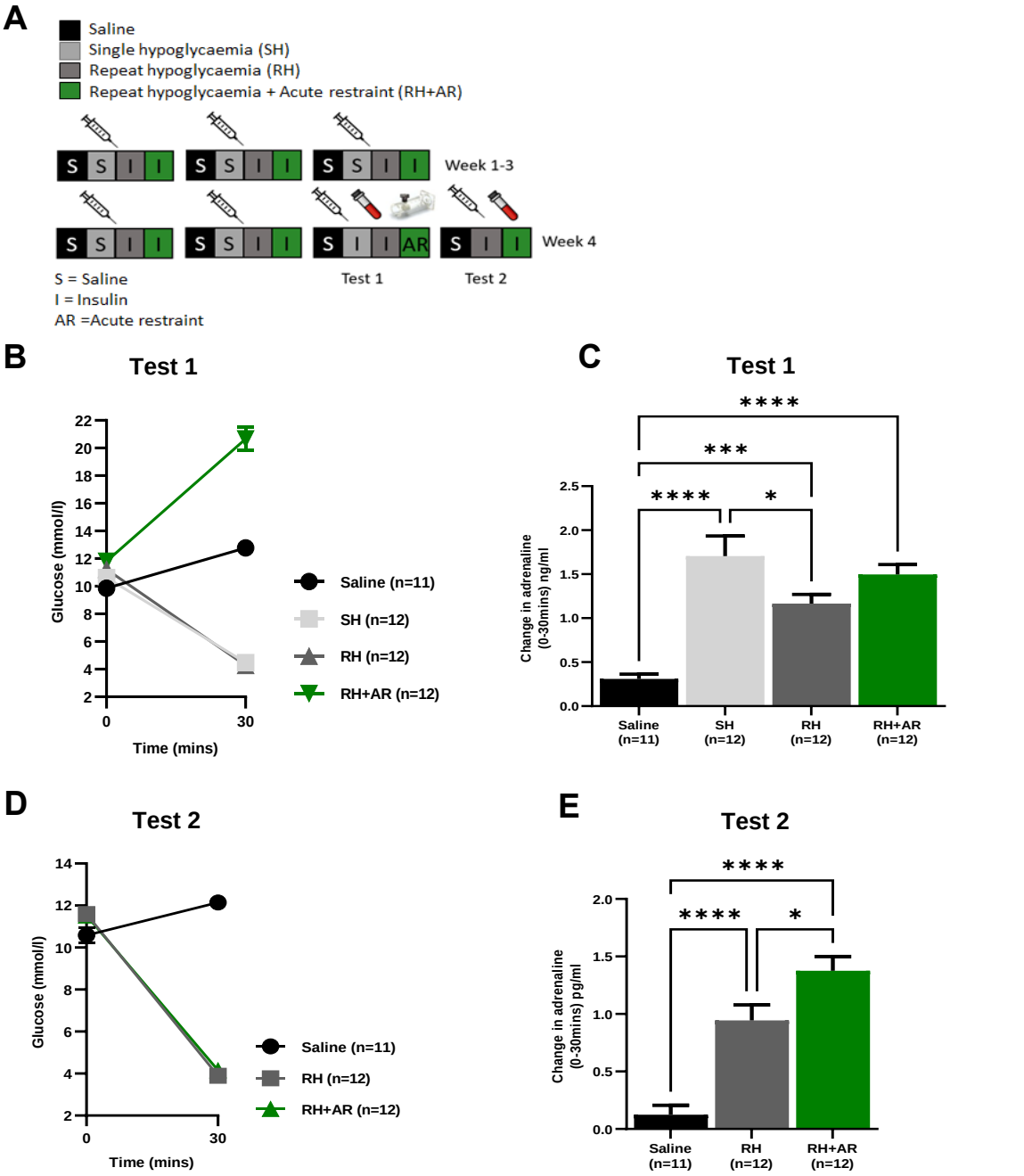

Figure 4.3: Dishabituation with acute restraint

A: Study Protocol
B: Test 1 glucose profiles at 0 and 30 min after s.c. insulin/saline injection, or AR. SH and RH mice displayed a drop in blood glucose, whilst RH+AR mice experienced hyperglycaemia due to restraint stress.
C: Test 1 adrenaline response (change in adrenaline 0-30 min after injection) following s.c. insulin/saline injection or AR. SH, RH and RH+AR mice showed a significant increase in adrenaline release, when compared with saline. The adrenaline response in RH mice was significantly reduced, when compared with SH. RH+AR mice displayed a non-significant increase in adrenaline response, when compared with RH (****p<0.0001, SH versus saline; ***p<0.001, RH versus saline; ****p<0.0001, RH+AR versus saline; *p<0.05, RH versus SH; one-way ANOVA with Tukey's *post hoc* test).
D: Test 2 glucose profiles at 0 and 30 min after s.c. insulin or saline injection. RH and RH+AR groups reached comparable blood glucose nadir at 30 min.
E: Test 2 adrenaline response (change in adrenaline 0-30 min after injection) following s.c. insulin or saline injection. RH and RH+AR mice showed a significantly increased adrenaline response, when compared with saline. Importantly, the adrenaline response in RH-AR mice was significantly increased, when compared with RH, signifying dishabituation (****p<0.0001, RH versus saline and RH+AR versus saline; *p<0.05, RH+AR versus RH; one-way ANOVA with Tukey's *post hoc* test).

4.4 Discussion

Cellular adaptations to RH are multiple (**Figure 1.10**) and to a greater or lesser extent may all contribute to the development of IAH. As McCrimmon *et. al.,* have outlined extensively, these adaptations in the face of profound energy deficit, may ultimately confer benefits to survival (McNeilly and McCrimmon, 2018, McCrimmon, 2017). At a neuronal network or whole organism level, these adaptations can be compared to classical habituation (McCrimmon, 2017).

4.4.1 Experiment 1

In this Chapter, I tested whether IAH carries key hallmarks of habituation, building on previous work in the field (McNeilly et al., 2017, Vickneson et al., 2021, Farrell et al., 2020). All experiments were conducted in the mouse model of IAH, which was characterised in Chapter 3. In showing that experimental RH leads to impairment of the sympathoadrenal response, measured through adrenaline release, the defining hallmark of habituation was satisfied. Namely, repeated stimulation, leads to an attenuation in response. We postulated that other repeated homotypic stressors would also lead to the habituation of the sympathoadrenal response. Therefore, we selected repeated restraint stress, which is primarily a psychological stressor and is known to robustly activate the HPA axis and autonomic nervous system (Girotti et al., 2006). As we predicted, repeated restraint was also capable of reducing the sympathoadrenal response to a subsequent episode of restraint stress, paralleling the findings for RH. The percentage reduction in adrenaline release, relative to SH and SR, was 55.9% and 43.0% respectively. The depth or magnitude of habituation is dependent on many factors. Although, the duration and frequency of the two stimuli were kept the same, the two stimuli are very different in nature, hypoglycaemia being a profound physiological stress, and restraint a strong psychological stress. This experiment did not test RH and restraint in combination, therefore stimulus generalisation (another hallmark of habituation, in which response impairment to one stimulus exhibits generalisation to another stimulus) could not be assessed. However, our data show that RH and RR can both habituate the sympathoadrenal response. As such, both stimuli are likely to engage neuronal networks which converge, but which contain different sensory elements. Therefore, we can postulate that habituation of the sympathoadrenal response, following RH, is not specific to hypoglycaemia, rather to a repeated stimulus. This has been indirectly tested through experiments which show an attenuated sympathoadrenal response to moderate exercise or cold pressor stimuli, in patients with prior hypoglycaemia (Galassetti et al., 2001, Kinsley et al., 1994). Generalisation of habituation is classically described as requiring the interchange of two similar, or homotypic stimuli (Grissom and Bhatnagar, 2009).

However, it remains unclear what characteristics make stimuli similar enough to allow generalisation of habituation. An alternative explanation could be that generalisation of habituation occurs when two stimuli share common integrative neuronal networks, resulting in a comparable habituation of the motor response. It is also interesting that in the same cross-tolerance experiments, involving cold pressor, moderate exercise and hypoglycaemia, the HPA axis response was unaffected. This suggests differential processing of stimuli within networks controlling the HPA response, and those responsible for the sympathoadrenal response (Galassetti et al., 2001, Kinsley et al., 1994).

4.4.2 Experiment 2

The second experiment involved testing whether the sympathoadrenal response recovered following withdrawal of the habituating stimulus (hypoglycaemia) for 4 weeks. We postulated that upon re-testing, the sympathoadrenal response to a final episode of hypoglycaemia would increase. As predicted, adrenaline levels following a 4-week withdrawal period had increased by 77.8%, demonstrating spontaneous recovery. Therefore, this criterion of habituation was also satisfied in our mouse mode of IAH. These data are consistent with classical studies in patients with IAH. Fanelli *et al.,* showed that in patients with type 1 diabetes and IAH for <7 years (termed short duration in this study), strict hypoglycaemia avoidance led to improvements in hypoglycaemia symptoms, neuroendocrine responses and CRR thresholds after just 2 weeks and normalisation at 3 months (Fanelli et al., 1993). A second study examined patients with longer-duration type 1 diabetes and IAH (>10 years duration), demonstrating that following 3 weeks of strict hypoglycaemia avoidance autonomic symptoms, neuroendocrine response and CRR thresholds all improved (Cranston et al., 1994). In both studies, the duration of diabetes and glycaemic control were used as a proxy of the prior exposure to hypoglycaemia. Interestingly, despite differences in diabetes duration and glycaemic control, patients in both studies demonstrated recovery after 2-3 weeks of hypoglycaemia avoidance. This is significant, as it suggests that irrespective of prior severity or quantity of hypoglycaemia episodes experienced, recovery occurs by avoiding the homotypic stressor. There are very few experiments examining spontaneous recovery in other systems. Studies examining spontaneous recovery within the HPA axis also are limited. However, Bhatnagar *et al.,* showed that habituation of HPA activity to repeated restraint did not fully recover after 3 weeks without restraint in rats (Bhatnagar et al., 2002). This may be explained by the classical observations by Thompson and Spencer, who provided the basis for our current understanding of habituation. They noted that the length of time required for spontaneous recovery was

extremely variable even for responses that were known to recover (Thompson and Spencer, 1966). It is also possible that the time taken for recovery depends on the nature of the homotypic stressor and the response system in question, making comparisons difficult.

4.4.3 Experiment 3

In the final experiment, we tested whether dishabituation of the impaired sympathoadrenal response was possible using a heterotypic stimulus. Heterotypic stimuli are capable of eliciting response sensitisation, which is the amplification of a response. This can be followed by dishabituation of the response to the homotypic stressor (Herman, 2013, Costa-Ferreira et al., 2016). Response sensitisation is often referred to at a neuronal level, as facilitation. The findings in experiment 1 highlighted that restraint stress for 30 mins led to a strong activation of the sympathoadrenal response and that it may serve as a good heterotypic stressor. Following the 4-week RH protocol, the adrenaline response was again attenuated in RH mice, but was increased in RH mice exposed to restraint stress. This suggested sensitisation, though the increase in adrenaline level was not statistically significant. Importantly, the next day, a final episode of hypoglycaemia led to a significant increase (58.3% increase) in adrenaline release in RH mice exposed to restraint stress, compared with RH mice, signifying dishabituation. These data are consistent with recent studies in rats and humans, which also demonstrate dishabituation of RH-impaired CRR, using other heterotypic stimuli (McNeilly et al., 2017, Vickneson et al., 2021, Farrell et al., 2020). It is interesting that dishabituation has been demonstrated with different heterotypic stimuli, suggesting that stimulus novelty is key to eliciting this effect. More significant still, therapies based on dishabituation could be explored. One barrier to this, is described by another hallmark of habituation, namely habituation of the dishabituating stimulus. Although, this was not directly tested in this Chapter, our investigations in experiment 1 demonstrated that repeated restraint habituates the sympathoadrenal response. Therefore, the utility of any heterotypic stimulus for dishabituation is likely to reduce on repetition. Combined, these data support the growing evidence that habituation underlies IAH.

4.4.4 Neuronal mechanisms for habituation

At a whole organism level, habituation provides a convincing explanation for the response impairments in IAH. Despite this, it is not precisely known how habituation evolves at a neuronal network or neuronal level. The two prevailing frameworks for understanding habituation are the dual process theory and the comparator theory, though many other models also exist (Uribe-Bahamonde et al., 2019, Steiner and Barry,

2014). Both models have merits and inconsistencies. However, to enable a neuronal and network level understanding of habituation, I will briefly outline both theories and how they may apply to IAH. In the dual process theory, if a repeated or familiar stimulus is applied (e.g., RH), then a pathway-specific neuronal decremental process occurs (habituation). Whereas, if a novel stimulus (e.g., restraint stress) is presented, then a pathway leading to an increased responsiveness occurs (sensitisation). An interaction, between habituating and sensitising pathways determines the final response (Groves and Thompson, 1970). Sokolov's comparator theory posits that a neuronal representation of expected and unexpected stimuli is built and constantly updated. With continued repeated presentation of the same stimulus (e.g. hypoglycaemia), this becomes expected and there is an inhibition of the response (Sokolov, 1960). Both theories make different predictions about the mechanism of dishabituation. The comparator process suggesting that dishabituation is a disturbance in the habituation process, whilst the dual process theory posits that dishabituation is a superimposed process of sensitisation (Steiner and Barry, 2014). Importantly both theories agree that there are neuronal networks which determine stress familiarity versus novelty. Although both theories provide a framework for understanding habituation within the brain, the specific neuronal networks and populations involved in habituation are not known. Applying these principles to the glucose-regulatory network, the control of habituation and sensitisation are likely to be located within integrative or pre-motor neuronal networks.

4.5 Summary

- The reduction in the sympathoadrenal response to RH carries the key hallmarks of habituation.
- RH, akin to other repeated homotypic stressors (repeated restraint stress), reduces the sympathoadrenal response to subsequent homotypic stress.
- Withdrawal of the habituating stimulus leads to recovery of the sympathoadrenal response on re-testing.
- Following RH, application of a heterotypic stimulus (acute restraint stress), leads to the recovery of the response to the original stimulus, demonstrating dishabituation.

4.6 Conclusion

Altogether, these data add to the already strong evidence that IAH carries important hallmarks of habituation. Despite this understanding, several mechanistic questions remain. It remains unclear whether changes in specific neuronal networks or neuronal populations account for habituation. It is also unclear if the cellular changes which lead to habituation of the CRR in patients with IAH are specific to hypoglycaemia, or whether non-specific cellular adaptations to a repeated stressor are responsible. This once again refocuses our attention to investigating the adaptation and possible habituation of specific neuronal populations following RH.

Chapter 5

The real-time recording of CRH^{PVH} neurons *in vivo*

5.1 Introduction

In Chapter 4, I provided evidence to support habituation as the underlying mechanism for the impairments seen in IAH. This was characterised using experimental RH, which acts as the habituating stimulus. Habituation remains poorly understood at a more granular level, but there is consensus that it is a process which relies on specific neural networks, the identity of which are unknown. Therefore, to understand how habituation develops in the glucose-regulatory network, studies which directly measure neuronal activity following RH are required. Researchers in this field have generally achieved this through *ex vivo* techniques, including electrophysiology in brain slices and the quantification of neuronal markers (e.g., cFos and FosB). Electrophysiological studies have focused on glucose-sensing elements within the glucose-regulatory network. These studies have concentrated largely on VMH neurons and have shown that RH alters glucose thresholds for their activation following RH (Kang et al., 2008, Song and Routh, 2006, Fioramonti et al., 2010). It remains unknown if this results from intrinsic changes within glucose-sensing cells, or if modulation from integrative networks is responsible (Belfort-DeAguiar et al., 2018). Only Sivitz *et al.,* has examined motor elements of the network using electrophysiology, showing that RH alters adrenal sympathetic nerve responsiveness (Sivitz et al., 2001).

Surprisingly, there is no electrophysiological data to show how RH affects neuronal activity within integrative or pre-motor networks. Therefore, neuronal marker studies have provided our best evidence for RH-related changes to integrative and pre-motor networks (Dodd et al., 2010, Al-Noori et al., 2008b, Evans et al., 2001, Sanders and Ritter, 2000). In Chapter 3, I provided evidence that integrative and pre-motor networks contain hypoglycaemia-responsive neurons, which adapt to RH. These investigations highlighted CRH^{PVH} neurons as a population which displays a high level of acute gene activation following SH and adaptive changes to RH, which we postulated could signify habituation. However, this approach cannot identify the precise kinetics or magnitude of neuronal activity. To this end, we wished to investigate the real-time activity of CRH^{PVH} neurons to stressors, including hypoglycaemia and identify if RH leads to diminished activity. This was investigated by using *in vivo* fibre photometry.

Fibre photometry is a relatively recent technique which allows the real-time measurement of intracellular calcium (a proxy for electrical activity) in a genetically defined neuronal population during normal behaviour *in vivo*. It provides a high resolution of temporal kinetics and a measure of the magnitude of neuronal activity. Recently, studies using fibre photometry have provided novel insights into neuronal populations within the PVH and other hypothalamic regions (Li et al., 2019, Berrios et al., 2021).

5.1.1 Objectives

In this Chapter, I investigated the *in vivo* activity of CRH^{PVH} neurons using fibre photometry. The overarching aim was to establish the kinetics and magnitude of CRH^{PVH} neuronal activity following SH and whether this diminished following RH. We postulated that RH, akin to other repeated stressors, leads to a reduction in CRH^{PVH} neuronal activity which might indicate habituation.

1) Characterise the CRH^{PVH} neuron response to acute stressors and food presentation

Recently, studies using fibre photometry have shown that CRH^{PVH} neurons respond rapidly with an increase in activity following exposure to a variety of psychological and physiological stressors (Kim et al., 2019a, Kim et al., 2019b). In addition, CRH^{PVH} neuronal activity is quickly reduced on food presentation in the fasted, but not in the fed state (Li et al., 2019). Therefore, we elected to investigate the response of CRH^{PVH} neurons to food presentation in the fed and fasted state, later using this test to screen each mouse. Subsequently, we characterised the CRH^{PVH} neuronal response to acute stressors. Experiments using acute stressors were performed with the aim of identifying a heterotypic stress stimulus and to inform future RH experiments.

2) Investigate the CRH^{PVH} neuron response to SH

CRH^{PVH} neurons display an acute increase in CRH mRNA and neuronal cFos induction following SH (Inouye et al., 2006, Al-Noori et al., 2008b). In this Chapter we investigated the CRH^{PVH} neuronal activity to SH, which has not previously been assessed *in vivo.* We postulated that CRH^{PVH} neurons would increase their activity following SH. We also wanted to understand the kinetic of the response to SH with respect to blood glucose levels.

3) Investigate the CRH^{PVH} neuron response to glucoprivation with 2-DG

Glucoprivation with 2-DG leads to a similar pattern of neuronal cFos induction in the PVH as insulin-induced hypoglycaemia (Dodd et al., 2010, Stanley et al., 2013). Though CRH^{PVH} cFos induction following 2-DG has not been investigated directly, it is likely this population is activated. In addition, 2-DG glucoprivation enables the investigation of the glucose-regulatory network, without the influence of insulin. This is important as there are known modulatory effects of central insulin signalling on the glucose-regulatory network (Diggs-Andrews et al., 2010). Therefore, we investigated CRH^{PVH} neuronal activity following systemic 2-DG administration. In combination with experiment 2, this experiment would help to identify if changes in CRH^{PVH} neuron activity are influenced by hypoglycaemia rather than insulin *per se*.

4) Investigate the CRH^{PVH} neuron response to RH

Following RH, the PVH displays attenuated cFos induction to subsequent hypoglycaemia, signifying reduced activity and possibly habituation (Al-Noori et al., 2008b, Evans et al., 2001). In Chapter 3, I demonstrated that CRH^{PVH} neurons are an important neuronal population which undergoes adaptive changes following RH. We postulated that CRH^{PVH} neurons, as a population, would demonstrate a real-time reduction in neuronal activity following a homotypic stressor (RH). We also wanted to investigate if CRH^{PVH} neurons would remain responsive to a heterotypic stressor.

5.2 Methods

5.2.1 Animals

Adult, male *Crh*-cre mice (Chapter 2) aged 8-16 weeks old were used for all studies in this Chapter. From the literature, the effect size of hypoglycaemia on CRH calcium transits was not known. However, from our understanding of CRH responses to other physiological and psychological stressors, we anticipated a small-medium effect size (Kim et al., 2019a, Kim et al., 2019b). As we hypothesised that CRH neuronal responses to hypoglycaemia are proportional to the sympathoadrenal response to hypoglycaemia, similar group sizes were selected for photometry experiments as for the characterisation of the mouse model of IAH (i.e., n= 5-6/group). Experiments were performed with separate cohorts of animals prepared in batches.

5.2.2 *In vivo* fibre photometry

Fibre photometry enables the real-time recording of neuronal activity in freely moving mice by detecting bulk changes in calcium-mediated fluorescence in the soma. This is achieved by using genetically encoded Ca^{2+} indicators such as GCaMP proteins, which can be delivered in AAV vectors into genetically defined neuronal populations. Neurons expressing the GCaMP protein are stimulated with an excitation light of a specific wavelength, leading to fluorescence. The fluorescence signal corresponds to intracellular calcium transits and is returned via the same optic fibre to the photometry system. By detecting changes in the fluorescence intensity, the calcium transit related to specific stimuli can be measured.

5.2.2.1 Intracranial surgery and optic fibre placement

Intracranial surgery was performed as described in the Chapter 2. AAVs carrying a Cre-dependent GCaMP construct (AAV1-hSyn-FLEX-jGCaMP7s-WPRE) were injected unilaterally into the PVH. AAV titre and injection coordinates and volumes are outlined in

Chapter 2. Optic fibre implantation was performed in the same sitting, immediately after intracranial injection and is described in Chapter 2. Intracranial injections and optic fibre implantations were primarily performed by me, however Mr Mehdi Boutagouga Boudjadja (D'Agostino Lab, University of Manchester) performed surgery for some animals used in the first experiment and assisted me in surgery for animals used in all the subsequent experiments. A 4–6-week post-operative period enabled recovery, transduction and neuronal expression of GCaMP. Animals were singly housed following surgery to prevent optic fibre displacement.

5.2.2.2 *In vivo* fibre photometry system

The fibre photometry system (Doric Lenses; Quebec, Canada) arrangement is shown in **Figure 5.1**. Excitation blue (465 nm) and purple (405 nm) light was modulated at different frequencies (211 Hz and 511 Hz, respectively) by a two-channel LED driver (LEDD_2; Doric Lenses) and sent through a fluorescence mini-cube. The mini-cube combines excitation light and separates output fluorescence light (FMC4_AE(405)_E(460-490)_F(500-550)_S; Doric Lenses). Excitation light was then passed down to the implanted optic fibre using an optic cable (Doric Lenses). The cable was connected to a pigtailed rotary joint (FRJ_1x1_PT_400/430/LWMJ-0.57_1m_FCM_0.06m_FCM; Doric Lenses), to allow free movement of the mice. Excitation 465 nm (Ca^{2+} dependent) and 405nm (isosbestic reference fluorescence) signals pass via the mini-cube to a photoreceiver unit. The signal is amplified and passes via a fibre photometry console (FPC), which synchronizes the output control and the input data acquisition. Data was collected via the Doric Neuroscience Studio Software (Doric Lenses), exported and then analysed.

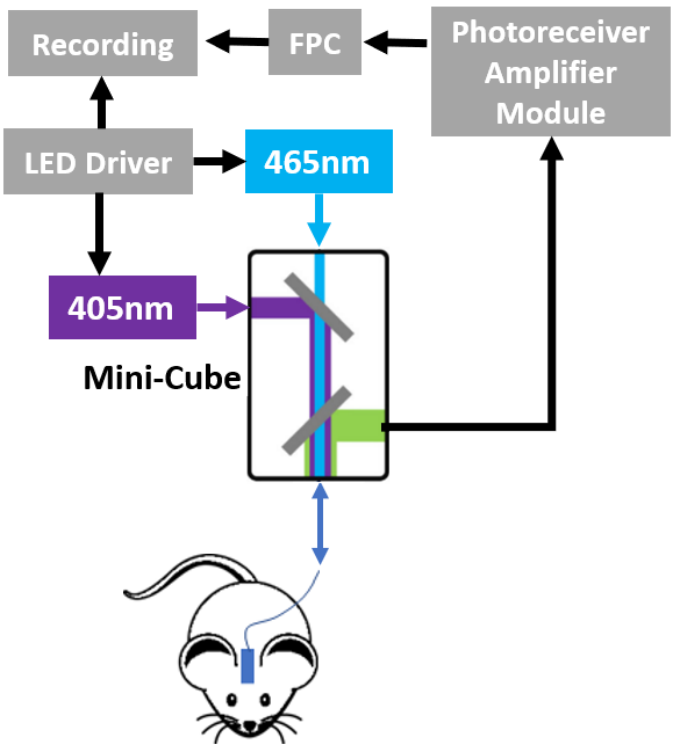

Figure 5.1: Fibre photometry system

Components and arrangement of fibre photometry system. The mini-cube contains a dichroic mirror which separates light based on wavelength and directs emission light to the photoreceiver unit. This is synchronised via the FPC.

FPC: Fibre photometry console

5.2.2.3 Photometry recording

Prior to recordings, animals were handled daily for 2 weeks and acclimatised to tethering. Depending on the experiment, animals were either fasted overnight (16 hr) or for 3 hr prior to recordings. Immediately prior to recording, animals were transferred from their home cage to an empty cage in the photometry system and tethered to the fibre patch cord. Tethering was achieved by connecting the implanted optic fibre to the patch cord with a plastic mating sleeve (Doric Lenses). They were then allowed to acclimatise to the photometry system cage for 30 min. Photometry recordings consisted of a 10 min baseline, presentation of a stimulus (e.g., hypoglycaemia), then a post-stimulus recording period which depended on the experiment. Animals were then returned to their home cage and food returned.

5.2.2.4 Photometry analysis

Photometry data analysis was performed using a custom-built MATLAB script which was solely developed by Mr Mehdi Boutagouga Boudjadja (D'Agostino Lab, University of Manchester). This script has been published and will be included in his PhD thesis (Gómez-Valadés et al., 2021).

In brief, the analysis script first removed signal artefact using a low-pass filter. The 465 nm and 405 nm fluorescence signals (F) were next normalised to their own respective baselines, to define ΔF/F $(F-F_{baseline})/F_{baseline}$. $F_{baseline}$ represented the mean of the fluorescence signal detected during the baseline pre-stimulus period (usually 10 min). The 405 nm ΔF/F was subtracted from the 465 nm ΔF/F to provide an additional level of normalisation. Data were down sampled to 1 Hz to create a manageable dataset.

Mr Mehdi Boutagouga Boudjadja assisted with the data analysis of photometry recordings for all experiments outlined in this Chapter. He also assisted with the development of a custom script to identify significant events in a long photometry trace (**Figure 5.2**).

5.2.2.5 Identifying significant events in a long photometry trace

Experiments involving hypoglycaemia or 2-DG, required a longer recording period and more than one stimulus. As a result, the identification of significant shifts in photometry signal was difficult and more open to interpretation. To provide a non-biased way of identifying the onset of significant events in a photometry trace, a separate analysis script was developed as part of my PhD. The main stages involved in this analysis are outlined in **Figure 5.2**. Significant events (termed S1, S2, S3 etc.) were compared to the recorded time that stimuli were presented or to biological measures.

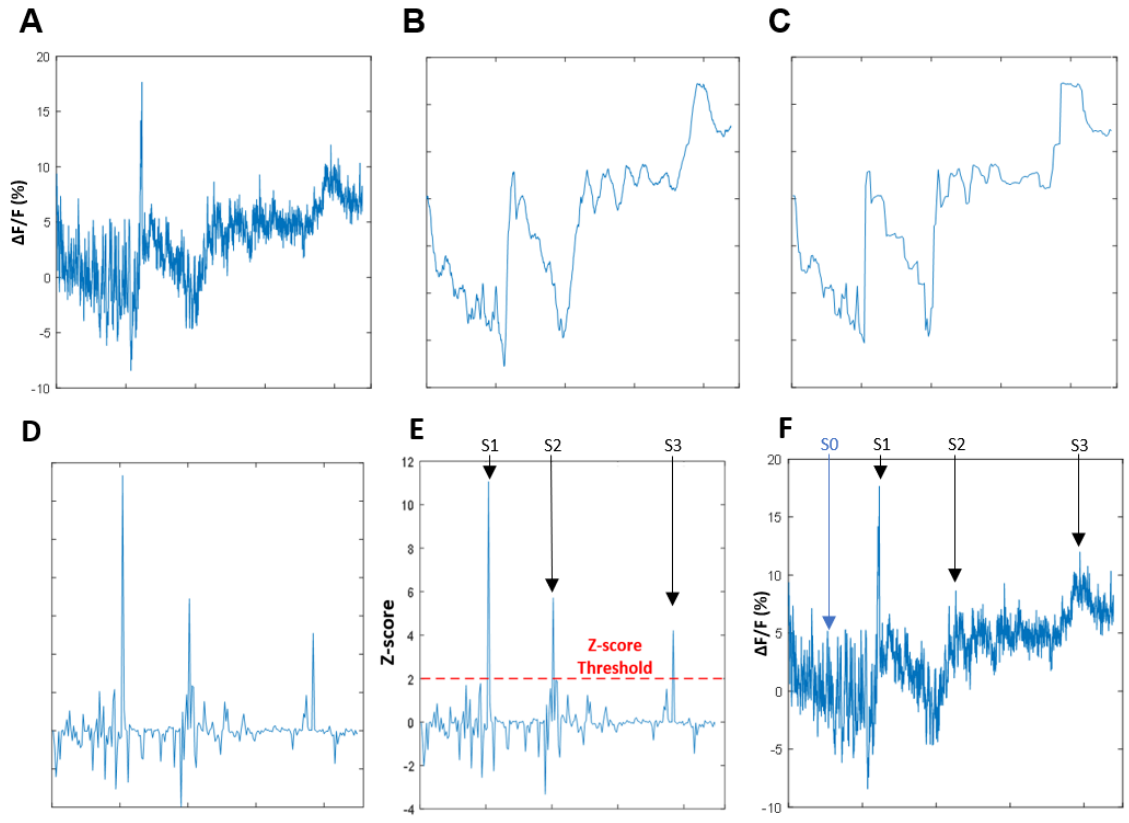

Figure 5.2: A custom method to identify significant events in a long photometry recording

A processed and normalised photometry recording (down sampled to 1 Hz) (A) undergoes a step-wise process to calculate significant events in a non-biased manner. This involves applying a moving average filter (B) to simplify the trace, whilst conserving the pattern. Identifying peaks (a point which has a greater value than either of its neighbours) within this trace (C) and differences between neighbouring peaks (D) enables the identification of the major shifts in signal. Conversion to a Z-score (E) allows a Z-score threshold to be applied (here z = 2) . Therefore, only shifts in signal beyond this threshold are identified as significant events (termed S1, S2, S3). These events can then be overlayed onto the original down-sampled trace, allowing temporal and then, quantitative identification of significant events in a long photometry trace. Significant events (S1-3) can be compared between animals and groups, or to a point during the baseline (termed S0) for comparisons within the same trace.

5.2.2.6 Photometry data presentation

Experiments were carried out in batches and animals receiving the same treatment were grouped across batches. The exception to this was the final RH experiment, where all animals were investigated concurrently.

Down-sampled data at 1 Hz acquisition was used in all figures and statistical analyses. Calcium transits were expressed as ΔF/F (%). In all figures, the pre-stimulus and post - stimulus periods were trimmed to reflect the duration of the stimulus. Statistical comparisons were performed using peak, average or area under the curve (AUC) for the ΔF/F (%).

5.2.2.7 Screening protocol

Experiments were not performed until 4-6 weeks after surgery to allow recovery and neuronal expression of GCaMP. Only animals identified to express GCaMP and demonstrate a stereotypical neuron response on screening (rapid inhibition of calcium signal on ingestion of food **Figure 5.3**) were included in experiments. Animals were acclimatised to the photometry system for three days before screening. This involved tethering the animals to the fibre patch cord for 30 min. Animals were also presented daily with a pellet of HED for three days before screening. This was to prevent neophobia and avoidance of the food during screening.

Screening photometry recordings were performed in overnight (16 hr) fasted mice at 10 am the following day. Animals were tethered to the fibre patch cord 30 min before recording commenced. Photometry recordings consisted of a 10 min baseline period, food presentation, then 10 min post-stimulus recording. Animals which responded with a clear inhibition in CRH^{PVH} activity were selected for further experiments.

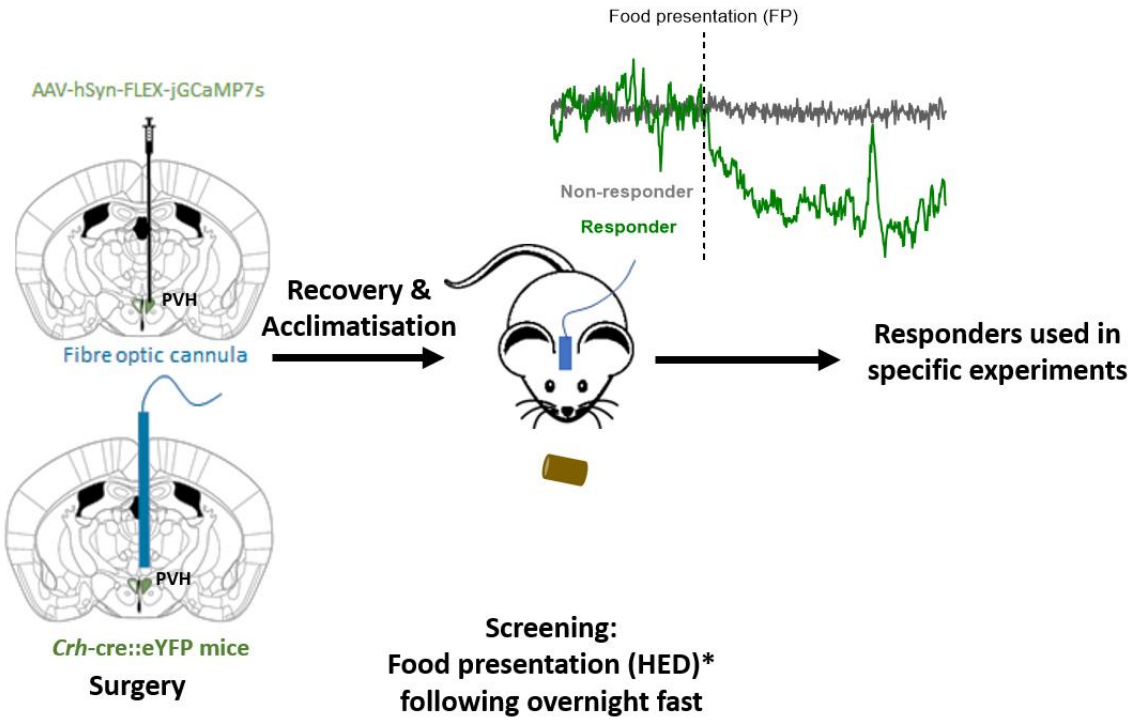

Figure 5.3: Screening protocol to identify responders

Optic fibre implantation was performed immediately after viral infection with GCaMP virus, during the same surgical procedure. Following a period of recovery and acclimatisation (4-6 weeks), animals were screened. Responders were defined as mice which exhibited an inhibition of PVH^{CRH} neuron activity on food presentation (FP) following overnight fast.

*High energy diet (HED) was used as this is highly appetitive and ensures timely food approach and ingestion on presentation.

5.2.3 Experimental stimuli

5.2.3.1 Single hypoglycaemia

Animals were fasted for 3 hr prior to recordings. During the recording, animals received s.c. insulin (1.75 U/kg) to induce hypoglycaemia. Recordings were performed for a further 35 min following s.c. insulin injection. At the end of the recording, all animals were returned to their home cage and given *ad libitum* access to food. Blood glucose levels were measured at baseline, prior to tethering and then at the end of the recording. This was to avoid additional stress related to measurements, which would impede identification of hypoglycaemia-specific effects. Once photometry experiments were completed, all animals underwent a final injection with s.c. insulin (1.75 U/kg). Blood glucose measurements were taken every 5 min for 35 min to enable correlation with the photometry trace. The hypoglycaemia and blood glucose measurement protocols are described in full in the Chapter 2**.**

5.2.3.2 Repeated hypoglycaemia

From previous experiments, we had observed that the time taken for maximal neuronal GCaMP expression varied, sometimes taking 6 weeks. Therefore, in this experiment, animals were allowed to recover for a 6-week period. This was followed by two separate food presentation screening tests (FP1 and FP2), which followed the same protocol as outlined in **Figure 5.3**. This was performed to check whether the GCaMP expression had stabilised, which would enable more reliable comparisons of calcium dynamics, across hypoglycaemia tests.

Animals were then recorded during their first episode of hypoglycaemia (Test 1) and then underwent the 4-week RH protocol, which was characterised in Chapter 3. On the last day of this protocol, all animals were recorded during a subsequent episode of hypoglycaemia (Test 2). Animals were then allowed to recover for a further 4 weeks and a final recording performed during hypoglycaemia (Test 3). Comparisons for each individual animal were performed to determine differences in calcium dynamics between recordings (tests). This was performed, as we had shown that spontaneous recovery of the sympathoadrenal response occurs after the withdrawal of hypoglycaemia for 4 weeks (Chapter 4). On the three test days, animals were also exposed to a heterotypic stressor of tail restraint (TR) for 20s. This was performed as we postulated that CRH^{PVH} would retain responsiveness to a heterotypic stressor, but not to a homotypic stressor (RH). At the end this experiment, blood glucose levels were measured at 5 min intervals in all the mice for 35 min following s.c. insulin.

5.2.3.3 2-DG induced glucoprivation

Glucoprivation using 2-DG allows the examination of neurons within the glucose-regulatory network without the need for supraphysiological doses of insulin. Animals were again fasted for 3 hr prior to recordings. During the recording, animals received i.p. 2-DG (500 mg/kg). Recordings were performed for a further 35 min following i.p 2-DG injection. Separately, saline group animals received i.p. saline. Animals in the saline group were not fasted, but acclimatisation and recording parameters were the same as for the 2-DG group. At the end of the recording, all animals were returned to their home cage and given *ad libitum* access to food.

5.2.3.4 Saline Injection

In separate experiments, animals received either s.c. or i.p. 0.9% NaCl (4 ml/kg) whilst tethered to the photometry system. Recordings were again performed for a further 35 min following saline injection and animals were then returned to their home cage.

5.2.3.5 Tail restraint

Tail restraint involved quickly catching the tail of tested mice and holding the tail firmly for 20 s, preventing escape. This was performed whilst tethered to the photometry system. The post-stimulus period varied depending on the experiment in question. A similar protocol has recently been published, showing rapid activation of CRH^{PVH} neurons (Kim et al., 2019a).

5.2.4 Verification of transfection and fibre placement

At the end of each experiment animals were perfused with fixative and brains dissected and processed (Chapter 2). Brain sections were sliced and sections containing the PVH were mounted onto microscope slides. GCaMP contains the GFP transgene, which was visible without the need for IHC. CRH neuron transduction with GCAMP and fibre placement was confirmed prior to inclusion of animals in the results (**Figure 5.4**). On-target transfection was defined as animals with 1) fluorescent-labelled neurons in the characteristic distribution of CRH neurons in middle-PVH sections and 2) a fibre tract dorsal to fluorescent-labelled neurons.

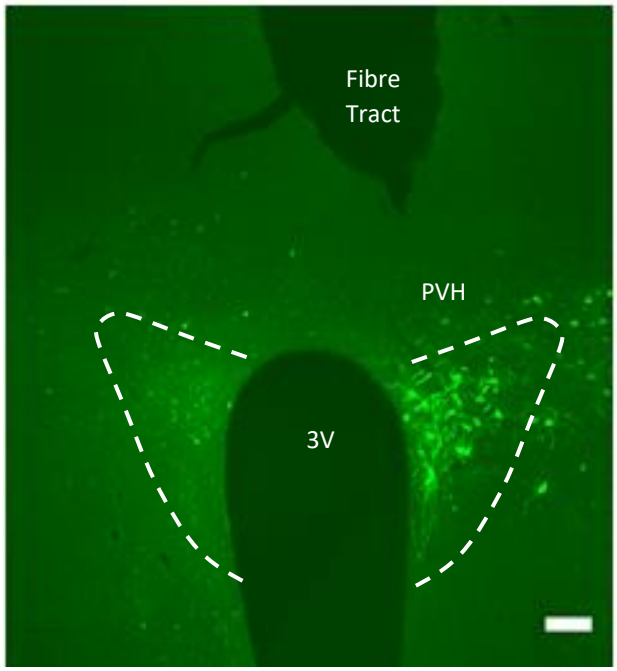

Figure 5.4: Verification of transfection and fibre placement

Brain slice showing unilateral GCaMP transfected CRH^{PVH} neurons (green). The optic fibre tract is directly above the PVH, confirming this was correctly positioned.
Scale bar represents 100 µm.

3V: 3rd Ventricle

5.3 Results

5.3.1 CRH^{PVH} neuron response to food presentation in the fed and fasted state

To establish a screening phase for subsequent experiments, we first conducted an experiment to investigate the response of CRH^{PVH} neurons to food presentation (FP) in the fed and fasted state. The calcium transits are show in **Figure 5.5A** and have been trimmed to show a 3 min baseline and 5 min post-stimulus period. Opening the cabinet and dropping the food pellet was associated with a transient increase in calcium signal. This was followed by a rapid reduction in calcium signal only in fasted mice (Average ΔF/F = -16.7 ± 4.7%) and not in the fed state (Average ΔF/F = 0.8 ± 1.4%) (**Figure 5.5A,B**). The calcium signal gradually increased from 4 min after FP, however, did not return to baseline levels during the recording period. These data confirmed that FP following an overnight fast, provides a minimally invasive approach for post-surgery screening and identification of responsive mice (i.e., correct surgery and transduction).

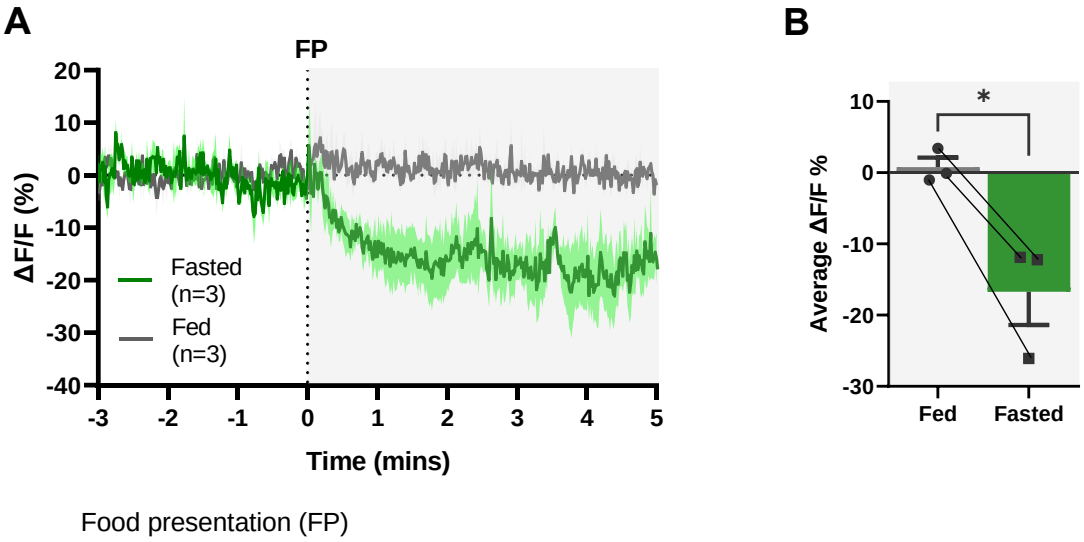

Figure 5.5: Food presentation in the fed and fated state

A: Plot of calcium transits for FP in the fed (grey) and fasted (green) state, aligned to FP time. The recording has been trimmed to show 3 min of baseline and the 5 min post-stimulus period. The dark colour indicates mean signal, lighter colour tones indicate SEM.
B: Average change in signal for 5-min window (grey background) following FP in fed and fasted state (*p<0.05; paired t-test).

5.3.2 CRH^{PVH} neuron response to acute stressors

Separate cohorts of male *Crh*-cre mice (cohort 1, n=4; cohort 2, n=5) were next investigated for their response to stressful stimuli. A trimmed plot of the calcium signal following injection and tail restraint stress is shown in **Figure 5.6A**. A time window of 30 s was selected as it was the average time take to scruff, inject and release the animal. Subcutaneous injection with 0.9% NaCl led to a rapid increase in calcium transit (Average ΔF/F = 16.0 ± 4.0%) in all mice. This was significantly increased when compared to a 30 s pre-stimulus baseline period (**Figure 5.6B**). After release of the mouse, the calcium signal reduced, however this did not return to baseline levels until around 5 mins post-injection.

Separately, a second cohort of *Crh*-cre mice (n=5), which were verified to be responders, underwent photometry recording during tail-restraint stress. The calcium transits aligned to time of TR are shown for 30 s pre- and 30 s post-TR (**Figure 5.6C**). Tail restraint for 20 s led to a rapid increase in calcium transit (Average ΔF/F = 18.0 ± 5.5%) in all mice. This raised level of calcium signal was sustained for the 20 s TR period and started to reduce on release of the mouse. This was significantly increased when compared with a 20 s pre-stimulus baseline period (**Figure 5.6D**). As with s.c. injection, on release of the mouse, the calcium signal reduced rapidly, however this did not return to baseline levels for another 2 mins.

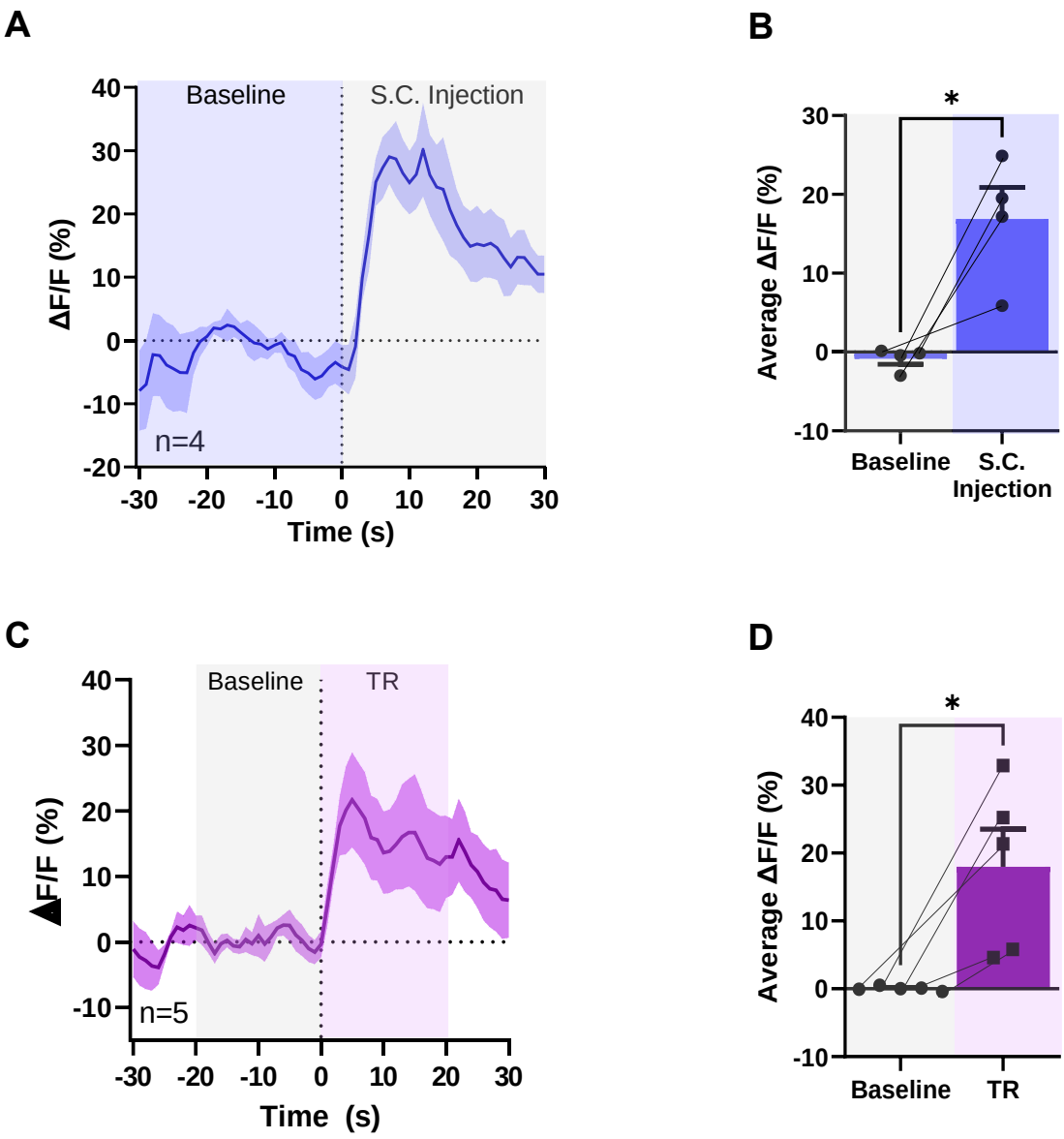

Figure 5.6: CRH^{PVH} neuron response to injection and trail restraint stress

A: Plot of calcium transits of CRH^{PVH} neurons aligned to the time of s.c. injection with saline. The recording has been trimmed to show 30 s of baseline and the 30 s post-stimulus period.
B: Mean signal for 30 s window at baseline (grey background) and following s.c. injection (blue background), (*p<0.05; paired t-test).
C: Plot of calcium transits of PVH^{CRH} neurons aligned to the time of tail restraint (TR) for 20 s. The recording has been trimmed to show 30 s of baseline and the 30 s post-stimulus period.
D: Mean signal for 20 s window at baseline (grey background) and following TR (purple background), (*p<0.05; paired t-test).
For plots of calcium signal, the dark colour indicates mean signal, light colour tones indicate SEM.

5.3.3 CRH^{PVH} neuron response to SH

Calcium transits in saline and SH-treated mice, along with a blood glucose profile are shown in **Figure 5.7A**. Significant events in the trace were identified using the custom script outlined in **Figure 5.2**, enabling S1 (s.c. injection onset) and S2 (hypoglycaemia onset) to be identified. The average S1 and S2, along with a baseline (S0) time points are identified on **Figure 5.7A**. S1 and S2 values were identified for individual animals and used in statistical comparisons (**Figure 5.7B-E**). Saline and SH groups both display similar baseline calcium transits showing a high level of tonic activity. Both groups also show a surprisingly similar increase in calcium signal following s.c. injection (average ΔF/F (30 s window) for saline = 13.2 ± 4.0%; SH = 13.0 ± 4.4%; **Figure 5.7D**). This increase in calcium signal is marked by S1, which was significantly increased relative to S0 in both saline and SH groups (**Figure 5.7B,C**). After S1, the calcium signal reduced in both groups, but remained at a higher level compared with baseline. In the SH group, the calcium signal noticeably increased from around 7 min after s.c. injection (S1). The point at which this increase became significant is marked by S2 (9 min after s.c. injection). The calcium signal at S2 was significantly increased in the SH group, relative to S0 and saline group (average ΔF/F (30 s window) at S2 for saline = 1.1 ± 1.5%; SH = 9.3 ± 3.6%; *p<0.05; **Figure 5.7A,C,D**). This corresponded with the timing of the fall in blood glucose and hypoglycaemia, when measured separately in the same mice. In contrast, the calcium signal at S2 in the saline group was comparable to baseline levels (**Figure 5.7B**). Post-S2, SH mice displayed a persistently elevated calcium signal until the end of the recording. Again, this sustained elevation corresponded with the low blood glucose level. On the other hand, the calcium signal post-S2, continued to decrease gradually in the saline group, reaching baseline levels and lower. Consistent with this, the area under the curve (AUC) for the calcium transit (post-S2) was significantly increased in the SH group, when compared with saline (**Figure 5.7E**).

Combined, the calcium dynamics of CRH^{PVH} neurons following SH, indicate that they increase their activity when blood glucose levels fall. Interestingly, this higher level of activity is sustained and persists whilst blood glucose levels remain low.

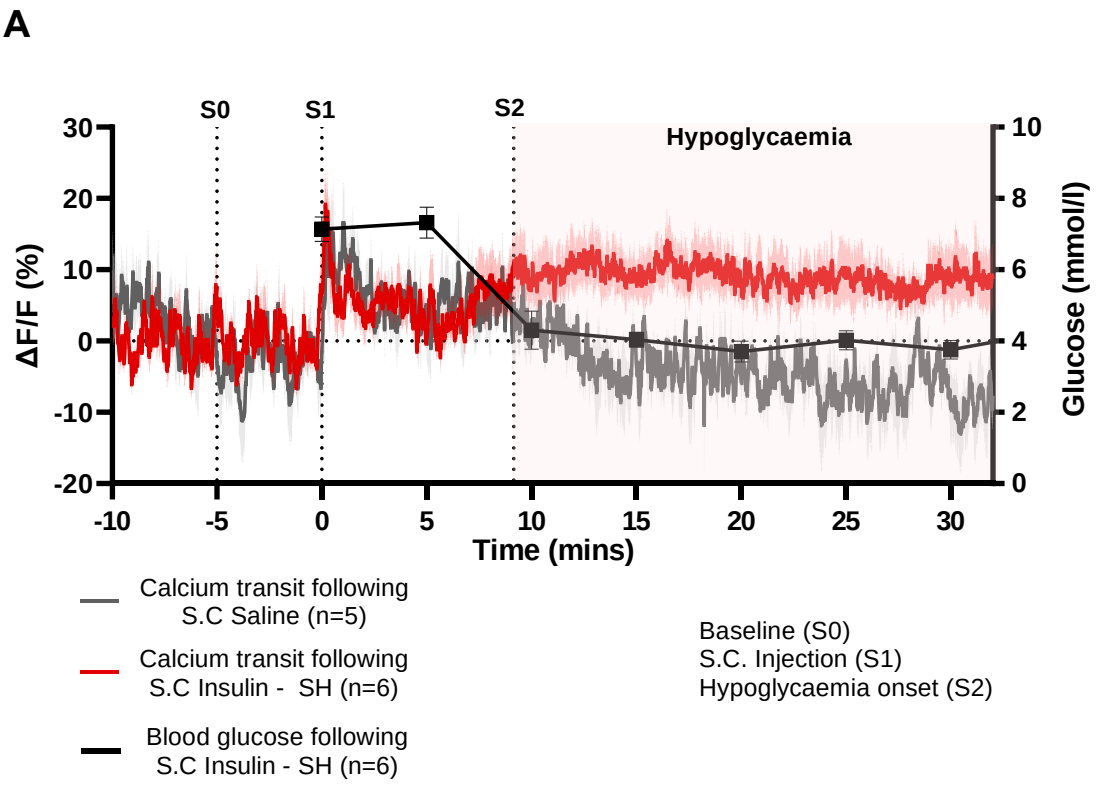
A
S0
S1
S2
Hypoglycaemia
ΔF/F (%)
Glucose (mmol/l)
Time (mins)
Calcium transit following S.C Saline (n=5)
Calcium transit following S.C Insulin - SH (n=6)
Blood glucose following S.C Insulin - SH (n=6)
Baseline (S0)
S.C. Injection (S1)
Hypoglycaemia onset (S2)

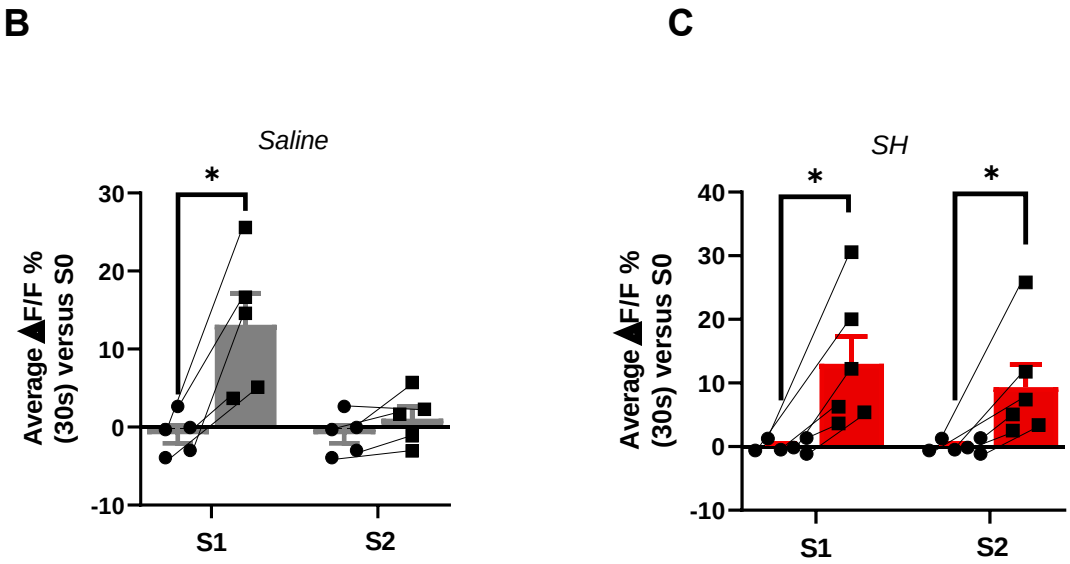
B
Saline
Average ΔF/F % (30s) versus S0
S1
S2
C
SH
Average ΔF/F % (30s) versus S0
S1
S2

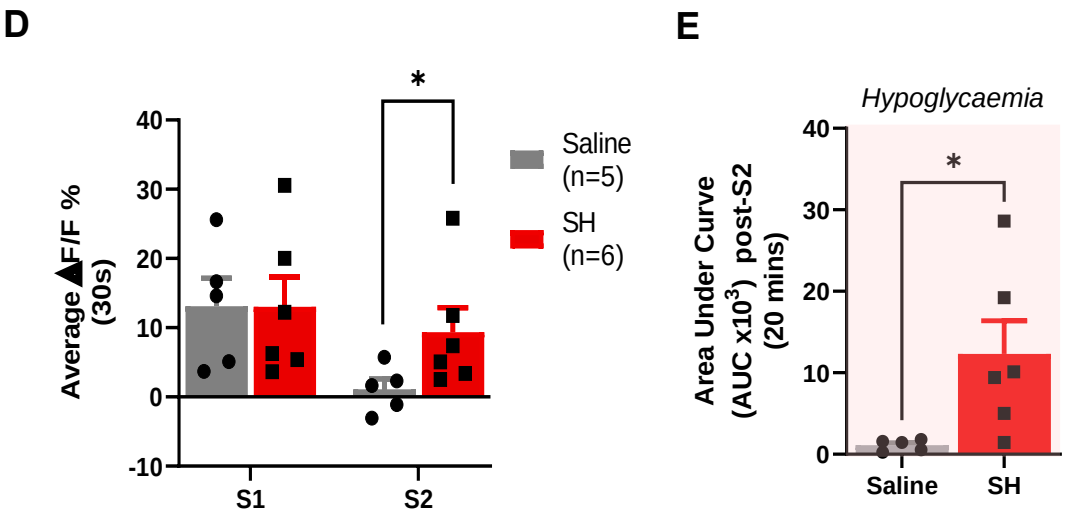

Figure 5.7: CRH^{PVH} neuron response to SH

A: Plot of calcium transits of CRH^{PVH} neurons aligned to the time of s.c. injection with saline or insulin (SH). Saline and SH group animals displayed similar calcium dynamics to s.c. injection (S1). SH mice show an increase in calcium signal at S2, which corresponds with a dropping blood glucose level (black line). Therefore, S2 marks hypoglycaemia onset. In parallel, the calcium signal in saline mice returned to baseline levels (S0).
B: Average calcium signal (30s window) at S1 and S2 compared with baseline (S0), in saline mice. S1 values were significantly increased relative to S0 (*p<0.05; paired t-test).
C: Average calcium signal (30s window) at S1 and S2 compared with baseline (S0), in SH mice. S1 and S2 values were significantly increased relative to S0 (*p<0.05, both versus S0; paired t-test).
D: Average calcium signal (30s window) at S1 and S2 for saline and SH groups. At S1, calcium signal values were similar. However, at S2, this was significantly increased in SH, compared to saline (*p<0.05, SH versus saline; unpaired t-test).
E: Area under the curve (AUC) for calcium signal (20min window post-S2) in saline and SH groups. The AUC was significantly higher in SH, compared to saline mice (*p<0.05, SH versus saline; unpaired t-test).
For plots of calcium signal, the dark colour indicates mean signal, light colour tones indicate SEM.

5.3.4 CRH^{PVH} neuron response to 2-DG-induced glucoprivation

Calcium transits in saline and 2-DG groups are shown in **Figure 5.8**. Significant events, termed S1 and S2, along with a baseline (S0) time point are marked on **Figure 5.8A.** S1 (i.p. injection onset) and S2 (2-DG induced glucoprivation onset) values were also identified for individual animals and used in statistical comparisons (**Figure 5.8B-E**). Saline and 2-DG groups display similar baseline calcium transits and comparable elevations in signal following i.p. injection, identified as S1. The average calcium signal (30 s window) at S1 was significantly elevated in both groups, when compared with S0, signifying enhanced CRH^{PVH} neuronal activity. Post-S1, saline-treated mice display a gradual reduction in calcium signal, approaching baseline levels. The 2-DG group displayed an initial reduction in calcium signal post-S1, though this plateaued and then increased. The elevation in calcium signal was visibly different between 2-DG and saline groups by 9 min post-S1. The point at which this increase became significant in 2-DG-treated animals is marked by S2 and has been taken to represent the onset of glucoprivation. At S2, the calcium signal was notably elevated in the 2-DG group, compared with saline (average $\Delta F/F$ (30 s window) for saline = 0.1 ± 1.6%; 2-DG = 14.5 ± 5.0%; *$p<0.05$; **Figure 5.8D**). This was also significantly elevated when compared with S0, in the 2-DG group, but not in the saline group (**Figure 5.8B,C**). Post-S2, 2-DG animals displayed a sustained high calcium signal, remaining at this level until the end of the recording. In contrast, saline animals displayed reductions in calcium signal, leading to levels below that of baseline, by the end of the recording. This was reflected by a significantly increased AUC in the 2-DG group, when compared with saline (**Figure 5.8E**).

These data parallel findings in the previous section, suggesting CRH^{PVH} neuronal activity increases when glucose availability is reduced. In addition, this elevated activity level is maintained whilst hypoglycaemia or glucoprivation is present

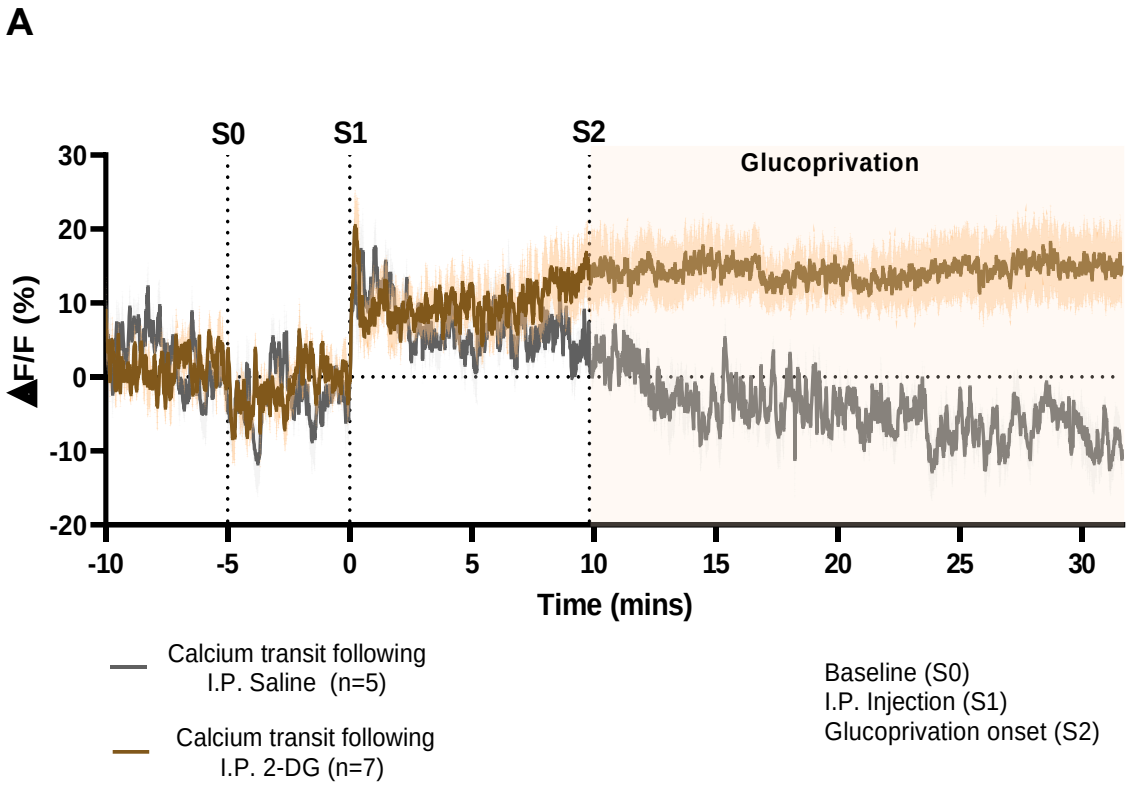
A
S0
S1
S2
Glucoprivation
30
20
10
0
-10
-20
▲F/F (%)
-10
-5
0
5
10
15
20
25
30
Time (mins)
Calcium transit following I.P. Saline (n=5)
Calcium transit following I.P. 2-DG (n=7)
Baseline (S0)
I.P. Injection (S1)
Glucoprivation onset (S2)

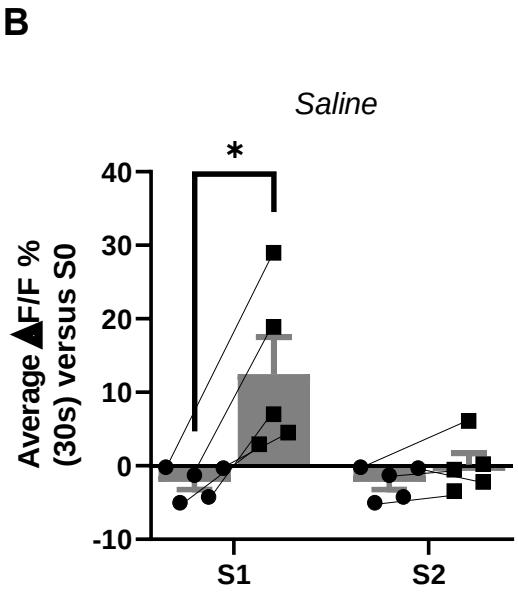
B
Saline
*
40
30
20
10
0
-10
Average ▲F/F % (30s) versus S0
S1
S2

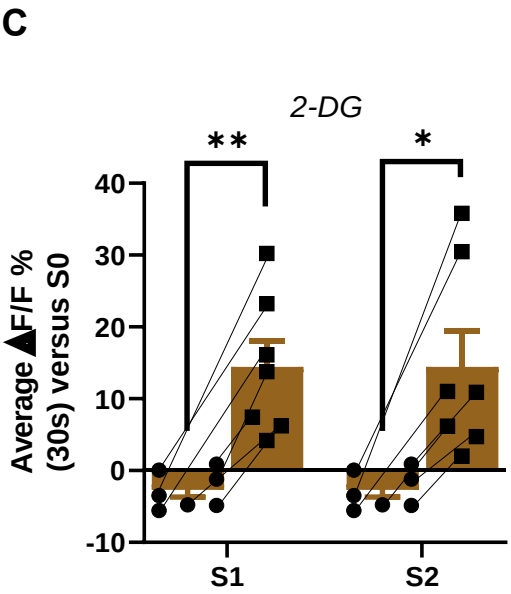
C
2-DG
**
*
40
30
20
10
0
-10
Average ▲F/F % (30s) versus S0
S1
S2

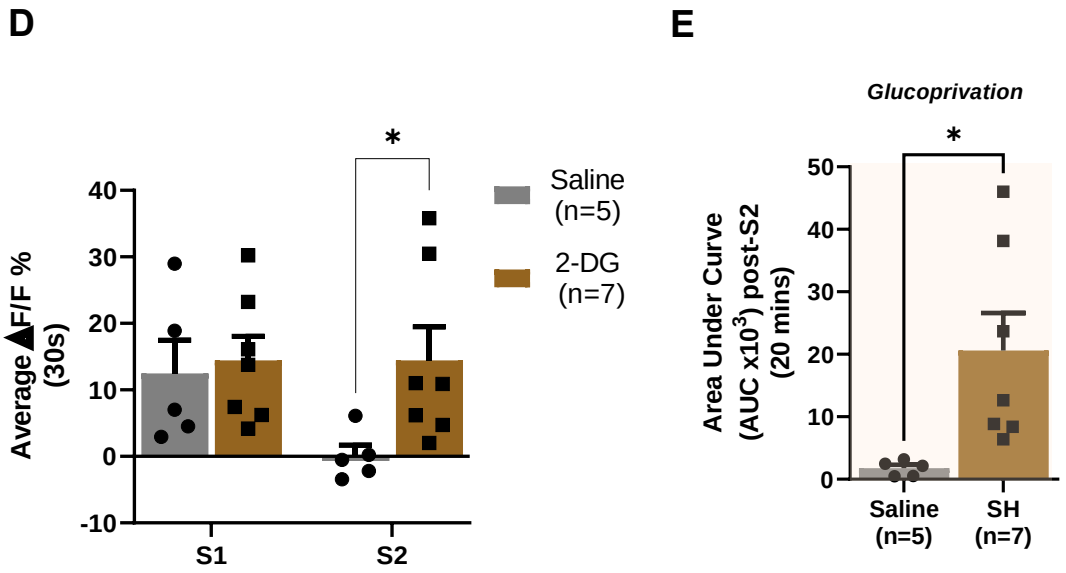

Figure 5.8: CRH^{PVH} neuron response to 2-DG induced glucoprivation

A: Plot of calcium transits of CRH^{PVH} neurons aligned to the time of i.p. injection with saline or insulin (SH). Saline and 2-DG groups displayed similar calcium dynamics to i.p. injection (S1). 2-DG led to an increase in calcium signal at S2, whilst saline led to a return of the signal to baseline levels (S0).
B: Average calcium signal (30 s window) at S1 and S2 compared with baseline (S0), in saline mice. S1 values were significantly increased when compared with S0 (*p<0.05; paired t-test).
C: Average calcium signal (30 s window) at S1 and S2 compared with baseline (S0) following 2-DG. S1 and S2 values were significantly increased when compared with S0 (*p<0.05, both versus S0; paired t-test).
D: Average calcium signal (30 s window) at S1 and S2 for saline and 2-DG groups. At S1, calcium signal values were similar. However, at S2, this was significantly increased in 2-DG, compared with saline (*p<0.05, 2-DG versus saline; unpaired t-test).
E: Area under the curve (AUC) for calcium signal (20 min window post-S2) in saline and 2-DG groups. The AUC was significantly higher in 2-DG, compared with saline (*p<0.05; unpaired t-test).
For plots of calcium signal, the dark colour indicates mean signal, light colour tones indicate SEM.

5.3.5 CRH^{PVH} neuron response to RH

5.3.5.1 CRH^{PVH} neuron response to RH, experimental protocol and screening

The RH experiment protocol is outlined in **Figure 5.9A**. The calcium transits for FP1 (green) and FP2 (blue) overlapped and showed similar dynamics (**Figure 5.9B**). Surprisingly, FP on both trials led to an initial rise in calcium signal. This was more pronounced than previously witnessed and may represent anticipatory stress. Reassuringly all animals demonstrated a reduction in calcium signal on approach to the food and consumption. The average calcium signal for the 10 min post-FP window during FP1 and FP2 is shown in **Figure 5.9C.** This demonstrated the similar calcium dynamics, suggesting GCaMP expression had stabilised.

A

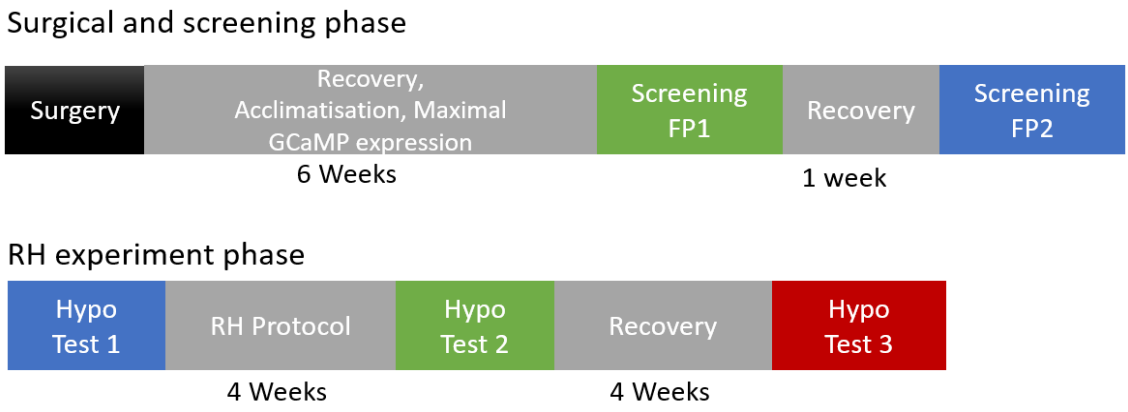

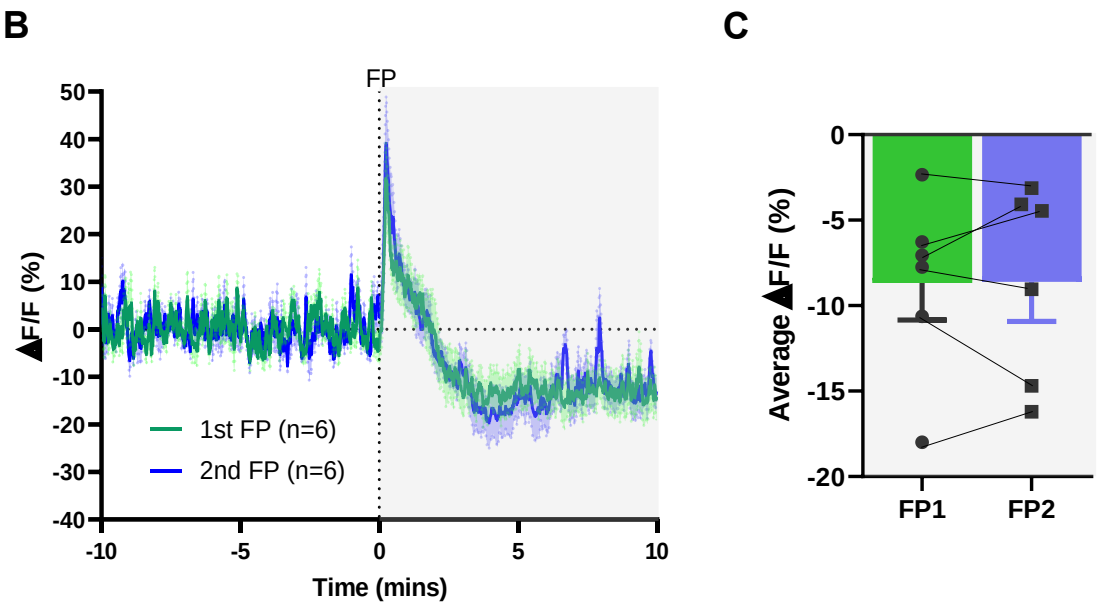

Figure 5.9: CRH^{PVH} neuron response to RH, experimental protocol and screening

A: Experimental protocol.
B: Plot of calcium transits for FP1 (green) and FP2 (blue) following overnight fast. Grey background marks the post-stimulus period of 10 min.
C: Average calcium signal for 10 min following FP for each animal during FP1 and FP2, showing similar calcium dynamics.

5.3.5.2 CRH^{PVH} neuron response during Test 1, 2 and 3

The calcium transits for the Tests 1, 2 and 3 are shown in **Figure 5.10A**. The blood glucose profile is overlayed to aid interpretation. S1 (s.c. injection), S2 (hypoglycaemia onset) and S3 (tail restraint) were identified for each mouse and the average time point for all tests plotted on **Figure 5.10A**.

During all tests, the calcium transit was low at baseline and increased rapidly following s.c. insulin injection (S1). The peak calcium signal at S1 was higher during Test 1, when compared to Test 2 and 3, respectively, but the kinetics of the response was very similar. At S2, the calcium signal for all tests increased at a similar time, reaching a plateau. Strikingly, this increase was attenuated in Test 2, compared with Test 1 (average ΔF/F at S2 (30s window) for Test 1 = 28.7 ± 9.8%; Test 2 = 13.5 ± 3.3%; **Figure 5.10B**), though this was not statistically significant. During all tests, the calcium signal remained at a constant level between S2 and S3, due to hypoglycaemia. Over this period, the AUC for the calcium transit was less in Test 2, relative to Test 1, however not reaching statistical significance (**Figure 5.10C)**. Similarly, the peak calcium signal between S2 and S3 was lower following RH (Peak ΔF/F for Test 1 = 41.6 ± 10.2%; Test 2 = 21.5 ± 3.4%), however was not statistically significant (**Figure 5.10D**). Tail restraint (S3) lead to a small additional increase in calcium signal in all tests and will be discussed separately in

5.3.5.3. Blood glucose levels, taken at the end of the recording (35 min post-injection) are shown in **Figure 5.10E**, showing lower blood glucose levels in Test 2, following RH.

Following the 4-week recovery period, the calcium transits follow the same pattern in Test 3, when compared with Test 2. This included overlapping calcium signal kinetics at baseline and at S1, where animals in both groups display similar elevations in signal. At around 7 min post-S1, the calcium signal increases in both tests, overlapping with a fall in blood glucose level. However, the peak calcium signal value was significantly greater during Test 3, when compared to Test 2 (Peak ΔF/F for Test 3 = 28.5 ± 5.2%; Test 2 = 21.5 ± 3.4%; *p<0.05; **Figure 5.10D**). Tail restraint (S3), once more lead to a small additional increase in calcium signal in both test and is discussed in **5.3.5.3**. In support of recovery of the CRR, blood glucose levels taken at the end of the recording (35 min post-injection) were increased in Test 3, when compared to Test 2 (**Figure 5.10E)**.

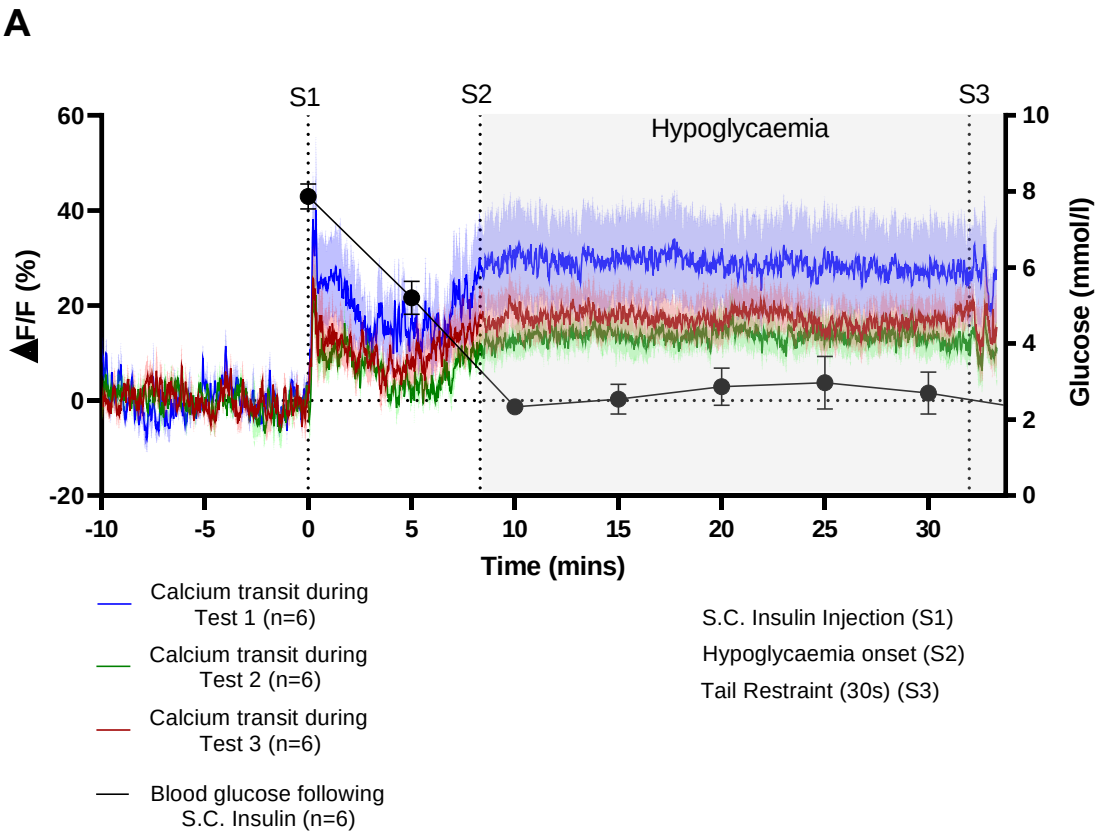

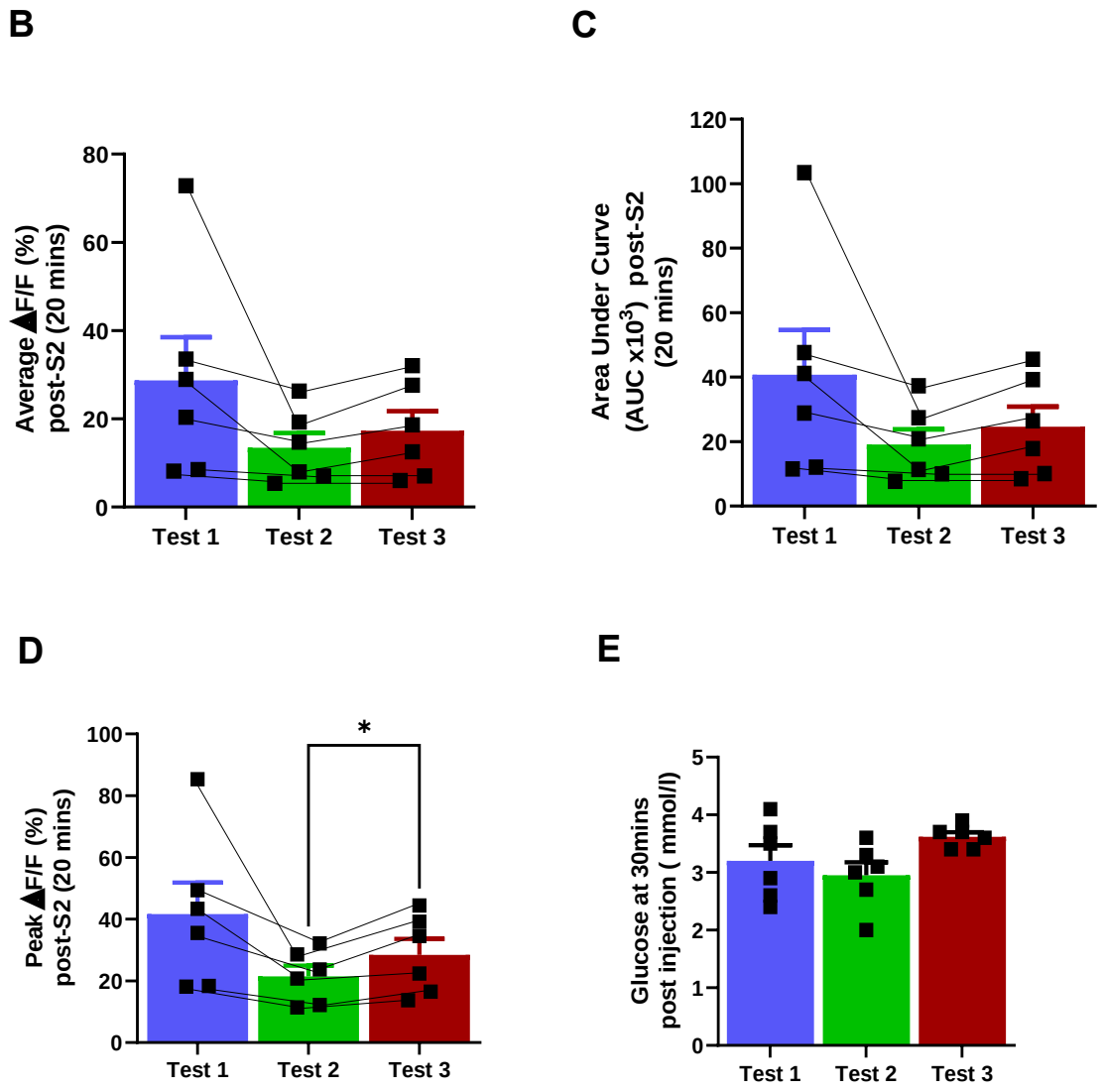

Figure 5.10: CRH^{PVH} neuron response during Tests 1, 2 and 3

A: Plot of calcium transits of CRH^{PVH} neurons aligned to the time of s.c. insulin injection on Test 1 (blue) and Test 2 (green). Blood glucose levels are overlayed to highlight hypoglycaemia-related effects. Prior RH led to a smaller increase in calcium signal during hypoglycaemia (Test 2). A 4-week recovery period led to an increase in calcium signal during a subsequent episode of hypoglycaemia (Test 3).
B: Average calcium signal post-S2 (20 mins) during hypoglycaemia, for Tests 1, 2 and 3. S2-onset was separately identified for each animal.
C: Area under the curve (AUC) for calcium signal (20 min window post-S2) for Tests 1, 2 and 3. This provided a measure of the cumulative calcium transit during hypoglycaemia.
D: Peak calcium signal (during 20 min post-S2) was significantly higher in Test 3, compared with Test 2 (*$p<0.05$; repeated measures ANOVA with Sidak's *post hoc* test).
E: Blood glucose levels at 35 min after injection for all animals in Tests 1, 2 and 3.
Repeated measures ANOVA with Sidak's *post hoc* test was used in the statistical analysis for this experiment.

5.3.5.3 CRH^{PVH} neuron response to tail restraint

Tail restraint (TR) for 20 s led to a rapid increase in CRH^{PVH} neuronal calcium signal (**Figure 5.6 C,D**). Importantly, as a stimulus, it is a heterotypic stressor when compared with RH. Animals were exposed to TR at the end of each test, to enable the primary effect of hypoglycaemia to be assessed without interference. The CRH^{PVH} neuronal calcium transit following TR is show for the three tests in **Figure 5.11A**. The increase in calcium signal which related to TR was identified for each mouse and is termed S3. The average S3 timepoint is plotted on **Figure 5.11A**. The calcium transits were aligned to S3 to enable comparisons between tests. TR led to a rapid increase in calcium signal on all test days. This was reflected by a similar average, AUC, and peak calcium signal (ΔF/F) for Test 1 and Test 2 (**Figure 5.11B-D**). TR during Test 3 led to a non-significant increase in average, AUC, and peak calcium signal (ΔF/F). However, this effect was primarily driven by one animal, which displayed disproportionately elevated calcium signal following TR during Test 3 when compared with the previous tests (**Figure 5.11B-D**). Following 20 s of TR, the calcium signal returned to baseline levels. Taken together, the kinetics and magnitude of the calcium transit were preserved across all three tests.

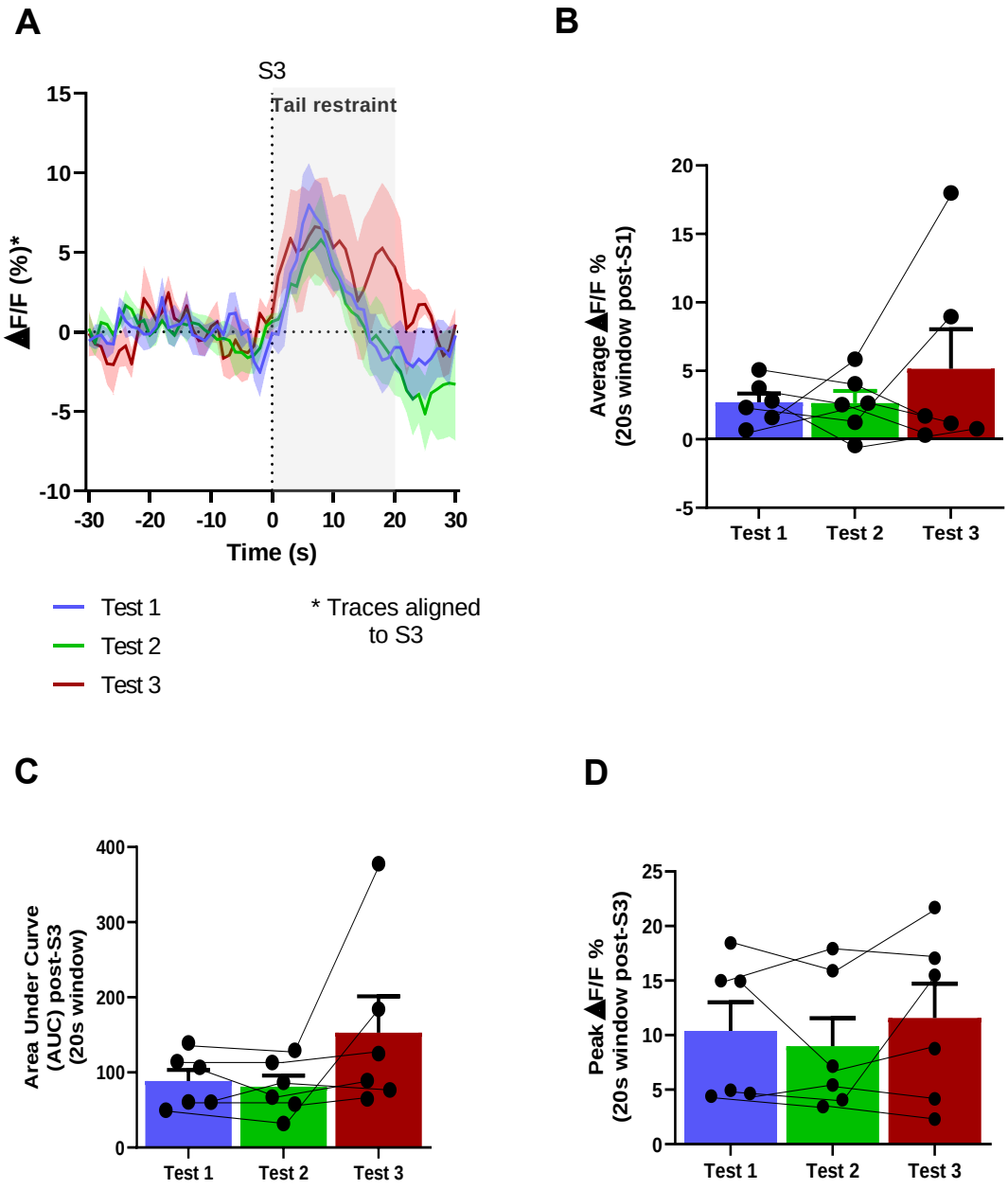

Figure 5.11: CRH^{PVH} neuron response to tail restraint

A: Plot of calcium transits of CRH^{PVH} neurons aligned to average time of TR (S3) for Test 1 (blue), Test 2 (green) and Test 3 (red). Calcium dynamics for the three tests overlap and are preserved.
B: Average calcium signal (20 s window post-S3) for the three tests.
C: Area under the curve (AUC) for calcium signal (20s window post S3) for the three tests.
D: Peak calcium signal (20 s window post-S3) for the three tests.
Repeated measures ANOVA with Sidak's *post hoc* test was used in the statistical analysis for this experiment.

5.4 Discussion

Adaptive changes within the glucose-regulatory network and in specific brain regions, like the PVH, may culminate in IAH (Chapter 3). At a whole-organism level, our data add support to the theory that habituation underlies IAH (Chapter 4). The PVH is thought to contain primarily pre-motor and integrative glucose-regulatory networks. These modulatory neuronal networks are a credible locus for habituation. Likewise, CRH^{PVH} neurons represent an important neuronal population in the modulation of neuroendocrine responses to novel or familiar stress and, as we postulate, to RH (Kim et al., 2019b). Consequently, CRH^{PVH} neurons were selected as the focus of our investigations.

In Chapter 5, we used *in vivo* fibre photometry to characterise the real-time dynamics of the CRH^{PVH} neuronal response to acute and repeated stressors. The primary aim of these investigations was to demonstrate that CRH^{PVH} neurons are activated acutely by hypoglycaemia and that this activation is altered and possibly habituated following RH. We postulated that RH, acting as a repeated homotypic stressor would lead to reduced neuronal responsiveness, whereas responses to heterotypic stress would be preserved. Secondary aims were to characterise the dynamics of CRH^{PVH} neuronal activity following other stimuli, which included food presentation, injection stress and tail-restraint stress.

The first experiment involved characterising the calcium dynamics of CRH^{PVH} neurons to food presentation in the fasted and fed state. This was performed with the primary aim of establishing a post-surgery screening test, which was minimally invasive and could identify responding animals for use in subsequent experiments. Food presentation (FP) led to a reduction in calcium signal only in the fasted state and not in the fed state, which was consistent with existing literature (Li et al., 2019). Fasting is an interoceptive stressor and is known to activate CRH neurons, shown by increased cFos expression and by corticosterone release (Li et al., 2019, Bains et al., 2015). Therefore, it is likely that after fasting, FP inhibits CRH^{PVH} neuronal activity as a mechanism to relieve stress (Li et al., 2019). From our data, we cannot confirm whether CRH^{PVH} neuronal activity is raised after fasting. However, the calcium signal on FP remains low for several minutes after consummatory activity had finished (**Figure 5.5**). This suggests that a new baseline of CRH^{PVH} neuronal activity is reached after termination of the stressor (fasting). Interestingly, it has been reported that the bulk of the reduction in calcium signal preceded food intake (Li et al., 2019). If this is true, this may suggest inhibition of CRH^{PVH} neuronal activity on sensory detection of food. This was not examined in our investigation. However, pairing photometry and video recordings would enable this to be identified. In this experiment, we elected to use a pellet of high-energy diet (HED), as this is highly appetitive and overcomes neophobia. Although we did not directly compare

this with normal diet, there is evidence that palatability and rewarding value of food relates to the magnitude of CRH^{PVH} inhibition (Yuan et al., 2019, Kim et al., 2019a).

Aversive stimuli have similarly been shown to rapidly activate CRH^{PVH} neuronal activity, which is in keeping with the well documented role of CRH^{PVH} neurons in neuroendocrine and behavioural responses to stress (Füzesi et al., 2016, Bains et al., 2015). In mice, rapid elevations in calcium transits relating to CRH^{PVH} neuronal activity are witnessed during a variety of stimuli, including forced-swim test, tail restraint, predator odour and i.p. injection of lithium chloride (causing gastric malaise) (Kim et al., 2019a). In this Chapter, we confirmed that s.c. injection with saline and tail restraint (TR), both applied for a short period of time (<30 s) lead to an instant increase in calcium signal, corresponding with increased CRH^{PVH} neuronal activity (**Figure 5.6**). From our observations, most of the initial rise in activity was on approach to scruff the mouse (s.c. injection) or to catch the tail (TR). This corroborates published data, showing the approach and capture of the animal leads to a rapid rise in CRH^{PVH} neuronal calcium signal (Kim et al., 2019a). Though both s.c. injection with saline and TR led to calcium dynamics which corresponded to the onset and termination of the stimulus, CRH^{PVH} neuronal activity failed to return to baseline for several minutes. It is possible that this persistent neuronal activity may reflect neuropeptide release and the regulation of the neuroendocrine HPA axis. Thus, CRH^{PVH} neuronal activity in the immediate and post-stimulus phase, may serve to direct different responses and behaviours. This is supported by optogenetic studies which show that the immediate activation of CRH^{PVH} neurons elicits rapid defensive behaviours, paralleling behaviours which follow acute stress (Kim et al., 2019a, Spruijt et al., 1992, Füzesi et al., 2016).

We next examined the calcium dynamics of CRH^{PVH} neurons following SH and 2-DG (**Figure 5.7 & 5.8**). We postulated that both stimuli would lead to activation of CRH^{PVH} neurons, with a corresponding elevation in calcium signal. In both treatments, injection led to a rapid increase in signal, termed S1. This was followed by a reduction in signal, though this failed to return to baseline levels. Importantly in both treatments, the calcium signal increased again, becoming a significant change at S2. This was taken to be the onset of hypoglycaemia (SH) or glucoprivation (2-DG). In both treatments, the calcium signal after S2 plateaued, remaining at an elevated level until the end of the recording. The delay in the rise in calcium signal between S1 and S2 was likely due to the time taken for the drugs to reach systemic circulation and activate sensing elements. This was corroborated by blood glucose measurements in the same group of mice, which identified that s.c. insulin (1.75 U/kg) led to a drop in blood glucose between 5 and 10 min after injection, causing hypoglycaemia (**Figure 5.7**). Blood glucose levels remained low until around 35 min after injection, following which rapid recovery occurred. The

blood glucose profile following SH, strongly suggests that hypoglycaemia leads to elevated CRH^{PVH} neuronal activity. However, it should be acknowledged glucose was measured in the same mice but on a separate day. Systemic administration of 2-DG at a similar dose in rats and mice leads to stimulation of the CRR and hyperglycaemia. This hyperglycaemia was noted at around 15 min after injection and persisted for over 2 hrs (Garfield et al., 2014, Sanders and Ritter, 2000). Glucose measurements were not performed in our experiment involving 2-DG, as the separation of stress-induced hyperglycaemia attributed to tethering, injection or 2-DG would not be possible. We did not directly test if the changes which follow SH could be related to hyperinsulinaemia, which may modulate the CRR (Lingenfelser et al., 1996, Davis et al., 1993). However, as both SH and 2-DG lead to a state of cellular glucose depletion, it is likely that our observations relate this this and not to hyperinsulinaemia.

The severity or aversive salience of a stimulus is difficult to quantify and depends on context and prior experience (Kim et al., 2019b). As a result, we did not compare the magnitude of CRH^{PVH} neuronal calcium dynamics for different stressors. In addition, as different cohorts of animals were used for each experiment, appropriate comparison would not be possible. However, we noted that the temporal kinetics of the stressor and CRH^{PVH} neuronal activity did closely align. Stressors with rapid onset and termination, including injection and tail restraint, lead to corresponding short-lived elevations in calcium signal. Whilst longer duration, physiological stressors, such as hypoglycaemia and glucoprivation lead to persistently elevated calcium signals, signifying a high level of sustained CRH^{PVH} neuronal activity.

In the final experiment, we investigated whether CRH^{PVH} neuronal calcium dynamics change following RH, demonstrating habituation. We postulated that CRH^{PVH} neuronal calcium dynamics would alter with RH, acting as a homotypic stressor, but not to tail restraint, which represented a heterotypic stressor. In addition, we tested whether spontaneous recovery of the response occurs on withdrawal of the habituation stimulus. This was performed by measuring the CRH^{PVH} neuronal calcium transit for each animal on three tests, with each animal acting as their own comparison. Test 1 and Test 2 were separated by the 4-week RH protocol, characterised in Chapter 3. An additional test was performed after a 4-week recovery period (Test 3) (**Figure 5.9A**). Animals first underwent a long post-surgery screening phase to establish stable GCaMP expression and calcium transits to FP (**Figure 5.9B,C**). Surprisingly, FP led to a transient but substantial elevation in calcium signal on opening the photometry system and dropping the food pellet (**Figure 5.9B**). A possible explanation for this is that animals in this cohort had associated opening the cabinet with an impending stressful experience. This conditioned response to stress may be detrimental for detecting changes in calcium signal to short

duration stimuli. However, in this experiment FP still led to a reduction in CRH^{PVH} neuronal activity which was consistent across FP1 and FP2. Subsequently, all animals underwent a photometry recording on the first (Test 1) and last (Test 2) day of the 4 week-RH protocol. The calcium dynamics on both tests followed the same pattern as was previously observed. However, following RH (Test 2) there was attenuation in the calcium signal in all animals, relative to Test 1, during the window of hypoglycaemia (S2-S3) (**Figure 5.10**). The magnitude of response attenuation varied, and in most animals, this was only a small reduction. It is possible that this reflected differences between animals in the degree to which RH led to impairment of the CRR. We did not take CRR hormone measurements in this experiment. This may have provided a functional correlate to the CRH^{PVH} neuronal response and explained the variability. However, blood sampling whilst recoding would have been technically challenging and produced an additional source of stress, affecting calcium dynamics. Strikingly after a 4-week recovery period, CRH^{PVH} neuronal calcium dynamics normalise following a final episode of hypoglycaemia (Test 3) (**Figure 5.10**). Specifically, the peak calcium signal increased during the window of hypoglycaemia. Again, the magnitude of response recovery was small between Test 2 and Test 3, but this was consistent across all animals. It should be noted that though the calcium signal increased at a 4-week period, this did not fully normalise.

At the end of each of the three tests, animals received tail restraint for 20 s. As we had predicted, this led to similar elevations in calcium signal, aligning to the onset of TR (S3; **Figure 5.11**). The was reflected in similar average, AUC and peak calcium signal on the three test occasions. The calcium signal on Test 3 showed a non-significant increase, however this was driven by the response of one particularly responsive animal.

Combined, these data show hallmarks of habituation at the level of the CRH^{PVH} neuron. Specifically, RH, acting as a homotypic stressor, leads to reduction in CRH^{PVH} neuronal calcium signal, which then recovers if the habituating stimulus is withdrawn for 4-weeks. On the other hand, the CRH^{PVH} neuronal calcium signal is preserved to the heterotypic stress of TR, when applied infrequently. These data support a growing understanding that CRH^{PVH} neurons are capable of rapidly tailoring neuroendocrine responses and behaviours depending on stress familiarity (Kim et al., 2019a, Kim et al., 2019b, Füzesi et al., 2016, Bains et al., 2015). Interestingly, habituation of CRH^{PVH} neuronal activity to repeated presentations of a loud white noise stimulus has been demonstrated in mice (Kim et al., 2019b). Consistent with our own findings, the response recovered, following a 3-week period of white noise abstinence. Significantly, Kim *et al.* identified that stress familiarity alone was the primary driver for habituation of responses and was independent of negative feedback from corticosterone release (Kim et al., 2019b). These findings

challenge the canonical view of corticosterone as the main inhibitory control on CRH^{PVH} neurons (Bittar et al., 2019, Kim and Iremonger, 2019). Indeed, our data corroborates findings in other *in vivo* studies that CRH^{PVH} neurons are rapidly activated by aversive stimuli and that the removal of the stimulus alone is sufficient to reduce activity to baseline (Kim et al., 2019a, Kim et al., 2019b). The temporal kinetics of this reduction cannot be explained by hormone-mediated negative feedback. In addition, the observation that rewarding or appetitive stimuli lead to a rapid inhibition of CRH^{PVH} neuronal activity, suggests that neuronal circuits, via fast neurotransmitter release modulate CRH^{PVH} neuronal activity (Yuan et al., 2019). This hypothesis will be revisited in Chapter 6 and Chapter 7.

In this Chapter, *in vivo* fibre photometry was used to measure CRH^{PVH} calcium transits, using the calcium indicator GCaMP. Though this provides a sensitive measure of changes in Ca^{2+} concentration which precede neuronal action potentials, it remains a proxy of neuronal activity (Wang et al., 2021). Therefore, findings should be correlated with electrophysiological data. Though *in vivo* fibre photometry has poorer temporal resolution than traditional electrophysiological techniques, it does provide access to a genetically-defined neuronal population (Li et al., 2019).

It must also be acknowledged that the calcium signal is dependent on several factors, principle of which is the position of the optic fibre and distribution of the genetically-defined neuronal population being studied (Wang et al., 2021). In our experience, an important source of variability occurred from differences in the implanted optic fibre position and CRH^{PVH} neuronal transfection. Fortunately, CRH^{PVH} neurons form an anatomically distinct population, meaning responses from other CRH neuron populations would not have been captured.

It is likely that in future studies, stricter criterion is required to define responders in the screening phase. This will allow inclusion of animals into experiments only if they reach a defined threshold of CRH neuronal activity inhibition on food presentation. Further work is required to define this threshold.

5.5 Summary

- CRH^{PVH} neuronal activity rapidly increases following s.c. injection and tail restraint stress, and decreases on food presentation in fasted mice.
- Following SH or 2-DG glucoprivation, CRH^{PVH} neuronal signal increases and demonstrates similar response kinetics.
- Following SH, the rise in CRH^{PVH} neuronal activity corresponds with a fall in blood glucose and hypoglycaemia.
- Following RH, the CRH^{PVH} neuronal response reduces to a subsequent episode of hypoglycaemia, signifying habituation.
- After 4-week recovery and re-test, a final episode of hypoglycaemia leads to CRH^{PVH} neuronal response recovery.
- CRH^{PVH} neuronal activity attenuates with homotypic stressors (RH), but remains intact following a heterotypic stress (TR).
- CRH^{PVH} neurons are an important hypoglycaemia-responsive population which habituates to RH.

5.6 Conclusion

These data provide evidence that habituation of the CRR after RH, can be detected not only at the whole organism level, but also at a neuronal population level. In this Chapter we have examined habituation within a pre-motor/integrative network using *in vivo* fibre photometry. Corroborating previous studies, we showed that CRH^{PVH} neurons display rapid and biphasic responses which depend on prior experience of the stimulus, the nutritive state and valence of the stimulus.

We found that elevations in CRH^{PVH} neuronal activity are paired to hypoglycaemia, demonstrating the real-time involvement of CRH^{PVH} neurons in the CRR. Importantly, we identified that CRH^{PVH} neurons alter responses according to the familiarity of the stress, demonstrating attenuated responses to homotypic RH stress, but intact responses to heterotypic TR stress.

These data, add to evidence that CRH^{PVH} neurons are integral to both immediate and long-term responses to stress. Crucially, CRH^{PVH} neurons orchestrate immediate behaviours which are likely to be controlled through neuronal circuits, rather than hormone feedback. It is not yet clear if CRH^{PVH} neurons, acting via neuronal circuits, also control immediate counter-regulatory responses when an organism is faced with hypoglycaemia.

Chapter 6

The role of CRH^{PVH} neurons in the sympathoadrenal response to hypoglycaemia

6.1 Introduction

CRH^{PVH} neurons have been viewed classically to control physiological responses to stress via a hormone cascade, resulting in glucocorticoid-mediated central and peripheral effects. This process, which can require several minutes to affect brain circuits, is at odds with observations that CRH^{PVH} neurons can drive rapid behaviours after stress (Droste et al., 2008, Füzesi et al., 2016). In support of this, we have shown in Chapter 5 that CRH^{PVH} neuronal activity is immediately enhanced on presentation of a stressor and rapidly terminates on its removal. In addition, the optogenetic stimulation of CRH^{PVH} neurons in mice, leads to immediate defensive behaviours (Füzesi et al., 2016). Similarly, in vivo fibre photometry studies show a rapid increase in CRH^{PVH} neuronal activity immediately before an escape response (Daviu et al., 2020). These observations suggest that CRH^{PVH} neurons may have a preparative role in directing autonomic output before fight or flight. It is not yet fully understood how CRH^{PVH} neurons contribute to autonomic responses to physiological stressors, such as hypoglycaemia.

In hypoglycaemia research, the most detailed body of work linking CRH^{PVH} neuronal function with the sympathoadrenal response, has involved the study of CRH neuropeptide release and signalling pathways. CRH neurons are characterised by their release of CRH and a family of related peptides including urocortins 1-3. These neuropeptides, in turn, act via CRH receptors (CRHR1 and CRHR2) to stimulate sympathetic outflow, manifested by changes in heart rate and blood pressure, as well as elevations in glucose and CRR hormone release (Brown et al., 1982, McCrimmon et al., 2006b). CRH signalling, likely via CRHR1 ensures an appropriate sympathoadrenal response to stressors, including hypoglycaemia (Flanagan et al., 2003).

It is possible that CRH^{PVH} neurons exert a controlling influence on autonomic regions through direct axonal projections. Indeed, PVH neurons project to the rVLM, which in turn provides a major excitatory input to sympathetic preganglionic vasomotor neurons of the spinal intermediolateral cell column (IML) (Milner et al., 1993). Interestingly, Lee et al., reported that in rats, around 30% of rostral VLM-projecting PVH neurons express CRH, though the functional significance of this connection was not investigated (Lee et al., 2013). Recently, there has also been interest in intra-PVH micro-circuits, which may enable CRH^{PVH} neurons to regulate autonomic function during stress (Ramot et al., 2017, Jiang et al., 2018). These intra-PVH circuits involve monosynaptic connections with a population of $CRHR1^{PVH}$ neurons, which subsequently send excitatory, long-range projections to autonomic regions, potentiating autonomic outflow during stress (Jiang et al., 2018).

Therefore, CRH^{PVH} neurons can influence autonomic function through a variety of glucocorticoid-independent pathways. In addition, our data in Chapters 3 and 5 suggest that CRH^{PVH} neurons are activated acutely following SH. However, there are no studies which directly examine the functional significance of CRH^{PVH} neurons to the sympathoadrenal response. Or, whether specific neuronal circuits involving CRH^{PVH} are activated following hypoglycaemia.

6.1.1 Objective

1) **Investigate the functional significance of CRH^{mpdPVH} neurons to the sympathoadrenal response following hypoglycaemia**

Hypoglycaemia activates CRH^{PVH} neurons and, as we have shown, leads to increased neuronal cFos in the mpdPVH region (Chapter 3). In Chapter 5, we showed that SH leads to elevations in the in vivo calcium signal in CRH^{PVH} neurons. In addition, it is known that hypoglycaemia increases CRH mRNA and HPA axis activation, providing indirect measures of CRH^{PVH} neuronal activation (Inouye et al., 2006, Chan et al., 2002). CRH^{PVH} neurons are increasingly seen as having HPA axis-independent functions and can direct autonomic activity, including following hypoglycaemia (Füzesi et al., 2016, Flanagan et al., 2003, McCrimmon et al., 2006b). However, the functional significance of CRH^{PVH} neuronal activity to the sympathoadrenal response and glucose homeostasis has not been directly investigated. To this end, we used a chemogenetic approach to study the effects of CRH^{mpdPVH} activation or inhibition, on glucose and sympathoadrenal responses, including to hypoglycaemia. We postulated that CRH^{mpdPVH} neuronal activity drives circuits which elevate blood glucose and promote sympathoadrenal activity, independent of the HPA axis.

2) **Investigate connections between CRH^{mpdPVH} neurons and autonomic regions involved in the sympathoadrenal response following hypoglycaemia**

PVH neurons, including CRH^{mpdPVH} neurons could influence autonomic function through a variety of pathways, involving CRH peptide signalling, intra-PVH circuits or through direct connections to the hindbrain. Indeed, in rats and mice, at least a proportion of CRH^{PVH} neurons do project to the rVLM and NTS (Lee et al., 2013, Zhao et al., 2017). However, it is not clear whether hindbrain-projecting PVH neurons are hypoglycaemia-responsive, or what their neuropeptide or receptor phenotype is. Consequently, we used a neuronal tracing and immunohistochemistry approach to understand the anatomy and phenotype of hindbrain-projecting PVH neurons. We were particularly interested in connections to the rVLM C1 group, as this catecholaminergic (CA) neuronal population is central to the sympathoadrenal response to hypoglycaemia and glucoprivation (Ritter

et al., 2019, Li et al., 2018). We postulated that a CRH^{mpdPVH} → rVLM connection is activated following SH, outlining a pathway which enables CRH^{mpdPVH} neurons to control sympathoadrenal output.

6.2 Methods

6.2.1 Animals

Adult male *Crh*-cre::eYFP (Chapter 2), aged 8-10 weeks, old were used for all chemogenetic studies in this Chapter.
For chemogenetic studies, group sizes were established using a power calculation and by factoring in a 20-30% attrition rate to account for any mice that had insufficient transduction. From pilot work in our lab (Luckman, unpublished) involving the chemogenetic activation of *Crh*-cre::hM3Dq neurons in the PVH (performed as a cross-over and analysed using a paired Student's t-test; alpha = 0.05) a moderate effect size (0.57) means an n = 12 was required to achieve a power of 93%.

Adult male *Crh*-cre::eYFP (Chapter 2), aged 8-10 weeks, old were also used for retrograde tracing studies to establish projections from CRH^{mpdPVH} → rVLM. For the retrograde tracing studies, adult male *VGlut2*-cre::eYFP (Chapter 2), aged 8-16 weeks, were used to establish projections from $VGlut2^{PVH}$ → rVLM.

The TRAP2 mouse ($Fos^{2A\text{-}iCreER}$; Jax strain #030323; C57BL/6J background) is a knock-in line which expresses tamoxifen-inducible, improved Cre recombinase (*icre/ERT2*) driven by *Fos* promoter/enhancer elements (DeNardo et al., 2018). This system enables the permanent genetic access to neurons which are activated by a specific stimulus (e.g., hypoglycaemia). TRAP2 mice aged 16-10 weeks were used in the final study in this Chapter.

Animals were acclimatised to the holding room and handled daily for 2 weeks prior to each experiment.

6.2.2 Chemogenetic activation of CRH^{mpdPVH}

Intracranial surgery

Crh-cre::eYFP mice (n=12) underwent intracranial surgery, as described in Chapter 2. AAVs carrying a Cre-dependent stimulatory DREADD construct (AAV8-hSyn-DIO-hM3D(Gq)-mCherry) were injected bilaterally into the mpdPVH region. AAV titre, coordinates and injection volumes are outlined in the Chapter 2. After surgery, animals

were left in their home cages for three weeks to enable recovery, viral transfection and gene transduction.

Experiment

The experiment was performed as a cross-over study on two test days (test 1 and test 2), which were separated by one week. On test days, mice were fasted for 3 hr in the morning and then randomised to receive either an i.p. injection of saline or clozapine-N-oxide (CNO; 1 mg/kg; Tocris) in a volume of 4 ml/kg. Blood glucose levels were checked at baseline (pre-injection) and every 30 min for 120 min post-injection, by tail-tip blood sampling. In addition, blood samples were taken at baseline and at 30 min after injection to measure adrenaline levels. Blood glucose testing, blood sampling and ELISA methods are described in Chapter 2. All animals received both treatments over the two test days enabling paired comparisons.

Immunohistochemistry

Viral transfection of CRH^{mpdPVH} neurons and neuronal activation was verified using triple immunohistochemistry for mCherry (stimulatory DREADD), cFos and GFP (*Crh*-cre::eYFP). This was achieved by administrating a final dose of CNO (i.p., 1 mg/kg) to all animals. Two hours later, animals were perfused with fixative and brains dissected and processed for immunohistochemistry. Processing of brain sections and immunohistochemistry methods are outlined in Chapter 2. Neurons, in the relevant regions of interest, were stained for mCherry (red-fluorescent secondary antibody), cFos (blue-fluorescent secondary antibody) and GFP (green-fluorescent secondary antibody). Only animals with on-target and bilateral viral transfection (n = 6) were included in the results.

6.2.3 Chemogenetic inhibition of CRH^{mpdPVH}

Intracranial surgery

Crh-cre::eYFP mice (n=12) underwent intracranial surgery in two batches. This time, AAVs carrying a Cre-dependent inhibitory DREADD construct (AAV8-hSyn-DIO-hM4D(Gi)-mCherry) were injected bilaterally into the mpdPVH region. Injection co-ordinates, AAV titre and injection volumes are outlined in the Chapter 2. After surgery, animals were again left in their home cages for three weeks to enable recovery and viral transfection.

Experiment 1

As we had experienced difficulties with previous batches of the inhibitory DREADD virus, we elected to first test whether glucose and corticosterone responses were attenuated following hypoglycaemia. This experiment was also performed as a cross-over study on two test days (test 1 and test 2), which were separated by one week.

On test days, mice were fasted for 3 hr in the morning and then randomised to receive either an i.p. injection of saline or CNO (1 mg /kg). All animals then received s.c insulin (1.75 U/kg) to induce hypoglycaemia. Blood glucose levels were checked at baseline and every 30 min for 120 min, via tail tip blood sampling. In addition, blood samples were taken at baseline and at 30 min to measure corticosterone levels.

Experiment 2

Next, following optimisations in virus titre (reduced to 1.9 x 10^{12} particles/µl) and injection volume (3 x 32 nl), we repeated the above experiment. In this experiment glucose and adrenaline responses were measured following hypoglycaemia. The experimental protocol was otherwise identical to Experiment 1.

Immunohistochemistry

Viral transfection of CRH^{mpdPVH} neurons was verified using dual-label immunohistochemistry for mCherry (inhibitory DREADD), and GFP (*Crh*-cre::eYFP). Only animals with on-target and bilateral viral transfection (n = 9 in Experiment 1 and n = 8 in Experiment 2) were included in the final results.
As i.p. CNO would inhibit transfected neurons, we did not perform cFos immunohistochemistry, as the absence of cFos is more difficult to interpret.

6.2.4 Retrograde tracing to investigate PVH→ rVLM connections using Fluoro-Gold

Intracranial surgery

Crh-cre::eYFP (n=6) and *VGlut2*-cre::eYFP mice (n=5) were injected unilaterally with the blue retrograde tracer Fluoro-Gold (FG) into the rVLM C1 group. Injection co-ordinates and volumes are outlined in the Chapter 2. After surgery, animals were left in their home cages for three weeks to enable recovery and transport of the tracer.

Immunohistochemistry

Animals were administered s.c insulin (1.75 U/kg) and 2 hr later were perfused, enabling tissue fixation at peak cFos protein expression. Hypoglycaemia-activated PVH→rVLM neurons were identified using immunohistochemistry. For PVH sections, this first involved separating anterior, middle, and posterior PVH sections, based on their distance from bregma. Next, sections underwent dual-label immunohistochemistry for cFos and GFP (*Crh*-cre::eYFP or *VGlut2*-cre::eYFP). In other PVH sections, immunohistochemistry for cFos and CRHR1 was performed. The endogenous fluorescence of the retrograde tracer was visualised for colocalisation in all PVH sections. For rVLM sections, dual-label immunohistochemistry was performed for cFos and TH (CA neurons in the C1 group). The endogenous fluorescence of the retrograde tracer was visualised to establish the injection site. Only on-target animals were included in counts (*Crh*-cre::eYFP (n=4) and *VGlut2*-cre::eYFP mice (n=3)).

6.2.5 Anterograde tracing to investigate PVH→ rVLM connections using TRAP2 mice

This study was performed with the aim of investigating projections from hypoglycaemia-activated PVH neurons to the rVLM. The TRAP2 mouse had not yet been validated in our laboratory, therefore this study was an adjunct to the retrograde tracing study outlined in the previous section.

TRAP2 System

The TRAP2 system uses the cFos gene locus to drive the expression of the tamoxifen-inducible Cre recombinase (CreER) along with a transgenic or AAV-delivered, Cre-dependent effector. In this experiment, an AAV containing a Cre-dependent channel rhodopsin (ChR2)-mCherry construct was injected unilaterally into the mpdPVH. When a neuron is activated following a stimulus (e.g., hypoglycaemia) CreER is produced. However, this is only able to enter the nucleus and catalyse recombination in the presence of tamoxifen (4-OHT) (DeNardo et al., 2018). Therefore, Cre recombination can be paired to neuronal activation following hypoglycaemia, by coordinating the administration of tamoxifen and insulin. In the literature, this technique is often referred to as “TRAPing”, and neurons which undergo successful Cre recombination in the presence of tamoxifen are referred to as “TRAPed”. The TRAP2 system is explained pictorially in **Figure 6.1**.

Intracranial Surgery

Male and female TRAP2 mice (male n=8 and female n=8) were injected unilaterally with AAVs carrying a Cre-dependent ChR2-mCherry construct (AAV8-EF1a-DIO-hChR2(H134R)-mCherry-WPRE-HGHpA) into the mpdPVH. The Cre-dependent expression of Chr2-mCherry in the neuronal cell membrane enables the anterograde tracing of neuronal connections. Injection co-ordinates, viral titre and volumes are outlined in the Chapter 2. After surgery, animals were left in their home cages for two weeks to enable recovery and transfection of cells.

Experiment: Hypoglycaemia-TRAPing of mpdPVH neurons

On the day of the experiment, animals were fasted for 3 hr in the morning then randomised to receive either s.c. insulin (1.75 U/kg) to induce SH, or volume matched saline. One hour later, animals then received either i.p. 4-OHT (10 mg/kg) or volume matched saline. In mice receiving i.p. 4-OHT, this would lead to Cre recombination of the ChR2-mCherry construct in transfected mpdPVH neurons, leading to stimulus-specific neuronal TRAPing. The groups were, therefore, as follows: SH/saline (n=5), saline/4-OHT (n=5) and SH/4-OHT (n=6). Food was returned to cages 1 hr after s.c injection and animals were left undisturbed for the next 24 hr. Ten days later, animals were perfused.

Immunohistochemistry

All animals were administered s.c insulin (1.75 U/kg) and 2 hr later were perfused with fixative to enable cFos quantification. Only on-target animals (SH/saline (n=4), saline/4-OHT (n=5) and SH/4-OHT (n=4)) were included in subsequent analysis. This was established by the presence of unilateral injection tract in the mpdPVH region.

I next used immunohistochemistry to identify TRAPed PVH neurons and to confirm if TRAPed neurons expressed cFos following hypoglycaemia. This was performed to assess if the TRAPing protocol was specific to hypoglycaemia. For PVH sections, this involved dual-label immunohistochemistry for mCherry (ChR2-mcherry expression in TRAPed neurons) and cFos. For hindbrain sections containing the LC, NTS and rVLM, dual-label immunohistochemistry was performed for mCherry (fibre staining) and TH (CA neurons).

6.2.6 Identification of transfection and quantification of neurons

Animals were included in the results of chemogenetic studies only if IHC demonstrated bilateral colocalisation of the viral reporter in >50% of CRH^{PVH} neurons. Investigators were blinded to the order of treatments received by each animal when checking transfection and during quantification.

For each animal, quantification of labelled neurons following chemogenetic and tracing experiments followed the same protocol. For each animal, neuronal counts were performed on a minimum of three brain sections (3-5 sections per region, depending on availability) which contained the region of interest, and then averaged to provide counts per section. For chemogenetic experiments counts were performed bilaterally. For tracing experiments, counts were performed unilaterally.

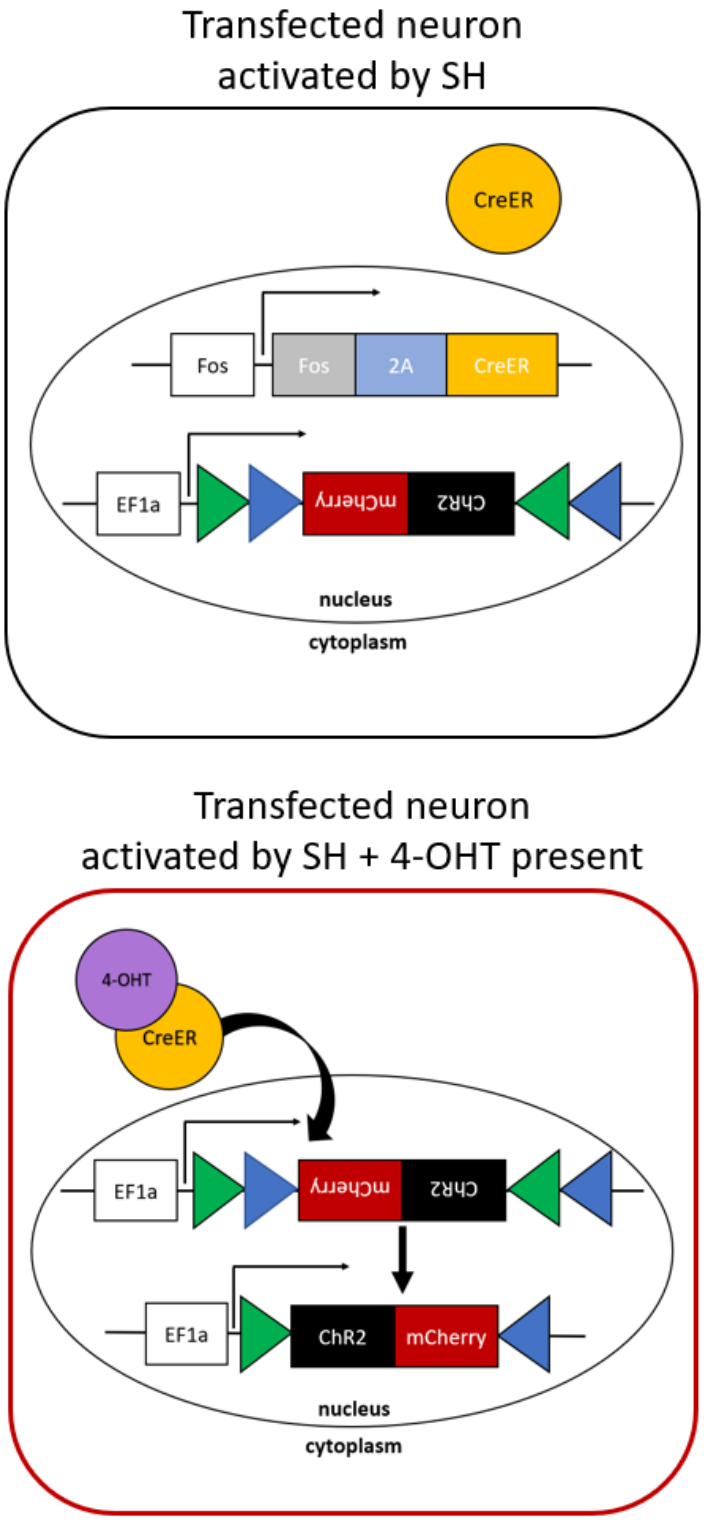

Figure 6.1: Schematic of TRAP2 system

In TRAP2 mice, neurons are first transfected with AAVs containing the effector of choice. In this experiment AAVs containing a Cre-dependent ChR2-mCherry construct. Activation of neurons (e.g., by SH) leads to CreER expression, which is unable to enter the nucleus. Only in the presence of 4-OHT, can CreER enter the nucleus. Cre-recombination leads to inversion of the ChR2-mcherry construct in the correct orientation, enabling effector transcription.

6.3 Results

6.3.1 Chemogenetic activation of CRH^{mpdPVH}

In the first experiment, the involvement of CRH^{mpdPVH} neurons in the activation of the sympathoadrenal response was investigated. This was achieved though the selective expression of the stimulatory DREADD (hM3Dq-mcherry) in CRH^{mpdPVH} neurons, by using the *Crh*-cre::eYFP mouse. The fusion of the DREADD with mCherry allowed visualisation of the receptor expression. Neuronal labelling for mCherry was localised to the PVH and was restricted to CRH neurons. This was demonstrated by colocalisation of mCherry with GFP (*Crh*-cre::eYFP) (**Figure 6.2**). Only animals displaying on-target and bilateral transfection in the PVH were included in the results.

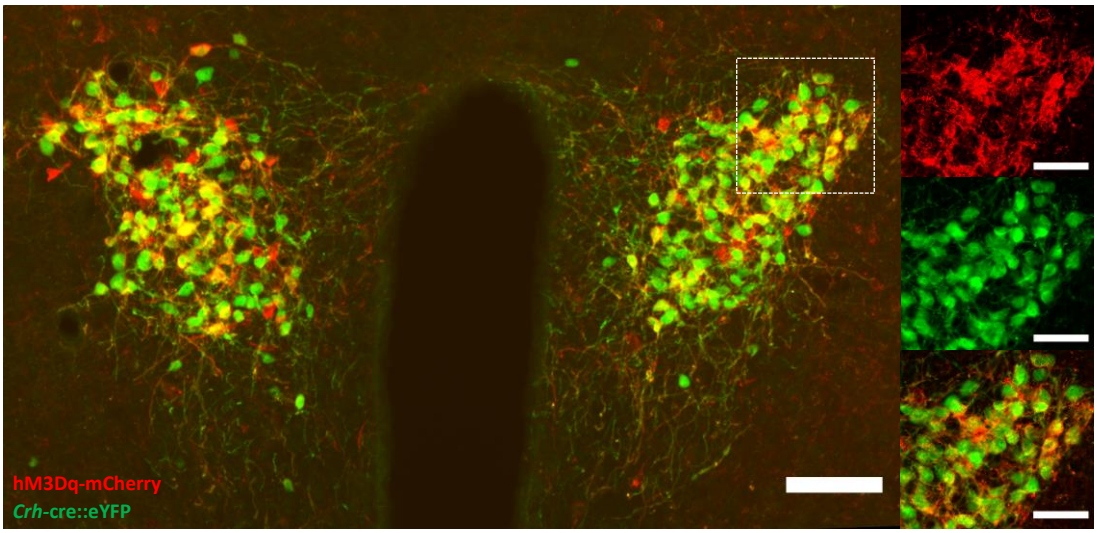

Figure 6.2: Expression of the stimulatory DREADD in PVH of *Crh*-cre::eYFP mice

Main image shows Cre-dependent hM3Dq-mCherrry (red) expression, restricted to the PVH and colocalisation with GFP-labelled CRH neurons (green). Dual-labelled cells appear yellow. Magnified images show mCherry- and GFP-labelled neurons, and colocalisation in the mpdPVH. Main image scale bar represents 100 µm. Magnified image scale bar represents 50 µm.

In a cross-over experiment, animals received either i.p. saline or CNO, followed by blood glucose and adrenaline measurements (**Figure 6.3**). Treatment with saline led to stress-related increases in blood glucose levels. However, activation of CRH^{mpdPVH} neurons following CNO injection led to a rapid and significantly greater increase in blood glucose at 30 min, when compared with saline injection. Blood glucose levels remained significantly elevated until 90 min after CNO, when compared with saline injection (**Figure 6.3A**). This was highlighted by a significant increase in the change in blood glucose (0-30 min) and area under the curve (AUC) for the glucose profile following CNO injection, when compared with saline administration (**Figure 6.3B,C**). Importantly the

change in adrenaline levels (0-30 min) was significantly elevated follow i.p. CNO, when compared with saline treatment.

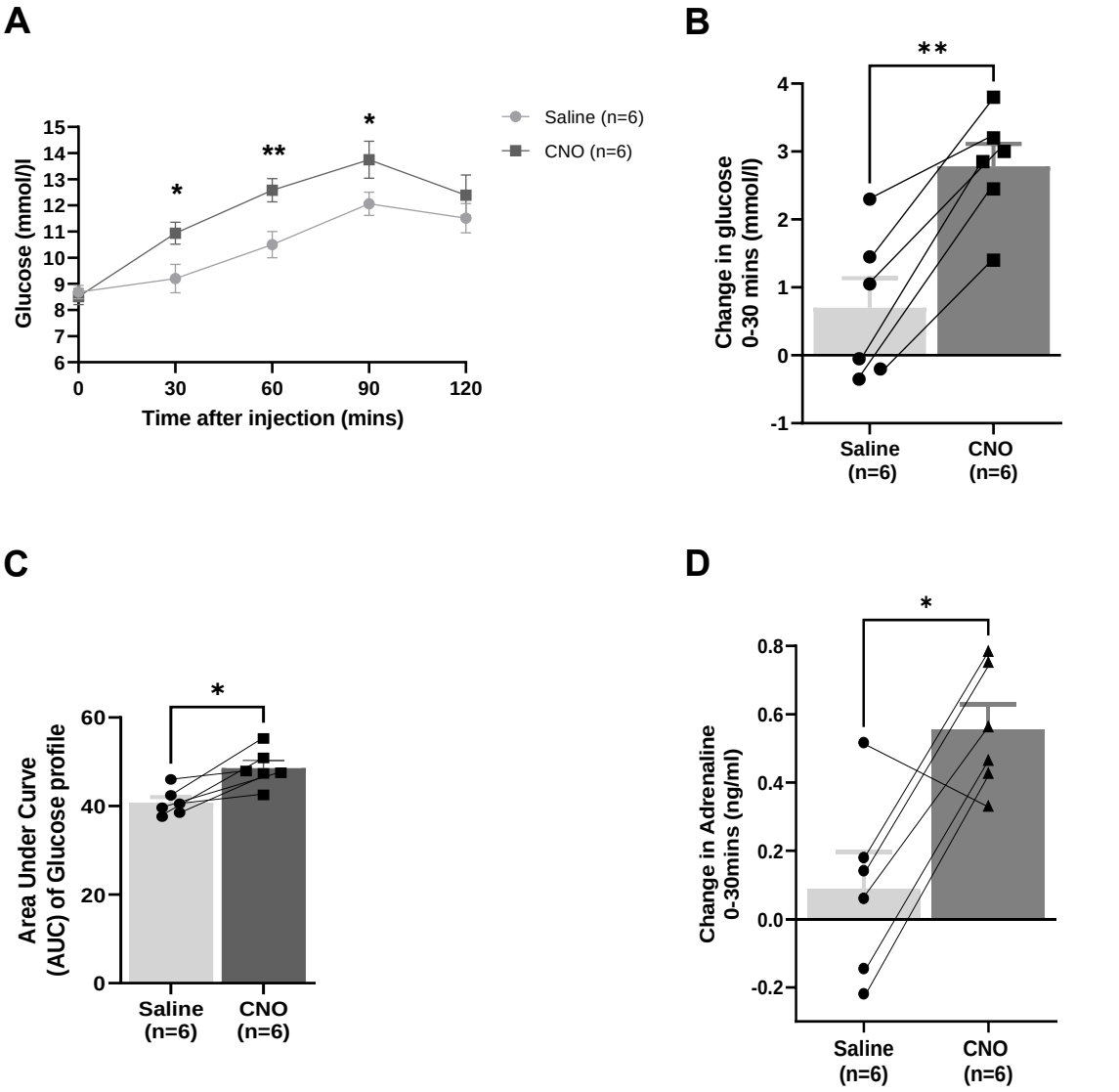

Figure 6.3: Blood glucose and adrenaline levels following chemogenetic activation of CRH^{mpdPVH} neurons

A: Mean blood glucose profile for the 120 min following saline or CNO injection. Blood glucose levels were significantly elevated at 30-, 60- and 90-min time points following CNO, when compared with saline treatment (*p<0.05, **p<0.01; repeated measures two-way ANOVA with Sidak's *post hoc* test).
B: Change in glucose (0-30 min) was significantly increased following CNO, versus saline treatment (**p<0.01; paired t-test).
C: Area under the curve (AUC) of glucose profiles for saline and CNO injection. AUC was significantly elevated following CNO treatment (*p<0.05; paired t-test).
D: Change in adrenaline release (0-30 min) following saline and CNO injection. Treatment with CNO led to a significant increase in adrenaline release when compared with saline (*p<0.05; paired t-test was used to identify differences in sympathoadrenal response within the same animal, dependent on treatment with saline or CNO).
Data presented as mean ± SEM. n=6 with on-target transfection.

Activation of CRH^{mpdPVH} neurons was further confirmed by immunohistochemistry for cFos. Representative images for mPVH sections stained for mCherry (red), GFP (green) and cFos (blue) are shown in **Figure 6.4A**. In mPVH sections, cFos was abundantly expressed following CNO injection, signifying high levels of neuronal activation. Importantly, 83.4 ± 3.3% of cFos-expressing neurons in the PVH colocalised with GFP, signifying that they were predominantly CRH neurons. Over 75% (78.4 ± 7.6 %) of GFP-labelled CRH neurons colocalised with mCherry, signifying high levels of transfection with the stimulatory DREADD. A subsequent analysis showed that 64.4 ± 8.3% of transduced (hM3Dq+) CRH neurons were activated following CNO. Importantly the percentage of activated hM3Dq+ CRH neurons showed a strong linear correlation (r = 0.85) with the adrenaline response (expressed as change in percentage adrenaline response following treatment with CNO, when compared with saline) (**Figure 6.4B**). Though activation in transfected CRH neurons was much lower in two animals, this was still correlated to the adrenaline response, suggesting this was a real effect.

Interestingly the chemogenetic activation of CRH^{mpdPVH} neurons led to specific, stereotyped behaviours. Notably there was enhanced digging and escape behaviours in most of the animals within minutes of CNO injection. Unfortunately, a formal assessment of behaviours was not performed in this experiment.

We postulated that CRH^{mpdPVH} neurons connect with hindbrain autonomic regions including the rVLM, providing a potential pathway which controls adrenaline release following hypoglycaemia. CA neurons in the C1 body of the rVLM are particularly important to the sympathoadrenal response (**Figure 6.5A**). Sections containing the rVLM (-6.5 to -7.2 mm from bregma) in the same cohort of mice were stained for TH with a green-fluorescent secondary antibody, to enable identification of CA neurons in the C1 cell group (**Figure 6.5B**). Sections were also stained for cFos to assess activation of TH^{C1rVLM} neurons. The activation of transfected CRH^{mpdPVH} neurons led to high levels of cFos in the rVLM, including, but not limited to TH neurons. Consistent with the literature the percentage of TH^{C1rVLM} neurons activated showed a strong linear correlation (r = 0.88) with adrenaline release (expressed as change in percentage adrenaline response following treatment with CNO, when compared with saline) (**Figure 6.5C**). Interestingly, the activation of TH^{C1rVLM} neurons also showed a strong linear correlation (r = 0.88) with the percentage of transduced CRH^{mpdPVH} neurons activated following CNO injection. These data suggest a functionally significant pathway between CRH^{mpdPVH} and TH^{C1rVLM} neurons which controls adrenaline release. However, the functional significance of this pathway to hypoglycaemia was not yet clear.

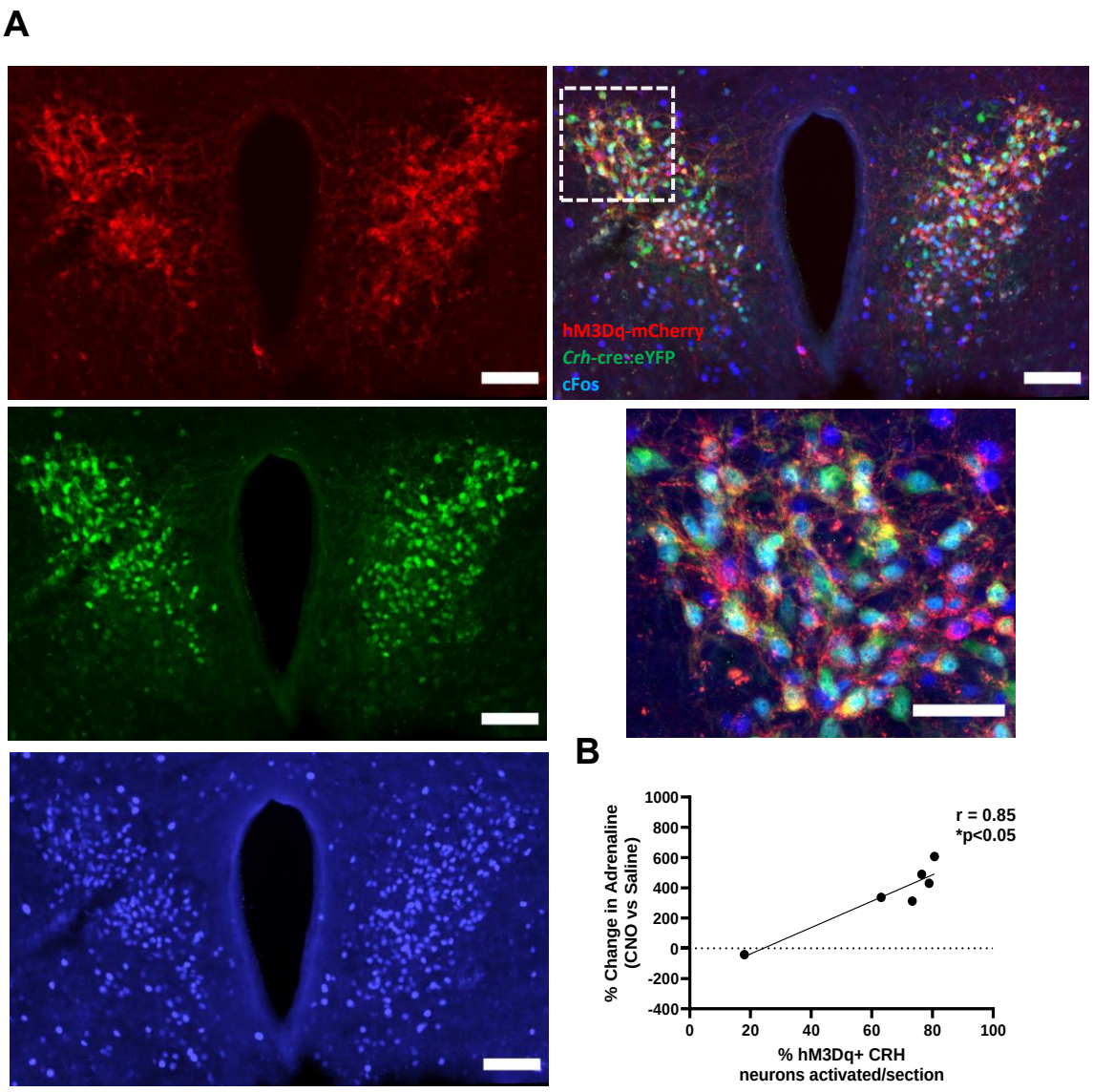

Figure 6.4: cFos induction in PVH following chemogenetic activation of CRH^{mpdPVH} neurons

A: Representative images of hM3Dq-mCherry- (red), GFP- (green) and cFos- (blue) labelled neurons in the mPVH following i.p. CNO injection. Merged and magnified images showing colocalisation are also included. Main image scale bar represents 100 µm, magnified image scale bar 50 µm.
B: Plot of % change in adrenaline response (CNO vs saline) for each animal and corresponding % hM3Dq+ CRH neurons activated following i.p. CNO (*p<0.05, r = 0.85; Pearson correlation).
Data presented as mean ± SEM. n=6 animals, n = 3-5 sections per animal.

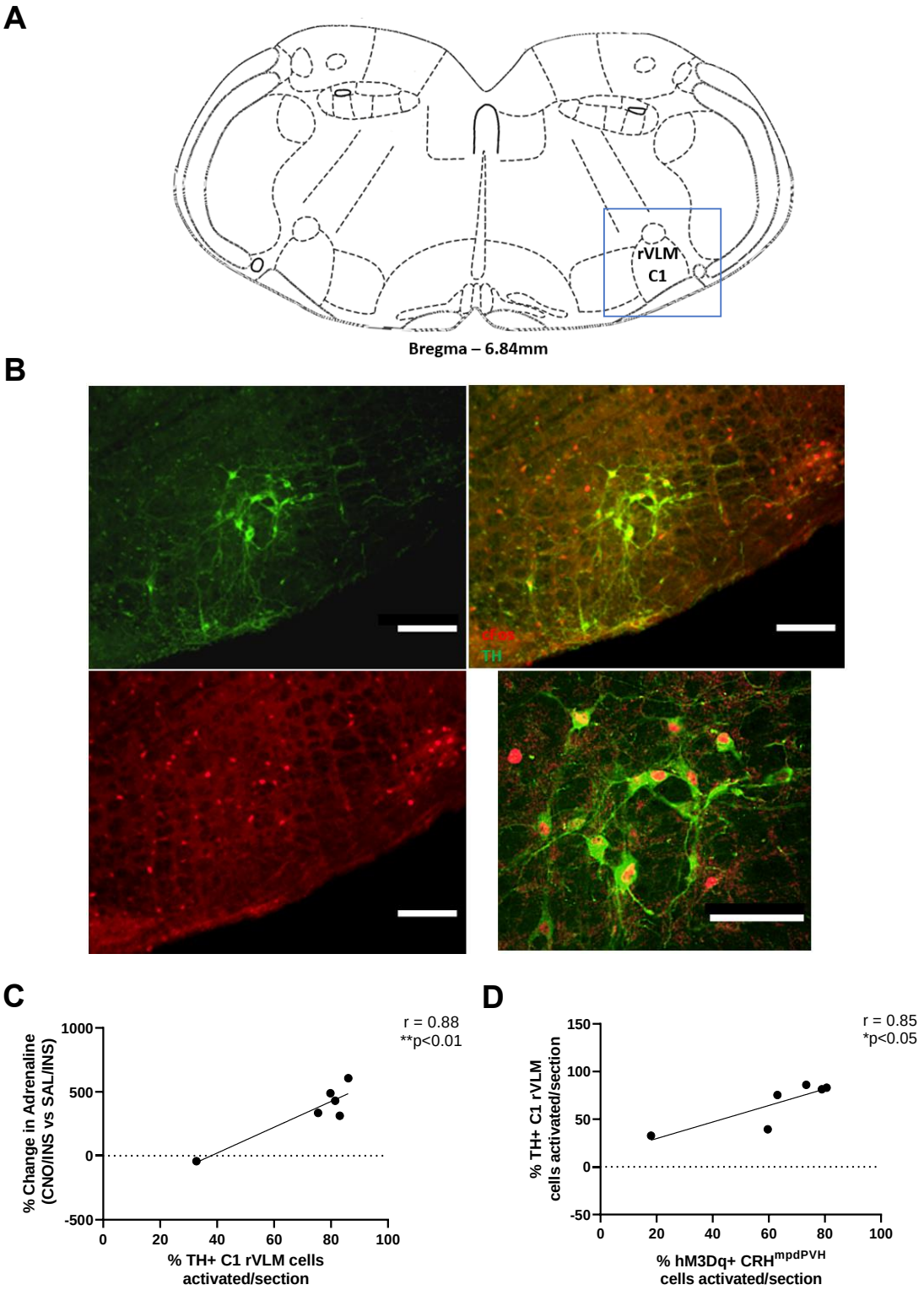

Figure 6.5: cFos induction in the rVLM following chemogenetic activation of CRH^{mpdPVH} neurons

A: Brain atlas coronal section through the rVLM C1 group (bregma -6.84 mm)
B: Representative images of TH- (green) and cFos- (red) labelled neurons in the rVLM C1 group. Merged and magnified images showing colocalisation are also included. Main image scale bar represents 100 µm, magnified image scale bar 50 µm.
C: Plot of % change in adrenaline response (CNO vs SAL) and corresponding % TH+ rVLM C1 neurons activated following CNO injection (**p<0.01, r = 0.88; Pearson correlation).
D: Plot of % TH+ rVLM C1 neurons activated and % hM3Dq+ CRH^{mpdPVH} neurons activated following CNO injection (*p<0.05, r = 0.85; Pearson correlation).
Data presented as mean ± SEM. n=6 animals, n = 3-5 sections per animal.

6.3.2 Chemogenetic inhibition of CRH^{mpdPVH}

Next, the functional significance of CRH^{mpdPVH} neurons to the hypoglycaemia CRR was assessed using the inhibitory DREADD (hM4Di-mCherry). We decided to first examine whether the inhibition of CRH^{mpdPVH} neurons affects glucose and corticosterone levels during insulin-induced hypoglycaemia. We postulated that measuring corticosterone release would be a more sensitive initial test for the chemogenetic inhibition of CRH^{mpdPVH} neurons.

Experiment 1

In this first experiment, hM4Di-mcherry was expressed selectively in the CRH^{mpdPVH} neurons of *Crh*-cre::eYFP mice. Blood glucose measurements were terminated early in this experiment because several animals displayed high levels of stress behaviours. These data are shown in **Figure 6.6**. Following s.c. insulin injection, blood glucose levels were reduced to a similar levels at 30 min, with prior saline and prior CNO injection, respectively (**Figure 6.6A**). This was followed by a very similar blood glucose profile after both treatments. Glucose profiles and recovery following hypoglycaemia was similar in both groups. However, corticosterone levels were reduced following prior CNO injection, when compared with prior saline injection (**Figure 6.6**).

Sections containing the mPVH underwent dual-label immunohistochemistry for mCherry and GFP, to visualise transfected CRH^{mpdPVH} neurons (**Figure 6.7A**). Neuronal labelling for hM4Di-mCherry was restricted to the PVH. However, <50% of CRH^{mpdPVH} neurons (43.8 ± 6.6%) displayed transfection with the inhibitory DREADD. In addition, non-specific colocalisation was seen. The percentage of transduced CRH^{mpdPVH} neurons and the percentage change in corticosterone release (expressed as change in percentage corticosterone response following treatment with CNO, when compared with saline) showed weak negative correlated (**Figure 6.7B**). Though this correlation was not statistically significant, these data suggest that the inhibition of CRH^{mpdPVH} neurons may correspond to reduced corticosterone release during hypoglycaemia. These data also highlighted that further optimisations to the transfection specificity were required.

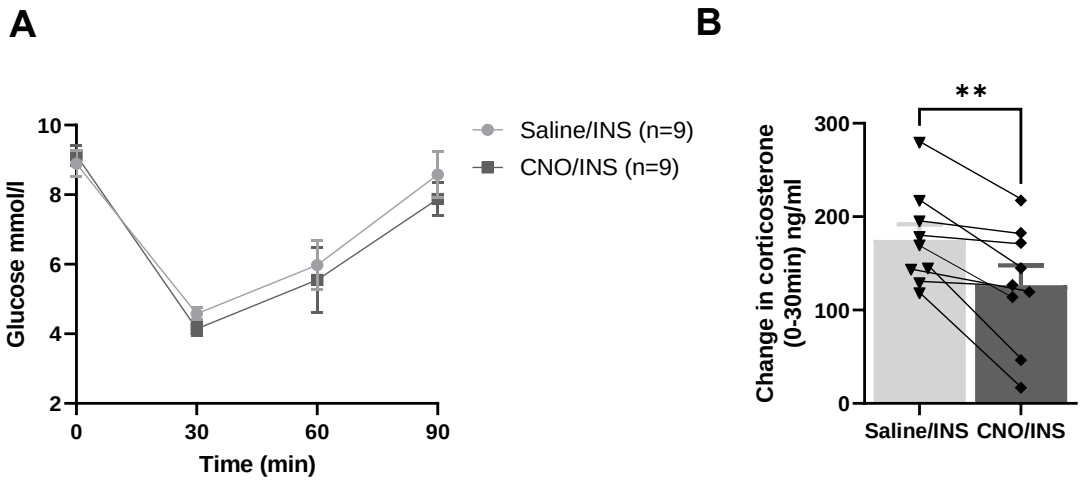

Figure 6.6: Blood glucose and corticosterone levels following chemogenetic inhibition of CRH^{mpdPVH} neurons

A: Mean blood glucose profile for the 90 min following insulin injection, with prior saline or CNO treatment. Blood glucose levels were similar at all timepoints between mice previously treated with saline or CNO.
B: Change in corticosterone (0-30 min) was significantly lower following prior CNO treatment, when compared with prior saline treatment (**p<0.01; paired t-test).
Data presented as mean ± SEM. n=9 animals.

A

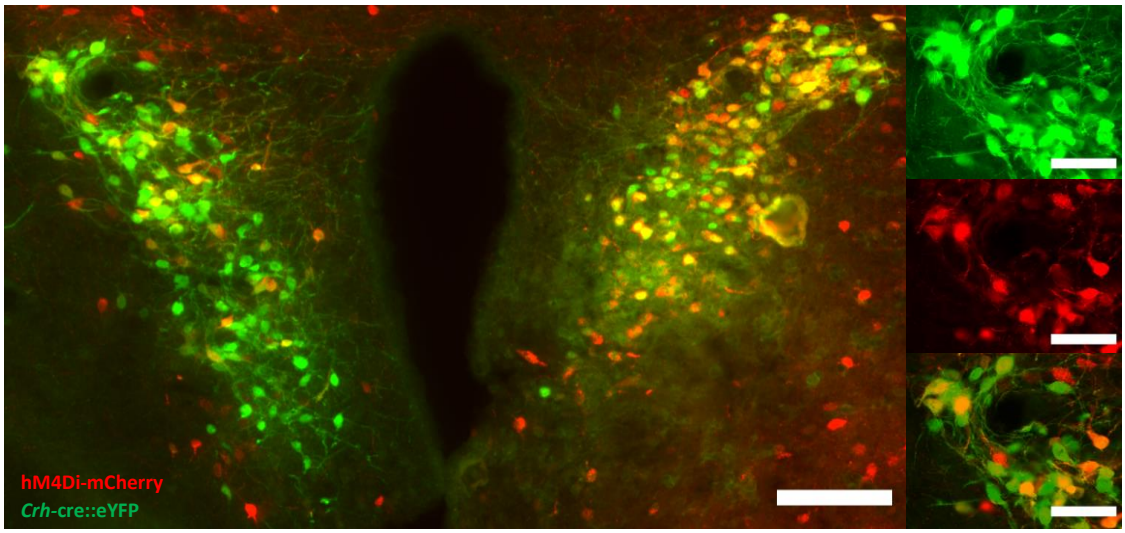

B

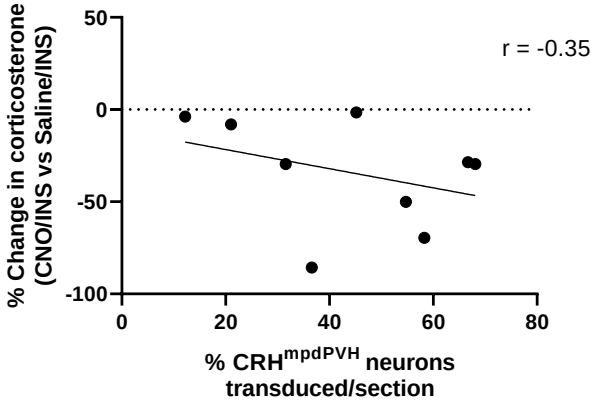

Figure 6.7: Expression of the inhibitory DREADD in PVH of *Crh*-cre::eYFP mice and correlation with corticosterone release

A: Main image shows Cre-dependent hM4Di-mCherrry (red) expression in the PVH and colocalisation with GFP-labelled CRH neurons (green). Dual-labelled cells appear yellow. Scale bar represents 100 µm. Magnified images show mCherry- and GFP-labelled neurons and colocalisation in the mpdPVH. Main image scale bar represents 100 µm, magnified image scale bar represents 50 µm.
B: Plot of % change in corticosterone response (CNO/INS vs saline/INS) and corresponding % hM4Di+ CRH^{mpdPVH} neurons, showing a weak negative correlation (p=ns, r = -0.35; Pearson correlation).
Data presented as mean ± SEM. n=9 animals, n = 3-5 sections per animal.

Experiment 2

In the next experiment, a similar approach was taken to investigate the functional significance of CRH^{mpdPVH} neurons to the sympathoadrenal response during hypoglycaemia. Following optimisations, the inhibitory DREADD was again injected into *Crh*-cre::eYFP mice. Blood glucose and adrenaline data are shown in **Figure 6.8**. Following s.c. insulin injection, blood glucose levels at 30 min reached a similar nadir, when animals were treated with prior saline and prior CNO injection, respectively (**Figure 6.8A**). This was followed by separation in the blood glucose profiles at the 60 min timepoint, with CNO/INS treatment leading to lower blood glucose levels. At the 90 min timepoint, blood glucose levels were significantly reduced with CNO/INS treatment, when compared with saline/INS treatment. These data suggested a delay in glucose recovery following hypoglycaemia, with prior CNO treatment. This was also evidenced by a significant reduction in the AUC for the glucose profile, when animals were treated with CNO, compared with saline (**Figure 6.8B**). In parallel, the change in adrenaline release (0-30 min) was significantly reduced with CNO/INS treatment, when compared with saline/INS. In combination, these data suggested a functional role of CRH^{mpdPVH} neurons in CRR following hypoglycaemia, evidenced by delayed glucose recovery and impaired adrenaline release.

Subsequently, sections containing the mPVH underwent dual-label immunohistochemistry for mCherry and GFP, to visualise transfected CRH^{mpdPVH} neurons (**Figure 6.9A**). Only animals displaying on-target and bilateral transfection in the PVH were included in the results. In this experiment, neuronal labelling for hM4Di-mCherry was restricted to the PVH and 72.4 ± 7.2 % of CRH^{mpdPVH} neurons displayed transfection with the inhibitory DREADD. Colocalisation showed much greater specificity to CRH neurons, when compared with the previous experiment. However, a small number of transduced neurons did not colocalise with mCherry. Importantly, there was a strong negative correlation ($r = -0.71$) between the percentage of transduced CRH^{mpdPVH} neurons and the percentage change in adrenaline release (expressed as change in percentage adrenaline response following treatment with CNO/INS, when compared with saline/INS) (**Figure 6.9B**). These data confirm that adrenaline and glucose responses to hypoglycaemia are impaired when CRH^{mpdPVH} neurons are inactivated. Together, these data indicate that the chemogenetic stimulation or inhibition of CRH^{mpdPVH} neurons leads to functionally significant changes to the sympathoadrenal response, including during hypoglycaemia.

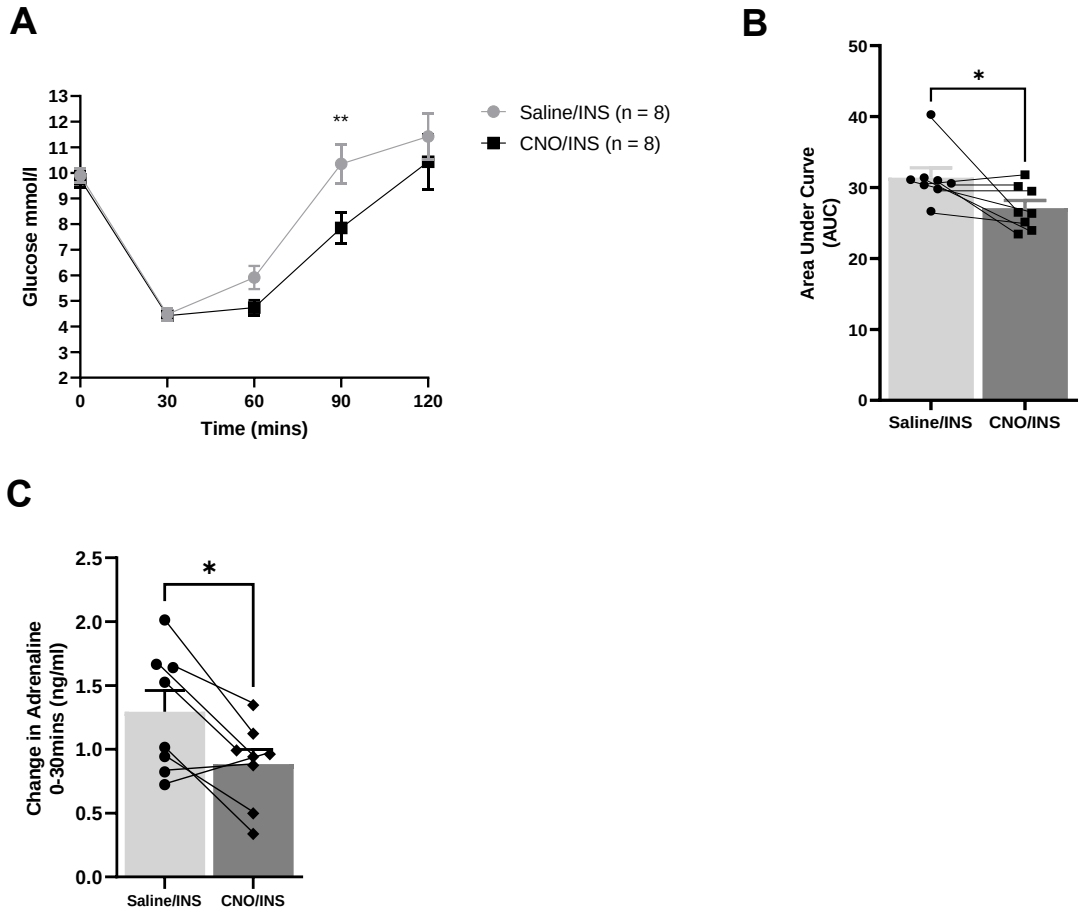

Figure 6.8: Blood glucose and adrenaline levels following chemogenetic inhibition of CRH^{mpdPVH} neurons

A: Mean blood glucose profile for the 120 min following insulin injection, with prior saline or CNO treatment (saline/INS and CNO/INS groups). Blood glucose levels diverged at 60 min and were significantly reduced with CNO/INS treatment, when compared with saline/INS (**p<0.01; repeated measures ANOVA with Sidak's *post hoc* test).

B: Area under the curve (AUC) for glucose profile was significantly reduced following CNO/INS, when compared with saline/INS (*p<0.05; paired t-test).

C: Change in adrenaline (0-30min) was significantly reduced following CNO/INS, when compared with saline/INS (*p<0.05; paired t-test paired t-test was used to identify differences in sympathoadrenal response within the same animal, dependent on treatment with saline or CNO).

Data presented as mean ± SEM. n=8 animals with on-target transfection.

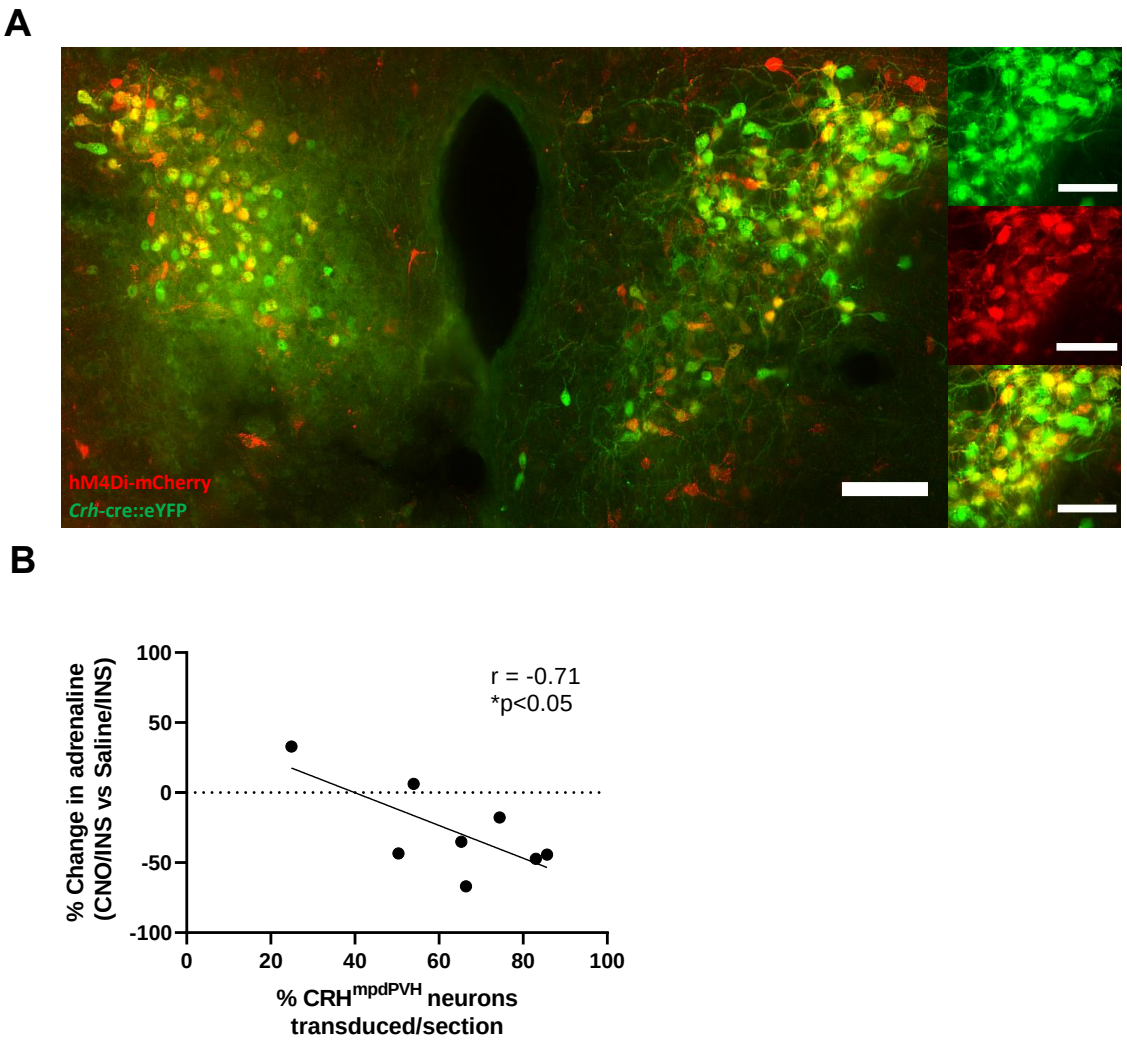

Figure 6.9: Expression of the inhibitory DREADD in PVH of *Crh*-cre::eYFP mice and correlation with adrenaline release

A: Main image shows Cre dependent hM4Di-mCherrry (red) expression in the PVH and colocalisation with GFP-labelled CRH neurons (green). Dual-labelled cells appear yellow. Scale bar represents 100 µm. Magnified images show mCherry- and GFP-labelled neurons and colocalisation in the mpdPVH. Main image scale bar represents 100 µm, magnified image scale bar represents 50 µm.
B: Plot of % change in adrenaline response (CNO/INS vs saline/INS) and corresponding % hM4Di+ CRH^{mpdPVH} neurons, showing a strong negative correlation (*p<0.05; r = -0.71; Pearson correlation).
Data presented as mean ± SEM. n=8 animals, n = 3-5 sections per animal.

6.3.3 Retrograde tracing to investigate PVH→ rVLM connections using Fluoro-Gold

In the previous section, CRH^{mpdPVH} neurons were identified as functionally significant to the hypoglycaemia CRR. However, the pathway which mediates this effect is unclear. We postulated that a direct excitatory neuronal circuit between the PVH and the rVLM may control the sympathoadrenal response following hypoglycaemia. We postulated that the identity of some rVLM-projecting PVH neurons ($PVH^{\rightarrow rVLM}$) was CRH^{mpdPVH} neurons.

Brain sections containing the rVLM C1 group were first dual-labelled for cFos (red-fluorescent secondary antibody) and TH (green-fluorescent secondary antibody) to identify CA neurons in the C1 group. The injection site and distribution pattern following FG injections was assessed by visualising the endogenous blue fluorescence of the tracer, alongside cFos and TH staining (**Figure 6.10C**). Intracranial injections showed good localisation to the rVLM. However, there was some spread of FG more dorsally and in the injection tract. The rostro-caudal spread of FG was restricted to the rVLM. However, in most animals FG spread also involved the C1/A1 cell group, which is immediately caudal to the C1 group.

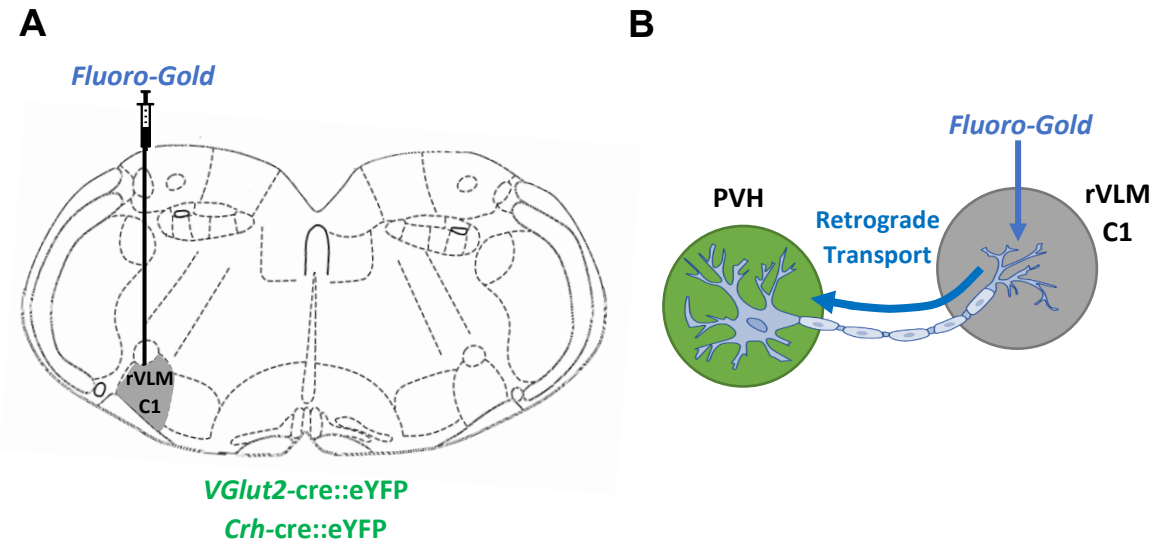

C

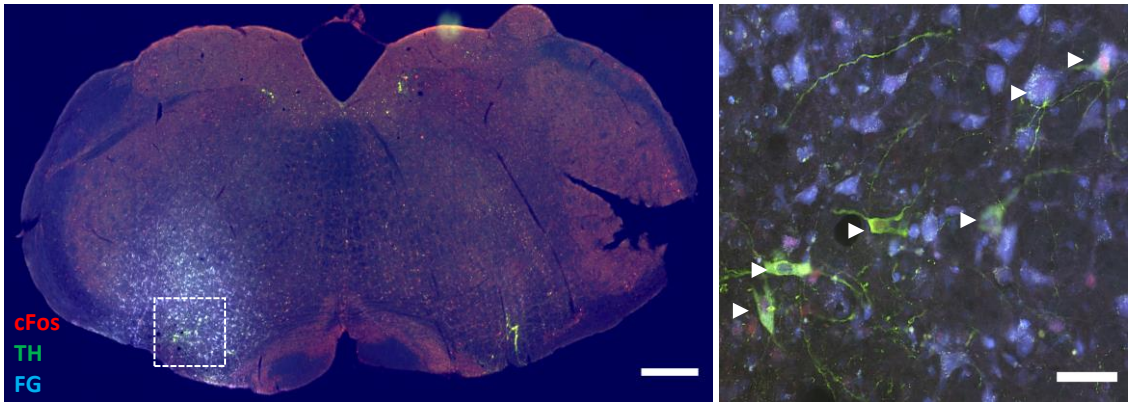

Figure 6.10: Retrograde injection approach to identify PVH$^{\rightarrow rVLM}$ neurons

A: Brain atlas coronal section showing the injection side. FG injection into the rVLM C1 group (bregma -6.84 mm) was performed in *VGlut2*-cre::eYFP and *Crh*-cre::eYFP mice.
B: Diagram showing retrograde tracing approach for this experiment.
C: Representative IHC image showing injection site of FG (blue) into the rVLM C1 region. TH+ CA neurons in the rVLM C1 are identified by arrows. Main image scale bar represents 500 µm, magnified image scale bar represents 50 µm.

Subsequently, in on-target animals from both cohorts of mice (*VGlut2*-cre::eYFP and *Crh*-cre::eYFP mice), the anatomical distribution of SH-activated PVH$^{\rightarrow rVLM}$ neurons was investigated. This was achieved by staining anterior (aPVH), middle (mPVH), and posterior PVH (pPVH) sections for cFos. Sections were then visualised for neuronal cFos and FG colocalisation, identifying SH-activated PVH$^{\rightarrow rVLM}$ neurons. Representative images for PVH sub-regions, displaying FG- and cFos-labelled neurons are shown in **Figure 6.11A**.

FG-labelled neurons were identified in all sub-regions and were predominantly unilateral, though a small number of contralateral PVH neurons were also labelled. FG labelling in the mPVH and pPVH regions was found ventro-laterally within the PVH, largely sparing the periventricular region of the PVH. In addition, only a small number of FG-labelled neurons were identified in the mpdPVH region. Consistent with the literature, the greatest number of FG-labelled neurons were present in the pPVH and then the mPVH (**Figure 6.11B**). Only a small number of aPVH neurons were found to be labelled with FG. The percentage of activated (cFos-labelled) neurons was similar in both pPVH (64.1 ± 3.9 %) and mPVH (58.3 ± 2.8%), and lower for the aPVH (34.1 ± 4.1 %) (**Figure 6.11C**). These data demonstrated that pPVH and mPVH sub-regions display the highest number of SH-activated PVH$^{\rightarrow rVLM}$ neurons.

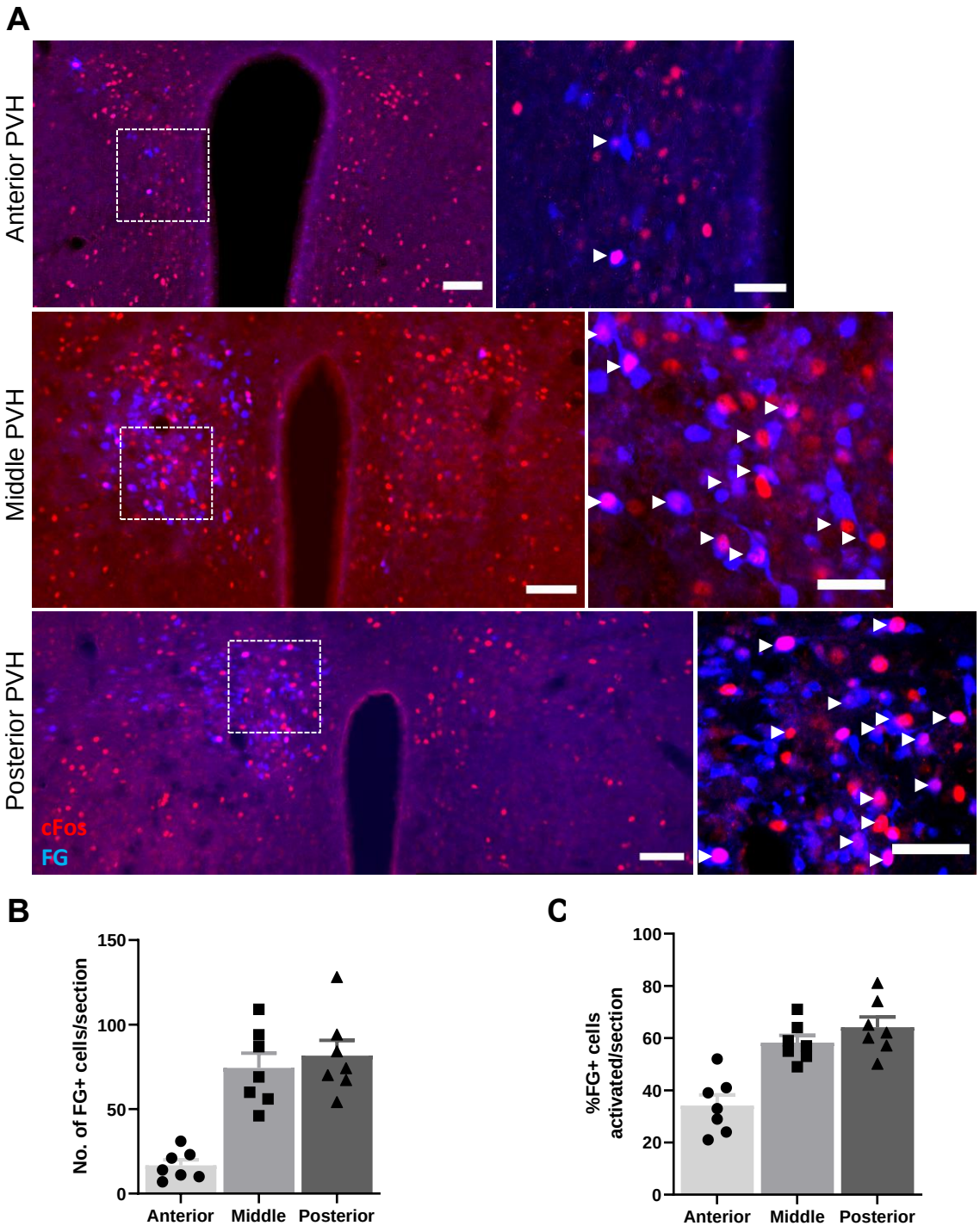

Figure 6.11: Anatomical location of SH-activated PVH$^{\rightarrow rVLM}$ neurons

A: Representative images of the anterior, middle, and posterior PVH following intracranial injection in the rVLM C1 group with FG. Neurons are stained for cFos (red) and FG (blue). Colocalisation of cFos and FG identifies SH-activated PVH$^{\rightarrow rVLM}$ neurons. Main image scale bar represents 100 µm, magnified image scale bar 50 µm.
B: Number of PVH$^{\rightarrow rVLM}$ neurons (FG+) in the PVH sub-regions
C: Percentage of PVH$^{\rightarrow rVLM}$ neurons (FG+) activated (cFos+) following SH in PVH sub-regions
Data presented as mean ± SEM. n=7 animals (*VGlut2*-cre::eYFP mice, n = 3; *Crh*-cre::eYFP mice, n = 4). n = 3-5 sections per sub-region, per animal.

The pPVH is known to contain glutamatergic neurons which project to autonomic regions in the spinal cord and hindbrain. However, this remains poorly characterised for aPVH and mPVH regions. This was further investigated by using brain sections from *VGlut2*-cre::eYFP mice. Sections were labelled for cFos and GFP to identify glutamatergic, SH-activated $PVH^{\rightarrow rVLM}$ neurons. A representative image of the mPVH, showing cFos-, GFP- and FG-labelled neurons is shown in **Figure 6.12A**. In all sub-regions, >70% of FG-labelled neurons colocalised with GFP, identifying them as glutamatergic $PVH^{\rightarrow rVLM}$ neurons. Colocalisation for FG, cFos and GFP was greatest in the pPVH and marginally less in the mPVH (**Figure 6.12B**). In all sub-regions, >80% of cFos and FG dual-labelled neurons also colocalised with GFP (**Figure 6.12C**). This demonstrated that irrespective of sub-region, SH-activated $PVH^{\rightarrow rVLM}$ neurons are predominately glutamatergic. Also, pPVH and mPVH regions are likely to contribute to the excitation of the rVLM during hypoglycaemia.

Glutamatergic PVH neurons are a highly heterogenous population and include CRH neurons. As the main aim of this Chapter was to understand circuits involving CRH^{mpdPVH} neurons, a further phenotypic investigation was performed. In this experiment, sections from *Crh*-cre::eYFP mice were labelled for cFos and GFP to identify SH-activated $CRH^{PVH\rightarrow rVLM}$ neurons. A representative image of the mPVH, showing cFos-, GFP- and FG-labelled neurons is shown in **Figure 6.13A**. A high proportion of CRH neurons were activated by SH in all regions, corroborating my findings in Chapter 3. Surprisingly, only a small number of cFos and FG dual-labelled neurons also colocalised with GFP (**Figure 6.13B**). This was highest in the mPVH, which contains the greatest number of CRH neurons. Interestingly, colocalisation of cFos, FG and GFP was not specific to the mpd region in the mPVH. Within the mPVH, only a small proportion (16.1 ± 2.5%) of cFos and FG dual-labelled neurons also colocalised with GFP (**Figure 6.13C**). These data highlighted that only a small percentage of SH-activated $PVH^{\rightarrow rVLM}$ neurons are phenotypically CRH neurons. Though, most of these neurons reside within the mPVH, they are not specific to the mpd region.

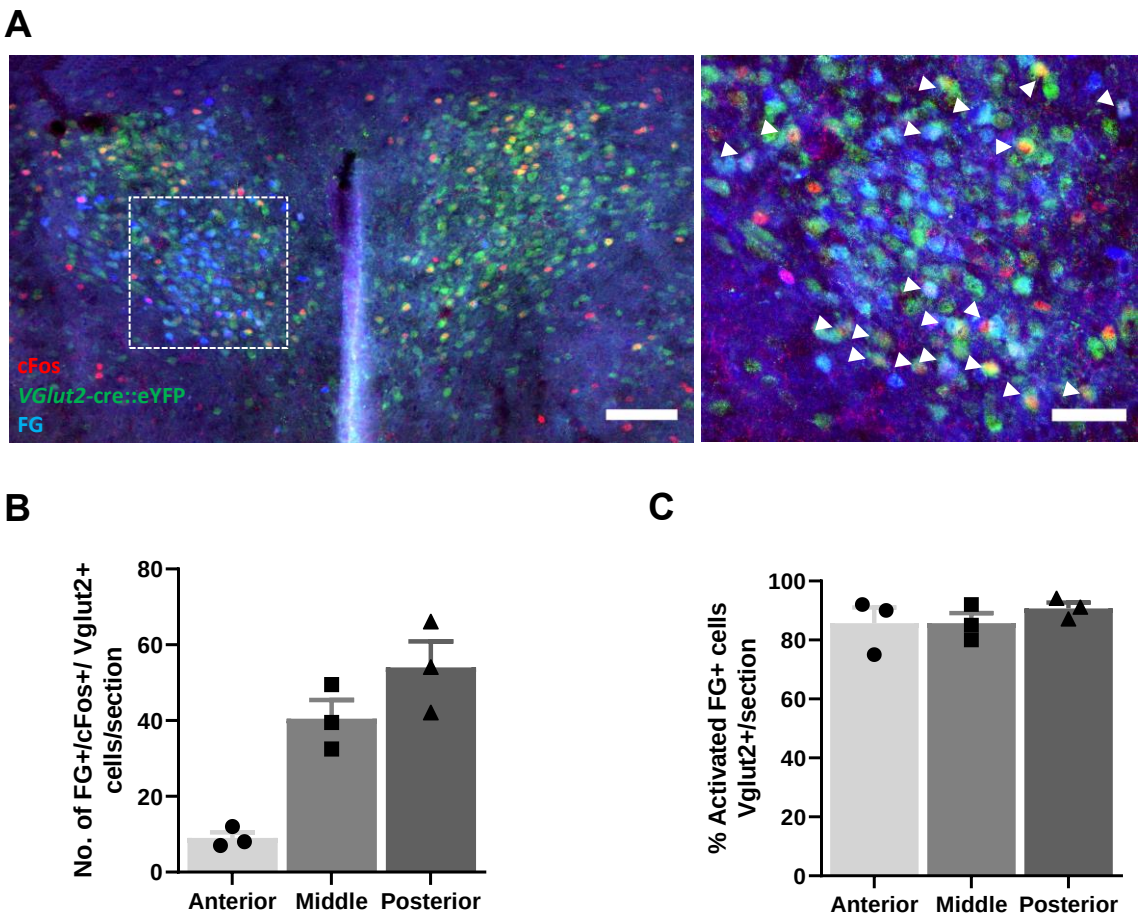

Figure 6.12: Anatomical location of SH-activated VGlut2 $^{PVH\rightarrow rVLM}$ neurons

A: Representative image of the mPVH following intracranial injection in the rVLM C1 group with FG. Neurons are stained for cFos (red), GFP (green) and FG (blue). Colocalisation of cFos, GFP and FG identifies SH-activated VGlut2$^{PVH\rightarrow rVLM}$ neurons and are marked with white arrows. Main image scale bar represents 100 µm and magnified image scale bar 50 µm.
B: Number of SH-activated VGlut2$^{PVH\rightarrow rVLM}$ neurons (FG+, cFos+ and GFP+) in different PVH sub-regions.
C: Percentage of SH-activated PVH$^{\rightarrow rVLM}$ neurons (cFos + and FG+) which colocalised with VGlut2 (GFP+). Data presented as mean ± SEM. n=3 animals, n = 3 sections per sub-region, per animal.

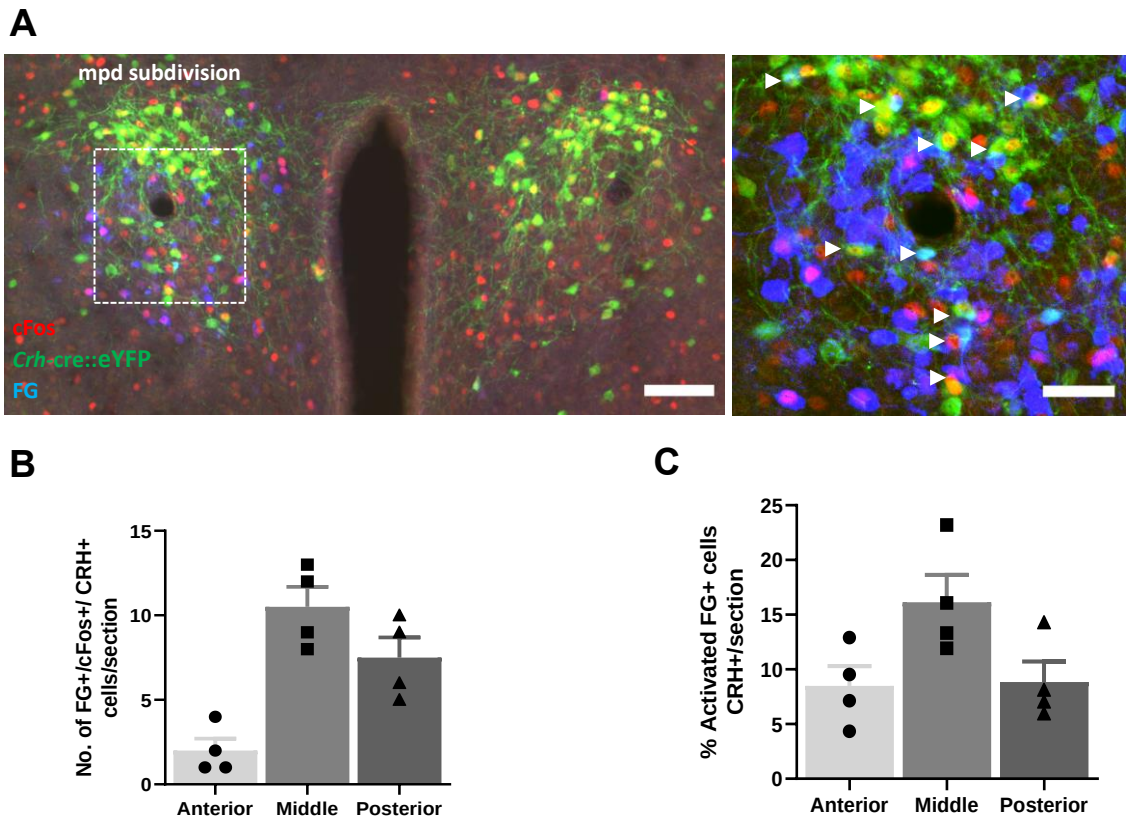

Figure 6.13: Anatomical location of SH-activated CRH$^{PVH→rVLM}$ neurons

A: Representative image of the mPVH following intracranial injection in the rVLM C1 group with FG. Neurons are stained for cFos (red), GFP (green) and FG (blue). Colocalisation of cFos, GFP and FG identifies SH-activated CRH$^{PVH→rVLM}$ neurons and are marked with white arrows. Main image scale bar represents 100 µm and magnified image scale bar 50 µm.
B: Number of SH-activated CRH$^{PVH→rVLM}$ neurons (FG+, cFos+ and GFP+) in different PVH sub-regions.
C: Percentage of SH-activated PVH$^{→rVLM}$ neurons (cFos + and FG+) which colocalised with CRH (GFP+)
Data presented as mean ± SEM. n=4 animals, n = 3 sections per sub-region, per animal.

Although a direct SH-activated $CRH^{PVH \rightarrow rVLM}$ connection was identified in the previous section, CRH neurons accounted for <20% of all SH-activated $PVH^{\rightarrow rVLM}$ neurons. Though this connection may be sufficient to control sympathoadrenal output, it is likely that alternative pathways also exist. Recently, intra-PVH circuits have been shown to have functional significance to autonomic activation (Jiang et al., 2018). Therefore, CRH signalling, via CRHR1-expressing PVH neurons was next investigated.

This was investigated in the same cohorts of *VGlut2*-cre::eYFP and *Crh*-cre::eYFP mice, which had received unilateral FG injection into the rVLM. Brain sections were labelled for cFos and CRHR1. A representative image of the mPVH, showing neurons labelled with cFos, CRHR1 and FG is shown in **Figure 6.14A**. Neurons which express CRHR1 were found abundantly throughout the rostro-caudal extent of the PVH. CRHR1 labelling was dense and distributed evenly in all sub-divisions of the mPVH (**Figure 6.14A**). The number of cFos, CRHR1 and FG colocalised neurons was greatest in the pPVH, with marginally fewer colocalised neurons in the mPVH (**Figure 6.14B**). In all sub-regions, >70% of cFos and FG dual-labelled cells, also colocalised with CRHR1. This signified that the majority of SH-activated $PVH^{\rightarrow rVLM}$ neurons express CRHR1. SH-activated $CRHR1^{PVH \rightarrow rVLM}$ neurons provide an alternative pathway by which CRH^{mpdPVH} neurons can control autonomic functions, including the sympathoadrenal response to hypoglycaemia.

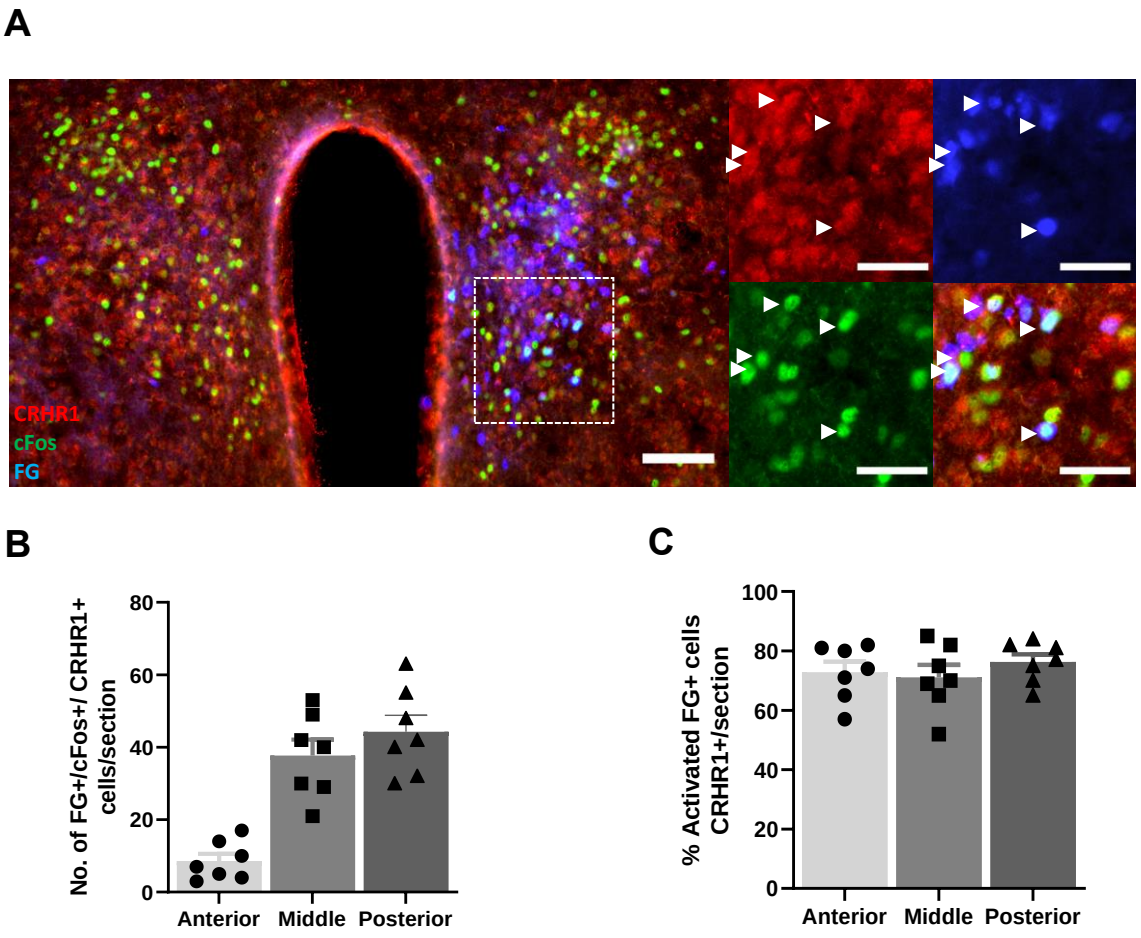

Figure 6.14: Anatomical location of SH-activated CRHR1$^{PVH→rVLM}$ neurons

A: Representative image of the mPVH following intracranial injection in the rVLM C1 group with FG. Neurons are stained for CRHR1 (red), cFos (green) and FG (blue). Colocalisation of CRHR1, cFos and FG identifies SH-activated CRHR1$^{PVH→rVLM}$ neurons. Main image scale bar represents 100 µm, magnified image scale bar 50 µm.
B: Number of SH-activated CRHR1$^{PVH→rVLM}$ neurons (CRHR1+, cFos+ and FG+) in the PVH sub-regions.
C: Percentage of SH-activated PVH$^{→rVLM}$ neurons (cFos + and FG+) which colocalised with CRHR1.
Data presented as mean ± SEM. n=7 animals (*VGlut2*-cre::eYFP, n = 3; *Crh*-cre::eYFP mice, n = 4). n = 3 sections per sub-region, per animal.

6.3.4 Anterograde tracing to investigate PVH→ rVLM connections using TRAP2 mice

An anterograde tracing study, which used the TRAP2 system was conducted to further investigate the PVH→rVLM connection. The experiment protocol is shown in **Figure 6.15A**. Identification of PVH neurons which expressed ChR2-mCherry and were acutely responsive to hypoglycaemia was achieved using dual-label immunohistochemistry. Representative images of the PVH in animals receiving SH/saline, saline/4-OHT and SH/4-OHT are shown in **Figure 6.15B**. Animals receiving SH/saline, did not express ChR2-mCherry in the PVH, as 4-OHT is required for Cre-dependent recombination in activated neurons. Following saline/4-OHT treatment, a very low level of ChR2-mCherry expression was seen unilaterally in the PVH. Transduced cells were identified by neuronal membrane staining with mCherry. In animals treated with SH/4-OHT, there was an increase in mCherry-labelled neurons in the PVH. Again, only a small number of neurons were labelled, however, >90% of mCherry labelled neurons, colocalised with cFos in animals treated with SH/4-OHT. This indicated that despite small numbers of mCherry-labelled neurons, treatment with SH/4-OHT led to a high level of transduction specificity to SH-activated PVH neurons. In this group, the number and location of transduced PVH neurons was surprising. Transduced PVH neurons were located unilaterally, adjacent to the injection site, however, contralateral fibre staining was also seen in some animals. Despite injections targeting the mpdPVH region, most mCherry-labelled neurons were located ventrally within the PVH. The number of ChR2-mCherry labelled PVH neurons, for each group, is shown in **Figure 6.15C**.

A

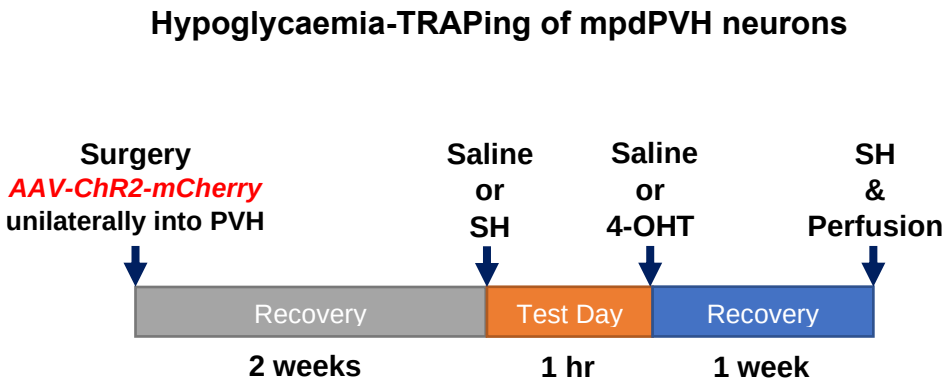

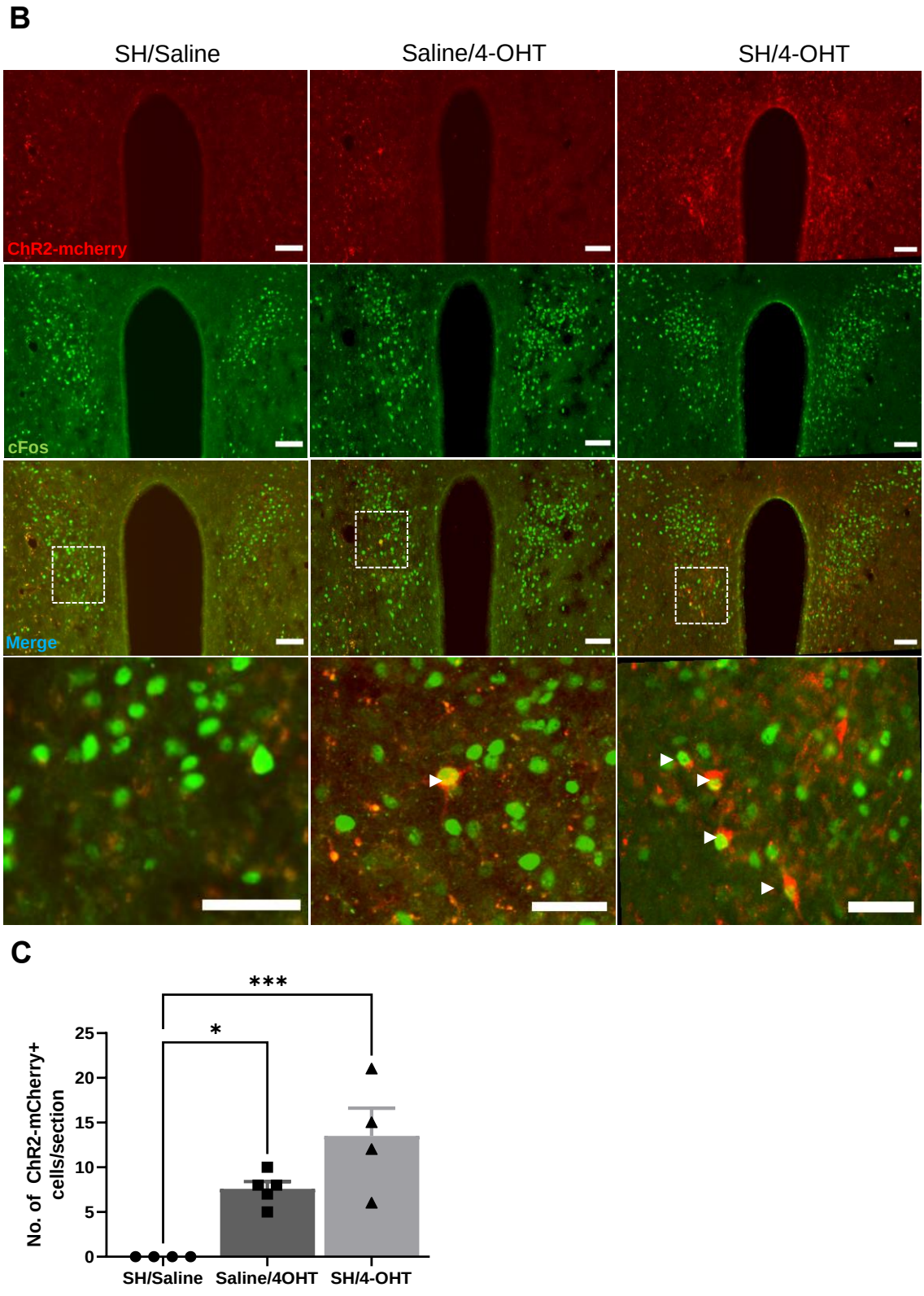

Figure 6.15: Hypoglycaemia-TRAPing of mpdPVH neurons

A: Study protocol.
B: Representative images of the mPVH following unilateral intracranial injection with AAV-ChR2-mCherry into the mpdPVH in SH/saline, saline/4-OHT and SH/4-OHT groups. Neurons are stained for ChR2-mCherry (red) and cFos (green). Main image scale bar represents 100 µm, magnified image scale bar 50 µm.
C: Number of ChR2-mCherry-labelled neurons in the mPVH after SH/saline, saline/4-OHT and SH/4-OHT groups.
Data presented as mean ± SEM. n=4-5 animals with on-target transfection, n = 3-5 sections, per animal.

Subsequently, PVH projections to hindbrain autonomic regions were assessed in relevant brain sections in SH/saline, saline/4-OHT and SH/4-OHT groups. Sections containing the LC, NTS and rVLM were labelled with ChR2-mCherry to identify fibres projecting from PVH neurons. Representative images of the rVLM C1 group, caudal NTS and LC are shown in **Figure 6.16A-C**. In animals receiving SH/saline, fibres were not visible in any hindbrain region as, in the absence of 4-OHT, Cre-dependent recombination was not possible. Following saline/4-OHT a very low level of fibre staining was seen in the rVLM C1 groups, but not in the NTS or LC. Importantly, animals treated with SH/4-OHT consistently displayed fibres in the rVLM C1 group and the caudal NTS (cNTS), but not in the LC. For the rVLM, fibres were only seen surrounding CA neurons in the rVLM C1 group (**Figure 6.16A**). In the cNTS, fibres were also distributed in proximity to CA neurons, including the A2/C2 neuron group. However, fibres were also seen sporadically in the AP and DMX regions. This confirmed that SH-activated PVH neurons project directly to hindbrain catecholaminergic regions, including the rVLM and cNTS. These connections may enable SH-activated PVH neurons to modulate autonomic output.

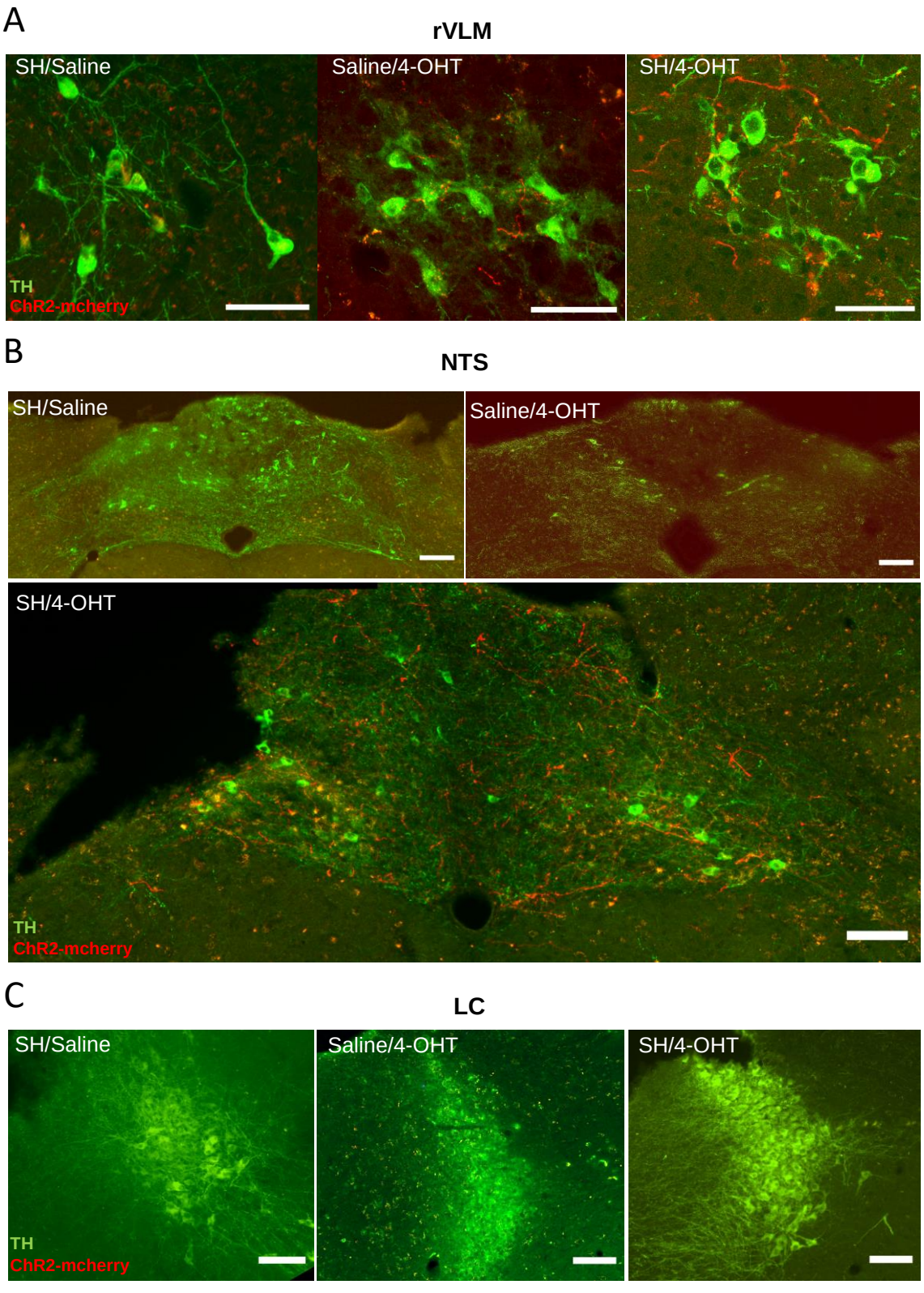

Figure 6.16: Hindbrain projections of hypoglycaemia TRAPed PVH neurons

A: Representative images of rVLM C1 group in SH/saline, saline/4-OHT and SH/4-OHTgroups. CA neurons are labelled with TH (green) and fibres are labelled with ChR2-mCherry (red).
B: Representative images of caudal NTS in SH/saline, saline/4-OHT and SH/4-OHT groups.
C: Representative images of LC in SH/saline, saline/4-OHT and SH/4-OHT groups.
Main image scale bar represents 100 µm, magnified image scale bar 50 µm.
Data presented as mean ± SEM. n=4-5 animals, n = 3-5 sections, per animal.

6.4 Discussion

In previous chapters, CRH^{mpdPVH} neurons were identified as a hypoglycaemia-activated neuronal population, which displays adaptive changes in activity following RH. These findings suggested a functional role for CRH^{mpdPVH} neurons in the hypoglycaemia CRR. We postulated that CRH^{mpdPVH} neurons also regulate sympathoadrenal responses to stressors, including hypoglycaemia, through connections with hindbrain autonomic regions.

To this end, we first performed a series of chemogenetic experiments to establish the functional significance of CRH^{mpdPVH} neurons to the sympathoadrenal response. The chemogenetic stimulation of CRH^{mpdPVH} neurons led to a rapid rise in blood glucose and adrenaline release within 30 min. This supported the hypothesis that CRH^{mpdPVH} neurons enable immediate activation of the sympathoadrenal response. This was supported by a strong positive correlation between the percentage of CRH^{mpdPVH} neurons chemogenetically activated and the adrenaline response. Subsequently, after optimisations, we were able to demonstrate that the chemogenetic inhibition of CRH^{mpdPVH} neurons attenuated both the corticosterone and adrenaline response to hypoglycaemia. Importantly, this attenuated hormone release translated to impaired recovery from hypoglycaemia. This was further substantiated by the finding that the degree of adrenaline response impairment correlated with the percentage of CRH^{mpdPVH} neurons transduced. Collectively these experiments provided direct evidence that CRH^{mpdPVH} neurons are important to the sympathoadrenal response to hypoglycaemia. These data also add weight to the argument that CRH^{PVH} neuronal activity is not limited to HPA axis activation following hypoglycaemia. We did not directly compare the relative importance of corticosterone and adrenaline release to the hypoglycaemia CRR. However, it is known that HPA axis-mediated effects are not immediate, often taking hours to influence hypoglycaemia recovery (De Feo et al., 1989). Whereas CRH^{mpdPVH} neurons, through diverse pathways, are rapidly activated by stress and can control immediate behavioural responses (Füzesi et al., 2016, Bains et al., 2015). This suggests that pathways exist which allow CRH^{mpdPVH} neurons to access autonomic regions, enabling immediate responses to stress. We postulated that CRH^{mpdPVH} regulate the sympathoadrenal response to hypoglycaemia, through connections with hindbrain autonomic regions including the rVLM.

Catecholaminergic neurons in the rVLM C1 body, which are marked by TH expression, form a pre-motor network which controls the sympathoadrenal response (Ritter et al., 2019). We hypothesised that TH^{C1rVLM} neurons may, in turn, be modulated by CRH^{mpdPVH} neurons. This was evidenced by our own chemogenetic studies, which demonstrated

that the chemogenetic activation CRH^{mpdPVH} led to a strong positive correlation between the percentage of TH^{C1rVLM} neurons activated and the adrenaline release. Importantly, the activation of TH^{C1rVLM} neurons and transduced CRH^{mpdPVH} neurons was strongly correlated, suggesting a functional connection. Other investigators have also shown a direct, excitatory PVH→rVLM connection, which is capable of rapidly increasing blood glucose levels through sympathoadrenal activation (Zhao et al., 2017, Jiang et al., 2018). However, the phenotype and anatomical location of SH-activated $PVH^{\rightarrow rVLM}$ neurons remains unclear.

We addressed this question by first injecting the retrograde tracer Fluoro-Gold (FG) unilaterally into the rVLM and characterising SH-activated PVH neurons which were labelled with FG. Using immunohistochemistry, we identified that SH-activated $PVH^{\rightarrow rVLM}$ neurons were located ipsilateral to the rVLM injection site and were predominantly located in mPVH and pPVH sub-regions. This is substantiated by the literature and indicated that neurons which are located more caudally in the PVH project to autonomic regions in the hindbrain and spinal cord (Biag et al., 2012, Zhao et al., 2017). Over 80% of SH-activated $PVH^{\rightarrow rVLM}$ neurons were identified as glutamatergic, confirming excitatory PVH→rVLM connections. Electrophysiological and optogenetic studies have corroborated this finding, showing that CA neurons in the rVLM receive excitatory inputs from the PVH and the activation of this circuit increases blood glucose levels (Zhao et al., 2017, Kalsbeek et al., 2004). Further confirmation of an SH-activated $PVH^{\rightarrow rVLM}$ connection was achieved by using the TRAP2 mouse. Here, AAVs containing ChR2-mCherry were injected unilaterally into the PVH to enable tracing of projections. In this experiment, pairing SH with 4-OHT injection led to Cre-dependent recombination of the ChR2-mCherry in activated PVH neurons. Unfortunately, only a small number of PVH neurons displayed mCherry labelling after saline/4-OHT and SH/4-OHT groups. In addition, despite injections targeting the mpdPVH region, most mCherry-labelled neurons were located ventrally within the PVH. These observations may indicate that only a subset of SH-activated PVH neurons were TRAPed in this experiment. It is likely that optimisation in the timing of SH and 4-OHT administration may lead to improved neuronal transduction.

In this experiment, only animals in the SH/4-OHT group displayed fibres near CA neurons in the cNTS and rVLM C1 (but not in the LC). In our investigations, the cNTS received particularly dense axonal projections from the PVH. Similar observations have been made in rats, suggesting PVH→NTS connections are important in the modulation of NTS activity following stress (Geerling et al., 2010, Zheng et al., 1995). Interestingly, CRH^{PVH} neurons have also been shown to project directly to the NTS and the stimulation of this circuit alters cardiovascular function (Wang et al., 2019). NTS neurons also project

directly to the rVLM, providing an indirect pathway, by which PVH neurons can influence the sympathoadrenal response (Geerling et al., 2010).

In our retrograde tracing study, we found that SH-activated $PVH^{\rightarrow rVLM}$ neurons were located more ventrally in the mPVH and did not segregate to a particular mPVH subdivision. We also identified that the mpdPVH subdivision, where most CRH neurons reside, contained relatively few SH-activated $PVH^{\rightarrow rVLM}$ neurons. Similarly, only a small percentage (<20%) of SH-activated $PVH^{\rightarrow rVLM}$ neurons were phenotypically CRH neurons. This corroborated findings by Zhao *et al.,* who reported that 10% of $PVH^{\rightarrow rVLM}$ neurons were phenotypically CRH neurons (Zhao et al., 2017). We were not able to selectively activate $CRH^{\rightarrow rVLM}$ neurons, therefore, we are unable to directly answer whether this connection is functionally significant to the sympathoadrenal response. In addition, the chemogenetic experiments performed in this Chapter were not projection specific. It is likely that other direct and indirect pathways enable CRH^{mpdPVH} neurons to also control the sympathoadrenal response following hypoglycaemia.

CRH and urocortin peptide release into the PVH and from axon terminals, provides another mechanism by which CRH^{mpdPVH} can control the sympathoadrenal response. CRH-deficient mice demonstrate reduced hypoglycaemia-induced adrenaline release, consistent with an impaired sympathoadrenal response (Jacobson et al., 2000). Whilst complete removal of CRH leads to profound CRR deficits, the manipulation of specific cell- and receptor-specific CRH signalling pathways also has potent effects. In the VMH of rats, CRH appears to act via CRHR1 to amplify the CRR to hypoglycaemia, whilst urocortin 1 (UCN1) acts via CRHR2 and suppresses this response (McCrimmon et al., 2006b). There is a close anatomical connection between PVH UCN3 neurons and the VMH, with dense projections of UCN3 nerves seen in the VMH (Chen et al., 2011). UNC3 acts on the VMH via the CRHR2 to alter glucose sensing. Specifically, UCN3 priming of both GE and GI VMH neurons led to a reduction in glucose level threshold, before a significant change in membrane potential was observed (McCrimmon et al., 2006b). This is significant as UCN3 treatment, in effect, mimics the response of glucose-sensing neurons to RH, by altering thresholds for glucose responsiveness (McCrimmon et al., 2006b).

CRH signalling is not limited to the PVH and VMH. CRH^{PVH} neurons innervate the ARC, which contains neurons which co-express agouti-related peptide (AgRP) and CRHR1 (Kuperman et al., 2016). In mice, with selective absence of CRHR1 in AgRP neurons, hepatic glucose production was reduced during fasting (Kuperman et al., 2016). In a separate study, CRHR1 antagonism reduced stress-induced noradrenaline release and hyperthermia (Griebel et al., 2002). These studies provide evidence that CRH acting via CRHR1 stimulates sympathetic outflow, including sympathetic-medicated hepatic

glucose production, and is complementary to the role of VMH CRHR1 in the hypoglycaemia CRR (Kuperman et al., 2016). Interestingly, CRH peptide has been shown to be released alongside glutamate from nerve terminals and may act to enhance the amplitude of excitatory postsynaptic currents in CA neurons (Wang et al., 2019, Jia and Mifflin, 2017). This could provide an added mechanism by which CRH neurons modulate activity in distal locations.

Recently, it has been shown that CRH^{mpdPVH} may also control autonomic function via monosynaptic connections with a population of $CRHR1^{PVH}$ neurons (Jiang et al., 2018). Interestingly, this population of $CRHR1^{PVH}$ neurons does not express any classical neuropeptide marker of PVH neurons (e.g., OXT, CRH, AVP, TRH), however they do have a distinct electrophysiological signature. Importantly, they send excitatory long-range projections to autonomic regions, including the rVLM and NTS, potentiating autonomic outflow during stress (Jiang et al., 2018, Elsaafien et al., 2021). Accessing this specific population of $CRHR1^{PVH}$ neurons was not possible, however, in this Chapter we examined CRHR1 expression in SH-activated $PVH^{\rightarrow rVLM}$ neurons. CRHR1 expression was present in >70% of SH-activated $PVH^{\rightarrow rVLM}$ neurons. This supports the theory that CRH^{mpdPVH} neurons, through direct connections and via intra-PVH CRH peptide release, can access a large proportion of SH-activated $PVH^{\rightarrow rVLM}$ neurons.

We did not explore other intra-PVH connections, such as to the dorsal parvicellular (dp) PVH, which is known to contain, spinally projecting autonomic neurons (Biag et al., 2012). It is possible that CRH^{mpdPVH} neurons, either via CRH peptide release or through a direct connection with the dpPVH, may activate the sympathoadrenal response. We were also not able to identify if distinct sub-populations of CRH^{PVH} neurons project to the median eminence and to hindbrain autonomic centres. We found that most $CRH^{PVH\rightarrow rVLM}$ neurons were located ventral to the mpdPVH region, which may mark these neurons as a distinct subpopulation. Biag *et al.,* used tail vein injections with FG to mark median eminence projecting neurons, identifying that FG-labelled PVH neurons were anatomically distinct to those which projected to the spinal cord or DMX (Biag et al., 2012). Future work which examines the projection patterns of CRH^{PVH} neurons, using similar methods, may resolve this question.

Our investigations have focused on an excitatory PVH→rVLM connection involving CRH^{mpdPVH} and CRHR1 neurons. However, we must acknowledge that connections between the PVH and rVLM are likely to be reciprocal. PVH-projecting rVLM neurons have been documented and are thought to influence feeding responses following hypoglycaemia (Ritter et al., 2019, Li et al., 2018, Ritter et al., 1998). Our own retrograde tracing studies have shown that hypoglycaemia-activated TH^{C1rVLM} neurons also project to the PVH. Both the PVH and rVLM show anatomical segregation based on projection

patterns and function (Li et al., 2018, Aguilera and Liu, 2012). This suggests that reciprocal connections between the PVH and rVLM may involve different sub-populations within both regions. Crosstalk between the PVH and rVLM may enable a more coordinated and rapid response to stress. CRHR1 neurons may play an important role in modulating both HPA-axis and autonomic response to stress (Elsaafien et al., 2021, Jiang et al., 2019).

6.5 Summary

- Chemogenetic activation of CRH^{mpdPVH} neuronal activity rapidly increases blood glucose and adrenaline release.
- Chemogenetic inhibition of CRH^{mpdPVH} neuronal activity during hypoglycaemia impairs blood glucose recovery and adrenaline release.
- CRH^{mpdPVH} have a functional role in the sympathoadrenal response to hypoglycaemia.
- The majority of SH-activated $PVH^{\rightarrow rVLM}$ neurons are glutamatergic and colocalise with CRHR1.
- Only a small percentage of SH-activated CRH^{mpdPVH} neurons project to the rVLM.
- Hypoglycaemia “TRAPed” PVH neurons project to hindbrain catecholaminergic regions, including the rVLM C1 group and NTS, but not the LC.

6.6 Conclusion

In this Chapter we have identified CRH^{mpdPVH} neurons as functionally important to the sympathoadrenal response during hypoglycaemia. We also provided evidence that this is achieved via pathways which converge on hindbrain autonomic regions, including the rVLM. Our experiments demonstrated that SH-activated $PVH^{\rightarrow rVLM}$ neurons are principally glutamatergic and are distributed more caudally within the PVH. Surprisingly, only a small proportion of SH-activated $PVH^{\rightarrow rVLM}$ neurons are phenotypically CRH neurons. Though we have shown that a direct $CRH^{mpdPVH} \rightarrow TH^{rVLMC1}$ circuit exists, we are not able to say whether this is connection is sufficient to control the sympathoadrenal response. However, our findings supplement the literature and show that alternative pathways may enable CRH^{mpdPVH} neurons to control rVLM activity (**Figure 6.17**). We can postulate that in addition to sending axons to the median eminence, CRH^{mpdPVH} also send collaterals within the PVH to neurons which express CRHR1. CRHR1 neurons, in turn, project to catecholaminergic neurons in the rVLM, regulating the sympathoadrenal response. RH may initiate a decremental process which leads to attenuated activation

of CRH^{mpdPVH} neurons. A neuronal circuit involving the PVT may be responsible for this and will be investigated in Chapter 7.

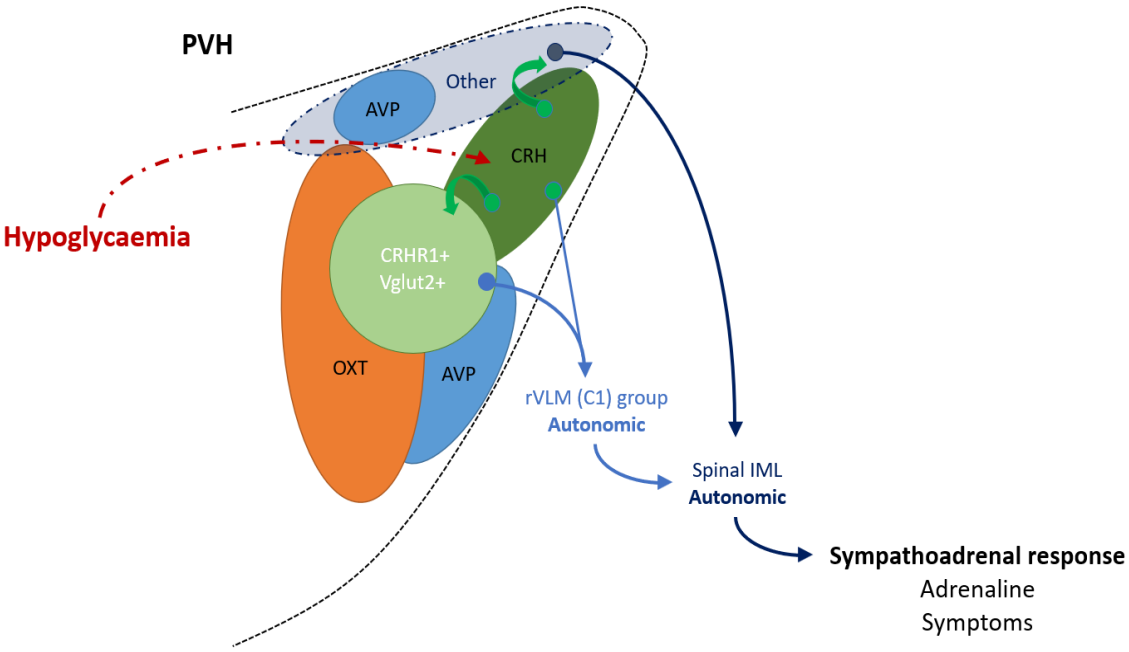

Figure 6.17: Proposed circuit diagram by which CRH^{mpdPVH} neurons control the sympathoadrenal response

Chapter 7

Is the PVT responsible for habituation?

7.1 Introduction

The paraventricular nucleus of the thalamus (PVT) integrates signals relating to threat, arousal, and reward. The PVT is a structure which is elongated rostro-caudally and exerts significant top-down control on diverse behaviours, through connections with cortical, limbic, and homeostatic circuits (Campus et al., 2019).

Signals conveying changes in blood glucose, including from GI neurons in the VMH, are also received by the PVT, leading to activation (Khodai et al., 2018, Labouebe et al., 2016). This is also true of glucoprivic signals, induced by the administration of 2-DG, which induces strong PVT neuronal cFos in rats (Dodd et al., 2010). The full extent of inputs to the PVT from hypoglycaemia-activated regions is not clear and, interestingly, PVT neurons which express GLUT2, a glucose transporter, may themselves be involved in glucose detection (Labouebe et al., 2016). These PVT GLUT2 transporter neurons are GI, and genetic inactivation of GLUT2 in the CNS of mice, causes an increase in sucrose seeking behaviour (Labouebe et al., 2016). Also, optogenetic activation of PVT GLUT2 transporter neurons projecting to the NAc, mimics hypoglycaemia and leads to enhanced effortful sucrose seeking in mice (Labouebe et al., 2016). Similarly, an rVLM→PVT→NAc circuit has been identified as important to glucoprivic food seeking (Sofia Beas et al., 2020). These studies demonstrate that the PVT is regulated by blood glucose levels and that hypoglycaemia may stimulate PVT-mediated motivated and effortful food seeking. However, the importance of the PVT in controlling neuroendocrine responses to hypoglycaemia is unclear.

In Chapter 3, I identified the PVT as a stress- and hypoglycaemia-responsive region, which displayed an increase in neuronal markers of adaptation following RH. This finding was consistent with the literature and a growing understanding that the PVT plays an important role in stress habituation (Herman, 2013). Lesions of the PVT block the habituation of the HPA-axis response to repeated restraint stress (Bhatnagar et al., 2002). It is not known if the PVT also regulates the habituation of responses to other repeated stressors such as RH. Interestingly, these studies confirmed that only the posterior sub-region of the PVT (pPVT) was involved in stress habituation (Bhatnagar et al., 2002). The circuitry of neuronal connections with the PVT is complex and there is some evidence that anterior PVT (aPVT) and pPVT regions have distinct inputs and outputs. A greater understanding of connections, both to and from PVT sub-regions, may improve our understanding of the control of habituation.

Any control of HPA-axis habituation by the pPVT would predict that there are neuronal circuits which connect with the PVH and, specifically, with CRH^{mpdPVH} neurons. Monosynaptic retrograde tracing studies have shown that a small number of

glutamatergic PVT neurons ($GLUT^{PVT}$) project directly to CRH^{mpdPVH} neurons (Yuan et al., 2019). This excitatory connection does not explain the regulation of stress habituation by the pPVT. As the major outputs of the PVT are glutamatergic, it is likely that populations of inhibitory neurons act as intermediary relays between $GLUT^{pPVT}$ and CRH^{mpdPVH} neurons. The anatomical location of these intermediary relays is not known, but from examining the literature, they may include the aBNST, CeA and NAc (Vertes and Hoover, 2008, Kirouac, 2015, Hsu et al., 2014). The ventral region of the aBNST is of particular interest as it contains a sizable population of GABAergic neurons which project directly to CRH^{PVH} neurons (Yuan et al., 2019, Radley and Sawchenko, 2015).

Our findings in Chapter 6 show the functional significance of CRH^{mpdPVH} neurons to the sympathoadrenal response during hypoglycaemia. Therefore, it is possible that a circuit involving the pPVT and vBNST, could modulate CRH^{mpdPVH} neuronal activity after RH, leading to habituation of the sympathoadrenal response.

7.1.1 Objectives

1) Investigating differences in afferent projections to the aPVT and pPVT

The PVT displays anatomical differences along its rostro-caudal extent and there is growing interest in identifying whether distinct functional sub-regions exist. This has traditionally involved separating the PVT into aPVT and pPVT sub-regions, which show differences in function and connections, though results have proven variable (Gao et al., 2021, Moga et al., 1995). Whether projections to the PVT originate from hypoglycaemia-responsive brain regions is unknown. To this end, I elected to investigate projections to the aPVT and pPVT from brain regions which display high levels of cFos following SH. We hypothesised that the aPVT and pPVT will show differences in the location and density of afferent projections from SH-activated brain regions.

2) Identifying direct connections between CRH^{mpdPVH} neurons and the PVT

A small number of studies have examined connections between the PVT and PVH, suggesting reciprocal connections between the two regions (Hsu et al., 2014, Kirouac, 2015). However, specific connections between CRH^{mpdPVH} and $GLUT^{PVT}$ neurons are not characterised. Investigating the circuitry between these neuronal populations may help to explain how the PVT controls neuroendocrine responses to acute and chronic stress. This was also achieved by conducting a tracing study to identify hypoglycaemia-responsive neurons which connect the PVT and PVH. We postulated that direct connections between hypoglycaemia-responsive CRH^{mpdPVH} and $GLUT^{PVT}$ neurons exist.

3) Investigating the importance of pPVT neurons in the RH-induced habituation of the sympathoadrenal response

The pPVT is important in the control of HPA-axis response habituation to repeated restraint stress. This may also be true for the control of habituation of other responses, including the sympathoadrenal response following RH. We decided to perform a genetic lesioning study to identify the functional significance of the pPVT to the RH-induced habituation of the sympathoadrenal response. We postulated that ablation of $GLUT^{pPVT}$ neurons would abolish habituation of the sympathoadrenal response following RH.

4) Identifying intermediary GABAergic neuronal populations which may enable the PVT to limit CRH^{mpdPVH} activity following RH

As PVT projection neurons have been identified as glutamatergic, it is likely that an intermediary inhibitory relay enables the PVT to dampen responses following RH (Do-Monte et al., 2017, Radley and Sawchenko, 2015). We hypothesised that following RH, increasing activity in a $GLUT^{pPVT}$ is relayed via an intermediary GABAergic neuronal population. This GABAergic relay may, in turn, project to the PVH, inhibiting CRH^{mpdPVH} activity following RH. The identify of potential GABAergic relays is not known, however, they may include the NAc, the ventral region of the aBNST (vBNST) and CeA. Therefore, we conduced further tracing studies to establish the anatomical location of the predominant GABAergic input.

5) Investigating the importance of GABAergic ventral BNST neurons to the RH-induced habituation of the sympathoadrenal response

The vBNST has been noted to contain populations of GABAergic neurons, which provide inhibitory tone to the PVH, regulating the HPA-axis response (Radley and Sawchenko, 2015). There is also evidence that the vBNST differentially regulates HPA-axis responses to acute and chronic stress paradigms (Choi et al., 2008). Therefore, this region may also regulate responses to repeated stressors such as RH. We hypothesised that GABAergic neurons in the vBNST are functionally important to the RH-induced habituation of the sympathoadrenal response.

7.2 Methods

7.2.1 Afferent projections to the aPVT and pPVT from SH-activated regions

Adult male and female *Crh*-cre::eYFP mice, aged 8-16 weeks old, were injected unilaterally with the blue retrograde tracer Fluoro-Gold (FG) either into the aPVT (n = 6) or pPVT (n = 7). Mice, injection co-ordinates and volumes are outlined in Chapter 2. After surgery, animals were left in their home cages for three weeks to enable recovery and transport of the tracer. Animals were handled daily for two weeks prior to administration of s.c insulin (1.75 U/kg), and 2 hr later were perfused with. Brains were dissected and processed for immunohistochemistry as described in Chapter 2. Animals which received on-target injections into the aPVT (n=3) or pPVT (n=4), underwent immunohistochemistry for cFos and FG labelling. A quantification of FG-labelled neurons in hypoglycaemia-activated regions, was performed for the aPVT and pPVT, respectively.

7.2.2 Identifying direct connections between CRH^{mpdPVH} neurons and the PVT

In a separate cohort, *Crh*-cre::eYFP mice (n=5) were injected unilaterally with FG into the mpdPVH (Chapter 2). The same post-operative recovery period and handling procedures were undertaken before receiving s.c insulin (1.75 U/kg). Processed brain sections were assessed for on-target injections into the mpdPVH. Animals which received on-target injections into the mpdPVH (n=3) underwent immunohistochemistry for cFos. Neurons in the pPVT which were labelled with both cFos and FG identified SH-activated pPVT→PVH neurons.

Separately, sections containing the PVH were identified from animals which had received FG injections into the pPVT (**7.2.1**). Immunohistochemistry to label cFos and GFP (*Crh*-cre::eYFP), with FG, identified SH-activated CRH^{mpdPVH}→pPVT neurons.

7.2.3 Investigating the importance of pPVT neurons to the sympathoadrenal response following SH and response habituation following RH

Intracranial Surgery

Adult male and female *VGlut2*-cre::eYFP mice, aged 8-16 weeks old, were injected medially into the pPVT with AAVs carrying a Cre-dependent caspase construct (AAV5-flex-taCasp3-TEVp) or control injections with Cre-dependent mCherry construct (AAV5-hSyn-DIO-mCherry). Here, the Cre-dependent expression of caspase triggers neuronal apoptosis restricted to $GLUT^{pPVT}$ neurons. Mice, injection co-ordinates, viral titre and volumes are outlined in the Chapter 2.

The group size for AAV-caspase experiments was guided by the literature and a 20-30% attrition rate was added to account for any mice that had insufficient transduction. A similar study in rats required a group size of n = 6-9 animals to provide sufficient power to identify whether pPVT lesioning alters stress responses to repeated stressors (Bhatnagar et al., 2002).

Separate cohorts of animals were used to investigate the importance of the pPVT in the sympathoadrenal response to SH and RH, respectively. Surgery and experiments were performed in batches. After surgery, animals were left in their home cages for two weeks to enable recovery, transfection of cells. Animals were handled daily during this period.

Experiment 1: Importance of the pPVT in the sympathoadrenal response to SH

Animals in caspase and control groups (n=8 per group) underwent a crossover experiment and were randomised to receive either s.c. insulin (1.75 U/kg) or volume matched s.c. saline on two test days (test 1 and test 2). Groups were as follows: saline/control, SH/control, saline/caspase and SH/caspase. On test days, blood glucose levels were measured every 30 min for 120 min after injection. Adrenaline levels were measured at baseline and 30 min after injection. Blood sampling and analysis methods are described in full in Chapter 2.

Experiment 2: Importance of the pPVT in the RH-induced habituation of the sympathoadrenal response

In a separate cohort of animals, caspase and control groups were subjected to the 4-week RH protocol. Here, animals in both groups, were randomised to receive, saline, SH or RH. The groups were as follows: saline/control (n = 8), SH/control (n = 9), RH/control (n = 9), saline/caspase (n = 8), SH/caspase (n =8), and RH/caspase (n = 9). On the test day, animals received either s.c. insulin (1.75 U/kg) or volume matched saline, depending on the group. Blood samples for glucose and adrenaline were taken as above.

Immunohistochemistry

At the end of both experiments, all animals were perfused with fixative. Dissected brains were then processed and sections containing the pPVT identified. Only on-target animals were included in subsequent analysis. For caspase-treated animals, immunohistochemistry was used to label for GFP (eYFP), identifying numbers of remaining $GLUT^{pPVT}$ neurons. For control animals, dual-label immunohistochemistry for mCherry and GFP enabled identification of transduced $GLUT^{pPVT}$ neurons.

7.2.4 Identifying intermediary GABAergic neuronal populations which may enable the PVT to control CRH^{mpdPVH} activity following RH

VGlut2-cre::eYFP mice were used also to identify SH-activated $GLUT^{pPVT}$ neuronal efferent projections to GABAergic relays in the NAc, vBNST and CeA. Separately, a cohort of *Gad2*-GFP mice was used to identify whether SH-activated GABAergic neurons in the NAc, vBNST and CeA projected to the PVH. Adult mice of both sexes were used. All animals were injected unilaterally with FG into the relevant brain regions. In *VGlut2*-cre::eYFP mice, FG was injected into either the NAc, vBNST or CeA. *Gad2*-GFP mice were injected with FG into the PVH (see Chapter 2 for co-ordinates).

All animals subsequently received s.c insulin (1.75 U/kg) and 2 hr later were perfused with fixative. Processed brain sections were assessed for on-target injections and then underwent immunohistochemistry for cFos, GFP and FG.

7.2.5 Investigating the importance of GABAergic vBNST neurons to the RH-induced habituation of the sympathoadrenal response

Intracranial Surgery

Adult male and female *Gad2*-cre mice were injected bilaterally into the vBNST with AAVs carrying a Cre-dependent tetanus toxin (TetTox) construct (AAVDJ-CMV-DIO-eGFP-2A-TeNT) or control injections with Cre-dependent mCherry construct (AAV5-hSyn-DIO-mCherry). Here, the Cre-dependent expression of tetanus toxin leads to the inactivation of transmitter release from $GABA^{vBNST}$ neurons. Mice, injection co-ordinates, viral titre and volumes are outlined in the Chapter 2. Surgery and experiments were performed in batches. After surgery, animals were left in their home cages for two weeks to enable recovery, transfection of cells. Animals were handled daily during this period.

The group size for AAV-TetTox experiments was also guided by the literature, with a 20-30% attrition rate again added for insufficient transduction. Similar studies were not available, however Fos and circuit-mapping studies in rats, which targeted the vBNST

typically required a group size of n = 5 animals to be sufficiently powered to detect neuronal and hormone changes following repeated stress (Radley and Sawchenko, 2011, Radley and Sawchenko, 2015).

Experiment

Animals in TetTox and control groups were subjected to the 4-week RH protocol. Here, animals in both groups, were randomised to receive, saline, SH or RH. The groups were as follows: saline/control (n=8), SH/control (n=8), RH/control (n=9), saline/TetTox (n=8), SH/TetTox (n=9) and RH/TetTox (n=9). On the test day, animals received either s.c. insulin (1.75 U/kg) or volume matched s.c. saline, depending on the group. Blood glucose and adrenaline levels were measured as described in Chapter 2.

Immunohistochemistry

Sections containing the vBNST were identified and immunohistochemistry performed to identify the accuracy of targeting and the number of neurons transfected. As both the TetTox and control constructs were fused with GFP, this enabled the identification of transfected $GABA^{vBNST}$ neurons. Only on-target animals were included in subsequent analysis.

7.2.6 Identification and quantification of neurons

Animals were included in the results of chemogenetic studies (AAV-caspase and AAV-TetTox experiments) only if IHC demonstrated on-target viral transduction. For AAV-caspase this was by demonstrating the loss of *VGlut2*+ cells in the pPVT. For Investigators were blinded to the order of treatments received by each animal. For AAV-TetTox this required bilateral colocalisation of the viral reporter in >50% of $GABA^{vBNST}$ neurons. Investigators were blinded to the order of treatments received by each animal when checking transfection and during quantification.

For each animal, quantification of labelled neurons followed the same protocol. Neuronal counts were performed on a minimum of three brain sections (3-5 sections per region, depending on availability), which contained the region of interest, and then averaged. In the first study, midline injection of FG into the PVT led to the labelling of neurons in brain regions bilaterally. Therefore, only in this instance, were counts performed bilaterally for brain regions with retrograde labelled neurons.

7.3 Results

7.3.1 Afferent projections to the aPVT and pPVT from SH-activated regions

An investigation of afferent projections to the aPVT and pPVT from SH-activated regions was first performed using immunohistochemistry (**Figure 7.1**).

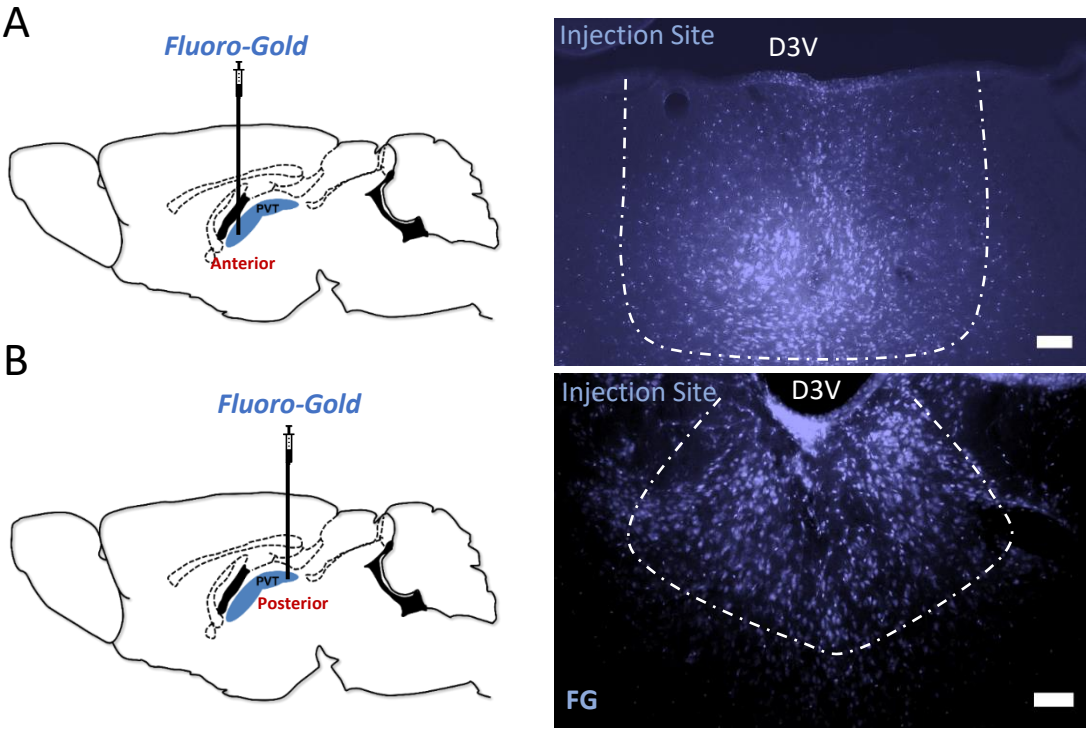

Figure 7.1: Retrograde tracing approach to identify afferents to the PVT

A: FG injection into the aPVT and representative immunohistochemistry image of injection site.
B: FG injection into the pPVT and representative immunohistochemistry image of injection site.
Scale bars represent 100 µm. n = 3-4 animals per group, n = 3 sections per sub-region, per animal.

Coronal brain sections from the entire rostro-caudal extent of the brain were labelled with cFos (red-fluorescent secondary antibody). Visualisation of the endogenous blue fluorescence of FG-labelled neurons, alongside cFos, enabled identification of SH-activated brain region which project to the aPVT or pPVT (**Figure 7.2** and **Figure 7.3**). This revealed that multiple brain regions contained FG-labelled neurons. There was a bilateral distribution of retrogradely labelled neurons in similar anatomical locations following midline FG injection into the aPVT or pPVT. Brain regions which contained high levels of cFos expression, alongside FG labelling, were selected for further analysis. These SH-activated, PVT-projecting brain regions are shown in **Figure 7.2** and **Figure 7.3**. Though several SH-activated brain regions projected to both the aPVT and pPVT, the density of FG-labelled neurons within these brain regions differed (**Figure 7.4**). Cortical regions showed the highest density of FG labelling, and included the cingulate

cortex (CG1), secondary somatosensory cortex (S2) and the infralimbic cortex (IL). Interestingly, cortical labelling with FG was greater in animals receiving injections into the pPVT compared with the aPVT. A low level of FG labelling was noted throughout the hypothalamus and peri-hypothalamic regions in both groups. However, FG labelling concentrated in the VMH, PVH, medial preoptic area (MPO), lateral preoptic area (LPO) and zona incerta (ZI). FG labelling in the PVH was greater after injections into the pPVT, when compared with the aPVT. Though VMH neurons do not express cFos, a moderate density of FG labelling was seen in this region, following injections into both PVT sub-regions. On the other hand, FG labelling in the MPO was greater after injections into the aPVT, when compared with the pPVT. The most striking difference in FG labelling was seen in the aBNST. Here, FG-labelled neurons congregated in the medial (mBNST) and ventral divisions (vBNST) of the aBNST in both groups. However, a much higher number of aBNST neurons were labelling followed injection into the pPVT, when compared with the aPVT. A similar, but less pronounced difference was seen in the lateral septal nucleus (LSV), which contained moderate/high levels of FG labelling. Within the hindbrain, only the rVLM contained small numbers of FG-labelled neurons, which projected to both PVT sub-regions. These data show that the PVT receives extensive inputs from multiple SH-activated brain regions. Interestingly, this study highlights greater cortical and limbic inputs to the pPVT, when compared with the aPVT.

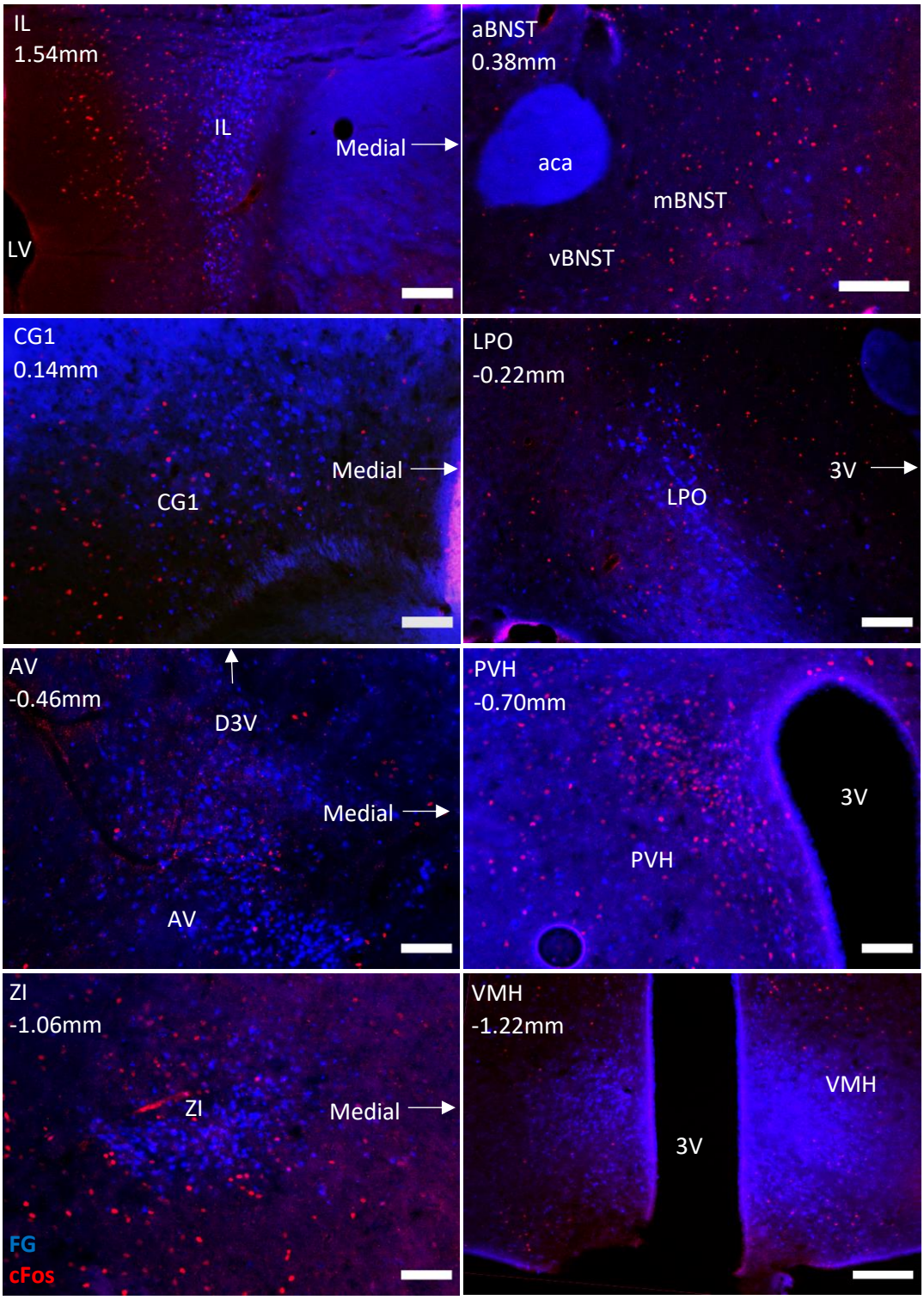

Figure 7.2: Afferent projections to the aPVT from SH-activated neurons

Representative images of SH-activated brain regions following intracranial injection with FG into the aPVT. Neuronal labelling with cFos (red) and FG (blue) is shown for each brain region. The distance relative to bregma is shown for each anatomical region.
Scale bar represents 100 µm.

IL: infralimbic cortex; **CG1**: cingulate cortex (area 1); **LPO**: lateral preoptic area; **AV**: anteroventral nucleus of the thalamus; **ZI**: zona incerta; **LV**: lateral ventricle; **mBNST**: medial division of the aBNST; **vBNST**: ventral division of the aBNST; **3V**: 3rd Ventricle

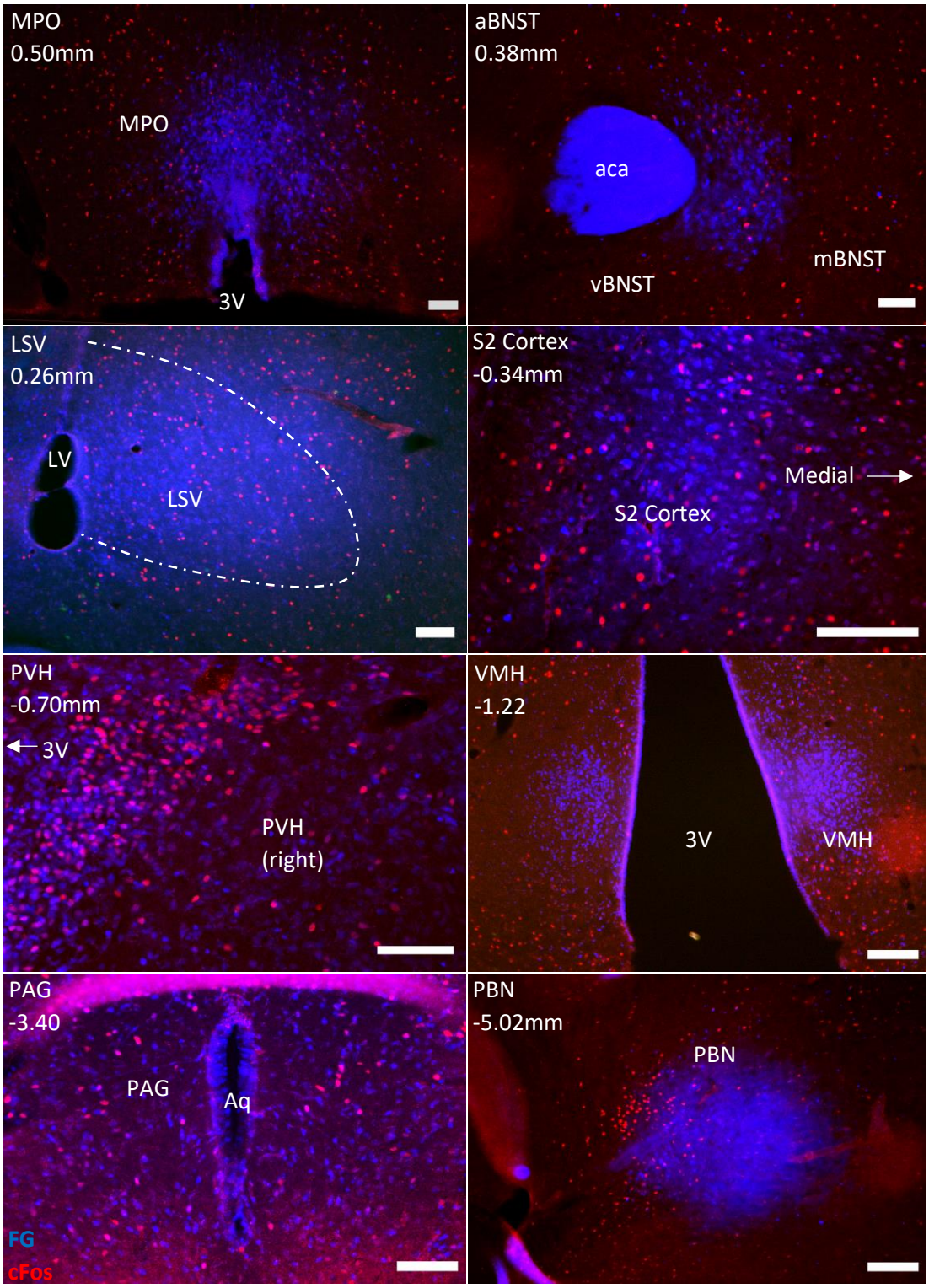

Figure 7.3: Afferent projections to the pPVT from SH-activated neurons

Representative images of SH-activated brain regions following intracranial injection with FG into the pPVT. Neuronal labelling with cFos (red) and FG (blue) is shown for each brain region. The distance relative to bregma is shown for each anatomical region.
Scale bar represents 100 µm.

LSV: latera septal nucleus; **S2**: secondary somatosensory cortex; **MPO**: medial preoptic area; **LV**: lateral ventricle; **mBNST**: medial division of the aBNST; **vBNST**: ventral division of the aBNST; **PAG**: periaqueductal grey; **PBN**: parabrachial nucleus; **Aq**: cerebral aqueduct; **3V**: 3rd Ventricle**.**

Structure	aPVT	pPVT
IL	++	+++
MPO	++	+
aBNST	+	+++
LSV	++	+++
CG1 Cortex	++	+++
LPO	++	++
S2 Cortex	+++	+++
AV	++	++
PVH	+	++
VMH	++	++
ZI	++	++
PAG	+	++
PBN	++	++
rVLM	+	+

Figure 7.4: Relative number of SH-activated neurons which project to the aPVT and pPVT from different brain regions

The number of cFos +ve, FG-labelled neurons: +light labelling ,<50 neurons; ++ moderate labelling, 50-150 neurons +++; high labelling, >200 neurons per section. Counts were performed bilaterally for each brain region.

IL: infralimbic cortex; **MPO**: medial preoptic area; **LSV**: latera septal nucleus; **CG1**: cingulate cortex (area 1); **LPO**: lateral preoptic area; **S2**: secondary somatosensory cortex; **AV**: anteroventral nucleus of the thalamus; **ZI**: zona incerta; **PAG**: periaqueductal grey; **PBN**: parabrachial nucleus.

7.3.2 Identifying direct connections between CRH^{mpdPVH} neurons and the pPVT

Subsequently, a retrograde tracing study was performed to identify direct connections between CRH^{mpdPVH} neurons and the pPVT. Injection of FG into the pPVT was confirmed by visualising the endogenous blue florescence of FG (**Figure 7.5A**). In animals with on-target injections, sections containing the mPVH were labelled for cFos and GFP, alongside FG, to identify SH-activated CRH^{mpdPVH}→pPVT neurons (**Figure 7.5B**). FG-labelled neurons were scattered throughout the hypothalamus, though more concentrated in the PVH and VMH. In the PVH, just under 20% of FG-labelled neurons, colocalised with GFP, identifying them as CRH neurons (**Figure 7.5C**). A smaller number of PVH neurons were labelled with cFos, FG and CRH, identifying them as SH-activated CRH^{mpdPVH}→pPVT neurons (**Figure 7.5D**). These triple colocalised CRH neurons were seen throughout the PVH but were more concentrated within the mpdPVH region. Interestingly, these CRH^{mpdPVH} neurons accounted for 39.2 ± 8.1% of SH-activated PVH$^{→pPVT}$ neurons (**Figure 7.5E**). This suggests that there is a significant CRH^{mpdPVH}→pPVT neuronal connection.

In parallel, injections of FG into the mpdPVH were performed to identify SH-activated pPVT→PVH neuron connections. The injection of FG led to spread of the retrograde tracer beyond the boundary of the mpdPVH. However, FG injection was confined to the mPVH region in animals included in this study (**Figure 7.6A**). Sections containing the pPVT were labelled with cFos and visualised alongside FG, enabling the identification of SH-activated pPVT→PVH neurons (**Figure 7.6B**). Dense neuronal labelling with FG was found throughout the pPVT. FG-labelled neurons were more numerous than cFos-labelled neurons. Many FG-labelled pPVT neurons colocalised with cFos, identifying them as SH-activated pPVT→PVH neurons (**Figure 7.6C**). Interestingly, 35.9 ± 9.3 % of cFos-labelled pPVT neurons colocalised with FG. This demonstrated an important projection from SH-activated pPVT neurons is to the PVH. Combined, a direct, reciprocal connection between SH-activated neurons in the PVH and pPVT exists and includes CRH^{mpdPVH} neurons.

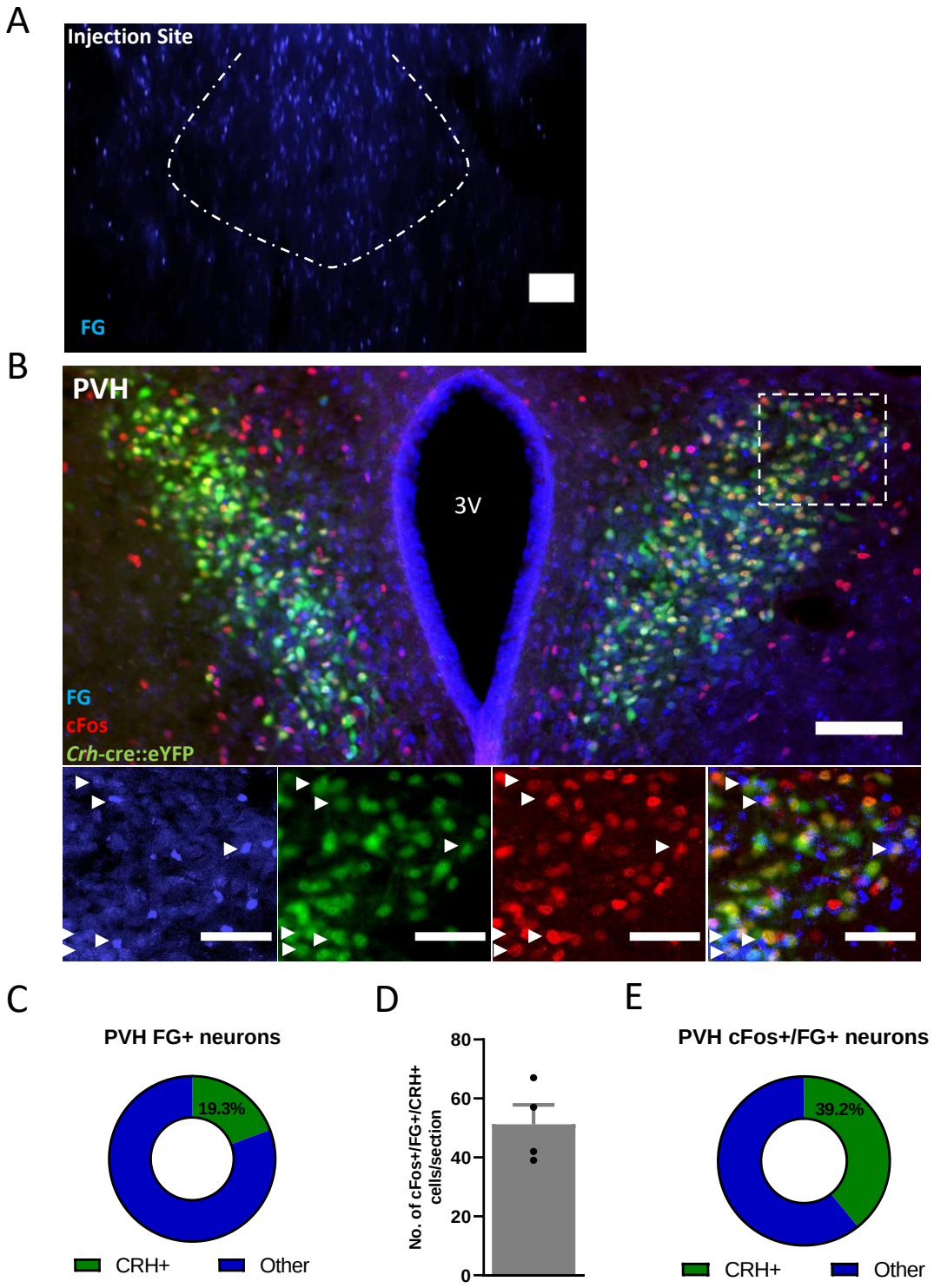

Figure 7.5: SH-activated CRH^{mpdPVH}→pPVT neuron connection

A: Representative image of the pPVT FG injection site. Scale bar represents 100 µm.
B: Representative image of the mPVH following FG injection into the pPVT. Neurons are stained for cFos (red), FG (blue) and GFP (green). Colocalisation of cFos, FG and GFP identifies SH-activated CRH^{mpdPVH}→pPVT neurons, which are marked with white arrows. Main image scale bar represents 100 µm, magnified image scale bar 50 µm.
C: Plot showing the percentage of FG+ neurons in the PVH which are CRH+(GFP+).
D: Number of colocalised cFos+, FG+ and CRH+ neurons in the PVH.
E: Plot showing the percentage of cFos+/FG+ dual-labelled PVH neurons, which are CRH+ (GFP+).
Data presented as mean ± SEM. n = 4 animals, n = 3-5 sections per sub-region, per animal.

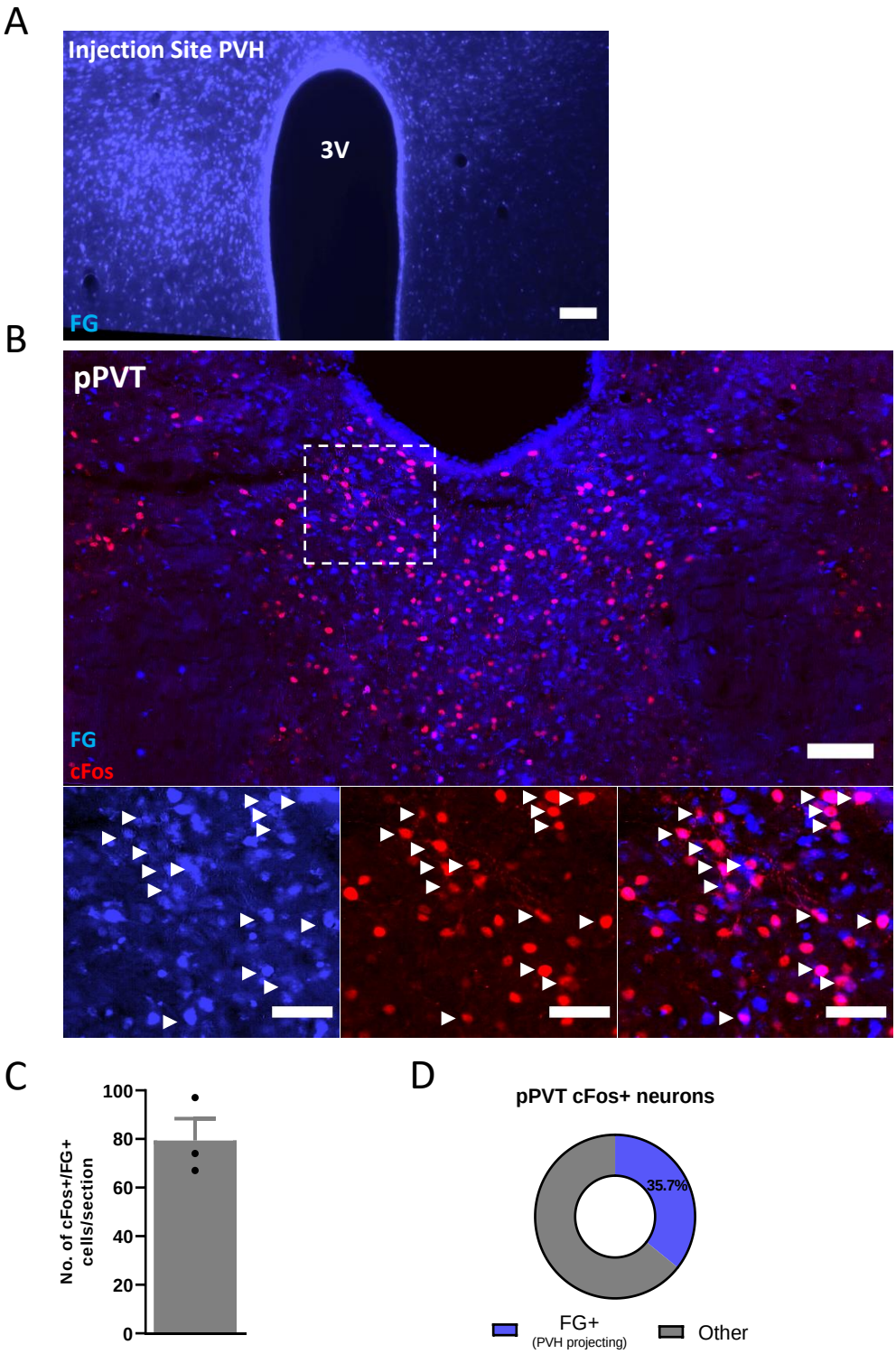

Figure 7.6: SH-activated pPVT→PVH neuron connection

A: Representative image of the mPVH FG injection site. Scale bar represents 100 µm.
B: Representative image of the pPVT following FG injection into the mPVH. Neurons are stained for cFos (red) and FG (blue). Colocalisation of cFos and FG identifies SH-activated $CRH^{mpdPVH \rightarrow pPVT}$ neurons, which are marked with white arrows. Main image scale bar represents 100 µm, magnified image scale bar 50 µm.
C: Number of colocalised cFos+ and FG+ neurons in the pPVT.
D: Plot showing the percentage of cFos+ neurons in the pPVT which are PVH-projecting (FG+).
Data presented as mean ± SEM. n = 3 animals, n = 3-5 sections per sub-region, per animal.

7.3.3 Investigating the importance of pPVT neurons to the sympathoadrenal response following SH

In this study, I investigated whether GLUT^{pPVT} neurons are functionally important to the sympathoadrenal response following SH. As the main projection and SH-activated neuronal population in the pPVT is glutamatergic, *VGlut2*-cre::eYFP mice were used in this experiment. The study design is outlined pictorially in **Figure 7.7**.

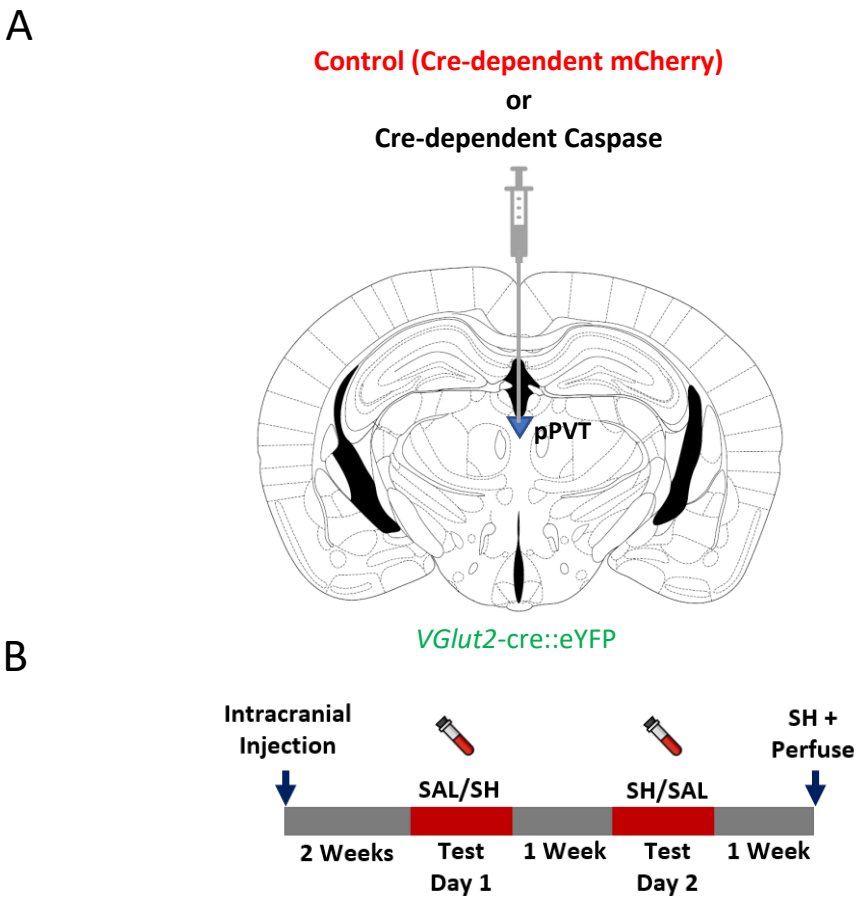

Figure 7.7: Study design to investigate the importance of pPVT neurons to the sympathoadrenal response following SH

A: Diagram showing intracranial injection into the pPVT with AAVs containing control (Cre-dependent mCherry) or Cre-dependent caspase constructs into *VGlut2*-cre::eYFP mice.
B: Study timeline, showing cross-over design. Animals were exposed to either saline or SH on test days and glucose and adrenaline levels were measured.

On test days, blood glucose levels following s.c insulin or saline injection were similar between control and caspase groups, showing a small stress-induced increase after the injection (**Figure 7.8A**). Animals in both treatment groups also experienced a similar reduction in blood glucose following SH and comparable recovery of blood glucose levels after hypoglycaemia (**Figure 7.8A**). Blood glucose measurements were terminated at 90 min as animals were displaying increased stress behaviours. The adrenaline response was also comparable for animals in both treatment groups, following saline and SH (**Figure 7.8B**).

Representative images of the pPVT in control and caspase-treated animals are shown in **Figure 7.8C**. GLUT^{pPVT} neurons transfected with the control virus are highlighted by staining for mCherry. Post-experimental validation of GFP (eYFP) staining indicated a significant reduction in the number of GLUT^{pPVT} neurons in animals injected with the caspase virus (**Figure 7.8D**). This confirmed that the ablation of GLUT^{pPVT} neurons did not affect the glucose or sympathoadrenal response following SH.

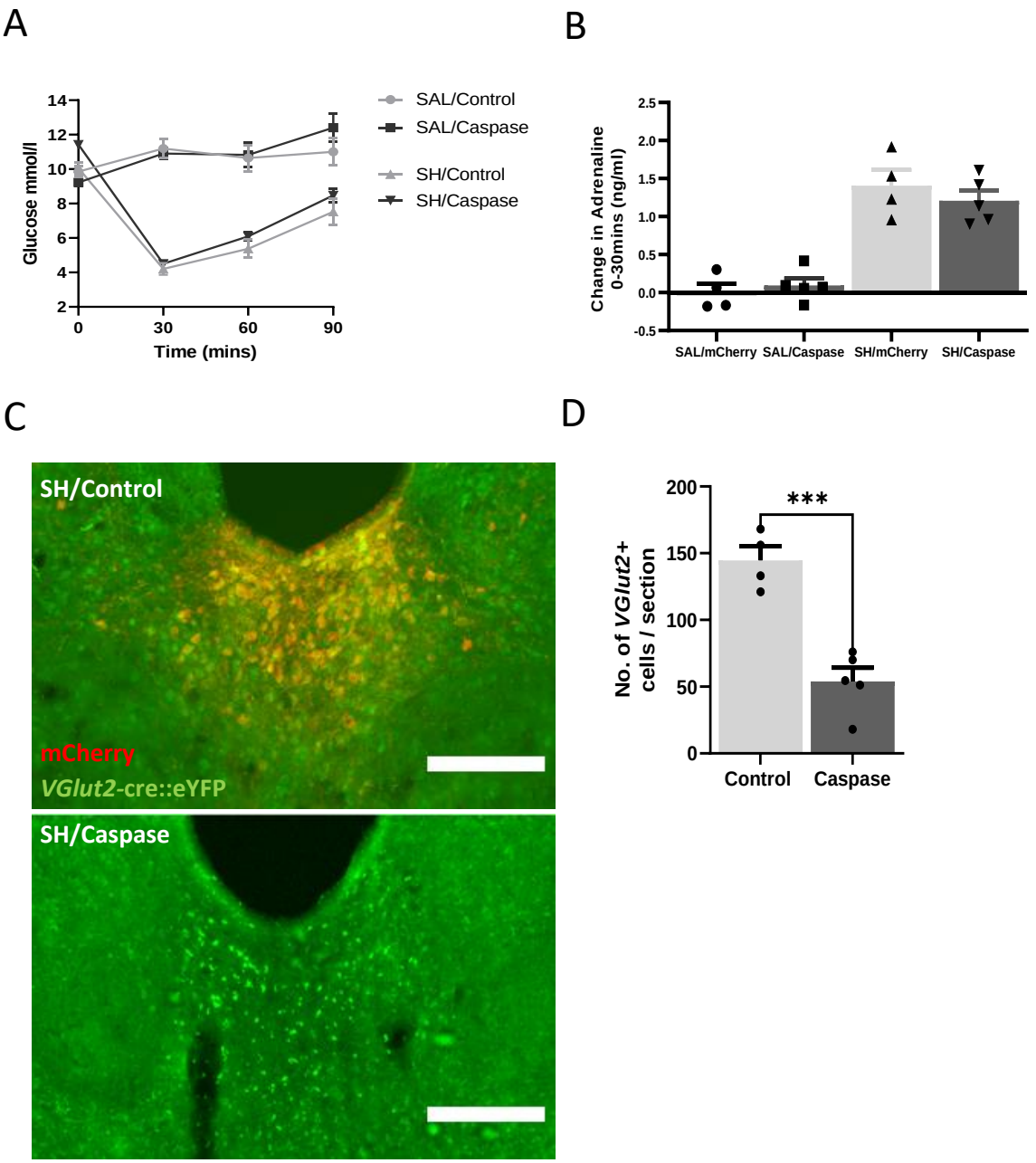

Figure 7.8: The importance of pPVT neurons to the sympathoadrenal response following SH

A: Mean blood glucose profile for the 90 min following injection, in SAL/control, SAL/caspase, SH/control and SH/caspase groups (repeated measures ANOVA with Sidak's *post hoc* test).
B: Change in adrenaline release (0-30 min) following injection in in SAL/control, SAL/caspase, SH/control and SH/caspase groups. Adrenaline levels were similar in control and caspase groups.
C: Representative image of the pPVT injection site in control and caspase-treated animals. In control animals, transfected VGlut2 neurons (green) were labelled with mCherry (red). Caspase injection led to ablation of VGlut2 neurons. Scale bare represents 100 µm.
D: Number of VGlut2+ cells in the pPVT in control and caspase groups. Transfection with caspase led to a significant reduction in VGlut2 cells (***p<0.001, unpaired t-test).
Data presented as mean ± SEM. n = 4-6 per group. n = 3-5 sections per sub-region, per animal.

7.3.4 Investigating the importance of pPVT neurons to the RH-induced habituation of the sympathoadrenal response

Subsequently, I investigated the functional significance of GLUT^{pPVT} neurons to the habituation of the sympathoadrenal response following RH. A similar experimental approach was taken, which is summarised in **Figure 7.9**.

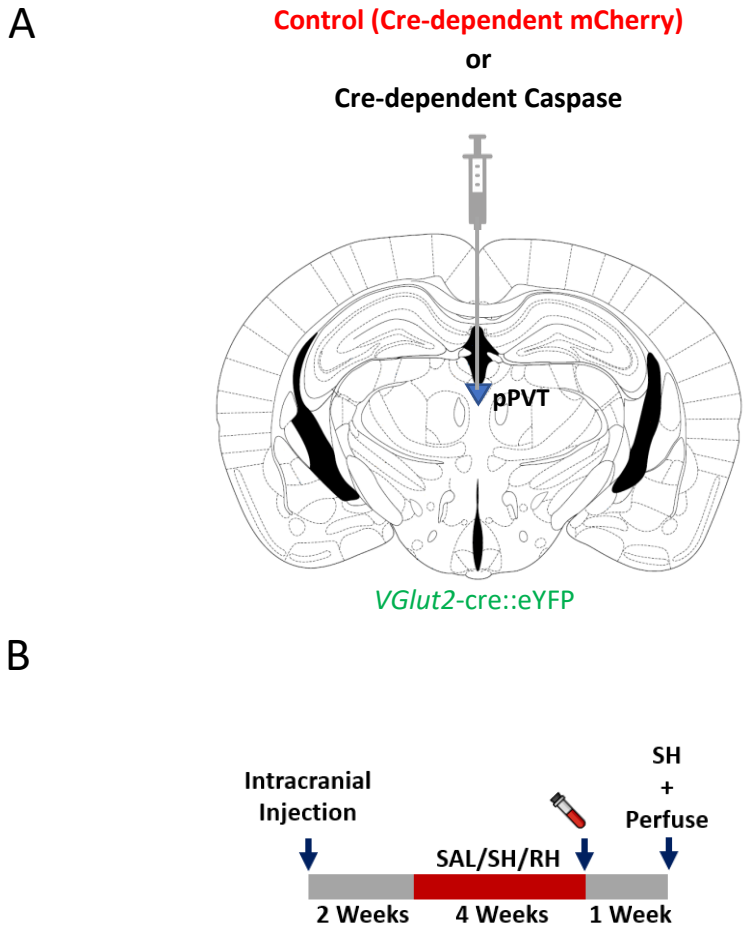

Figure 7.9: Study design to investigate the importance of pPVT neurons to the RH-induced habituation of the sympathoadrenal response

A: Diagram showing intracranial injection into the pPVT with AAVs containing control (Cre-dependent mCherry) or Cre-dependent caspase constructs into *VGlut2*-cre::eYFP mice.
B: Study timeline. Animals were randomised to SAL, SH or RH group and on the final day the glucose and adrenaline levels were measured.

On the final day of the RH protocol, glucose and adrenaline measurements were taken after a final injection of s.c. insulin or volume-matched saline. The blood glucose profile for 90 min after injection is shown in **Figure 7.9A**. Blood glucose levels reached a similar nadir in SH- and RH-treated groups and approached baseline levels at 90 min after injection. Blood glucose measurements were terminated at 90 min as animals were displaying increased stress behaviours. At the 90 min blood glucose time point, RH/caspase animals showed a trend towards faster recovery from hypoglycaemia, when compared with RH/control animals. However, this difference was not found to be statistically significant.

The adrenaline release was at a low level in saline-treated groups (SAL/control and SAL/caspase groups) and increased to a comparable level in SH-treated groups (SH/control and SH/caspase) (**Figure 7.9B**). Importantly, in control groups, RH treatment led to a significant attenuation in adrenaline release, when compared with SH, demonstrating the consistency of the RH protocol. Interestingly, the adrenaline release following a final episode of hypoglycaemia was preserved in the RH/caspase group. This was significantly increased when compared with the RH/control group (**Figure 7.9C**).

Representative images of the pPVT in RH/control and RH/caspase groups are shown in **Figure 7.10A**. Post-experimental validation of GFP (eYFP) staining confirmed a significant reduction in the number of $GLUT^{pPVT}$ neurons following AAV-caspase injection (**Figure 7.10B**). This demonstrated that ablating $GLUT^{pPVT}$ neurons blocked habituation of the adrenaline response due to RH.

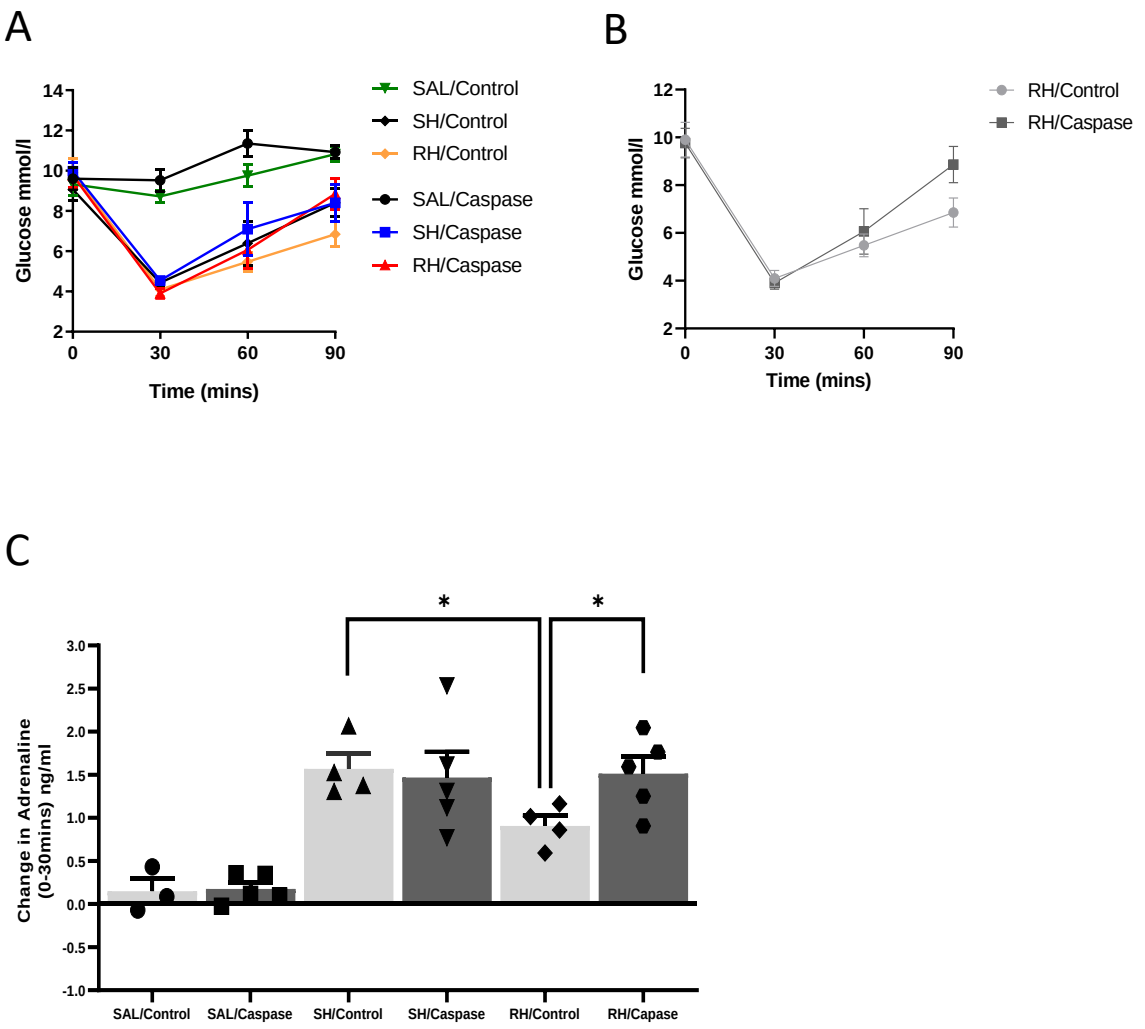

Figure 7.10: The importance of pPVT neurons to the RH-induced habituation of the sympathoadrenal response

A: Mean blood glucose profile for the 90 min following injection, in control and caspase groups.
B: Mean blood glucose profile for the 90 min following injection, in all RH/control and RH/caspase groups. Glucose recovery showed a trend towards faster recovery in the RH/caspase group.
C: Change in adrenaline release (0-30 min) following injection, in control and caspase groups. The adrenaline response was significantly attenuated in the RH/control group, when compared with SH/control group. Whereas this attenuation was blunted in the RH/caspase group, which displayed significantly increased adrenaline levels, when compared with RH/control (*p<0.05, SH/control versus RH/control; *p<0.05, RH/caspase versus RH/control; one-way ANOVA with Sidak's *post hoc* test).
Data presented as mean ± SEM. n = 3-5 per group.

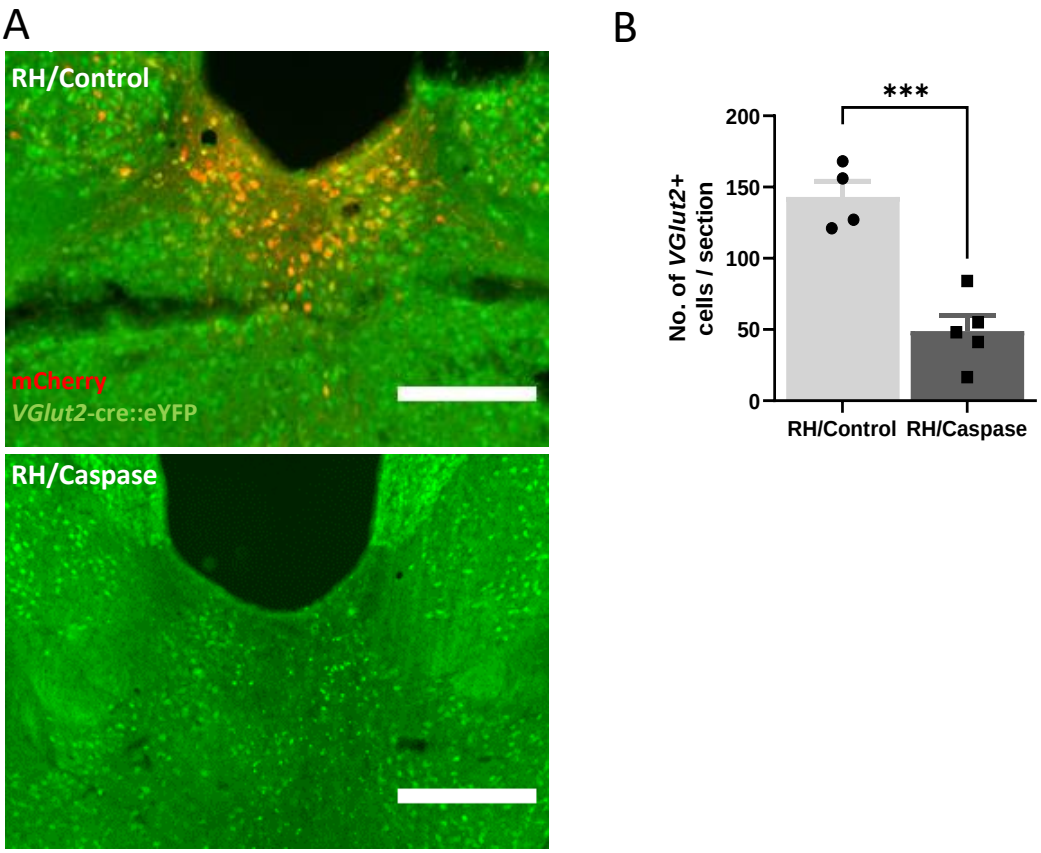

Figure 7.11: Validation of ablation of VGlut2^{pPVT} neurons following AAV-caspase transfection

A: Representative image of the pPVT injection site in control and caspase-treated animals. In control animals, transfected VGlut2 neurons (green) were labelled with mCherry (red). Caspase injection led to ablation of VGlut2 neurons. Scale bar represents 100 µm.
B: Number of VGlut2+ cells in the pPVT in control and caspase groups. Transfection with caspase led to a significant reduction in VGlut2 cells (***p<0.001, unpaired t-test).
Data presented as mean ± SEM. n = 3-5 per group. n = 3-5 sections per animal.

7.3.5 Identifying intermediary GABAergic neuronal populations which may enable the pPVT to control CRH^{mpdPVH} activity following RH

In this Chapter, I demonstrated reciprocal connections between SH-activated neurons in the mpdPVH and pPVT. However, the major outputs of the PVT are glutamatergic (GLUT) neurons which project directly to the NAc, vBNST and CeA. We postulated that the pPVT controls the RH-induced habituation of the sympathoadrenal response through connections with an intermediary GABAergic neuronal population, which itself projects to the PVH (CRH^{mpdPVH} neurons) (**Figure 7.12**).

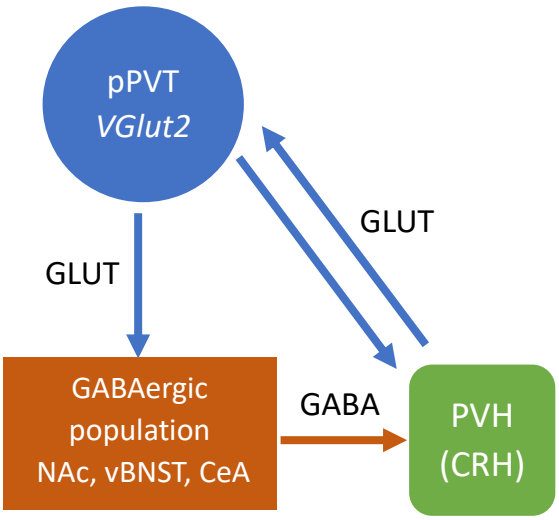

Figure 7.12: Proposed neuronal circuit diagram to explain the pPVT control of RH-induced habituation of the sympathoadrenal response

The identity of the GABAergic relays was investigated using retrograde tracing with FG. First, projections from SH-activated GLUT^{pPVT} neurons to possible GABAergic relay populations were investigated (**Figure 7.13**). Representative images of the injection site along with the corresponding pPVT section are shown in **Figures 7.14 - 7.16**. Following unilateral injection with FG into the NAc, vBNST or CeA, neurons labelled with FG were found ipsilaterally within the pPVT. Interestingly, the anatomical location of FG labelled neurons in the pPVT was slightly different for the three injection sites. NAc projecting pPVT neurons were located more ventrally within the pPVT. Whereas vBNST and CeA projecting pPVT neurons were distributed more dorsally within the pPVT, adjacent to the dorsal 3rd ventricle. The majority (>90%) of FG-labelled pPVT neurons colocalised with GFP (*VGlut2*-cre::eYFP), identifying them as glutamatergic neurons and confirming their projection to the NAc, vBNST and CeA. Several pPVT neurons were labelled with cFos, GFP and FG following injections into all three brain regions, identifying SH-activated GLUT^{pPVT} projection neurons (**Figure 7.17A**). A greater number of SH-activated GLUT^{pPVT} neurons project to the NAc, compared with to the vBNST and CeA. However,

a higher percentage of GLUT^{pPVT} neurons which project to the vBNST were SH activated **Figure 7.17B**. This suggested that a SH-activated GLUT^{pPVT}→vBNST connection may be particularly important within this arm of the neuronal circuit.

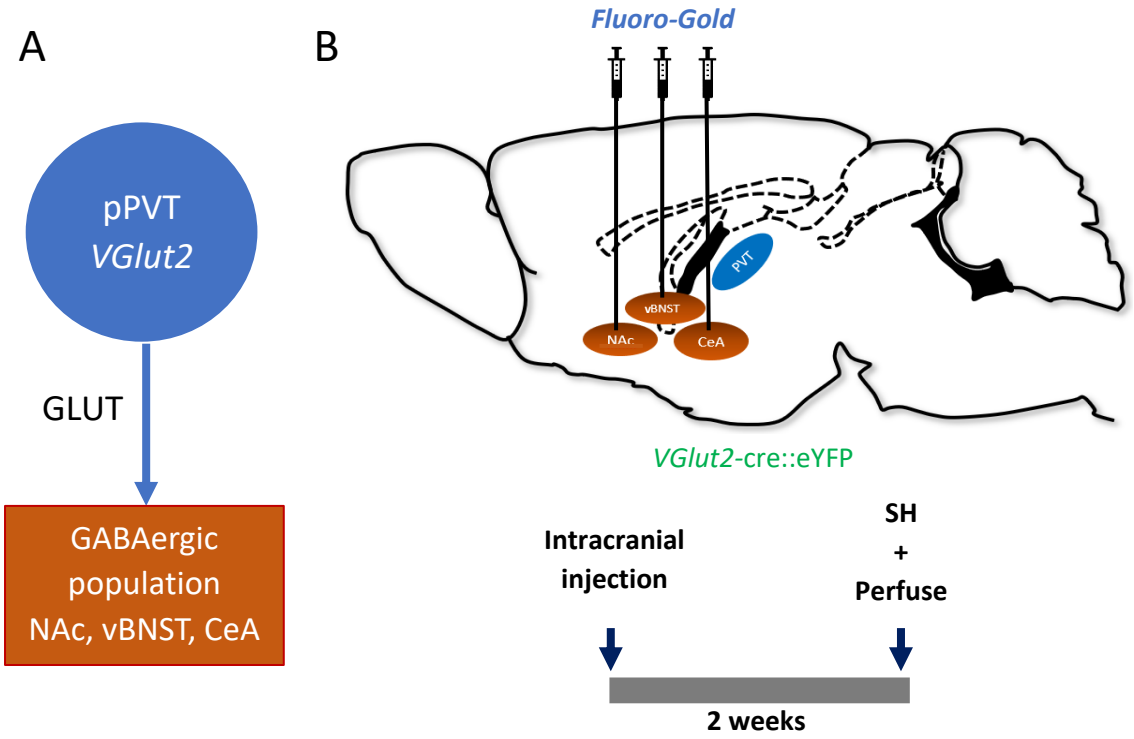

Figure 7.13: The investigation of SH-activated GLUT^{pPVT}→GABA neuronal connection

A: Circuit diagram showing the proposed connection between glutamatergic neurons in the pPVT and the NAc, vBNST and CeA, which all contain GABAergic neuronal populations.
B: Study protocol showing FG injection into either the NAc, vBNST or CeA in *VGlut2*-cre::eYFP mice.

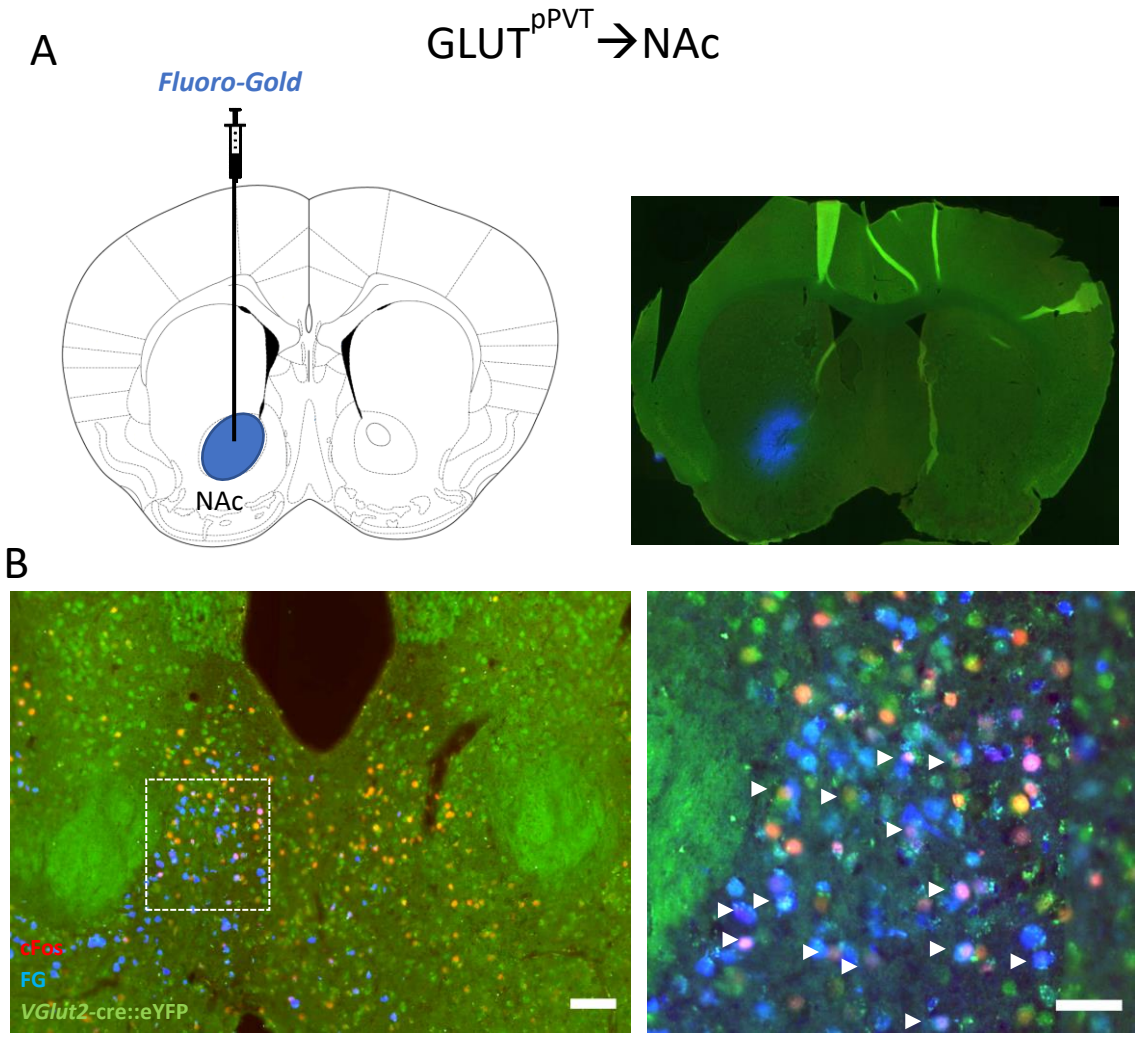

Figure 7.14: SH-activated GLUT^{pPVT}→NAc neuron connection

A: Brain atlas diagram of injection site in the NAc and representative whole-brain section showing FG (blue) localised to the NAc.
B: Representative image of the pPVT following FG injection into the NAc. Neurons are stained for cFos (red), FG (blue) and GFP (green). Colocalisation of cFos, FG and GFP identifies SH-activated GLUT^{pPVT}→NAc neurons, which are marked with white arrows. Main image scale bar represents 100 µm, magnified image scale bar 50 µm.
n = 3 per group. n = 3-5 sections per animal.

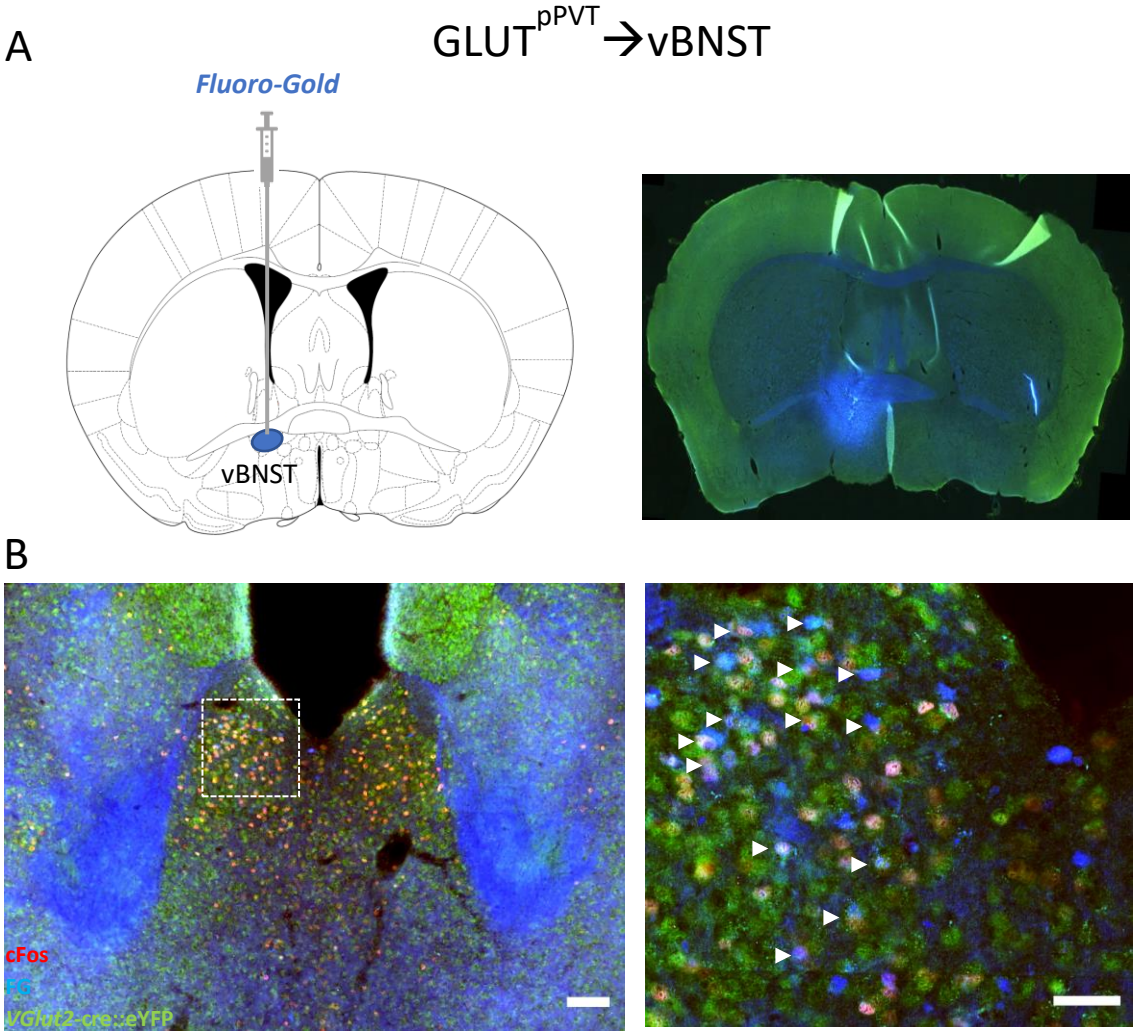

Figure 7.15: SH-activated GLUT^{vBNST}→vBNST neuron connection

A: Brain atlas diagram of injection site in the vBNST and representative whole-brain section showing FG (blue) localised to the vBNST.
B: Representative image of the pPVT following FG injection into the vBNST. Neurons are stained for cFos (red), FG (blue) and GFP (green). Colocalisation of cFos, FG and GFP identifies SH-activated GLUT^{pPVT}→vBNST neurons, which are marked with white arrows. Main image scale bar represents 100 µm, magnified image scale bar 50 µm.
n = 3 per group. n = 3-5 sections per animal.

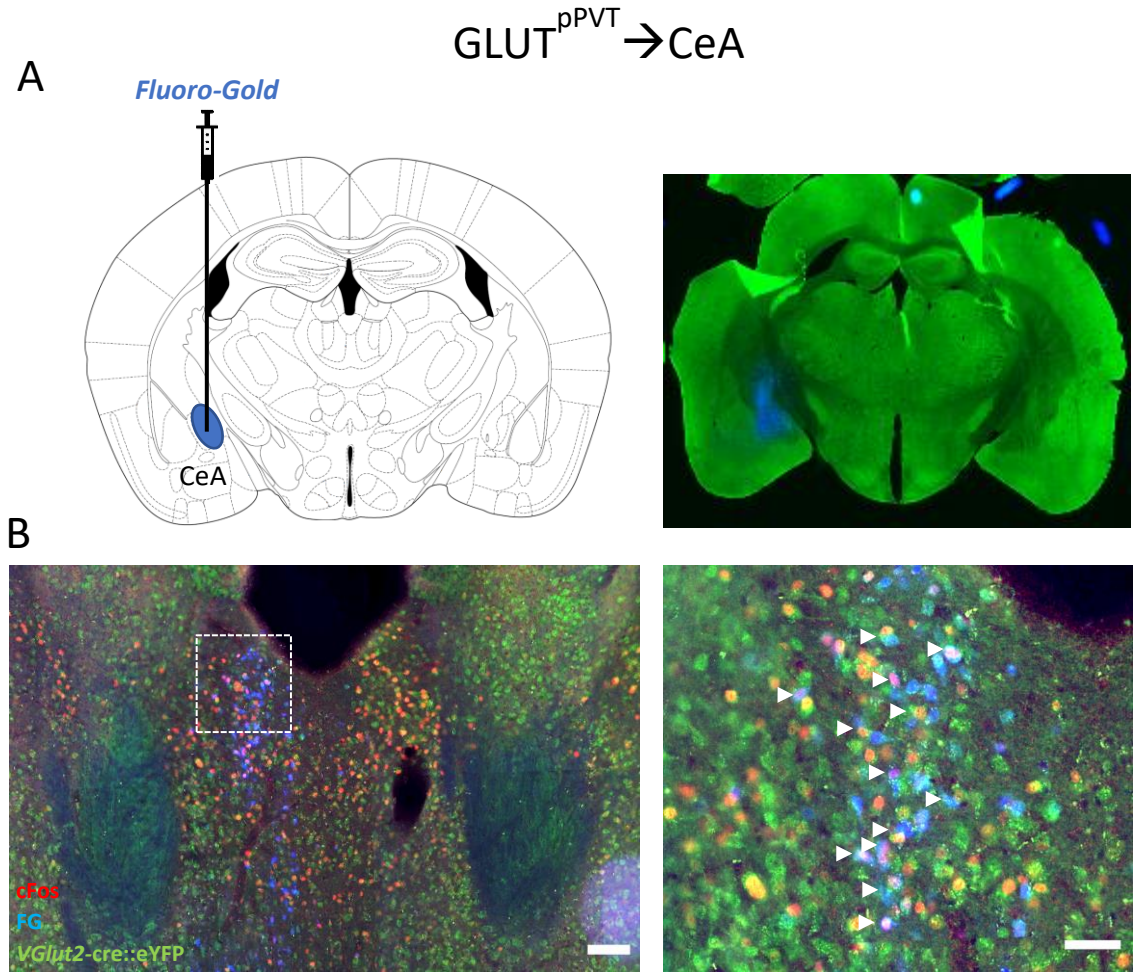

Figure 7.16: SH-activated GLUT^{pPVT}→CeA neuron connection

A: Brain atlas diagram of injection site in the CeA and representative whole-brain section showing FG (blue) localised to the CeA.
B: Representative image of the pPVT following FG injection into the CeA. Neurons are stained for cFos (red), FG (blue) and GFP (green). Colocalisation of cFos, FG and GFP identifies SH-activated GLUT^{pPVT}→CeA neurons, which are marked with white arrows. Main image scale bar represents 100 µm, magnified image scale bar 50 µm.
n = 3 per group. n = 3-5 sections per animal.

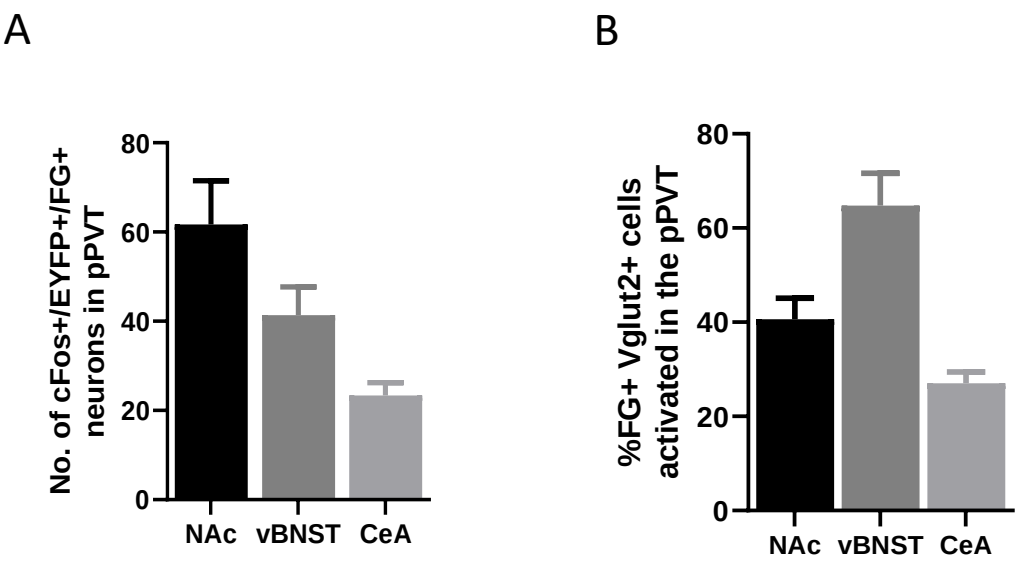

Figure 7.17: Projection-specific cell counts for SH-activated GLUT^{pPVT} neurons

A: Number of colocalised cFos+, VGlut2+ and FG+ neurons in the pPVT following injection into the NAc, CeA and vBNST, respectively.
B: Percentage of FG+ and VGlut2+ colocalised cells which were activated (cFos+), following SH for the NAc, CeA or vBNST, respectively.
Data presented as mean ± SEM. n = 3 per group.

Subsequently, projections from GABAergic neurons in the NAc, vBNST or CeA to the mpdPVH was investigated. The experimental approach is summarised in **Figure 7.18**.

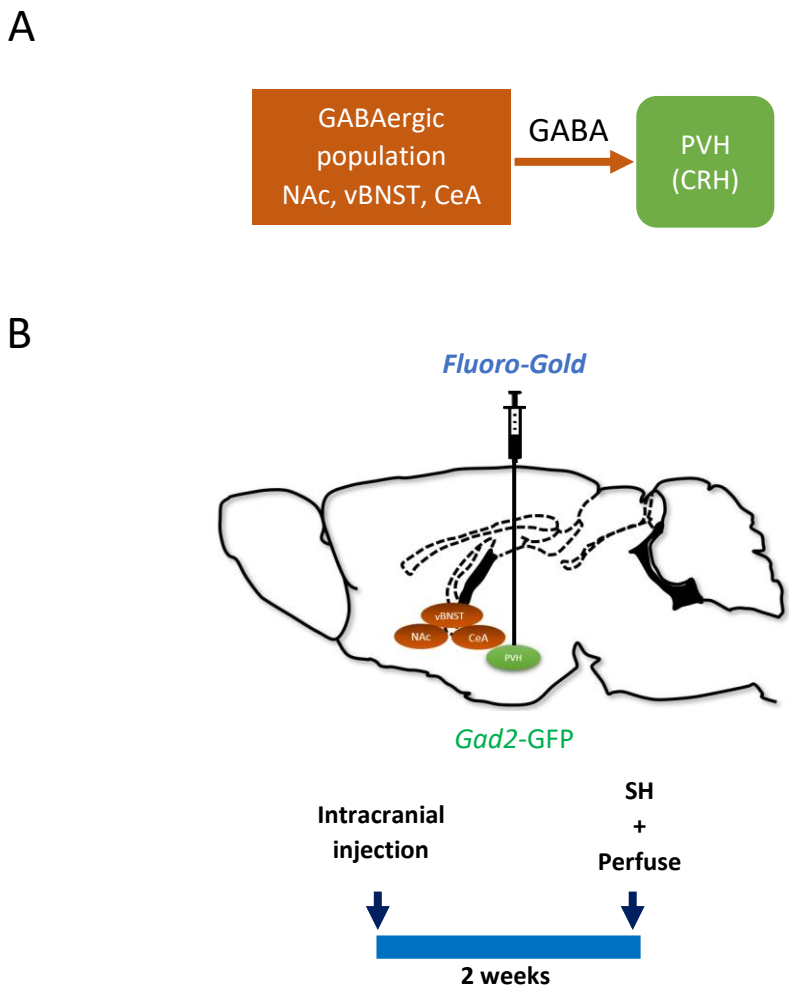

Figure 7.18: The investigation of a SH-activated GABA→mpdPVH neuronal connection

A: Circuit diagram showing the proposed connection between GABAergic neurons in the NAc, vBNST or CeA and the mpdPVH.
B: Study protocol showing FG injection into the mpdPVH in *Gad2*-GFP mice.

Injections of FG into the mpdPVH led to spread of the retrograde tracer beyond the boundary of the mpdPVH division. However, FG injection was still confined to the mPVH region in on-target animals (**Figure 7.19A**). Sections containing the NAc, vBNST and CeA were assessed for labelling with FG, identifying mpdPVH projecting neurons. Representative images for the NAc, vBNST and CeA are shown in **Figure 7.19B-D**. GFP labelling, which identified Gad2+ (GABA) neurons, were concentrated in the lateral NAc, vBNST and CeA. In all three brain regions, a high proportion of GABA neurons colocalised with cFos, indicating activation. The unilateral injection of FG into the mpdPVH led to ipsilateral neuronal labelling in all three brain regions. Surprisingly only a small number (<5 FG+ neurons/section) of FG-labelled neurons were found in the CeA

and BNST (**Figure 7.19B,C**). However, these mpdPVH-projecting neurons were not found to colocalise with GFP, suggesting they were not GABA neurons. The vBNST contained large numbers of GAD neurons throughout its rostro-caudal extent (**Figure 7.19D**). The quantification of vBNST FG-labelled neurons was performed at three bregma levels (+0.26mm, +0.14mm and +0.02mm), allowing a greater understanding of the anatomical location of mpdPVH-projecting neurons. At all anatomical levels of the vBNST >85% of GABA neurons were found to colocalise with cFos, indicating activation following SH (**Figure 7.19E**). In addition, GABA neurons were identified at all levels of vBNST, which colocalised with both cFos and FG. The greatest number of neurons colocalising with cFos, Gad2 and FG was identified at bregma +0.14mm (**Figure 7.19F**). At this bregma level >55% of cFos and Gad2 dual-labelled neurons also colocalised with FG. This indicated that a large proportion of SH-activated $GABA^{vBNST}$ neurons project to the mpdPVH.

Combined, the experiments in this section identified that the $GABA^{vBNST}$ neurons may act as an intermediary relay, allowing $GLUT^{pPVT}$ neurons to control CRH^{mpdPVH} activity.

A

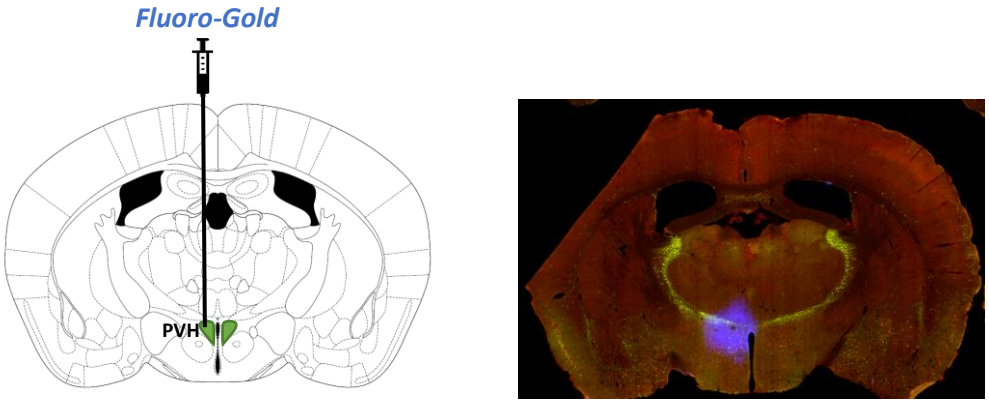

B

GABA^{NAc}→mpdPVH

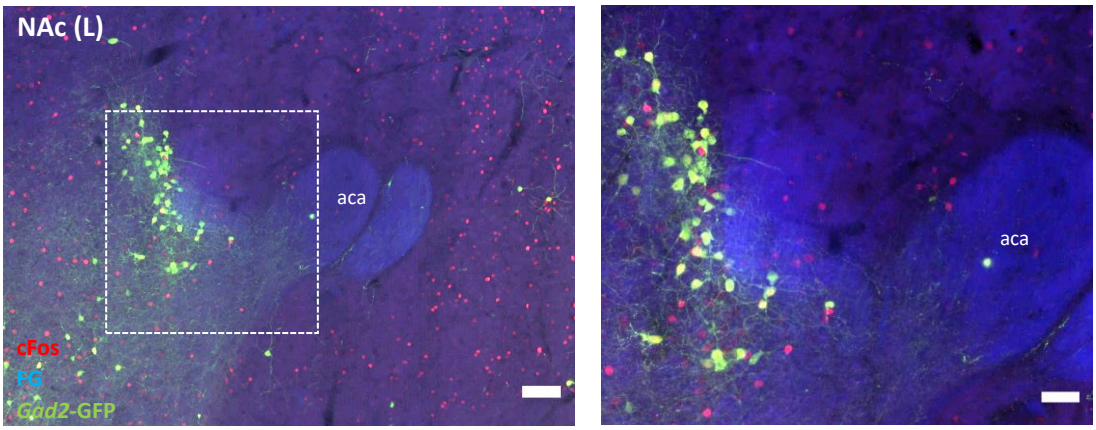

C

GABA^{CeA}→mpdPVH

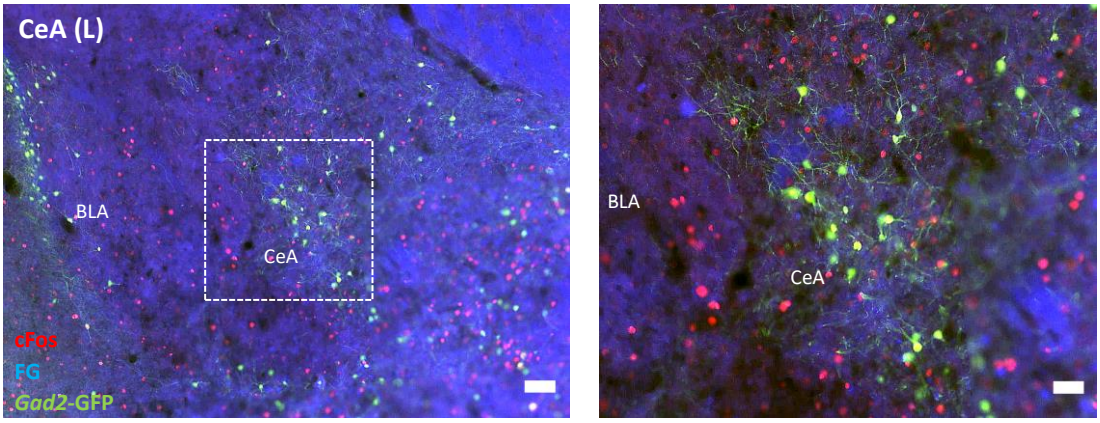

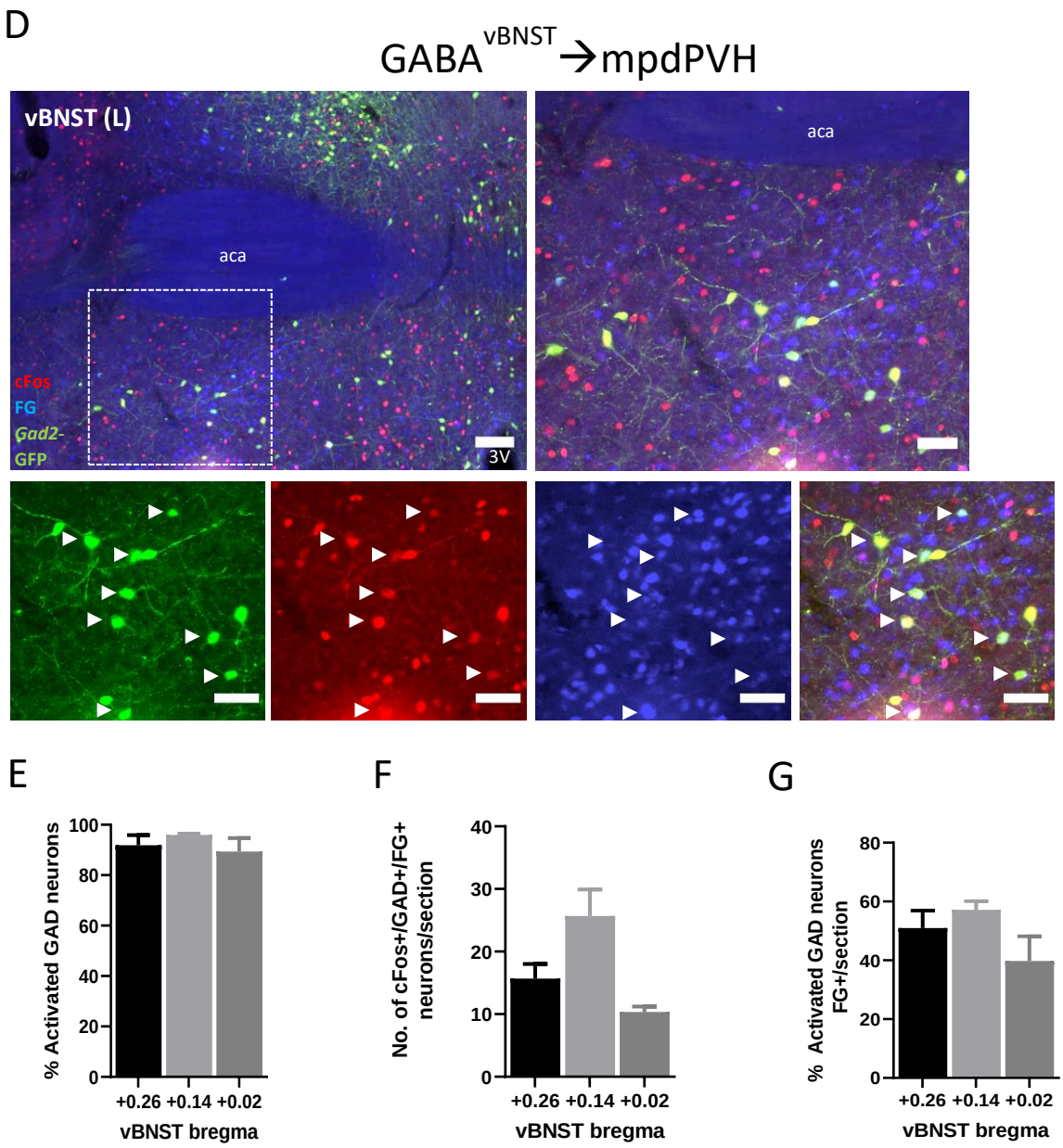

Figure 7.19: The investigation of a SH-activated GABA→mpdPVH neuronal connection

A: Brain atlas diagram of injection site in the mpdPVH and representative whole-brain section showing FG (blue) spread following injection.
B: Representative image of the NAc (left) following FG injection into the mpdPVH. Neurons are stained for cFos (red), FG (blue) and GFP (green).
C: Representative image of the CeA (left) following FG injection into the mpdPVH. Neurons are again stained for cFos, FG and GFP.
D: Representative image of the vBNST (left) following FG injection into the mpdPVH. Neurons are again stained for cFos, FG and GFP. Magnified images showing cFos, FG, GFP labelling and colocalisation is also shown. White arrows identify neuronal colocalisation with cFos, FG and GFP. This identifies SH-activated GABA^{vBNST}→mpdPVH neurons.
E: The percentage of Gad2+ neurons at different levels of the vBNST which are activated following SH.
F: Number of colocalised cFos+, FG+ and GFP+ neurons at different levels of the vBNST.
G: The percentage of SH-activated Gad2+ neurons which project to the mpdPVH at different levels of the vBNST.
Main image scale bar represents 100 µm, magnified image scale bar 50 µm.
n = 3. n = 3-5 sections per animal.

7.3.6 Investigating the importance of GABAergic vBNST neurons to the RH-induced habituation of the sympathoadrenal response

In the previous section, a GLUT^{pPVT}→GABA^{vBNST}→mpdPVH circuit was identified. However, the functional significance of GABA^{vBNST} to RH-induced habituation of the sympathoadrenal response is not known. This was investigated by disabling GABA^{vBNST} neurons using AAV-TetTox and measuring the sympathoadrenal response following RH. The experimental protocol is outlined in **Figure 7.20**.

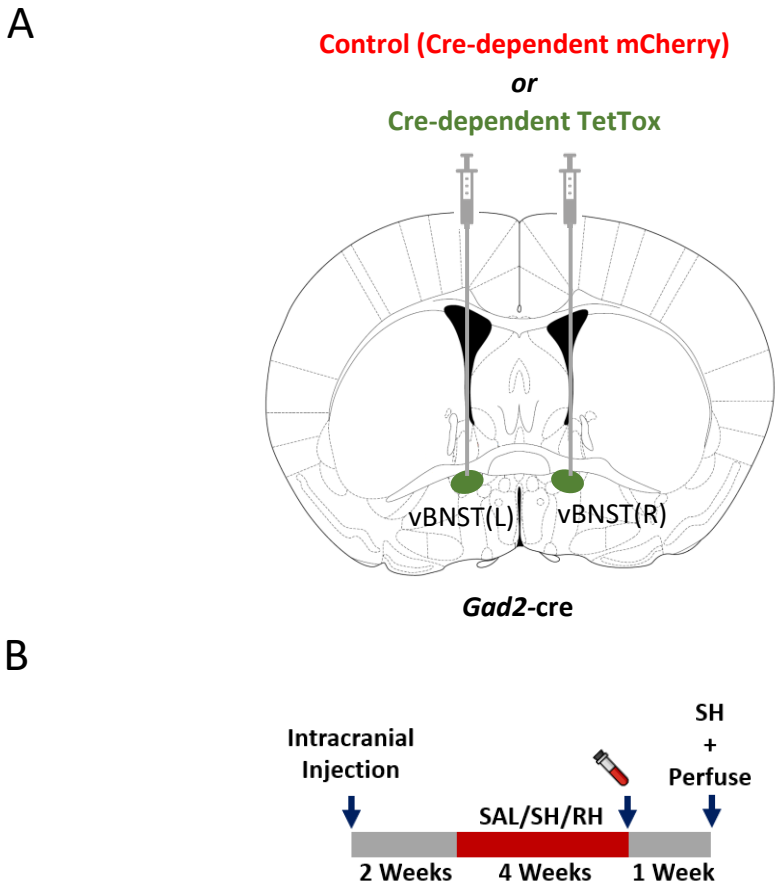

Figure 7.20: Study design to investigate the importance of GABA^{vBNST} neurons to the RH-induced habituation of the sympathoadrenal response

A: Diagram showing intracranial injection into the vBNST with AAVs containing control (Cre-dependent mCherry) or Cre-dependent tetanus toxin (TetTox) constructs into *Gad2*-cre mice.
B: Study timeline. Animals were randomised to SAL, SH or RH groups and on the final day glucose and adrenaline levels were measured.

Animals in both injection groups underwent the RH protocol and, on the last day, glucose and adrenaline measurements were taken after a final injection of s.c. insulin or volume-matched saline. The blood glucose profile for 120 min after injection is shown in **Figure 7.21A**. All SH- and RH-treated groups reached a similar blood glucose nadir at 30 min after injection and showed similar recovery in blood glucose levels by 120 min. At the 90 min blood glucose time point, the RH/TetTox group showed a trend towards quicker recovery from hypoglycaemia, when compared with RH/control animals (**Figure 7.21B**). However, this difference was not found to be statistically significant. Subsequently, both groups reached a similar blood glucose level at 120 min.

Plasma adrenaline following saline treatment was at a low level in SAL/control and SAL/TetTox groups. As expected, insulin injection led to an increase in adrenaline in the SH/control and SH/TetTox groups, when compared with saline treatment (**Figure 7.21C**). However, the adrenaline response was more varied in the SH/TetTox group and lower than in the SH/control group (not statistically significant). In control groups, RH treatment led to a significant attenuation in adrenaline release, when compared with SH, signifying habituation. Importantly, the adrenaline release following a final episode of hypoglycaemia was preserved in the RH/TetTox group. This was significantly increased when compared with the RH/control group (**Figure 7.21C**).

Representative images of the vBNST in RH/control and RH/TetTox groups are shown in **Figure 7.22A**. The post-experimental validation of GFP (eYFP) staining confirmed the location and specificity of transfected $GABA^{vBNST}$ neurons following injection with AAV-TetTox and AAV-mCherry (**Figure 7.22B**). $GABA^{vBNST}$ neurons in the RH/TetTox continued to express cFos, demonstrating they retain responsiveness to glutamatergic inputs. The number of transfected Gad2 neurons in RH/control and RH/TetTox groups is shown in **Figure 7.22C**.

Collectively, these data demonstrate that the selective silencing of $GABA^{vBNST}$ neurons also blocked the habituation of the adrenaline response due to RH. These findings are consistent with the hypothesis that a $GLUT^{pPVT} \rightarrow GABA^{vBNST} \rightarrow$mpdPVH circuit is functionally important to the RH-induced habituation of the sympathoadrenal response..

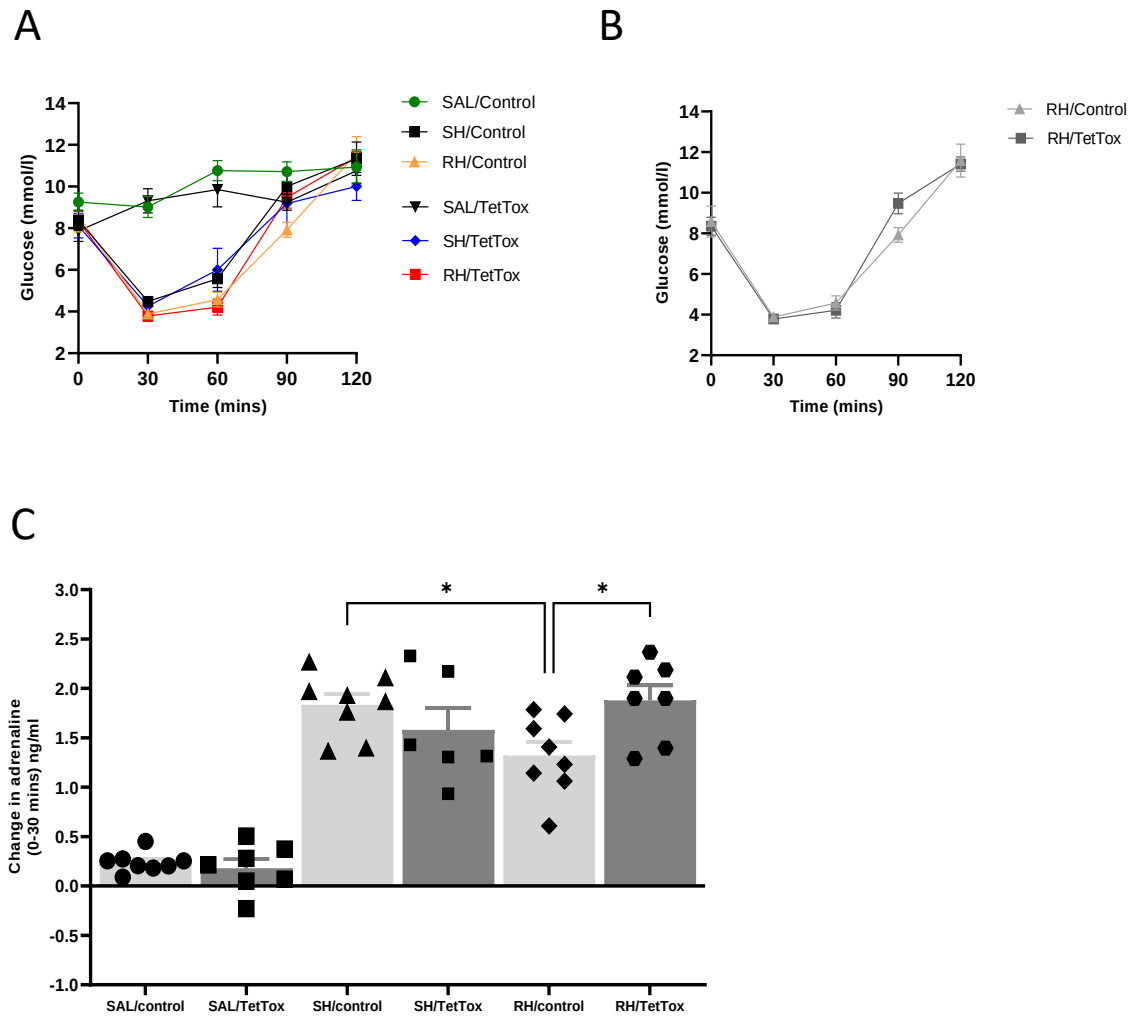

Figure 7.21: The importance of GABAergic vBNST neurons to the RH-induced habituation of the sympathoadrenal response

A: Mean blood glucose profile for the 120 min following injection, in control and TetTox groups.
B: Mean blood glucose profile for the 120 min following injection, in RH/control and RH/TetTox groups (repeated measures ANOVA with Sidak's *post hoc* test).
C: Change in adrenaline release (0-30 min) following injection, in control and TetTox groups. The adrenaline response was significantly attenuated in the RH/control group, when compared with SH/control group. Whereas this attenuation was blunted in the RH/TetTox group, which displayed significantly increased adrenaline levels, when compared with RH/control (*p<0.05, SH/control versus RH/control; *p<0.05, RH/TetTox versus RH/Control; one-way ANOVA with Sidak's *post hoc* test).
Data presented as mean ± SEM. n= 6-8 per group.

A

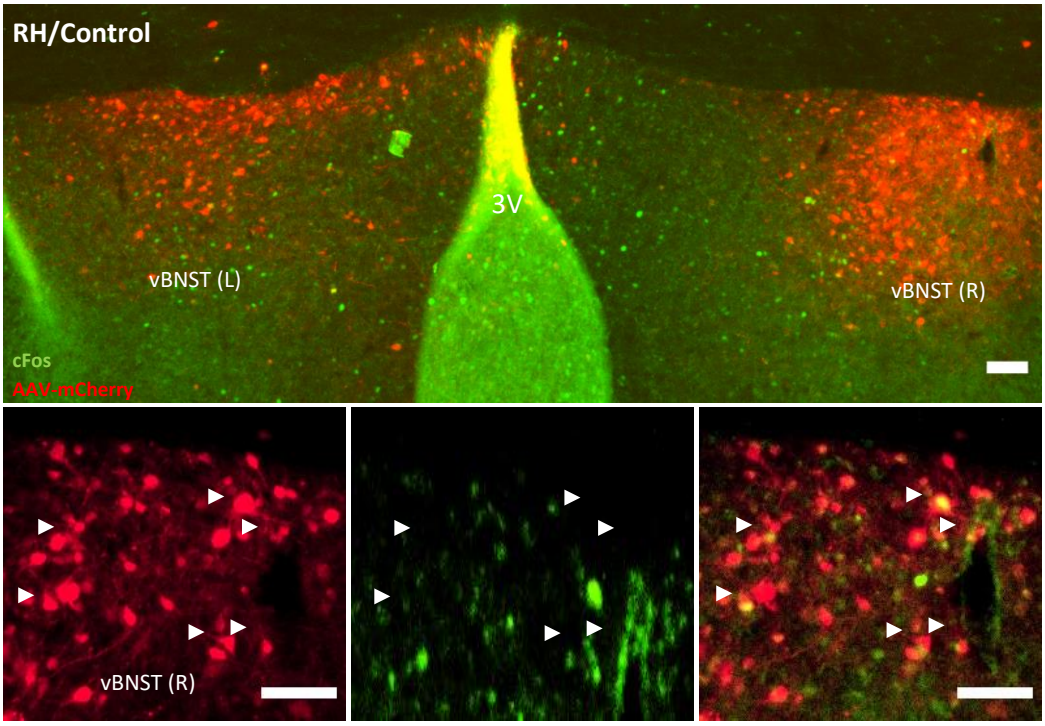
RH/Control
3V
vBNST (L)
vBNST (R)
cFos
AAV-mCherry
vBNST (R)

B

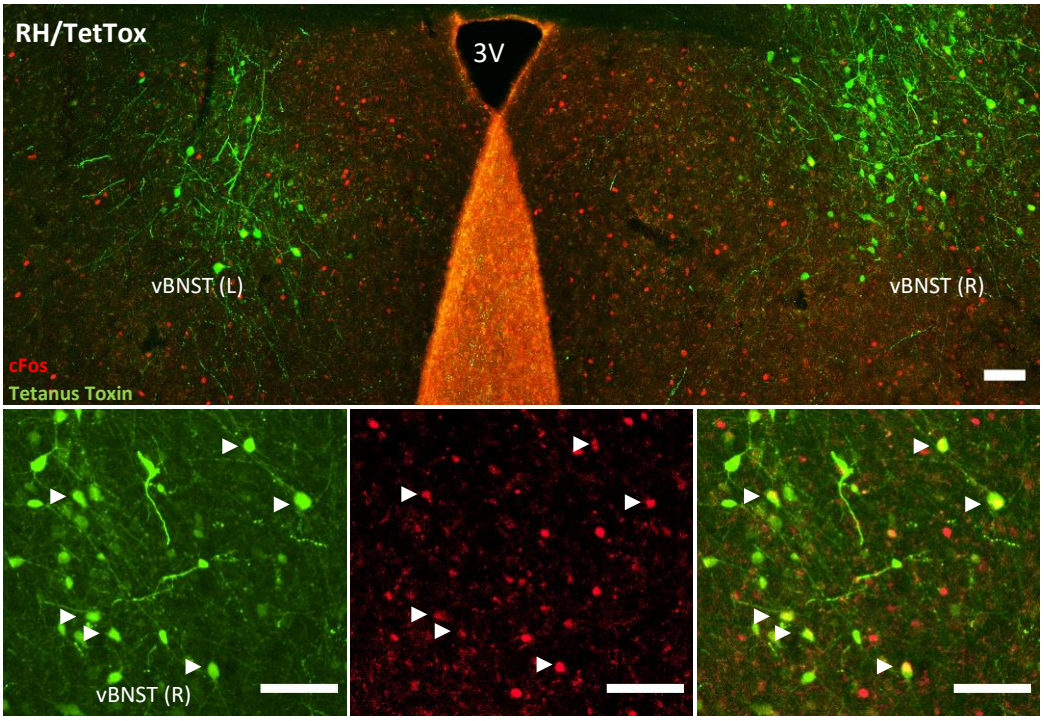
RH/TetTox
3V
vBNST (L)
vBNST (R)
cFos
Tetanus Toxin
vBNST (R)

C

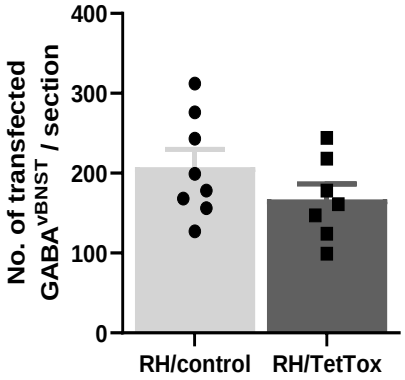

Figure 7.22: Validation of transfection of GABA^{vBNST} neurons following AAV-TetTox injection

A: Representative image of the vBNST in RH/control animal following bilateral injection with AAV-mCherry. Transfected Gad2 neurons were labelled with mCherry (red). Neuronal cFos (green) labelling identifies SH-activated neurons. Magnified images show mCherry, cFos and dual-labelled neurons in the vBNST. Main image scale bar represents 100 µm, magnified image scale bar 50 µm.
B: Representative image of the vBNST in RH/TetTox animal following bilateral injection with AAV-TetTox. Transfected Gad2 neurons were labelled with GFP (TetTox). Neuronal cFos (red) labelling identifies SH-activated GABA neurons, which are marked with white arrows. Magnified images show TetTox, cFos and dual-labelled neurons in the vBNST. Main image scale bar represents 100 µm, magnified image scale bar 50 µm.
C: Number of transfected Gad2 neurons in the vBNST (bilaterally) in the RH/control and RH/TetTox groups. n = 7-8 per group. n = 3 sections per animal.

7.4 Discussion

The PVT was highlighted in Chapter 3 as a region which displays high levels of cFos expression following SH and interestingly, persistently elevated cFos levels following RH. Also, FosB was found to be increased in the PVT following RH, signifying neuronal adaptation. In Chapter 3, I also identified that hypoglycaemia-activated PVT neurons were glutamatergic, corroborating the literature (Labouebe et al., 2016). This established that the PVT participates in the glucose-regulatory network, and we postulated that it may play an important role in network adaptations which follow RH.

The PVT is an interesting structure which integrates stress signals relating to both the internal and external environment, and its connections enable it to influence both motivational behaviour and homeostatic balance (Kirouac, 2015). Work from our own lab confirmed that this structure receives diverse inputs, including from GI neurons of the VMH (Khodai et al., 2019). A greater appreciation of how the PVT connects with other hypoglycaemia-activated brain regions may provide new insights into its function within the glucose-regulatory network. To this end, in the first section of this Chapter, I performed a neuronal tracing study to identify afferent projections to the PVT from hypoglycaemia-activated brain regions. This was also performed to understand differences in afferent projections to the aPVT and pPVT, respectively. Recently, differences in projection patterns, cell types and functions have between reported for different PVT sub-regions (Kirouac, 2015, Hsu et al., 2014, Gao et al., 2020). In this Chapter, by using retrograde tracing, I showed that both anterior and posterior sub-regions of the PVT receive inputs from multiple hypoglycaemia-activated brain regions. For both PVT sub-regions, there was significant overlap in the afferent projections, however, the density of projections varied. Both PVT sub-regions, received extensive inputs from medial prefrontal cortical regions (mPFC) including from the infralimbic cortex (IL), which also contained hypoglycaemia-activated neurons. Interestingly, the relative number of FG-labelled cells in the IL was greater following injection into the pPVT. Similar observations have been reported in the literature for rats (Kirouac, 2015, Li and Kirouac, 2012). Activity within the mPFC can modulate the expression of habituation of the HPA-axis response to repeated restraint, though this region is not necessary for the development of habituation (Weinberg et al., 2010).

FG labelling in hypoglycaemia-activated regions in the hypothalamus was similar following injections into the aPVT and pPVT, respectively. This was found to concentrate in the PVH and VMH, with more scattered labelling in other hypothalamic regions. This differs from reports in rats, which highlight the DMH as the primary hypothalamic input to the PVT (Li and Kirouac, 2012).

The FG labelling in hypoglycaemia-activated hindbrain structures included the PBN, PAG and rVLM. Low/moderate neuronal labelling with FG was present and was similar for the two PVT sub-regions. The PBN and PAG, which are both involved in the glucose-regulatory network, are known to integrate viscero-sensory inputs from the hindbrain, relaying this information to the forebrain via the PVT (Li and Kirouac, 2012, Krout et al., 2002). Interestingly, hindbrain catecholaminergic neurons, including in the rVLM, also project directly to the PVT (Sofia Beas et al., 2020). Inhibition of this connection was shown to preferentially impair glucoprivation-induced feeding responses, whilst preserving neuroendocrine responses (Sofia Beas et al., 2020).

As the current study centred on identifying afferent projections from hypoglycaemia-activated regions to the PVT, regions with low levels of cFos expression were not quantified. A notable example is the ventral subiculum (vSub), which is a component of the limbic network. The vSub is thought to regulate the HPA-axis, via inhibitory relays in the aBNST and to participate in stress memory retrieval through connections with the mammillary body (Herman and Mueller, 2006, Ledergerber and Moser, 2017). Notably, in rats, the vSub projects preferentially to the aPVT. It is possible that these projections enable the PVT to differentiate novel from familiar stressors.

It is also important to note that the tracing studies in this Chapter did not include a saline control group. Therefore, the specificity of cFos expression to hypoglycaemia, cannot be confirmed. That said, results in Chapter 3 show that saline injection leads to a very low level of cFos expression in most brain regions. Indeed, only the rVLM (which is known to be hypoglycaemia-activated) showed a low number of FG-labelled neurons (<50 neurons) following retrograde tracer injection into PVT sub-regions.

Though I have outlined potential differences in afferent projections to PVT sub-regions, this does not rule out intra-PVT integration of inputs. Of note is that efferent projections have been found to travel from the aPVT to the pPVT, but not in reverse (Vertes and Hoover, 2008). This suggests that information entering the PVT ultimately converges on the pPVT, where the final integrative functions are performed (Vertes and Hoover, 2008). This is corroborated by a large literature which supports greater responsiveness of the pPVT to a variety of stressors, when compared with the aPVT (Barson et al., 2020, Timofeeva and Richard, 2001, Gao et al., 2020). Our own observations with cFos expression in the PVT, suggest a greater relationship between the pPVT and repeated, rather than acute stress. This is consistent with studies in rats, which have confirmed the importance of the pPVT in the control of habituation of the HPA-axis response to repeated restraint stress (Bhatnagar et al., 2002).

The neuronal circuitry which underlies the pPVT control over HPA-axis function is not clear and may involve direct connections with CRH^{mpdPVH} neurons. In Chapter 6, I outlined the functional importance of CRH^{mpdPVH} neurons in the sympathoadrenal response following hypoglycaemia. Therefore, communication between the pPVT and mpdPVH neurons may also regulate sympathoadrenal activation. A retrograde tracing study to investigate direct connections between hypoglycaemia-activated pPVT and mPVH neurons was performed. This revealed that around 40% of SH-activated PVH→pPVT neurons were phenotypically CRH neurons. Also, around 35% of SH-activated pPVT neurons projected to the mPVH. These data are consistent with a small number of studies which report reciprocal connections between pPVT and CRH^{mpdPVH} neurons (Hsu et al., 2014, Yuan et al., 2019). In macaque monkeys, the PVT was confirmed to have a moderate density of CRH neuron fibres, whilst retrograde tracer injection into the PVT labelled PVH neurons (Hsu et al., 2014). In addition, the monosynaptic tracing of efferent projections to CRH^{PVH} neurons identified glutamatergic PVT neurons. As SH-activated pPVT and CRH^{mpdPVH} neurons are both glutamatergic neuronal populations, one explanation for this reciprocal connection is to enable feedback excitation of CRH^{mpdPVH} neurons. Feedback excitation is a process which enables a brief stimulus to trigger more prolonged neuronal activity (Li et al., 2006). This mechanism has been shown to be particularly important in memory formation and in maintaining motor responses following a threatening stimulus (Goldman-Rakic, 1995, Collins et al., 2002). Studies examining feedback excitation in stress-responsive networks are required to support this theory.

The functional importance of $GLUT^{pPVT}$ neurons to the sympathoadrenal response following SH was examined using an ablation strategy. This experiment confirmed that that $GLUT^{pPVT}$ neurons are not required for the normal sympathoadrenal response following SH. This finding was not unexpected as the glucose-regulatory network is complex and multiple parallel pathways exist which influence the sympathoadrenal response following hypoglycaemia (Verberne et al., 2014). Though these experiments did not directly examine the $GLUT^{pPVT}$→ CRH^{mpdPVH} projection, it is likely that this pathway is not functionally important to glucose and sympathoadrenal responses to SH. The pPVT has consistently been implicated in the regulation of responses to repeated and chronic stressors (Grissom and Bhatnagar, 2009, Bhatnagar et al., 2002, Bhatnagar and Dallman, 1998). Therefore, we postulated that the predominant function of $GLUT^{pPVT}$ neurons would be in the control of sympathoadrenal responses following RH and not SH. Consistent with our hypothesis, the ablation of $GLUT^{pPVT}$ neurons blocked the habituation of the sympathoadrenal response due to RH. This suggests that $GLUT^{pPVT}$ neurons, through an indirect circuit contribute to the habituation of the sympathoadrenal response following RH.

Though this experiment did not identify the circuitry which enables $GLUT^{pPVT}$ to inhibit sympathoadrenal activation following RH, our data supported an indirect connection with CRH^{mpdPVH} neurons. Moreover, if both HPA-axis and sympathoadrenal responses can be controlled by $GLUT^{pPVT}$ neurons, it is likely that CRH^{mpdPVH} neurons are involved. We hypothesised that following RH, an intermediary inhibitory neuronal population enables $GLUT^{pPVT}$ neurons to modulate CRH^{mpdPVH} neurons, leading to habituation of the sympathoadrenal response. The major excitatory outputs of the PVT are towards the extended amygdala (which includes the CeA and aBNST) and the nucleus accumbens (NAc) (Li and Kirouac, 2008). The projections to the NAc have been implicated previously with sugar seeking in response to hypoglycaemia (Labouebe et al., 2016). Both the CeA and NAc contain GABAergic neuronal populations which have been shown not to project extensively to CRH neurons in the PVH (Yuan et al., 2019). PVT projections to the aBNST are involved in processing states of negative valence (e.g. fear, anxiety) and these, in turn, do send a major GABAergic inhibitory input to the PVH (Radley and Sawchenko, 2015). Within the aBNST, the vBNST has been shown to differentially regulate HPA-axis responses to acute and chronic stress (Choi et al., 2008). Specifically, lesions of the vBNST elevated plasma ACTH and corticosterone responses to novel restraint in the rats previously exposed to chronic variable stress (CVS), but not in stress naive animals (Choi et al., 2008). Consequently, I performed further neuronal tracing studies to identify the most likely GABAergic intermediary relay. Though SH-activated $GLUT^{pPVT}$ neurons were found to project to the NAc, vBNST and CEA, only SH-activated $GABA^{vBNST}$ neurons were found to project to the mPVH. In rats, $GABA^{vBNST}$ neurons have been shown to maintain high levels of activation and increases in glutamate decarboxylase (GAD) expression following repeated restraint stress (Radley and Sawchenko, 2015). This elevated $GABA^{vBNST}$ neuronal activity corresponded with a habituated HPA-axis response, delineating an inhibitory circuit which controls CRH^{PVH} neuron activity (Radley and Sawchenko, 2015). Therefore, we elected to investigate the importance of $GABA^{vBNST}$ neurons to the RH-induced habituation of the sympathoadrenal response. The synaptic silencing of $GABA^{vBNST}$ neurons with tetanus toxin prevented the habituation of the sympathoadrenal response following RH. Somewhat unexpectedly, the silencing of $GABA^{vBNST}$ neurons in this experiment led to a lower (though not statistically different) sympathoadrenal response following SH, relative to controls. This was not related to differences in the number of silenced $GABA^{vBNST}$ neurons in the SH/TetTox and SH/control groups. A possible explanation is the presence of compensatory pathways which increase inhibitory tone onto PVH, when $GABA^{vBNST}$ neurons are inactivated. Indeed, a substantial proportion of PVH tonic inhibition is performed by local peri-PVH GABAergic neurons (Herman et al., 2002).

Collectively, these data indicated that increased activity in a regulatory $GLUT^{pPVT} \rightarrow GABA^{vBNST} \rightarrow CRH^{mpdPVH}$ forebrain pathway may result in the RH-induced habituation of the sympathoadrenal response and may underlie IAH. As the inhibition of either $GLUT^{pPVT}$ or $GABA^{vBNST}$ neurons prevented the reduction in adrenaline secretion normally associated with RH, we can be confident that this arm of the circuit is functionally significant. However, we have not directly evidenced that this inhibitory pathway is specific to CRH^{mpdPVH} neurons. This might be achieved through the projection-specific lesioning of $GABA^{vBNST} \rightarrow$ PVH neurons, which would require an intersectional approach. It is reassuring that the literature confirms that the major output from the vBNST is to the mpdPVH, suggesting that CRH^{mpdPVH} are the likely target (Herman et al., 2002, Gungor and Paré, 2016).

In this Chapter, an anatomical lesioning approach was used to selectively ablate $GLUT^{pPVT}$ neurons and to silence $GABA^{vBNST}$. This approach was taken to demonstrate that these neuronal populations are necessary for the development of RH-induced sympathoadrenal habituation. In future experiments, it would be interesting to identify whether driving the $GLUT^{pPVT} \rightarrow GABA^{vBNST}$ circuit, using chemogenetic or optogenetic techniques, leads to impaired sympathoadrenal activation, simulating response habituation.

Although we were able to selectively lesion $GLUT^{pPVT}$ neurons, we were not able to perform any further phenotyping to identify the sub-population which controls RH-induced habituation. It is likely that a genetically distinct $GLUT^{pPVT} \rightarrow GABA^{vBNST}$ population is responsible for the findings. Recently, investigators have proposed that the PVT is composed of two well-defined neuronal subtypes, termed type I and type II neurons, based on different gene expression, anatomy and function. Interestingly, type I neurons were found to restrict to the pPVT and signal aversive states, whereas type II neurons resided in the aPVT and were modulated by arousal (Gao et al., 2020). Type I neurons were genetically defined by their expression of the dopamine receptor D2 gene (*Drd2)*. We can postulate that type I pPVT neurons may be involved in the control of RH-induced habituation (Gao et al., 2020). Further understanding of the genetic identity and receptor expression of these $GLUT^{pPVT}$ neurons may assist in resolving this important neuronal circuit.

These data indicate a top-down neuronal control of RH-induced habituation which centres on $GLUT^{pPVT}$ neurons. Moreover, our data support that a neuronal circuit, involving fast neurotransmitter release is responsible for this phenomenon. Other mechanisms have not been investigated, including neuropeptide release, hormone signalling and structural alterations. These complementary mechanisms will be discussed further in Chapter 8.

7.5 Summary

- The aPVT and pPVT receive differential projection patterns from hypoglycaemia-activated brain regions.
- The pPVT receives inputs from neurons involved in the hypoglycaemia sympathoadrenal response, including CRH^{mpdPVH}.
- $GLUT^{pPVT}$ neurons are themselves activated after SH and project to the PVH.
- Lesioning $GLUT^{pPVT}$ neurons does not affect the sympathoadrenal response to acute hypoglycaemia.
- However, lesioning $GLUT^{pPVT}$ neurons prevents RH-induced habituation of the sympathoadrenal response.
- An intermediary $GABA^{vBNST}$ relay receives inputs from $GLUT^{pPVT}$ neurons and projects to the PVH.
- The synaptic inhibition of $GABA^{vBNST}$ neurons attenuates the RH-induced habituation of the sympathoadrenal response.

7.6 Conclusion

In this Chapter, I outlined a neuronal circuit which is necessary for the RH-induced habituation of the sympathoadrenal response. By combining neuronal tracing studies along with manipulating key nodes within this circuit, we have been able to identify a functionally important regulatory $GLUT^{pPVT} \rightarrow GABA^{vBNST} \rightarrow CRH^{mpdPVH}$ forebrain pathway. Interestingly, this circuit is not necessary for the normal sympathoadrenal response following an acute stress, SH. Rather, following RH, increased activity within this circuit, leads to response habituation and may contribute to the development of IAH. Our data suggests that $GLUT^{pPVT}$ neurons are critical to the expression of habituation. We can postulate that different sub-populations of $GLUT^{pPVT}$ neurons, through direct excitatory and indirect inhibitory connections with CRH^{mpdPVH} neurons, can provide a suppressive or stimulatory influence on the sympathoadrenal response. The preferential activation of excitatory or inhibitory pPVT circuits, may be dependent on stress familiarity, which requires the participation of limbic and cortical networks.

These findings provide further support to our hypothesis that activity in select integrative neuronal networks leads to habituation. It is possible that therapies which lead to dishabituation, also engage this circuit.

Chapter 8

General Discussion

8.1 Overview of Thesis

A mechanistic understanding of IAH is missing, though there is growing evidence that habituation within the central glucose-regulatory network may explain the disease (McNeilly and McCrimmon, 2018). This was investigated in my thesis by first characterising a mouse model of IAH which used experimental RH. This mouse model was shown to recapitulate key hallmarks of IAH, namely the impaired sympathoadrenal response and delayed recovery of blood-glucose levels following antecedent RH (Chapters 3 and 4). Subsequently, the characterisation and investigation of a hypoglycaemia-responsive brain network was performed using this model.

A major part of this thesis has involved the use of neuronal markers to identify activation following SH and adaptations following RH. This approach highlighted that, whilst many brain structures contain hypoglycaemia-activated neurons, their response patterns following RH differ. This confirmed that neuronal adaptations following RH, which may indicate habitation, are likely to occur in specific neuronal networks (Chapter 3).

Within the central glucose-regulatory network, CRH^{mpdPVH} neurons were highlighted as a critical neuronal population. My data provides evidence for habituation of CRH^{mpdPVH} neuronal activity with the repeated homotypic stress of RH, but not with heterotypic stress (Chapter 5). In unpublished work, our laboratory has shown that CRH neurons are not intrinsically sensitive to physiological changes in glucose, but that they do receive direct excitatory input from GI neurons in the VMH (Luckman, unpublished). This, together with the findings in my thesis, that CRH neurons are required for the hypoglycaemia-induced sympathoadrenal response and connect with sympathetic output systems from the brain (Chapter 6), demonstrates that they are a critical part pf the overall glucose-regulatory network. Finally, I investigated the role of the pPVT in the control of the RH-induced habituation of the sympathoadrenal response. Here, I propose a forebrain circuit which enables the pPVT to and modulate response habituation, dependent on stress familiarity (Chapter 7).

Through applying a sensory-motor integration framework to understand RH-induced habituation, I provide evidence that the expression of habituation is controlled through specific integrative neuronal networks. My data provide new insights into mechanisms which may underlie IAH. The following general discussion combines these results with theories regarding the neuronal mechanisms underlying IAH, evidence supporting habituation within integrative neuronal networks, and the potential for therapeutic applications.

8.2 Modelling IAH in animals

Establishing a robust animal model for IAH was the first aim of this doctoral thesis and was achieved using experimental RH in mice. This subsequently enabled the use of transgenic tools to interrogate neuronal circuitry. The merits of different parameters and protocols used in modelling IAH with experimental RH have been discussed in Chapter 3 and in a separate review (Sankar et al., 2020). In classical experiments by Heller and Cryer, impairment of the sympathoadrenal response following RH in rats was measured alongside other hormone and symptom levels (Heller and Cryer, 1991). In our animal model of IAH, the sympathoadrenal response, detected by measuring adrenaline release was our only direct measure of the CRR. The literature supports the importance of this arm of the CRR, not only in terms of glucose raising effects, but also in producing autonomic symptoms, which lead to hypoglycaemia awareness (Cryer, 2013, McCrimmon, 2017). It is likely that the sympathoneural component of the sympathoadrenal response, is most important for autonomic symptoms (DeRosa and Cryer, 2004). The sympathoneural response can be measured by sampling noadrenaline spill over from synaptic release into the circulation (Esler, 2011). Though there is evidence to suggest that very low blood glucose levels (<2 mmol/l) are required before increases in pancreatic noradrenaline are detected (Taborsky and Mundinger, 2012). Therefore, sympathetic activation, sufficient to produce biological effects, may be more reliably measured through sampling plasma adrenaline levels.

The most specific and clinically relevant measure of IAH in humans is hypoglycaemia symptoms. This has proven difficult to measure in animals. Even relatively simple behavioural CRR measurements, such as changes in food intake following RH or repeated 2-DG, have failed to produce consistent results (Sanders et al., 2006). Only one group have identified a possible surrogate measure of IAH, by a conditioned place preference (CPP) paradigm. Here, a reward-induced CPP was blunted with the aversive salience of SH. However, with prior RH, the negative valency of subsequent hypoglycaemia was lost and the CPP was preserved (Otlivanchik et al., 2016). This is an interesting paradigm and in parallel with sympathoadrenal measurements, could provide a more complete animal model of IAH in future work.

Hypoglycaemia is known to alter behaviours in rodents, but this often requires specialised tests to enable detection. Rats exposed to RH display increased anxiety-like behaviours using an elevated plus-maze performance (McNay, 2015). In mice, hypoglycaemia <2.8 mmol/l induces depression-like behaviours, which last beyond the period of hypoglycaemia. This was evidenced by increased immobility in a forced-swim test (FST) and reduced saccharin preference (Park et al., 2012). Interestingly, these behaviours arise due to autonomic activation and are likely to correlated with

measurements of sympathoadrenal activation. As our knowledge of animal behaviours improves, hypoglycaemia-specific behaviours may be identified, without the need for additional tests.

Taken together, we have sought to understand the evolution of sympathoadrenal impairment, which we believe is central to the pathophysiology of IAH. Whilst our animal model can be further optimised, it has proven effective in recapitulating this hallmark of IAH.

8.3 RH leads to habituation within a central glucose-regulatory network

Hypoglycaemia activates a central glucose-regulatory network, which can be understood by its separation into sensory, integrative, pre-motor and motor elements (Watts and Donovan, 2010). In Chapter 3, through quantification of neuronal cFos, I confirmed that SH leads to the acute activation of neuronal networks in multiple brain regions. However, following RH, the expression of FosB, a neuronal marker of adaptation, was significantly increased in a smaller number of integrative and pre-motor neuronal areas. Interestingly, in my investigations the aBNST, CeA, PVT, PVH and LC were found to express significantly higher levels FosB following RH.

It has been suggested that RH leads to a form of 'pre-conditioning,' preventing neuronal death to subsequent hypoglycaemia (Puente et al., 2010, McCrimmon, 2017). Cellular adaptations following RH, which have been described in this thesis as habituation, may conserve resources and enhance survival. However, in patients with insulin-treated diabetes and fundamentally altered physiology, these adaptations are detrimental, culminating in IAH. We believe that FosB, which can regulate neuronal and synaptic function, may be mechanistically involved in neuroplastic changes following RH. FosB and its splice variant ΔFosB accumulate in specific brain regions following other repeated physiological and psychological stress (Ohnishi et al., 2011, Corbett et al., 2017, Grueter et al., 2013, Knight et al., 2011). Increased expression of FosB in the NAc has been associated with enhanced stress tolerance and resilience (Vialou et al., 2010). Furthermore, the treatment of abnormal behaviours following chronic stress, requires the induction of ΔFosB in specific brain regions for treatment success (Vialou et al., 2010). Conversely, in other brain regions, such as the mPFC, increased ΔFosB results in enhanced psychological stress susceptibility (Vialou et al., 2014). FosB and ΔFosB ultimately exert their effects through the enhancement or repression of gene transcription. Within the NAc, ΔFosB accumulation leads to increased AMPA glutamate receptor subunit (GluR2) expression, but a suppression of dynorphin (Zachariou et al.,

2006). Whilst in the mPFC, ΔFosB leads to increased induction of the cholecystokinin-B receptor (Vialou et al., 2014).

FosB/ΔFosB expression is concentrated in specific brain structures following repeated stress and, notably, includes the PVH (Kovács et al., 2019). In keeping with our own data, CRH^{PVH} neurons have been consistently identified to express high levels of FosB/ΔFosB following a variety of repeated and chronic stress types (Kovács et al., 2019, Knight et al., 2011). Interestingly, CRH neurons in the CeA and aBNST do not show this pattern (Kovács et al., 2019). CRH^{PVH} neurons orchestrate complex neuroendocrine and behavioural responses to stress, contingent on stress familiarity (Kim et al., 2019b). It can be theorised that FosB/ΔFosB expression is required for stress adaptation in CRH^{PVH} neurons, including following RH. In rats exposed to RH, CRH^{PVH} neurons show the expected increases in FosB and in parallel, a significant decrease in the presynaptic marker synaptophysin (Al-Noori et al., 2008b). Though it is not known whether FosB represses synaptophysin, this study identified the presence of synaptic adaptations following RH, which my lead to habituation.

It remains unclear whether levels of FosB/ΔFosB expression correspond with cellular adaptations which confer an advantage or lead to pathology. This seems dependent on the neuronal population and the stimulus in question. Though I have focused on the Fos family of transcriptional factors and regulatory genes, diverse cellular mechanisms are initiated following RH (Beall et al., 2012). My data, confirm that FosB expression is restricted to specific hypoglycaemia-activated loci. I also postulate that its expression within a functional hypoglycaemia-activated neuronal circuit could identify critical nodes where habituation arises.

8.4 Habituation of the sympathoadrenal response underlies IAH

At a whole organism level, the response impairments which follow RH, have been compared convincingly with habituation (McNeilly and McCrimmon, 2018, McCrimmon, 2017). Consistent with this theory, my findings in Chapter 4 demonstrated classical features of habituation, when tested in our mouse model of IAH. These studies examined sympathoadrenal response impairment, which I have taken to be the key hallmark of IAH. First, I measured a reduced response to RH and repeated restraint, respectively. Second, I was able to recover the deficit by withdrawal of the habituating stimulus. Third, I dishabituated the sympathoadrenal response by applying a heterotypic stimulus. These studies are consistent with recent insights in rodents and humans (Farrell and McCrimmon, 2021, Vickneson et al., 2021, McNeilly et al., 2017).

Sympathoadrenal over activation can be deleterious to health, therefore, habituation may be a protective mechanism. For example, chronic or repeated sympathetic drive leads to a plethora of detrimental consequences, including cardiovascular disease, metabolic dysfunction and increased inflammation (Fisher and Paton, 2012). An alternative theory is that habituation allows conservation of energy resources by the brain. Though initiating the sympathoadrenal response is vital for glucose mobilisation and symptom awareness during hypoglycaemia, it is itself a metabolically costly activity. We can hypothesise that the energy costs for repeated activation of the sympathoadrenal response are weighed up against the survival benefit. Having survived prior hypoglycaemia, the set point and response magnitude is lowered, conserving energy, unless a more severe hypoglycaemic threat is encountered. We believe that this calculation is performed by specific neuronal networks and is dependent on stress familiarity, resulting in response habituation to conserve energy. This strategy carries significant risks and parallels can be drawn with observations in rodent models of repeated and chronic stress (Herman, 2013). For example, behavioural withdrawal and reduced locomotor activity following chronic stress may save immediate energy resources but, conversely, it limits identification of new food sources, more secure surroundings and mates (Herman et al., 2002). Why adaptations can sometimes become maladaptive is unclear, however, the presence of diabetes and insulin treatment are major drivers of this transition in IAH. We believe that in the non-diabetic patient, response habituation may have benefits through energy conservation and the prevention of tissue damage from excessive activation of the sympathoadrenal system. However, in the presence of diabetes, response habituation is maladaptive, culminating in IAH (Maggs and Sherwin, 1997, Cryer, 2013).

Another important observation from our work is that habituation of the sympathoadrenal response also occurred following repeated restraint, which is a very different type of stress to RH. The sympathoadrenal response is a vital and immediate survival response, which is initiated on exposure to a range of severe physiological and psychological stimuli (Maggs and Sherwin, 1997, Fukuhara et al., 1996, Goldstein, 2010). Therefore, different stress networks can interact by sharing common motor elements. This overlap between neuronal circuitry which mediate responses to different stressors is not restricted to motor networks. For example, CRH^{PVH} neurons, which perform integrative and pre-motor functions, are responsive to an array of physiological and psychological stimuli (Kim et al., 2019a, Kim et al., 2019b). The sharing of networks between homeostatic systems is likely to explain findings from cross-tolerance experiments in human. This includes, attenuated adrenaline release following a cold pressor tests and with moderate exercise, only in patients with prior hypoglycaemia (Galassetti et al., 2001, Kinsley et al., 1994).

These insights also suggest that where circuitry is shared, repeated applications of any stress can induce sympathoadrenal response habituation. Therefore, stress familiarity is the most important determinant of response habituation. It also suggests that identification of the locus of habituation may be achieved by studying networks which are common to different types of stress.

8.5 CRH^{mpdPVH} neurons are necessary for the hypoglycaemia CRR and habituation to RH

In this thesis, investigating the responsiveness and functional significance of CRH^{mpdPVH} neurons to the hypoglycaemia sympathoadrenal response has been an important objective. In addition, we hypothesised that CRH^{mpdPVH} neurons, which function as a vital stress integration and pre-motor axis, may be important in the development of habituation to RH. Our data from *ex vivo* and *in* vivo studies identify that CRH^{mpdPVH} neurons are rapidly activated following SH (Chapter 3 and Chapter 5). Furthermore, the majority of hypoglycaemia-activated mPVH neurons are in fact CRH^{mpdPVH} neurons. Our laboratory has used electrophysiological and circuit mapping techniques to confirm that CRH^{mpdPVH} neurons are not themselves intrinsically sensitive to hypoglycaemia, but they gather information from glucose-sensing elements, including from glucose-inhibited PACAP neurons in the VMH (Luckman, unpublished). It is likely that this is one of many redundant pathways which signal hypoglycaemic stress to CRH^{mpdPVH} neurons. Furthermore, using chemogenetic techniques, we have shown that CRH^{mpdPVH} are functionally important, not only to the HPA-axis but specifically to the sympathoadrenal response following hypoglycaemia (Chapter 6). We also have challenged the canonical view that CRH^{mpdPVH} neurons enact behavioural and neuroendocrine responses to hypoglycaemia, solely through activation of the HPA axis.

Sympathoadrenal activation by CRH^{PVH} neurons may be achieved through direct excitatory projections to hindbrain catecholaminergic neurons (Zhao et al., 2017). We have shown that there are direct connections between SH-activated CRH^{mpdPVH} neurons and hindbrain catecholaminergic neurons, which may facilitate rapid autonomic activation. CRH^{PVH} neurons are also known to send direct, excitatory projections to neighbouring hypothalamic nuclei, including the LH and ARC (Füzesi et al., 2016, Kuperman et al., 2016). Therefore, an indirect, excitatory circuit could also enable CRH^{PVH} neurons to control sympathoadrenal activity. Although we have not been able to identify if CRH^{mpdPVH} neurons send collaterals which signal the HPA and sympathoadrenal axes in parallel, our neuronal tracing studies suggest this coordinated stress response may be achieved through local, intra-PVH circuits. In this thesis, I demonstrated an intra-PVH circuit involving hypoglycaemia-activated CRHR1 neurons,

which send long-range glutamatergic projections from the mPVH to the rVLM. These findings, tie in with studies which recently identified a subpopulation of $CRHR1^{PVH}$ neurons, which are activated by intra-PVH CRH peptide release (Jiang et al., 2018, Jiang et al., 2019). Interestingly this population of $CRHR1^{PVH}$ neurons make local GABAergic synapses onto CRH neurons, and long-range glutamatergic synapses in the rVLM and NTS (Jiang et al., 2018, Jiang et al., 2019). CRH peptide release from the PVH also reaches neighbouring hypothalamic nuclei. Though this was not investigated, it is known that CRH peptide release facilitates activation of the sympathoadrenal response, by stimulating CRH receptors in neurons within the VMH and ARC (Kuperman et al., 2016, McCrimmon et al., 2006b). We believe that local and long-range glutamatergic projections, alongside CRH peptide release, enable CRH^{mpdPVH} neurons to achieve sympathoadrenal activation following acute hypoglycaemia.

CRH^{mpdPVH} neuronal activity is regulated by a multitude of central and peripheral signals, of which glucocorticoids have traditionally been thought of as most important (Aguilera and Liu, 2012). However, our *in vivo* fibre photometry results show rapid inhibition on food presentation following an overnight fast, and dynamics which correspond with the duration of the stimulus. These findings strongly indicate that HPA-axis-independent feedback mechanisms can rapidly modulate CRH^{mpdPVH} neurons. We believe this is likely to be via inhibitory neuronal circuits and fast neurotransmitter release. Such inhibitory circuits have been shown in other hypothalamic neuronal populations. For example, AgRP neurons in the ARC, which regulate energy homeostasis, are rapidly inhibited on sensory detection of food (Mandelblat-Cerf et al., 2015). Also, subfornical organ (SFO) Nos1 neurons, which regulate fluid homeostasis, are rapidly inhibited on water ingestion, even before water reaches the circulation (Zimmerman et al., 2016). As I will discuss, inhibitory circuits may also be important in controlling CRH^{mpdPVH} neuronal activity following repeated stress.

Following RH, CRH^{mpdPVH} neurons displayed reduced neuronal markers of acute activation and increased adaptive neuronal markers, consistent with habituation. This was supported by *in vivo* fibre photometry, which showed attenuated CRH^{mpdPVH} neuronal activity following RH, which recovered on withdrawal of the habituating stimulus. Of particular significance, CRH^{mpdPVH} neurons still responded after RH (without attenuation) to a heterotypic stimulus of acute restraint stress. Therefore, we hypothesise that following RH, the function of CRH neurons remains intact, but rather, inputs which signal hypoglycaemic stress undergo adaptation. One possible explanation is that RH leads to a stress-specific increase in inhibitory tone onto CRH^{mpdPVH} neurons. The PVH receives GABAergic inputs from multiple structures which can rapidly inhibit CRH neuron activity (Yuan et al., 2019). We believe that this inhibitory tone is dependent on stress

familiarity and may determine the strength of the stress response initiated by CRH^{mpdPVH} neurons. A neuronal circuit which may modulate CRH^{mpdPVH} neuronal activity following RH was identified in Chapter 7.

We have not examined the role of CRH peptide release *per se* on stress adaptation and possibly habituation. Interestingly, CRH peptide may mediate sustained effects following stress in several brain regions (Al-Noori et al., 2008b). For example, CRH signalling via CRHR1 in the hippocampus modulates dendritic length and branching (Chen et al., 2004, Swinny et al., 2004). Therefore, it is plausible that CRH peptide release, is a cellular mechanism which enables neuroplasticity within regions that encode stress memory. Another signalling pathway which may mediate stress adaptation is the endocannabinoid system. Endocannabinoid signalling is enhanced within the PVH by acute stress, it is attenuated by repeated homotypic stress, and it is reset by a novel or heterotypic stress (Bains et al., 2015).

Within the sensory-motor integration framework, these data suggest that CRH^{mpdPVH} neurons form integrative and pre-motor pathways, which enable stress integration, stress adaptation and effector functions (CRH peptide release and HPA-response initiation). Thus, CRH^{mpdPVH} have the capability to direct immediate and chronic stress responses, including following hypoglycaemia. We believe that CRH^{mpdPVH} neurons are, in fact, a final common pathway which directs HPA-axis and sympathoadrenal responses following stress. This ties in with recent studies which support cross-talk between neurosecretory and preautonomic PVH neurons that enable HPA axis activity to augment sympathetic drive following stress (Elsaafien et al., 2021, Jiang et al., 2019). Furthermore, we believe that through connections with the PVT and limbic structures, stress memory and familiarity modulate CRH^{mpdPVH} neuron activity, leading to response sensitisation with heterotypic stress and response habituation with homotypic stress.

8.6 A neuronal circuit involving the pPVT controls habituation

The identification of a neuronal circuit involving the pPVT, which controls habituation of the RH-induced sympathoadrenal response was a novel finding in this thesis. In Chapter 3, the pPVT, which contains integrative networks, was noted to maintain high levels of cFos, and to induce FosB following RH. We postulated that the pPVT and CRH^{mpdPVH} neurons would form a circuit which is necessary for stress habituation (Chapter 7). Since the PVT has been implicated previously in adaption to other repeated homotypic stressors, we manipulated glutamatergic cells in this structure (Bhatnagar et al., 2002). The ablation of adult $VGlut2^{pPVT}$ neurons had no effect on the sympathoadrenal response to SH, but it blocked the habituation observed after RH. Although we identified reciprocal glutamatergic connections between the mpdPVH and the pPVT, the precise role of this

interaction was not clear. We theorise that this direct connection enables feedback excitation, which maintains elevated CRH^{mpdPVH} activity acutely. We can hypothesise that this connection may also be important in the sensitised response to a heterotypic stressor.

We postulated that $GLUT^{pPVT}$ neurons drive an indirect inhibitory input onto CRH^{mpdPVH} neurons during RH. By disabling adult inhibitory GABAergic neurons in vBNST, one of the major output targets of the pPVT and inputs to CRH neurons, the RH-induced habituation of the sympathoadrenal response was again prevented. As functional inhibition of either $GLUT^{pPVT}$ or $GABA^{vBNST}$ neurons by genetic targeting prevented habituation, we assume that this circuit is driven by $GLUT^{pPVT}$ neurons. We believe stress familiarity enhances $GLUT^{pPVT}$ activity, which increases signalling through an inhibitory $GLUT^{pPVT} \rightarrow GABA^{vBNST} \rightarrow CRH^{mpdPVH}$ forebrain pathway, culminating in a habituated response. While this provides a coherent hypothesis, it is likely that other redundant pathways may play additional roles in stress habituation. That accepted, this pathway provides a validated component with which we can build on our understanding of a hypoglycaemia-responsive brain network.

$GABA^{vBNST}$ neurons have been identified as an important convergence site for stress-inhibitory influences originating from the limbic forebrain (Radley and Sawchenko, 2011, Radley and Sawchenko, 2015). The inputting structures include the PVT, lateral septum (LS), mPFC, amygdala and vSub. The vSub is of particular interest, as it is the main output node of the hippocampal formation and is important in memory retrieval (Ledergerber and Moser, 2017). In addition, through strong reciprocal connections with the PVT and BNST, the vSub can exert inhibitory control on the PVH (Kirouac, 2015). We postulate that the limbic forebrain, through connections with the PVT determines whether as stressor is novel or familiar.

Though we have outlined a neuronal circuit, operating by fast neurotransmitter release, which controls habituation of stress responses, other mechanisms likely exist. With regards to HPA-axis habituation, it has been suggested that glucocorticoid signalling is an important mechanism (Jaferi et al., 2003). Interestingly, the local blockade of glucocorticoid and mineralocorticoid receptors in the PVT prevented habituation without affecting responses to acute stress (Jaferi and Bhatnagar, 2006). Investigators have also reported structural alterations in stress integrative circuits, which include the retraction of basal dendrites in mPFC neurons following repeated restraint stress (Brown et al., 2005). Structural changes within neuronal circuits may explain the classical hallmark of habituation, whereby habituation becomes successively more rapid with each period of habituation training and spontaneous recovery.

We can postulate that within the mammalian brain, there are neuronal networks whose primary function is to monitor stimulus novelty versus familiarity and to limit a particular response if this has been previously experienced. We have described a cellular mechanism, based on a specific neuronal circuit, which can explain the reduction in the sympathoadrenal CRR following RH. The integrative brain networks, which include the pPVT, mPFC and vSub control habituation and possibly dishabituation, through connections with other integrative and pre-motor element. The proposed circuitry which controls habituation within the glucose-regulatory network is shown in **Figure 8.1**.

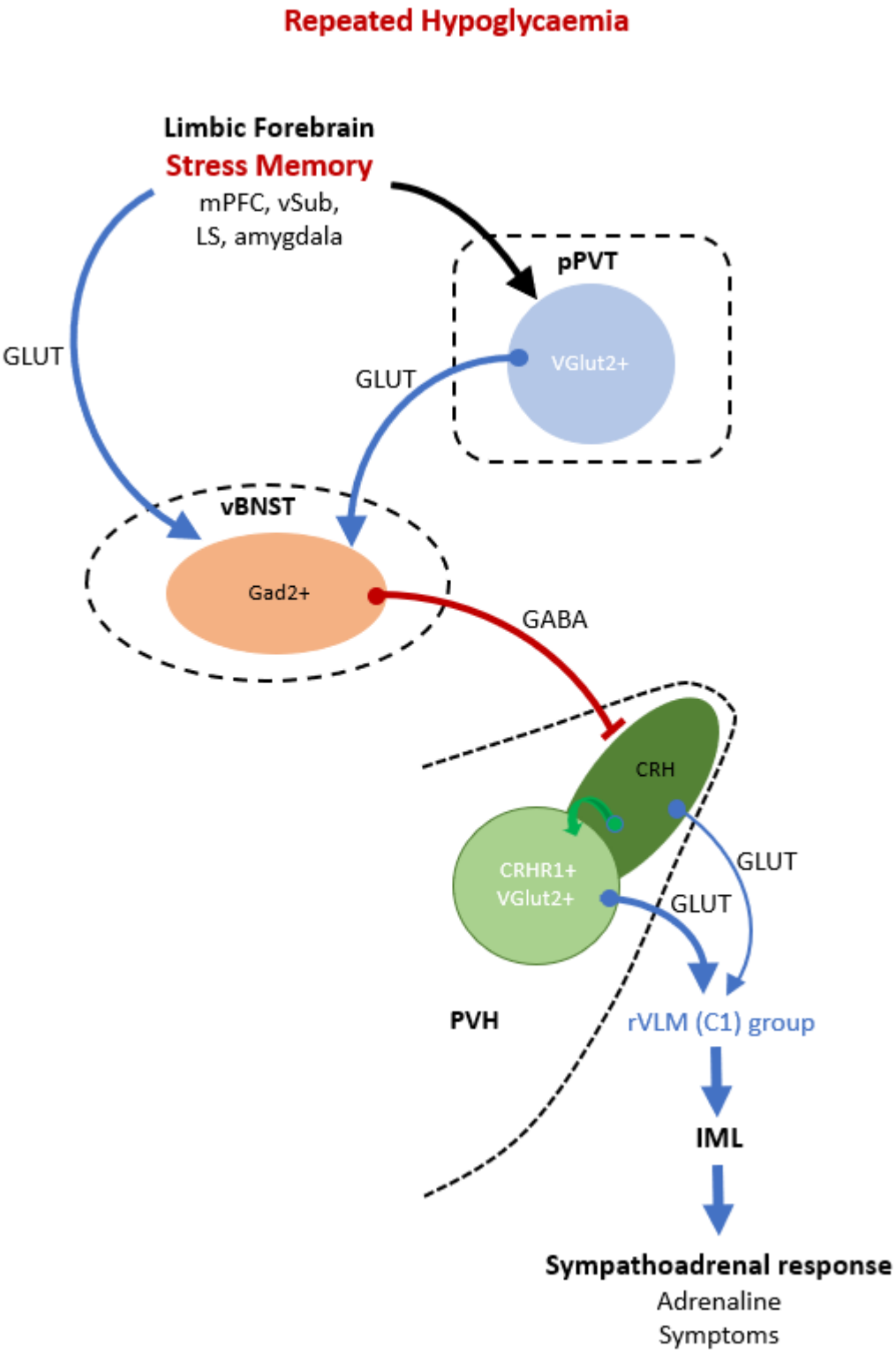

Figure 8.1: Proposed circuitry which controls habituation of the sympathoadrenal response following RH

We postulate that a circuit connecting the limbic forebrain, the pPVT, vBNST and PVH controls habituation of the sympathoadrenal response following repeated stress, such as RH. Stress memory is stored in the limbic forebrain and, together with the pPVT, a top-down inhibitory pathway is initiated. This involves increased activity in GABAergic vBNST neurons which inhibit CRH neurons in the PVH. Through direct and indirect pathways, decreased CRH neuronal activity translates to an attenuated sympathoadrenal response, leading to reduced symptoms and awareness.

mPFC: medial prefrontal cortex; **vSub**: ventral subiculum; **LS**: lateral septum.

8.7 Habituation within integrative neuronal networks underlies IAH

Adaptations within sensory, integrative/pre-motor or motor elements of the glucose-regulatory network separately have been proposed to explain sympathoadrenal response attenuation following RH. However, evidence from our own findings and recent literature support that habituation within integrative or pre-motor neuronal networks most convincingly explains IAH.

Habituation as the underlying mechanism for a decremental response, can be distinguished from sensory adaptation and motor fatigue by the process of dishabituation and stimulus specificity (the response still occurring to other heterotypic stimuli) (Rankin et al., 2009). In Chapter 4, dishabituation using a heterotypic stimulus led to response recovery when retested against the initial repeated stress. Heterotypic stress activates different sensory elements to the homotypic stress, but similar integrative, pre-motor and motor elements. Therefore, habituation must occur downstream of sensory networks and is separate from sensory adaptation. As dishabituation leads to a rapid recovery of the response, this also proves that motor elements and effector fatigue is not responsible. In Chapter 5, I demonstrated that CRH^{mpdPVH} neurons, which are not intrinsically glucose sensing, habituate to RH, but retain responsiveness to a heterotypic stimulus. Similarly, acute restraint leads to a potentiated response, relative to RH, showing motor elements remain intact to heterotypic but not homotypic stress. These arguments support our assertion that habituation arises in the integrative elements of the network. These insights are summarised in **Figure 8.2**.

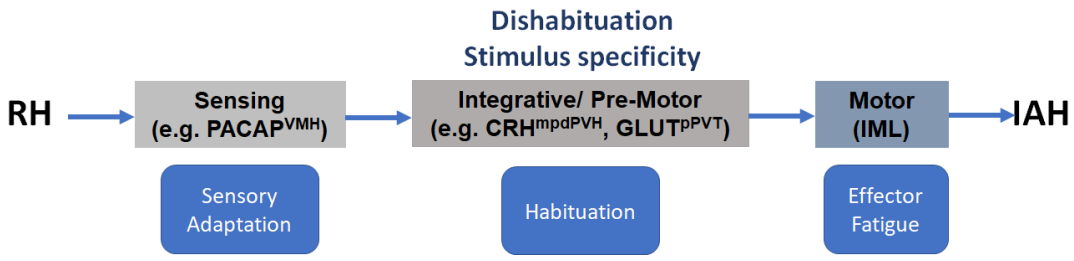

Figure 8.2: RH leads to habituation within integrative and pre-motor neuronal elements of the glucose-regulatory network

The glucose-regulatory network can be divided into sensing, integrative/pre-motor and motor elements. Examples of neuronal populations which are functionally important to each element of the glucose-regulatory system are shown. The presence of dishabituation and stimulus specificity in IAH, identifies that this is not due to sensory adaptation or effector fatigue. This localises adaptations to integrative or pre-motor networks.

IML: intermediolateral nucleus of the spinal cord.

It must be acknowledged that there is a large body of work which has investigated adaptations within glucose-sensing neurons following RH (Song and Routh, 2006, Kang et al., 2008, Osundiji et al., 2011). As autonomic symptoms improve following dishabituation it is possible that thresholds for glucose-sensing GI neuron activation also reset. However, this has not yet been shown using electrophysiological recording. If this is true, this suggests that a feedback mechanism, potentially arising in integrative networks, normalises glucose-sensing thresholds. We suppose that, in a complex system, no single mechanism necessarily accounts entirely for a specific type of adaptation (Rankin et al., 2009).

Several cellular adaptations which follow RH have been identified and may explain habituation (Chapter 1). Ultimately, these adaptations lead to synaptic alterations, which produce a habituated response (Bayne et al., 2020). The neuronal and synaptic mechanisms underlying habituation have been studied in simple animal models of habituation and most notably by Kandel in the sea snail, *Aplysia* (Pinsker et al., 1970). Stimulation of the siphon in *Aplysia* leads to a protective gill-withdrawal (sensory-motor) reflex, but this reflex can become habituated with repeated stimulation of the siphon. However, if a heterotypic stimulus (e.g., electric shock) to the tail is presented at the same time as stimulation of the siphon, there is a sensitised response and full gill withdrawal (Pinsker et al., 1970). The neuronal circuity for this response is fully resolved and is shown in **Figure 8.3**. Kandel found that with repeated stimulation of the siphon, sensory neurons retain sensitivity and continue to generate action potentials, but there is less presynaptic neurotransmitter release onto interneurons or motor neurons (Kandel et al., 2000). This is often termed as homosynaptic depression. It also has been shown that inhibition from separate pathways, can lead to reduced presynaptic neurotransmission. This process is known as heterosynaptic inhibition (Goldberg and Lukowiak, 1984). Importantly, there was no change in the sensitivity of postsynaptic receptors in Kandel's investigations (Pinsker et al., 1970).

On the other hand, sensitisation was found to be mediated by heterosynaptic facilitation, a process which increases the efficacy of synaptic transmission between the sensory neuron and follower neurons (interneuron or motor neuron), produced by excitation from facilitating interneurons. With sensitisation, an excitatory postsynaptic potential was generated in the motor neuron without increasing the response of the sensory neuron (Kandel et al., 2000). Habituation and sensitisation are characterised by neuroplasticity and the down regulation (habituation) or up regulation (sensitisation) of synaptic terminals at the sensory-interneuron and sensory-motor neuron synapse (Kandel et al., 2000). This is dependent on altered protein synthesis, which is controlled by multiple pathways, including cAMP-responsive element binding protein (CREB), protein kinase

C (PKC) and A (PKA) and interestingly, the activation of immediate-early genes, including cFos (Gandolfi et al., 2017, Kandel et al., 2000, Hawkins et al., 2006).

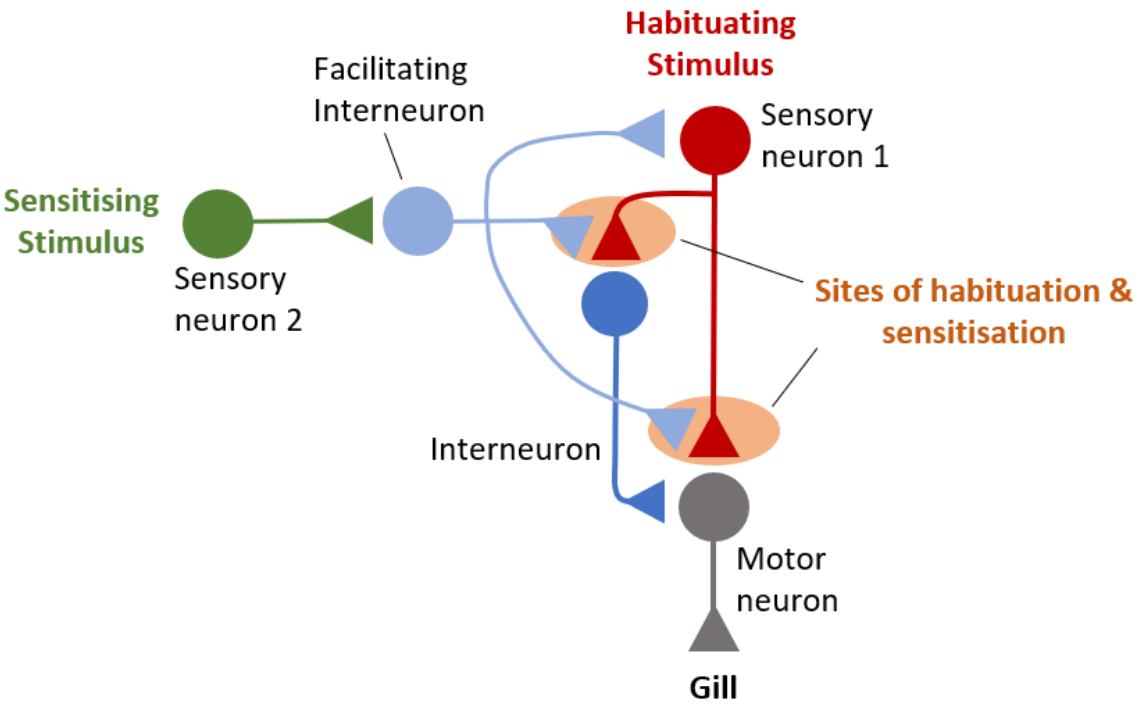

Figure 8.3: The circuitry underlying habituation and sensitisation in Kandel's *Aplysia* research

The sensory neuron 1 is activated by touching the siphon, whereas sensory neuron 2 is in the tail and is activated with alternative stimuli. Habituation was found to occur presynaptically at the sensory neuron 1-interneuron or sensory neuron 1-motor neuron synapse. Sensitisation was found to involve a separate pathway mediated by facilitating interneurons, which lead to presynaptic excitation (Kandel et al., 2000).

The comparator theory suggests that dishabituation is a disturbance in the habituation process, whilst the dual process theory predicts that dishabituation is a superimposed process of sensitisation (Steiner and Barry, 2014, Hawkins et al., 2006). In more recent work by Kandel in *Aplysia*, both reversal of habituation and superimposed sensitisation were detected (Hawkins et al., 2006). At a mechanistic level, dishabituation is also explained by heterosynaptic facilitation (Pinsker et al., 1970). It has been further postulated that dishabituation and sensitisation involve separate molecular mechanisms of facilitation, but lead to cellular and behavioural phenotypes that are indistinguishable (Gingrich and Byrne, 1985, Hawkins et al., 2006). In a model of IAH in rats, high-intensity exercise used as a dishabituating stimulus was associated with increased brain-derived neurotrophic factor (BDNF), which may aid in restoring normal glutamatergic hypothalamic neurotransmission (McNeilly et al., 2017, Farrell et al., 2020). It is unclear

whether different dishabituating stimuli harness separate cellular mechanisms or whether activation of a 'dishabituation network' enables response recovery.

By applying these mechanistic insights to our own data, we hypothesise that habituation following RH occurs between the sensing and integrative element interface. Within our hypothesised circuit, we believe that habituation results presynaptically to CRH^{mpdPVH} neurons. Following RH, CRH^{mpdPVH} neurons retain responsiveness to heterotypic (acute restraint) but not homotypic (hypoglycaemia) stress, this suggests that habituation occurs at synapses from glucose-sensing input neurons (e.g., $PACAP^{VMH}$). We hypothesise that an integrative forebrain pathway, driven by the pPVT, controls habituation at the glucose-sensing-CRH^{mpdPVH} neuron synapse through a process of heterosynaptic inhibition. Interestingly, lesions to the pPVT also block sensitisation of the HPA-axis response to novel stress, in chronically stressed animals (Bhatnagar and Dallman, 1998). We suggest that parallel pathways enable the pPVT to either inhibit (habituation) or excite (sensitisation) CRH^{mpdPVH} neurons, dependent on stress familiarity. These opposing effects may be possible through different pPVT neuronal subpopulations, which differ in anatomical location, projection patterns and functions (Gao et al., 2020).

Stress sensitisation also may be influenced by noradrenergic inputs from the LC and NTS, which project to the limbic forebrain, mpdPVH and VMH (Cunningham and Sawchenko, 1988, Herman, 2013). In addition, following chronic cold exposure, the responsiveness of the PVH can be increased with noradrenaline (NA), leading to HPA-axis sensitisation (Pardon et al., 2003). In our own investigations, RH led to increased FosB induction in the LC, suggesting adaptation. Noradrenergic inputs also surround the VMH where they are thought to modulate the hypoglycaemia CRR. NA levels increase in the VMH following systemic hypoglycaemia, but this increase is abolished if the VMH is perfused with glucose (Beverly et al., 2001, de Vries et al., 2005). Interestingly, NA, acting via β_2-adrenergic receptor activation, can stimulate glutamatergic neurotransmission in VMH neurons in the rat (Lee et al., 2007). The interplay between the noradrenergic system, glucose sensing and integrative elements remains unclear. However, this may provide an alternative pathway by which integrative networks can regulate sensing elements.

As dishabituation and sensitisation are both though to arise from heterosynaptic facilitation, we can postulate that circuits controlled by the pPVT or LC may also direct dishabituation. A hypothesised neuronal circuit to explain habituation and dishabituation in the glucose-regulatory network is shown in **Figure 8.4** and **Figure 8.5**.

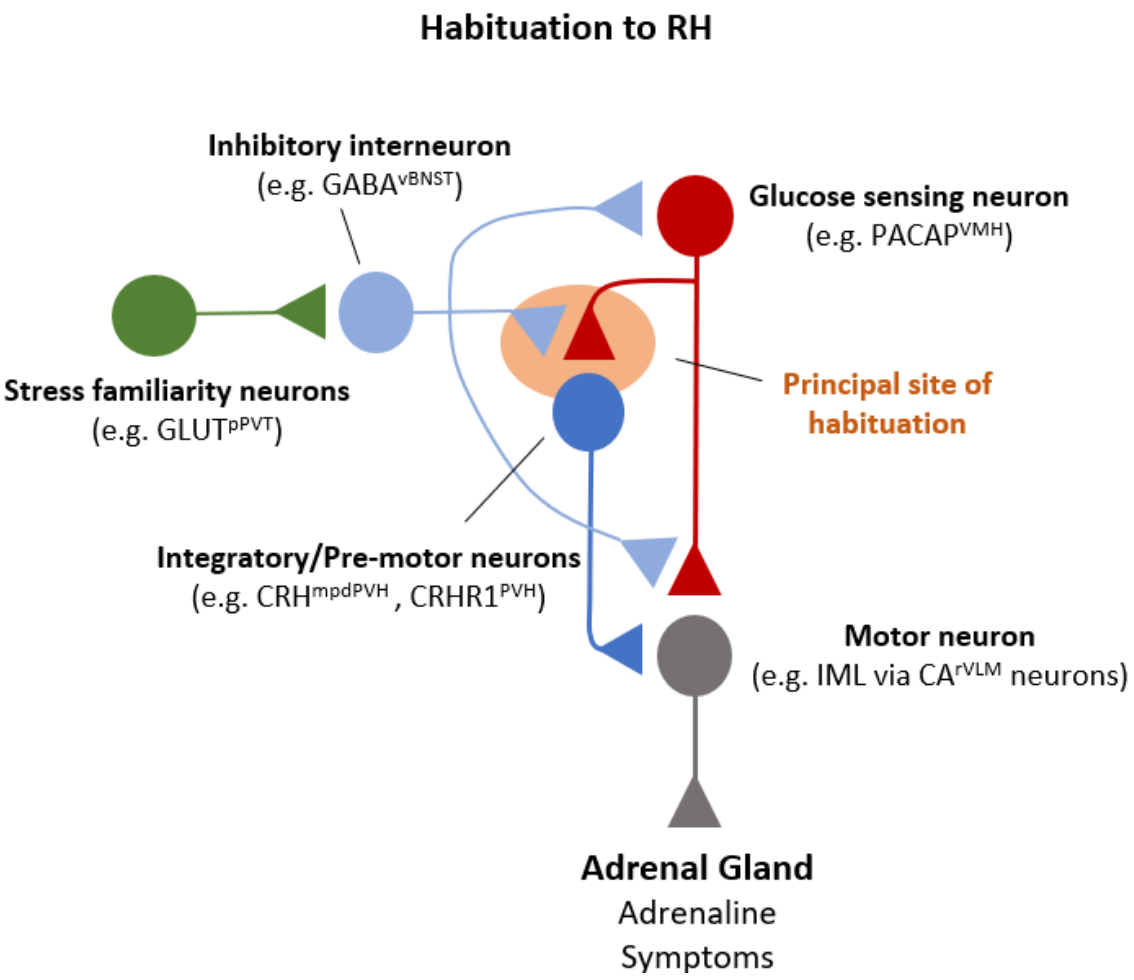

Figure 8.4: A proposed neuronal circuit model for habituation in the central glucose-regulatory network based on Kandel's *Aplysia* research

We postulate that habituation within the glucose-regulatory network is primarily driven by presynaptic inhibition at the sensory-integrative neuron synapse. This is likely to involve several mechanisms, including heterosynaptic inhibition. From our data, we propose that if a familiar stress is encountered, the limbic forebrain and pPVT drive an inhibitory circuit involving the vBNST. This inhibits presynaptic neurotransmission at the sensory-integrative neuron synapse, leading to reduced CRH^{mpdPVH} neuron activation. This attenuated activation is communicated to hindbrain catecholaminergic (CA) neurons, through cross-talk mechanisms, leading to an impaired sympathoadrenal response. We do not yet have strong evidence to support direct connections between glucose-sensing and motor elements in the mammalian brain. Therefore, this model is not without its limitations. This reinforces that the most likely site of habituation within the mammalian glucose-regulatory network is at the sensory-integrative neuron synapse.

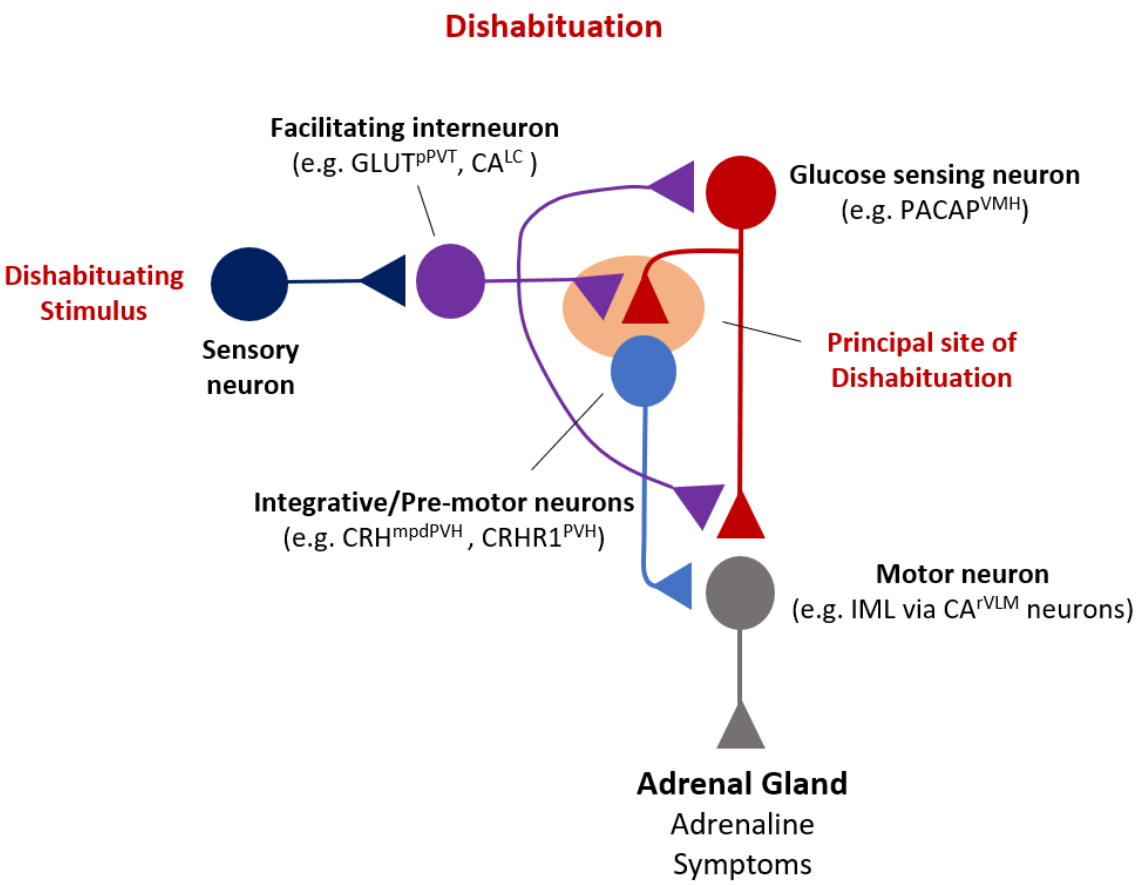

Figure 8.5: A proposed neuronal circuit model for dishabituation in the central glucose-regulatory network based on Kandel's *Aplysia* research

We postulate that dishabituation is mechanistically comparable to sensitisation and involves heterosynaptic facilitation. We propose that following RH, if a novel heterotypic stress is encountered, an excitatory circuit involving facilitating interneurons is activated. The identity of neuronal populations involved in facilitation is not known. We postulate that they may include a separate subpopulation of GLUT^{pPVT}, which we show project to the mpdPVH, or catecholaminergic neurons in the LC. Facilitation, through presynaptic excitation at the sensory-integrative neuron synapse would lead to increased activation of CRH^{mpdPVH} neurons. This would translate to an enhanced sympathoadrenal response. In parallel, facilitating interneurons may restore glutamatergic neurotransmission in glucose-sensing neurons. The precise mechanism for this is not clear but may involve noradrenaline release from an LC input.

8.8 Therapies based on habituation theory

In this thesis, I have outlined evidence which supports habituation of responses to RH as the primary driver for IAH. Treatments based on habituation theory could hypothetically involve those which prevent the development of habituation or therapies which lead to dishabituation.

Preventing patients from developing IAH is the ultimate treatment goal and normally requires the complete avoidance of hypoglycaemia. Despite improvements in the clinical management of diabetes, new technologies and therapeutics, patients with insulin-treated diabetes are likely to continue to experience RH and develop IAH in the foreseeable future. Since habituation is a core neurobiological process, its prevention is not possible. However, it is possible that its development could be delayed or even reversed though interventions which retrain symptom recognition. Two small scale studies have shown promise. The first is the DAFNE-Hypoglycaemia Awareness Restoration Training (DAFNE-HART) study, which focussed on psycho-educational interventions, akin to cognitive behavioural therapy, in a small cohort of patients with IAH and type 1 diabetes. The interventions targeted unhelpful thoughts relating to hypoglycaemia, instituted a structured guide to find subjective cues to blood glucose level, and explored theories linking thoughts with behaviours (de Zoysa et al., 2014). Importantly, this study demonstrated improved symptom awareness and reductions in severe hypoglycaemic episodes, without compromising blood glucose control (de Zoysa et al., 2014). The second is the “Blood glucose awareness training” (BGAT) programme, which targeted psychological barriers related to IAH. It can be considered as a form of biological feedback training, as it teaches individuals to recognise and regain normal autonomic function. This was achieved through training in interpretation of physical symptoms, cognitive performance and mood, as internal cues of blood glucose awareness hypoglycaemia (Cox et al., 2001, Kinsley et al., 1999). BGAT has been shown to reduce IAH, rates of severe hypoglycaemia and interestingly to improve sympathoadrenal response to subsequent hypoglycaemia (Cox et al., 2001, Kinsley et al., 1999). It is not clear if these improvements were due to hypoglycaemia avoidance, or if separate mechanisms led to symptom recovery. If the latter is true, this could indicate that psycho-educational treatments can also dishabituate.

Therapies which focus directly on dishabituation have also shown promise. Investigators have already provided excellent examples where two separate heterotypic stressors, high-intensity exercise and, separately, cold exposure can reinstate the sympathoadrenal response in rodent models of RH (McNeilly et al., 2017, Farrell et al., 2020). More importantly, the concept is translatable, since high-intensity exercise training increases both adrenaline and hypoglycaemia awareness in patients with type 1

diabetes (Farrell et al., 2020). It is not clear how long the therapeutic effect of dishabituation would last and it is likely that therapies based on this principle would need to be periodically re-visited. This is important as patients are likely to continue to experience RH. As with habituation, the response to dishabituation is likely to depend on the individual. This would require treatment regimens which are carefully calibrated to the individual. Other difficulties exist with this approach, including the likelihood that the dishabituating stimulus itself may become habituated with repetition. A solution to this could be to design treatment protocols which involve the interchange of a variety of dishabituating stimuli. This approach parallels chronic variable stress protocols, which elicit stress in an unpredictable manner and are less likely to habituate (Herman, 2013). However, treatments which dishabituate by activating the hypothalamo-sympathoadrenal axis through alternative sensory inputs, must strike the right balance. Excessive activation is inherently unpleasant and carries risks to health from repeated overactivation of stress axes. On the other hand, a mild stimulus is unlikely to bring about dishabituation.

Our data show that specific neuronal networks control the RH-induced habituation of the sympathoadrenal response. We can postulate that if the therapeutic targeting of specific neuronal populations becomes possible in the future, then we may be able to target the neuronal locus of habituation. In the context of our findings, the PVT is of particular interest as a therapeutic target. The blockade of glucocorticoid and mineralocorticoid signalling within the PVT prevents habituation of the HPA-axis to repeated restraint stress. In addition, neuropeptidergic circuits involving cholecystokinin (CCK) and orexin neurons which project to the PVT are important in HPA-axis sensitisation, which may also have mechanistic relevance to dishabituation (Jaferi and Bhatnagar, 2006, Heydendael et al., 2011). Unfortunately, our current ability to access pharmacologically specific neuronal populations is limited. Drug delivery into the brain is often complicated by inability to cross the blood-brain barrier, adverse side effects and lack of specificity to a particular brain region. Therefore, indirect ways of promoting signalling pathways or re-establishing basal physiology are more likely treatment approaches. For example, the finding that high-intensity exercise, in a rodent model of IAH, induces brain-derived neurotrophic factor (BDNF) and improves hypothalamic glutaminergic transmission (McNeilly et al., 2017).

8.9 Limitations and Future Directions

In this thesis I first characterised a nondiabetic mouse model of IAH which enabled investigations into the central glucose-regulatory network. It must be acknowledged that the findings in this thesis along with those gained from other nondiabetic animal models in the literature, will need validation in diabetic models and ultimately patients with IAH. For example, RH has differential effects on hippocampal tissue in diabetic and nondiabetic rodents (Zhou et al., 2018, McNeilly et al., 2016). Interestingly, RH seems to confer adaptations which improve cognition in non-diabetic rodents but features which indicate the opposite in diabetic rodents (McNay et al., 2006, Zhou et al., 2018, McNeilly et al., 2016). It is postulated that an important difference in the diabetic state is that chronic hyperglycaemia impairs the ability of cells to tolerate hypoglycaemia-induced oxidative stress (Bree et al., 2009). It is likely that other mechanisms are altered with diabetes. For example, it is not known if the chronic glucagon dysfunction in type 1 diabetes leads to changes within the glucose-regulatory network and adaptations within the sympathoadrenal axis. These questions, which require further study emphasise the importance of diabetic animal models in IAH research. However, it is reassuring that the core feature of sympathoadrenal response habituation following RH, has been demonstrated in mice, rats, and humans, with and without diabetes (Sankar et al., 2020, McNeilly and McCrimmon, 2018). Therefore, we are confident that important mechanistic insights can still be gained from our work.

Our mouse model of IAH mouse model focused on measuring habituation of the sympathoadrenal response. However, a direct behavioural measure indicative of symptoms awareness was missing. Further work to understanding hypoglycaemia-specific behaviours in animals is required to address this. This may be achieved by understanding whether stereotyped behaviours exhibited following other psychological and physical stress (e.g., escape, grooming, freezing, digging) are also exhibited after hypoglycaemia (Füzesi et al., 2016).

Our objective has been to understand neuronal mechanisms underlying IAH in the brain. This was because we postulated that habituation of the sympathoadrenal response occurs in central integrative neuronal networks. However, it must be acknowledged that in a complex system, peripheral changes at the level of the adrenal chromaffin cells may also contribute (Seaquist, 2018). Our genetic ablation and inhibitory studies have identified key nodes for both the hypoglycaemia CRR and habituation, controlled by CRH^{mpdPVH} neurons and $GLUT^{pPVT}$ neurons, respectively. However, more work is required to dissect the precise hierarchy of the whole-body, glucose-regulatory network.

An important technique used in this thesis has been the measurement of neuronal markers of acute activation (cFos) and adaptation (FosB). Both markers have widely adopted in elucidating neuronal circuitry and function, but they represent a snapshot of neuronal activity. Therefore, we were not able to establish if specific brain regions habituate to RH at an earlier or later stage in the pathophysiological process. In addition, as both cFos and FosB are regulatory proteins, they show basal expression which varies depending on the neuronal population. This emphasises the importance of control groups in experiments which quantify neuronal activation with cFos and FosB.

In this thesis, the focus has been to understand the RH-induced habituation of the sympathoadrenal response. This was poorly characterised for the autonomic nervous system and required application of the large literature which has examined habituation of the HPA axis. We found good concordance between our own findings and studies investigating HPA-axis habituation. A notable difference with the literature was our findings which supported the possibility of stimulus generalisation of the sympathoadrenal response with restraint and RH. Though this was tested indirectly in this thesis, this has been shown to be present in rodents exposed to cold stress after RH (Vickneson et al., 2021). These findings are at odds with a large body of work investigating HPA axis responses to understand habituation, which have failed to show generalisation of habituation for HPA-axis responses (Grissom and Bhatnagar, 2009, Costa-Ferreira et al., 2016). This discrepancy may be due to the type of stimulus used in these experiments, which are required to be sufficiently similar in nature to enable stimulus generalisation (Vickneson et al., 2021). It is reassuring that other key hallmarks of habituation can be observed within the HPA axis, including dishabituation (Herman, 2013, Costa-Ferreira et al., 2016). At a circuit level, our data support the involvement of the pPVT and CRH^{mpdPVH} neurons in the habitation of both axes. Further work is required to characterise the different mechanisms which mediate habituation within the HPA axis and the sympathoadrenal system, respectively. Though we postulate that the same neuronal circuit is also involved in dishabituation, dedicated investigations are needed to prove that this is the case.

More work is also required to delineate the phenotype of $GLUT^{pPVT}$ neuronal subpopulations which we hypothesise drive habituation and sensitisation/dishabituation. This could be achieved using an intersectional intracranial surgical approach, in transgenic lines, to provide projection-specific genetic access to this neuronal circuit. This would also enable more specific manipulations of the $GLUT^{pPVT} \rightarrow GABA^{vBNST} \rightarrow CRH^{mpdPVH}$ circuit, which we believe controls stress habituation.

A major area of further work also relates to the investigation of stress memory storage and retrieval, which is believed to involve the limbic forebrain. Within this network, the vSub is of particular interest, based on its memory retrieval functions and inhibitory connections with the PVT (Herman and Mueller, 2006, Ledergerber and Moser, 2017). It is possible that the vSub along with other limbic forebrain structures encode stress familiarity and, in concert with the pPVT, dictates stress habituation.

Comparing our neuronal tracing and circuit mapping data to the literature has shown that important connections within the glucose-regulatory network are conserved between the mouse and rat brain. However, the precise location of neuronal subpopulations, (e.g., CRH^{PVH} neurons) within structures can vary (Biag et al., 2012). Further, experimentation will be required to map this circuit into a much wider and complex glucose-regulatory network, and to determine if this framework translates into humans.

The specificity of this neuronal circuit to the human brain is unclear. However, imaging studies in humans consistently identify hypoglycaemia-induced altered activity in forebrain and thalamic structures (Arbelaez et al., 2008, Nwokolo et al., 2019b, Nwokolo et al., 2019a).

References

ADA 2005. Defining and Reporting Hypoglycemia in Diabetes. *A report from the American Diabetes Association Workgroup on Hypoglycemia,* 28**,** 1245-1249.

AGUILERA, G. & LIU, Y. 2012. The molecular physiology of CRH neurons. *Frontiers in neuroendocrinology,* 33**,** 67-84.

AHRÉN, B. & TABORSKY, G. J., JR. 1986. The mechanism of vagal nerve stimulation of glucagon and insulin secretion in the dog. *Endocrinology,* 118**,** 1551-7.

AKLAN, I., SAYAR ATASOY, N., YAVUZ, Y., ATES, T., COBAN, I., KOKSALAR, F., FILIZ, G., TOPCU, I. C., ONCUL, M., DILSIZ, P., CEBECIOGLU, U., ALP, M. I., YILMAZ, B., DAVIS, D. R., HAJDUKIEWICZ, K., SAITO, K., KONOPKA, W., CUI, H. & ATASOY, D. 2020. NTS Catecholamine Neurons Mediate Hypoglycemic Hunger via Medial Hypothalamic Feeding Pathways. *Cell Metab,* 31**,** 313-326.e5.

AL-NOORI, S., SANDERS, N. M., TABORSKY, G. J., JR., WILKINSON, C. W. & FIGLEWICZ, D. P. 2008a. Acute THPVP inactivation decreases the glucagon and sympathoadrenal responses to recurrent hypoglycemia. *Brain Res,* 1194**,** 65-72.

AL-NOORI, S., SANDERS, N. M., TABORSKY, G. J., JR., WILKINSON, C. W., ZAVOSH, A., WEST, C., SANDERS, C. M. & FIGLEWICZ, D. P. 2008b. Recurrent hypoglycemia alters hypothalamic expression of the regulatory proteins FosB and synaptophysin. *Am J Physiol Regul Integr Comp Physiol,* 295**,** R1446-54.

ALQUIER, T., KAWASHIMA, J., TSUJI, Y. & KAHN, B. B. 2007. Role of hypothalamic adenosine 5'-monophosphate-activated protein kinase in the impaired counterregulatory response induced by repetitive neuroglucopenia. *Endocrinology,* 148**,** 1367-75.

AMIEL, S. A. 2009. Hypoglycemia: From the Laboratory to the Clinic. *Diabetes Care,* 32**,** 1364-1371.

AMIEL, S. A., SHERWIN, R. S., SIMONSON, D. C. & TAMBORLANE, W. V. 1988. Effect of intensive insulin therapy on glycemic thresholds for counterregulatory hormone release. *Diabetes,* 37**,** 901-7.

ANDREW, S. F., DINH, T. T. & RITTER, S. 2007. Localized glucoprivation of hindbrain sites elicits corticosterone and glucagon secretion. *Am J Physiol Regul Integr Comp Physiol,* 292**,** R1792-8.

ARBELAEZ, A. M., POWERS, W. J., VIDEEN, T. O., PRICE, J. L. & CRYER, P. E. 2008. Attenuation of counterregulatory responses to recurrent hypoglycemia by active thalamic inhibition: a mechanism for hypoglycemia-associated autonomic failure. *Diabetes,* 57**,** 470-5.

ARBELAEZ, A. M., RUTLIN, J. R., HERSHEY, T., POWERS, W. J., VIDEEN, T. O. & CRYER, P. E. 2012. Thalamic activation during slightly subphysiological glycemia in humans. *Diabetes Care,* 35**,** 2570-4.

ARDIEL, E. L., GILES, A. C., YU, A. J., LINDSAY, T. H., LOCKERY, S. R. & RANKIN, C. H. 2016. Dopamine receptor DOP-4 modulates habituation to repetitive photoactivation of a C. elegans polymodal nociceptor. *Learn Mem,* 23**,** 495-503.

ARDIEL, E. L., YU, A. J., GILES, A. C. & RANKIN, C. H. 2017. Habituation as an adaptive shift in response strategy mediated by neuropeptides. *npj Science of Learning,* 2**,** 9.

ARMARIO, A., VALLÈS, A., DAL-ZOTTO, S., MÁRQUEZ, C. & BELDA, X. 2004. A single exposure to severe stressors causes long-term desensitisation of the physiological response to the homotypic stressor. *Stress,* 7**,** 157-72.

ARMBRUSTER, B. N., LI, X., PAUSCH, M. H., HERLITZE, S. & ROTH, B. L. 2007. Evolving the lock to fit the key to create a family of G protein-coupled receptors potently activated by an inert ligand. *Proceedings of the National Academy of Sciences,* 104**,** 5163-5168.

ASVOLD, B. O., SAND, T., HESTAD, K. & BJORGAAS, M. R. 2010. Cognitive function in type 1 diabetic adults with early exposure to severe hypoglycemia: a 16-year follow-up study. *Diabetes Care,* 33**,** 1945-7.
ATASOY, D., APONTE, Y., SU, H. H. & STERNSON, S. M. 2008. A FLEX Switch Targets Channelrhodopsin-2 to Multiple Cell Types for Imaging and Long-Range Circuit Mapping. *The Journal of Neuroscience,* 28**,** 7025-7030.
BAINS, J. S., CUSULIN, J. I. W. & INOUE, W. 2015. Stress-related synaptic plasticity in the hypothalamus. *Nature Reviews Neuroscience,* 16**,** 377-388.
BALCOMBE, J. P., BARNARD, N. D. & SANDUSKY, C. 2004. Laboratory routines cause animal stress. *Contemp Top Lab Anim Sci,* 43**,** 42-51.
BALFOUR, R. H., HANSEN, A. M. & TRAPP, S. 2006. Neuronal responses to transient hypoglycaemia in the dorsal vagal complex of the rat brainstem. *J Physiol,* 570**,** 469-84.
BARSON, J. R., MACK, N. R. & GAO, W.-J. 2020. The Paraventricular Nucleus of the Thalamus Is an Important Node in the Emotional Processing Network. *Frontiers in Behavioral Neuroscience,* 14.
BAYNE, M., ALVARSSON, A., DEVARAKONDA, K., LI, R., JIMENEZ-GONZALEZ, M., GARIBAY, D., CONNER, K., VARGHESE, M., SERASINGHE, M. N., CHIPUK, J. E., HOF, P. R. & STANLEY, S. A. 2020. Repeated hypoglycemia remodels neural inputs and disrupts mitochondrial function to blunt glucose-inhibited GHRH neuron responsiveness. *JCI Insight,* 5.
BEALL, C., ASHFORD, M. L. & MCCRIMMON, R. J. 2012. The physiology and pathophysiology of the neural control of the counterregulatory response. *Am J Physiol Regul Integr Comp Physiol,* 302**,** R215-23.
BELDA, X., FUENTES, S., DAVIU, N., NADAL, R. & ARMARIO, A. 2015. Stress-induced sensitization: the hypothalamic-pituitary-adrenal axis and beyond. *Stress,* 18**,** 269-79.
BELFORT-DEAGUIAR, R., GALLEZOT, J. D., HWANG, J. J., ELSHAFIE, A., YECKEL, C. W., CHAN, O., CARSON, R. E., DING, Y. S. & SHERWIN, R. S. 2018. Noradrenergic Activity in the Human Brain: A Mechanism Supporting the Defense Against Hypoglycemia. *J Clin Endocrinol Metab,* 103**,** 2244-2252.
BERRIOS, J., LI, C., MADARA, J. C., GARFIELD, A. S., STEGER, J. S., KRASHES, M. J. & LOWELL, B. B. 2021. Food cue regulation of AGRP hunger neurons guides learning. *Nature,* 595**,** 695-700.
BEVERLY, J. L., DE VRIES, M. G., BOUMAN, S. D. & ARSENEAU, L. M. 2001. Noradrenergic and GABAergic systems in the medial hypothalamus are activated during hypoglycemia. *Am J Physiol Regul Integr Comp Physiol,* 280**,** R563-9.
BHATNAGAR, S. & DALLMAN, M. 1998. Neuroanatomical basis for facilitation of hypothalamic-pituitary-adrenal responses to a novel stressor after chronic stress. *Neuroscience,* 84**,** 1025-39.
BHATNAGAR, S., HUBER, R., NOWAK, N. & TROTTER, P. 2002. Lesions of the posterior paraventricular thalamus block habituation of hypothalamic-pituitary-adrenal responses to repeated restraint. *J Neuroendocrinol,* 14**,** 403-10.
BIAG, J., HUANG, Y., GOU, L., HINTIRYAN, H., ASKARINAM, A., HAHN, J. D., TOGA, A. W. & DONG, H.-W. 2012. Cyto- and chemoarchitecture of the hypothalamic paraventricular nucleus in the C57BL/6J male mouse: a study of immunostaining and multiple fluorescent tract tracing. *The Journal of comparative neurology,* 520**,** 6-33.
BIESSELS, G. J. 2014. Hypoglycemia and cognitive decline in older people with type 2 diabetes: a bidirectional relationship. *Diabetic Hypoglycemia,* 6**,** 11-14.
BITTAR, T. P., NAIR, B. B., KIM, J. S., CHANDRASEKERA, D., SHERRINGTON, A. & IREMONGER, K. J. 2019. Corticosterone mediated functional and structural plasticity in corticotropin-releasing hormone neurons. *Neuropharmacology,* 154**,** 79-86.

BJORGAAS, M., SAND, T., VIK, T. & JORDE, R. 1998. Quantitative EEG during controlled hypoglycaemia in diabetic and non-diabetic children. *Diabet Med,* 15**,** 30-7.

BOLLI, G., DE FEO, P., COMPAGNUCCI, P., CARTECHINI, M. G., ANGELETTI, G., SANTEUSANIO, F., BRUNETTI, P. & GERICH, J. E. 1983. Abnormal glucose counterregulation in insulin-dependent diabetes mellitus. Interaction of anti-insulin antibodies and impaired glucagon and epinephrine secretion. *Diabetes,* 32**,** 134-41.

BORG, M. A., BORG, W. P., TAMBORLANE, W. V., BRINES, M. L., SHULMAN, G. I. & SHERWIN, R. S. 1999. Chronic hypoglycemia and diabetes impair counterregulation induced by localized 2-deoxy-glucose perfusion of the ventromedial hypothalamus in rats. *Diabetes,* 48**,** 584-7.

BORG, M. A., SHERWIN, R. S., BORG, W. P., TAMBORLANE, W. V. & SHULMAN, G. I. 1997. Local ventromedial hypothalamus glucose perfusion blocks counterregulation during systemic hypoglycemia in awake rats. *J Clin Invest,* 99**,** 361-5.

BORG, W. P., DURING, M. J., SHERWIN, R. S., BORG, M. A., BRINES, M. L. & SHULMAN, G. I. 1994. Ventromedial hypothalamic lesions in rats suppress counterregulatory responses to hypoglycemia. *J Clin Invest,* 93**,** 1677-82.

BORG, W. P., SHERWIN, R. S., DURING, M. J., BORG, M. A. & SHULMAN, G. I. 1995. Local ventromedial hypothalamus glucopenia triggers counterregulatory hormone release. *Diabetes,* 44**,** 180-4.

BOYLE, P. J. & CRYER, P. E. 1991. Growth hormone, cortisol, or both are involved in defense against, but are not critical to recovery from, hypoglycemia. *Am J Physiol,* 260**,** E395-402.

BOYLE, P. J., KEMPERS, S. F., O'CONNOR, A. M. & NAGY, R. J. 1995. Brain glucose uptake and unawareness of hypoglycemia in patients with insulin-dependent diabetes mellitus. *N Engl J Med,* 333**,** 1726-31.

BREE, A. J., PUENTE, E. C., DAPHNA-IKEN, D. & FISHER, S. J. 2009. Diabetes increases brain damage caused by severe hypoglycemia. *Am J Physiol Endocrinol Metab,* 297**,** E194-201.

BRIAN M. FRIER, S. H., RORY MCCRIMMON 2014. *Hypoglycaemia in Clinical Diabetes*, Wiley-Blackwell.

BRISCOE, V. J., ERTL, A. C., TATE, D. B. & DAVIS, S. N. 2008a. Effects of the selective serotonin reuptake inhibitor fluoxetine on counterregulatory responses to hypoglycemia in individuals with type 1 diabetes. *Diabetes,* 57**,** 3315-22.

BRISCOE, V. J., ERTL, A. C., TATE, D. B., DAWLING, S. & DAVIS, S. N. 2008b. Effects of a selective serotonin reuptake inhibitor, fluoxetine, on counterregulatory responses to hypoglycemia in healthy individuals. *Diabetes,* 57**,** 2453-60.

BROWN, M. R., FISHER, L. A., SPIESS, J., RIVIER, C., RIVIER, J. & VALE, W. 1982. Corticotropin-releasing factor: actions on the sympathetic nervous system and metabolism. *Endocrinology,* 111**,** 928-31.

BROWN, S. M., HENNING, S. & WELLMAN, C. L. 2005. Mild, Short-term Stress Alters Dendritic Morphology in Rat Medial Prefrontal Cortex. *Cerebral Cortex,* 15**,** 1714-1722.

BUIJS, R. M., CHUN, S. J., NIIJIMA, A., ROMIJN, H. J. & NAGAI, K. 2001. Parasympathetic and sympathetic control of the pancreas: a role for the suprachiasmatic nucleus and other hypothalamic centers that are involved in the regulation of food intake. *J Comp Neurol,* 431**,** 405-23.

BURDAKOV, D., KARNANI, M. M. & GONZALEZ, A. 2013. Lateral hypothalamus as a sensor-regulator in respiratory and metabolic control. *Physiology & Behavior,* 121**,** 117-124.

BURDAKOV, D. & LESAGE, F. 2010. Glucose-induced inhibition: how many ionic mechanisms? *Acta Physiol (Oxf),* 198**,** 295-301.

CAMPUS, P., COVELO, I. R., KIM, Y., PARSEGIAN, A., KUHN, B. N., LOPEZ, S. A., NEUMAIER, J. F., FERGUSON, S. M., SOLBERG WOODS, L. C., SARTER,

M. & FLAGEL, S. B. 2019. The paraventricular thalamus is a critical mediator of top-down control of cue-motivated behavior in rats. *Elife,* 8.
CANTERAS, N. S., SIMERLY, R. B. & SWANSON, L. W. 1994. Organization of projections from the ventromedial nucleus of the hypothalamus: a Phaseolus vulgaris-leucoagglutinin study in the rat. *J Comp Neurol,* 348**,** 41-79.
CAPRIO, S., GERETY, G., TAMBORLANE, W. V., JONES, T., DIAMOND, M., JACOB, R. & SHERWIN, R. S. 1991. Opiate blockade enhances hypoglycemic counterregulation in normal and insulin-dependent diabetic subjects. *American Journal of Physiology-Endocrinology and Metabolism,* 260**,** E852-E858.
CAREY, M., GOSPIN, R., GOYAL, A., TOMUTA, N., SANDU, O., MBANYA, A., LONTCHI-YIMAGOU, E., HULKOWER, R., SHAMOON, H., GABRIELY, I. & HAWKINS, M. 2017. Opioid Receptor Activation Impairs Hypoglycemic Counterregulation in Humans. *Diabetes,* 66**,** 2764-2773.
CARTER, M., DE LECEA, L. & ADAMANTIDIS, A. 2013. Functional wiring of hypocretin and LC-NE neurons: implications for arousal. *Frontiers in Behavioral Neuroscience,* 7.
CHAFETZ, M. D., PARKO, K., DIAZ, S. & LEIBOWITZ, S. F. 1986. Relationships between medial hypothalamic alpha 2-receptor binding, norepinephrine, and circulating glucose. *Brain Res,* 384**,** 404-8.
CHAN, O., CHAN, S., INOUYE, K., SHUM, K., MATTHEWS, S. G. & VRANIC, M. 2002. Diabetes impairs hypothalamo-pituitary-adrenal (HPA) responses to hypoglycemia, and insulin treatment normalizes HPA but not epinephrine responses. *Diabetes,* 51**,** 1681-9.
CHAN, O., CHENG, H., HERZOG, R., CZYZYK, D., ZHU, W., WANG, A., MCCRIMMON, R. J., SEASHORE, M. R. & SHERWIN, R. S. 2008. Increased GABAergic tone in the ventromedial hypothalamus contributes to suppression of counterregulatory responses after antecedent hypoglycemia. *Diabetes,* 57**,** 1363-70.
CHAN, O., PARANJAPE, S., CZYZYK, D., HORBLITT, A., ZHU, W., DING, Y., FAN, X., SEASHORE, M. & SHERWIN, R. 2011. Increased GABAergic output in the ventromedial hypothalamus contributes to impaired hypoglycemic counterregulation in diabetic rats. *Diabetes,* 60**,** 1582-9.
CHAN, O., PARANJAPE, S. A., HORBLITT, A., ZHU, W. & SHERWIN, R. S. 2013. Lactate-induced release of GABA in the ventromedial hypothalamus contributes to counterregulatory failure in recurrent hypoglycemia and diabetes. *Diabetes,* 62**,** 4239-46.
CHAN, O., ZHU, W., DING, Y., MCCRIMMON, R. J. & SHERWIN, R. S. 2006. Blockade of GABA(A) receptors in the ventromedial hypothalamus further stimulates glucagon and sympathoadrenal but not the hypothalamo-pituitary-adrenal response to hypoglycemia. *Diabetes,* 55**,** 1080-7.
CHEN, P., LIN, D., GIESLER, J. & LI, C. 2011. Identification of urocortin 3 afferent projection to the ventromedial nucleus of the hypothalamus in rat brain. *J Comp Neurol,* 519**,** 2023-42.
CHEN, T.-W., WARDILL, T. J., SUN, Y., PULVER, S. R., RENNINGER, S. L., BAOHAN, A., SCHREITER, E. R., KERR, R. A., ORGER, M. B., JAYARAMAN, V., LOOGER, L. L., SVOBODA, K. & KIM, D. S. 2013. Ultrasensitive fluorescent proteins for imaging neuronal activity. *Nature,* 499**,** 295-300.
CHEN, W. G., SCHLOESSER, D., ARENSDORF, A. M., SIMMONS, J. M., CUI, C., VALENTINO, R., GNADT, J. W., NIELSEN, L., HILLAIRE-CLARKE, C. S., SPRUANCE, V., HOROWITZ, T. S., VALLEJO, Y. F. & LANGEVIN, H. M. 2021. The Emerging Science of Interoception: Sensing, Integrating, Interpreting, and Regulating Signals within the Self. *Trends in neurosciences,* 44**,** 3-16.
CHEN, Y., BENDER, R. A., BRUNSON, K. L., POMPER, J. K., GRIGORIADIS, D. E., WURST, W. & BARAM, T. Z. 2004. Modulation of dendritic differentiation by corticotropin-releasing factor in the developing hippocampus. *Proc Natl Acad Sci U S A,* 101**,** 15782-7.

CHOI, D. C., EVANSON, N. K., FURAY, A. R., ULRICH-LAI, Y. M., OSTRANDER, M. M. & HERMAN, J. P. 2008. The anteroventral bed nucleus of the stria terminalis differentially regulates hypothalamic-pituitary-adrenocortical axis responses to acute and chronic stress. *Endocrinology,* 149**,** 818-826.

CHOUDHARY, P. & AMIEL, S. A. 2018. Hypoglycaemia in type 1 diabetes: technological treatments, their limitations and the place of psychology. *Diabetologia,* 61**,** 761-769.

CHOUDHARY, P., RICKELS, M. R., SENIOR, P. A., VANTYGHEM, M. C., MAFFI, P., KAY, T. W., KEYMEULEN, B., INAGAKI, N., SAUDEK, F., LEHMANN, R. & HERING, B. J. 2015. Evidence-informed clinical practice recommendations for treatment of type 1 diabetes complicated by problematic hypoglycemia. *Diabetes Care,* 38**,** 1016-29.

CLARKE, W. L., COX, D. J., GONDER-FREDERICK, L. A., JULIAN, D., SCHLUNDT, D. & POLONSKY, W. 1995. Reduced Awareness of Hypoglycemia in Adults With IDDM: A prospective study of hypoglycemic frequency and associated symptoms. *Diabetes Care,* 18**,** 517-522.

COIRO, V., PASSERI, M., DAVOLI, C., D'AMATO, L., GELMINI, G., FAGNONI, F., SCHIANCHI, L., BENTIVOGLIO, M., VOLPI, R. & CHIODERA, P. 1988. Oxytocin response to insulin-induced hypoglycemia in obese subjects before and after weight loss. *Journal of Endocrinological Investigation,* 11**,** 125-128.

COLLINS, D., BURKE, D. & GANDEVIA, S. 2002. Sustained contractions produced by plateau-like behaviour in human motoneurones. *The Journal of physiology,* 538**,** 289-301.

CORBETT, B. F., YOU, J. C., ZHANG, X., PYFER, M. S., TOSI, U., IASCONE, D. M., PETROF, I., HAZRA, A., FU, C. H., STEPHENS, G. S., ASHOK, A. A., ASCHMIES, S., ZHAO, L., NESTLER, E. J. & CHIN, J. 2017. DeltaFosB Regulates Gene Expression and Cognitive Dysfunction in a Mouse Model of Alzheimer's Disease. *Cell Rep,* 20**,** 344-355.

COSTA-FERREIRA, W., VIEIRA, J. O., ALMEIDA, J., GOMES-DE-SOUZA, L. & CRESTANI, C. C. 2016. Involvement of Type 1 Angiontensin II Receptor (AT1) in Cardiovascular Changes Induced by Chronic Emotional Stress: Comparison between Homotypic and Heterotypic Stressors. *Frontiers in Pharmacology,* 7.

COX, D. J., GONDER-FREDERICK, L., POLONSKY, W., SCHLUNDT, D., KOVATCHEV, B. & CLARKE, W. 2001. Blood glucose awareness training (BGAT-2): long-term benefits. *Diabetes Care,* 24**,** 637-642.

CRAIG, A. D. 2002. How do you feel? Interoception: the sense of the physiological condition of the body. *Nature Reviews Neuroscience,* 3**,** 655-666.

CRANSTON, I., LOMAS, J., MARAN, A., MACDONALD, I. & AMIEL, S. A. 1994. Restoration of hypoglycaemia awareness in patients with long-duration insulin-dependent diabetes. *Lancet,* 344**,** 283-7.

CRYER, P. E. 2004. Diverse causes of hypoglycemia-associated autonomic failure in diabetes. *N Engl J Med,* 350**,** 2272-9.

CRYER, P. E. 2013. Mechanisms of hypoglycemia-associated autonomic failure in diabetes. *N Engl J Med,* 369**,** 362-72.

CUNNINGHAM, E. T., JR. & SAWCHENKO, P. E. 1988. Anatomical specificity of noradrenergic inputs to the paraventricular and supraoptic nuclei of the rat hypothalamus. *J Comp Neurol,* 274**,** 60-76.

DAGOGO-JACK, S. E., CRAFT, S. & CRYER, P. E. 1993. Hypoglycemia-associated autonomic failure in insulin-dependent diabetes mellitus. Recent antecedent hypoglycemia reduces autonomic responses to, symptoms of, and defense against subsequent hypoglycemia. *J Clin Invest,* 91**,** 819-28.

DAVIS, M. R., MELLMAN, M. & SHAMOON, H. 1993. Physiologic hyperinsulinemia enhances counterregulatory hormone responses to hypoglycemia in IDDM. *J Clin Endocrinol Metab,* 76**,** 1383-5.

DAVIS, S. N., SHAVERS, C., MOSQUEDA-GARCIA, R. & COSTA, F. 1997. Effects of Differing Antecedent Hypoglycemia on Subsequent Counterregulation in Normal Humans. *Diabetes,* 46**,** 1328-1335.

DAVIU, N., FÜZESI, T., ROSENEGGER, D. G., RASIAH, N. P., STERLEY, T.-L., PERINGOD, G. & BAINS, J. S. 2020. Paraventricular nucleus CRH neurons encode stress controllability and regulate defensive behavior selection. *Nature Neuroscience,* 23**,** 398-410.

DE FEO, P., PERRIELLO, G., TORLONE, E., VENTURA, M. M., FANELLI, C., SANTEUSANIO, F., BRUNETTI, P., GERICH, J. E. & BOLLI, G. B. 1989. Contribution of cortisol to glucose counterregulation in humans. *Am J Physiol,* 257**,** E35-42.

DE VRIES, M. G., LAWSON, M. A. & BEVERLY, J. L. 2005. Hypoglycemia-induced noradrenergic activation in the VMH is a result of decreased ambient glucose. *Am J Physiol Regul Integr Comp Physiol,* 289**,** R977-81.

DE ZOYSA, N., ROGERS, H., STADLER, M., GIANFRANCESCO, C., BEVERIDGE, S., BRITNEFF, E., CHOUDHARY, P., ELLIOTT, J., HELLER, S. & AMIEL, S. A. 2014. A psychoeducational program to restore hypoglycemia awareness: the DAFNE-HART pilot study. *Diabetes Care,* 37**,** 863-6.

DENARDO, L. A., LIU, C. D., ALLEN, W. E., ADAMS, E. L., FRIEDMANN, D., DADGAR-KIANI, E., FU, L., GUENTHNER, C. J., LEE, J. H., TESSIER-LAVIGNE, M. & LUO, L. 2018. Temporal Evolution of Cortical Ensembles Promoting Remote Memory Retrieval. *bioRxiv***,** 295238.

DEROSA, M. A. & CRYER, P. E. 2004. Hypoglycemia and the sympathoadrenal system: neurogenic symptoms are largely the result of sympathetic neural, rather than adrenomedullary, activation. *American Journal of Physiology-Endocrinology and Metabolism,* 287**,** E32-E41.

DESOUZA, C., SALAZAR, H., CHEONG, B., MURGO, J. & FONSECA, V. 2003. Association of hypoglycemia and cardiac ischemia: a study based on continuous monitoring. *Diabetes Care,* 26**,** 1485-9.

DIABETES, C., COMPLICATIONS TRIAL RESEARCH, G., NATHAN, D. M., GENUTH, S., LACHIN, J., CLEARY, P., CROFFORD, O., DAVIS, M., RAND, L. & SIEBERT, C. 1993. The effect of intensive treatment of diabetes on the development and progression of long-term complications in insulin-dependent diabetes mellitus. *N Engl J Med,* 329**,** 977-86.

DIGGS-ANDREWS, K. A., ZHANG, X., SONG, Z., DAPHNA-IKEN, D., ROUTH, V. H. & FISHER, S. J. 2010. Brain Insulin Action Regulates Hypothalamic Glucose Sensing and the Counterregulatory Response to Hypoglycemia. *Diabetes,* 59**,** 2271-2280.

DIROCCO, R. J. & GRILL, H. J. 1979. The forebrain is not essential for sympathoadrenal hyperglycemic response to glucoprivation. *Science,* 204**,** 1112-4.

DO-MONTE, F. H., MINIER-TORIBIO, A., QUINONES-LARACUENTE, K., MEDINA-COLON, E. M. & QUIRK, G. J. 2017. Thalamic Regulation of Sucrose Seeking during Unexpected Reward Omission. *Neuron,* 94**,** 388-400.e4.

DODD, G. T., WILLIAMS, S. R. & LUCKMAN, S. M. 2010. Functional magnetic resonance imaging and c-Fos mapping in rats following a glucoprivic dose of 2-deoxy-D-glucose. *J Neurochem,* 113**,** 1123-32.

DONOVAN, C. M. 2002. Portal vein glucose sensing. *Diabetes Nutr Metab,* 15**,** 308-12; discussion 313-4.

DONOVAN, C. M., CANE, P. & BERGMAN, R. N. 1991a. Search for the hypoglycemia receptor using the local irrigation approach. *Adv Exp Med Biol,* 291**,** 185-96.

DONOVAN, C. M., HALTER, J. B. & BERGMAN, R. N. 1991b. Importance of hepatic glucoreceptors in sympathoadrenal response to hypoglycemia. *Diabetes,* 40**,** 155-8.

DONOVAN, C. M. & WATTS, A. G. 2014. Peripheral and central glucose sensing in hypoglycemic detection. *Physiology (Bethesda),* 29**,** 314-24.

DROSTE, S. K., DE GROOTE, L., ATKINSON, H. C., LIGHTMAN, S. L., REUL, J. M. & LINTHORST, A. C. 2008. Corticosterone levels in the brain show a distinct ultradian rhythm but a delayed response to forced swim stress. *Endocrinology,* 149**,** 3244-53.

DUNN, J. T., CRANSTON, I., MARSDEN, P. K., AMIEL, S. A. & REED, L. J. 2007. Attenuation of amydgala and frontal cortical responses to low blood glucose concentration in asymptomatic hypoglycemia in type 1 diabetes: a new player in hypoglycemia unawareness? *Diabetes,* 56**,** 2766-73.

ELSAAFIEN, K., KIRCHNER, M. K., MOHAMMED, M., EIKENBERRY, S. A., WEST, C., SCOTT, K. A., DE KLOET, A. D., STERN, J. E. & KRAUSE, E. G. 2021. Identification of Novel Cross-Talk between the Neuroendocrine and Autonomic Stress Axes Controlling Blood Pressure. *J Neurosci,* 41**,** 4641-4657.

ESLER, M. 2011. The sympathetic nervous system through the ages: from Thomas Willis to resistant hypertension. *Exp Physiol,* 96**,** 611-22.

EVANS, M. L., MCCRIMMON, R. J., FLANAGAN, D. E., KESHAVARZ, T., FAN, X., MCNAY, E. C., JACOB, R. J. & SHERWIN, R. S. 2004a. Hypothalamic ATP-sensitive K + channels play a key role in sensing hypoglycemia and triggering counterregulatory epinephrine and glucagon responses. *Diabetes,* 53**,** 2542-51.

EVANS, S. B., WILKINSON, C. W., BENTSON, K., GRONBECK, P., ZAVOSH, A. & FIGLEWICZ, D. P. 2001. PVN activation is suppressed by repeated hypoglycemia but not antecedent corticosterone in the rat. *Am J Physiol Regul Integr Comp Physiol,* 281**,** R1426-36.

EVANS, S. B., WILKINSON, C. W., GRONBECK, P., BENNETT, J. L., ZAVOSH, A., TABORSKY, G. J., JR. & FIGLEWICZ, D. P. 2004b. Inactivation of the DMH selectively inhibits the ACTH and corticosterone responses to hypoglycemia. *Am J Physiol Regul Integr Comp Physiol,* 286**,** R123-8.

FAN, X., DING, Y., BROWN, S., ZHOU, L., SHAW, M., VELLA, M. C., CHENG, H., MCNAY, E. C., SHERWIN, R. S. & MCCRIMMON, R. J. 2009. Hypothalamic AMP-activated protein kinase activation with AICAR amplifies counterregulatory responses to hypoglycemia in a rodent model of type 1 diabetes. *American Journal of Physiology-Regulatory, Integrative and Comparative Physiology,* 296**,** R1702-R1708.

FAN, X., DING, Y., CHENG, H., GRAM, D. X., SHERWIN, R. S. & MCCRIMMON, R. J. 2008. Amplified hormonal counterregulatory responses to hypoglycemia in rats after systemic delivery of a SUR-1-selective K(+) channel opener? *Diabetes,* 57**,** 3327-34.

FANELLI, C., PAMPANELLI, S., EPIFANO, L., RAMBOTTI, A. M., CIOFETTA, M., MODARELLI, F., DI VINCENZO, A., ANNIBALE, B., LEPORE, M., LALLI, C. & ET AL. 1994. Relative roles of insulin and hypoglycaemia on induction of neuroendocrine responses to, symptoms of, and deterioration of cognitive function in hypoglycaemia in male and female humans. *Diabetologia,* 37**,** 797-807.

FANELLI, C. G., EPIFANO, L., RAMBOTTI, A. M., PAMPANELLI, S., DI VINCENZO, A., MODARELLI, F., LEPORE, M., ANNIBALE, B., CIOFETTA, M., BOTTINI, P. & ET AL. 1993. Meticulous prevention of hypoglycemia normalizes the glycemic thresholds and magnitude of most of neuroendocrine responses to, symptoms of, and cognitive function during hypoglycemia in intensively treated patients with short-term IDDM. *Diabetes,* 42**,** 1683-9.

FARRELL, C. M. & MCCRIMMON, R. J. 2021. Clinical approaches to treat impaired awareness of hypoglycaemia. *Ther Adv Endocrinol Metab,* 12**,** 20420188211000248.

FARRELL, C. M., MCNEILLY, A. D., FOURNIER, P., JONES, T., HAPCA, S. M., WEST, D. & MCCRIMMON, R. J. 2020. A randomised controlled study of high intensity exercise as a dishabituating stimulus to improve hypoglycaemia awareness in people with type 1 diabetes: a proof-of-concept study. *Diabetologia,* 63**,** 853-863.

FEETHAM, C. H., O'BRIEN, F. & BARRETT-JOLLEY, R. 2018. Ion Channels in the Paraventricular Hypothalamic Nucleus (PVN); Emerging Diversity and Functional Roles. *Frontiers in Physiology,* 9.

FIGLEWICZ, D. P., VAN DIJK, G., WILKINSON, C. W., GRONBECK, P., HIGGINS, M. & ZAVOSH, A. 2002. Effects of repetitive hypoglycemia on neuroendocrine response and brain tyrosine hydroxylase activity in the rat. *Stress,* 5**,** 217-26.

FIORAMONTI, X., MARSOLLIER, N., SONG, Z., FAKIRA, K. A., PATEL, R. M., BROWN, S., DUPARC, T., PICA-MENDEZ, A., SANDERS, N. M., KNAUF, C., VALET, P., MCCRIMMON, R. J., BEUVE, A., MAGNAN, C. & ROUTH, V. H. 2010. Ventromedial Hypothalamic Nitric Oxide Production Is Necessary for Hypoglycemia Detection and Counterregulation. *Diabetes,* 59**,** 519-528.

FISHER, J. P. & PATON, J. F. R. 2012. The sympathetic nervous system and blood pressure in humans: implications for hypertension. *Journal of Human Hypertension,* 26**,** 463-475.

FLANAGAN, D. E., KESHAVARZ, T., EVANS, M. L., FLANAGAN, S., FAN, X., JACOB, R. J. & SHERWIN, R. S. 2003. Role of corticotrophin-releasing hormone in the impairment of counterregulatory responses to hypoglycemia. *Diabetes,* 52**,** 605-13.

FOSTER, N. N., AZAM, S. & WATTS, A. G. 2016. Rapid-onset hypoglycemia suppresses Fos expression in discrete parts of the ventromedial nucleus of the hypothalamus. *American Journal of Physiology - Regulatory, Integrative and Comparative Physiology,* 310**,** R1177-R1185.

FRIER, B. M. 2014a. Hypoglycaemia in diabetes mellitus: epidemiology and clinical implications. *Nat Rev Endocrinol,* 10**,** 711-22.

FRIER, B. M. 2014b. Impaired Awareness of Hypoglycaemia. *Hypoglycaemia in Clinical Diabetes.*

FRIER, B. M., JENSEN, M. M. & CHUBB, B. D. 2016. Hypoglycaemia in adults with insulin-treated diabetes in the UK: self-reported frequency and effects. *Diabetic Medicine,* 33**,** 1125-1132.

FRIER, B. M., SCHERNTHANER, G. & HELLER, S. R. 2011. Hypoglycemia and Cardiovascular Risks. *Diabetes Care,* 34**,** S132-S137.

FUJITA, S. & DONOVAN, C. M. 2005. Celiac-superior mesenteric ganglionectomy, but not vagotomy, suppresses the sympathoadrenal response to insulin-induced hypoglycemia. *Diabetes,* 54**,** 3258-64.

FUKUHARA, K., KVETNANSKY, R., CIZZA, G., PACAK, K., OHARA, H., GOLDSTEIN, D. S. & KOPIN, I. J. 1996. Interrelations between sympathoadrenal system and hypothalamo-pituitary-adrenocortical/thyroid systems in rats exposed to cold stress. *J Neuroendocrinol,* 8**,** 533-41.

FÜZESI, T., DAVIU, N., WAMSTEEKER CUSULIN, J. I., BONIN, R. P. & BAINS, J. S. 2016. Hypothalamic CRH neurons orchestrate complex behaviours after stress. *Nat Commun,* 7**,** 11937.

FUZESI, T., WITTMANN, G., LIPOSITS, Z., LECHAN, R. M. & FEKETE, C. 2007. Contribution of noradrenergic and adrenergic cell groups of the brainstem and agouti-related protein-synthesizing neurons of the arcuate nucleus to neuropeptide-y innervation of corticotropin-releasing hormone neurons in hypothalamic paraventricular nucleus of the rat. *Endocrinology,* 148**,** 5442-50.

GALASSETTI, P., MANN, S., TATE, D., NEILL, R. A., COSTA, F., WASSERMAN, D. H. & DAVIS, S. N. 2001. Effects of antecedent prolonged exercise on subsequent counterregulatory responses to hypoglycemia. *Am J Physiol Endocrinol Metab,* 280**,** E908-17.

GANDOLFI, D., CERRI, S., MAPELLI, J., POLIMENI, M., TRITTO, S., FUZZATI-ARMENTERO, M.-T., BIGIANI, A., BLANDINI, F., MAPELLI, L. & D'ANGELO, E. 2017. Activation of the CREB/c-Fos Pathway during Long-Term Synaptic Plasticity in the Cerebellum Granular Layer. *Frontiers in Cellular Neuroscience,* 11.

GAO, C., LENG, Y., MA, J., ROOKE, V., RODRIGUEZ-GONZALEZ, S., RAMAKRISHNAN, C., DEISSEROTH, K. & PENZO, M. A. 2020. Two genetically, anatomically and functionally distinct cell types segregate across anteroposterior axis of paraventricular thalamus. *Nat Neurosci,* 23**,** 217-228.

GAO, R., REN, L., ZHOU, Y., WANG, L., XIE, Y., ZHANG, M., LIU, X., KE, S., WU, K., ZHENG, J., LIU, X., CHEN, Z. & LIU, L. 2021. Recurrent non-severe hypoglycemia aggravates cognitive decline in diabetes and induces mitochondrial dysfunction in cultured astrocytes. *Mol Cell Endocrinol,* 526**,** 111192.

GARFIELD, A. S., SHAH, B. P., MADARA, J. C., BURKE, L. K., PATTERSON, C. M., FLAK, J., NEVE, R. L., EVANS, M. L., LOWELL, B. B., MYERS, M. G., JR. & HEISLER, L. K. 2014. A parabrachial-hypothalamic cholecystokinin neurocircuit controls counterregulatory responses to hypoglycemia. *Cell metabolism,* 20**,** 1030-1037.

GEDDES, J., SCHOPMAN, J. E., ZAMMITT, N. N. & FRIER, B. M. 2008. Prevalence of impaired awareness of hypoglycaemia in adults with Type 1 diabetes. *Diabet Med,* 25**,** 501-4.

GEERLING, J. C., SHIN, J.-W., CHIMENTI, P. C. & LOEWY, A. D. 2010. Paraventricular hypothalamic nucleus: axonal projections to the brainstem. *The Journal of comparative neurology,* 518**,** 1460-1499.

GEORGE, P. S., TAVENDALE, R., PALMER, C. N. & MCCRIMMON, R. J. 2015. Diazoxide improves hormonal counterregulatory responses to acute hypoglycemia in long-standing type 1 diabetes. *Diabetes,* 64**,** 2234-41.

GIMÉNEZ, M., GILABERT, R., MONTEAGUDO, J., ALONSO, A., CASAMITJANA, R., PARÉ, C. & CONGET, I. 2011. Repeated episodes of hypoglycemia as a potential aggravating factor for preclinical atherosclerosis in subjects with type 1 diabetes. *Diabetes care,* 34**,** 198-203.

GINGRICH, K. J. & BYRNE, J. H. 1985. Simulation of synaptic depression, posttetanic potentiation, and presynaptic facilitation of synaptic potentials from sensory neurons mediating gill-withdrawal reflex in Aplysia. *J Neurophysiol,* 53**,** 652-69.

GIROTTI, M., PACE, T. W. W., GAYLORD, R. I., RUBIN, B. A., HERMAN, J. P. & SPENCER, R. L. 2006. Habituation to repeated restraint stress is associated with lack of stress-induced c-fos expression in primary sensory processing areas of the rat brain. *Neuroscience,* 138**,** 1067-1081.

GOLD, A. E., MACLEOD, K. M. & FRIER, B. M. 1994. Frequency of Severe Hypoglycemia in Patients With Type I Diabetes With Impaired Awareness of Hypoglycemia. *Diabetes Care,* 17**,** 697-703.

GOLDBERG, J. I. & LUKOWIAK, K. 1984. Transfer of habituation in Aplysia: contribution of heterosynaptic pathways in habituation of the gill-withdrawal reflex. *J Neurobiol,* 15**,** 395-411.

GOLDMAN-RAKIC, P. S. 1995. Cellular basis of working memory. *Neuron,* 14**,** 477-85.

GOLDSTEIN, D. S. 2010. Adrenal responses to stress. *Cellular and molecular neurobiology,* 30**,** 1433-1440.

GÓMEZ-VALADÉS, A. G., POZO, M., VARELA, L., BOUDJADJA, M. B., RAMÍREZ, S., CHIVITE, I., EYRE, E., HADDAD-TÓVOLLI, R., OBRI, A., MILÀ-GUASCH, M., ALTIRRIBA, J., SCHNEEBERGER, M., IMBERNÓN, M., GARCIA-RENDUELES, A. R., GAMA-PEREZ, P., ROJO-RUIZ, J., RÁCZ, B., ALONSO, M. T., GOMIS, R., ZORZANO, A., D'AGOSTINO, G., ALVAREZ, C. V., NOGUEIRAS, R., GARCIA-ROVES, P. M., HORVATH, T. L. & CLARET, M. 2021. Mitochondrial cristae-remodeling protein OPA1 in POMC neurons couples Ca(2+) homeostasis with adipose tissue lipolysis. *Cell metabolism,* 33**,** 1820-1835.e9.

GRAVELING, A. J. & FRIER, B. M. 2009. Hypoglycaemia: an overview. *Prim Care Diabetes,* 3**,** 131-9.

GRIEBEL, G., SIMIAND, J., STEINBERG, R., JUNG, M., GULLY, D., ROGER, P., GESLIN, M., SCATTON, B., MAFFRAND, J. P. & SOUBRIE, P. 2002. 4-(2-Chloro-4-methoxy-5-methylphenyl)-N-[(1S)-2-cyclopropyl-1-(3-fluoro-4-methylphenyl)ethyl]5-methyl-N-(2-propynyl)-1, 3-thiazol-2-amine hydrochloride (SSR125543A), a potent and selective corticotrophin-releasing factor(1) receptor antagonist. II. Characterization in rodent models of stress-related disorders. *J Pharmacol Exp Ther,* 301**,** 333-45.

GRISSOM, N. & BHATNAGAR, S. 2009. Habituation to repeated stress: get used to it. *Neurobiology of learning and memory,* 92**,** 215-224.
GROVES, P. M. & THOMPSON, R. F. 1970. Habituation: a dual-process theory. *Psychol Rev,* 77**,** 419-50.
GRUETER, B. A., ROBISON, A. J., NEVE, R. L., NESTLER, E. J. & MALENKA, R. C. 2013. ΔFosB differentially modulates nucleus accumbens direct and indirect pathway function. *Proceedings of the National Academy of Sciences,* 110**,** 1923-1928.
GUNGOR, N. Z. & PARÉ, D. 2016. Functional Heterogeneity in the Bed Nucleus of the Stria Terminalis. *The Journal of neuroscience : the official journal of the Society for Neuroscience,* 36**,** 8038-8049.
HAN, J., PLUHACKOVA, K. & BÖCKMANN, R. A. 2017. The Multifaceted Role of SNARE Proteins in Membrane Fusion. *Frontiers in Physiology,* 8.
HARADA, K., KAMIYA, T. & TSUBOI, T. 2016. Gliotransmitter release from astrocytes: functional, developmental and pathological implications in the brain. *Frontiers in Neuroscience,* 9.
HAWKINS, R. D., COHEN, T. E. & KANDEL, E. R. 2006. Dishabituation in Aplysia can involve either reversal of habituation or superimposed sensitization. *Learning & memory (Cold Spring Harbor, N.Y.),* 13**,** 397-403.
HELLER, S. R. 2002. Abnormalities of the electrocardiogram during hypoglycaemia: the cause of the dead in bed syndrome? *Int J Clin Pract Suppl***,** 27-32.
HELLER, S. R. & CRYER, P. E. 1991. Reduced neuroendocrine and symptomatic responses to subsequent hypoglycemia after 1 episode of hypoglycemia in nondiabetic humans. *Diabetes,* 40**,** 223-6.
HENRIKSEN, M. M., ANDERSEN, H. U., THORSTEINSSON, B. & PEDERSEN-BJERGAARD, U. 2018. Hypoglycemic Exposure and Risk of Asymptomatic Hypoglycemia in Type 1 Diabetes Assessed by Continuous Glucose Monitoring. *J Clin Endocrinol Metab,* 103**,** 2329-2335.
HENRY, P. G., CRIEGO, A. B., KUMAR, A. & SEAQUIST, E. R. 2010. Measurement of cerebral oxidative glucose consumption in patients with type 1 diabetes mellitus and hypoglycemia unawareness using (13)C nuclear magnetic resonance spectroscopy. *Metabolism,* 59**,** 100-6.
HERMAN, J. 2013. Neural control of chronic stress adaptation. *Frontiers in Behavioral Neuroscience,* 7.
HERMAN, J. P. & MUELLER, N. K. 2006. Role of the ventral subiculum in stress integration. *Behavioural Brain Research,* 174**,** 215-224.
HERMAN, J. P. & TASKER, J. G. 2016. Paraventricular Hypothalamic Mechanisms of Chronic Stress Adaptation. *Frontiers in Endocrinology,* 7**,** 137.
HERMAN, J. P., TASKER, J. G., ZIEGLER, D. R. & CULLINAN, W. E. 2002. Local circuit regulation of paraventricular nucleus stress integration: Glutamate–GABA connections. *Pharmacology Biochemistry and Behavior,* 71**,** 457-468.
HERZOG, R. I., CHAN, O., YU, S., DZIURA, J., MCNAY, E. C. & SHERWIN, R. S. 2008. Effect of acute and recurrent hypoglycemia on changes in brain glycogen concentration. *Endocrinology,* 149**,** 1499-1504.
HERZOG, R. I., JIANG, L., HERMAN, P., ZHAO, C., SANGANAHALLI, B. G., MASON, G. F., HYDER, F., ROTHMAN, D. L., SHERWIN, R. S. & BEHAR, K. L. 2013. Lactate preserves neuronal metabolism and function following antecedent recurrent hypoglycemia. *J Clin Invest,* 123**,** 1988-98.
HEVENER, A. L., BERGMAN, R. N. & DONOVAN, C. M. 2000. Portal vein afferents are critical for the sympathoadrenal response to hypoglycemia. *Diabetes,* 49**,** 8-12.
HEYDENDAEL, W., SHARMA, K., IYER, V., LUZ, S., PIEL, D., BECK, S. & BHATNAGAR, S. 2011. Orexins/Hypocretins Act in the Posterior Paraventricular Thalamic Nucleus During Repeated Stress to Regulate Facilitation to Novel Stress. *Endocrinology,* 152**,** 4738-4752.
HOFFMAN, A. N., LORSON, N. G., SANABRIA, F., FOSTER OLIVE, M. & CONRAD, C. D. 2014. Chronic stress disrupts fear extinction and enhances amygdala and

hippocampal Fos expression in an animal model of post-traumatic stress disorder. *Neurobiology of Learning and Memory,* 112**,** 139-147.
HOFFMAN, G. E., SMITH, M. S. & VERBALIS, J. G. 1993. c-Fos and related immediate early gene products as markers of activity in neuroendocrine systems. *Front Neuroendocrinol,* 14**,** 173-213.
HSU, D. T., KIROUAC, G. J., ZUBIETA, J. K. & BHATNAGAR, S. 2014. Contributions of the paraventricular thalamic nucleus in the regulation of stress, motivation, and mood. *Front Behav Neurosci,* 8**,** 73.
HURST, P., GARFIELD, A. S., MARROW, C., HEISLER, L. K. & EVANS, M. L. 2012. Recurrent Hypoglycemia Is Associated with Loss of Activation in Rat Brain Cingulate Cortex. *Endocrinology,* 153**,** 1908-1914.
IKEMATSU, N., DALLAS, M. L., ROSS, F. A., LEWIS, R. W., RAFFERTY, J. N., DAVID, J. A., SUMAN, R., PEERS, C., HARDIE, D. G. & EVANS, A. M. 2011. Phosphorylation of the voltage-gated potassium channel Kv2. 1 by AMP-activated protein kinase regulates membrane excitability. *Proceedings of the National Academy of Sciences,* 108**,** 18132-18137.
INKSTER, B. & FRIER, B. M. 2012. The effects of acute hypoglycaemia on cognitive function in type 1 diabetes. *The British Journal of Diabetes & Vascular Disease,* 12**,** 221-226.
INOUYE, K. E., YUE, J. T., CHAN, O., KIM, T., AKIRAV, E. M., PARK, E., RIDDELL, M. C., BURDETT, E., MATTHEWS, S. G. & VRANIC, M. 2006. Effects of insulin treatment without and with recurrent hypoglycemia on hypoglycemic counterregulation and adrenal catecholamine-synthesizing enzymes in diabetic rats. *Endocrinology,* 147**,** 1860-70.
IQBAL, A. & HELLER, S. R. 2018. The role of structured education in the management of hypoglycaemia. *Diabetologia,* 61**,** 751-760.
JACOBSON, A. M., MUSEN, G., RYAN, C. M., SILVERS, N., CLEARY, P., WABERSKI, B., BURWOOD, A., WEINGER, K., BAYLESS, M., DAHMS, W. & HARTH, J. 2007. Long-term effect of diabetes and its treatment on cognitive function. *N Engl J Med,* 356**,** 1842-52.
JACOBSON, L., ANSARI, T. & MCGUINNESS, O. P. 2006. Counterregulatory deficits occur within 24 h of a single hypoglycemic episode in conscious, unrestrained, chronically cannulated mice. *Am J Physiol Endocrinol Metab,* 290**,** E678-84.
JACOBSON, L., MUGLIA, L. J., WENINGER, S. C., PACAK, K. & MAJZOUB, J. A. 2000. CRH deficiency impairs but does not block pituitary-adrenal responses to diverse stressors. *Neuroendocrinology,* 71**,** 79-87.
JAFERI, A. & BHATNAGAR, S. 2006. Corticosterone Can Act at the Posterior Paraventricular Thalamus to Inhibit Hypothalamic-Pituitary-Adrenal Activity in Animals that Habituate to Repeated Stress. *Endocrinology,* 147**,** 4917-4930.
JAFERI, A., NOWAK, N. & BHATNAGAR, S. 2003. Negative feedback functions in chronically stressed rats: role of the posterior paraventricular thalamus. *Physiology & Behavior,* 78**,** 365-373.
JANSEN, A. S., HOFFMAN, J. L. & LOEWY, A. D. 1997. CNS sites involved in sympathetic and parasympathetic control of the pancreas: a viral tracing study. *Brain Res,* 766**,** 29-38.
JIA, S. & MIFFLIN, S. 2017. Corticotropin-Releasing Hormone Regulates Spontaneous Excitatory Postsynaptic Currents on the Nucleus of the Solitary Tract. *The FASEB Journal,* 31**,** 861.10-861.10.
JIANG, L., HERZOG, R. I., MASON, G. F., DE GRAAF, R. A., ROTHMAN, D. L., SHERWIN, R. S. & BEHAR, K. L. 2009. Recurrent antecedent hypoglycemia alters neuronal oxidative metabolism in vivo. *Diabetes,* 58**,** 1266-74.
JIANG, Z., RAJAMANICKAM, S. & JUSTICE, N. J. 2018. Local Corticotropin-Releasing Factor Signaling in the Hypothalamic Paraventricular Nucleus. *J Neurosci,* 38**,** 1874-1890.
JIANG, Z., RAJAMANICKAM, S. & JUSTICE, N. J. 2019. CRF signaling between neurons in the paraventricular nucleus of the hypothalamus (PVN) coordinates stress responses. *Neurobiol Stress,* 11**,** 100192.

KAKALL, Z. M., KAVURMA, M. M., COHEN, E. M., HOWE, P. R., NEDOBOY, P. E. & PILOWSKY, P. M. 2019. Repetitive hypoglycemia reduces activation of glucose-responsive neurons in C1 and C3 medullary brain regions to subsequent hypoglycemia. *American Journal of Physiology-Endocrinology and Metabolism,* 317**,** E388-E398.

KALSBEEK, A., LA FLEUR, S., VAN HEIJNINGEN, C. & BUIJS, R. M. 2004. Suprachiasmatic GABAergic inputs to the paraventricular nucleus control plasma glucose concentrations in the rat via sympathetic innervation of the liver. *J Neurosci,* 24**,** 7604-13.

KAMITAKAHARA, A., XU, B. & SIMERLY, R. 2016. Ventromedial hypothalamic expression of Bdnf is required to establish normal patterns of afferent GABAergic connectivity and responses to hypoglycemia. *Mol Metab,* 5**,** 91-101.

KANDEL, E. R., SCHWARTZ, J. H., JESSELL, T. M., SIEGELBAUM, S., HUDSPETH, A. J. & MACK, S. 2000. *Principles of neural science*, McGraw-hill New York.

KANG, L., SANDERS, N. M., DUNN-MEYNELL, A. A., GASPERS, L. D., ROUTH, V. H., THOMAS, A. P. & LEVIN, B. E. 2008. Prior hypoglycemia enhances glucose responsiveness in some ventromedial hypothalamic glucosensing neurons. *Am J Physiol Regul Integr Comp Physiol,* 294**,** R784-92.

KAPLAN, G. B., LEITE-MORRIS, K. A., FAN, W., YOUNG, A. J. & GUY, M. D. 2011. Opiate Sensitization Induces FosB/ΔFosB Expression in Prefrontal Cortical, Striatal and Amygdala Brain Regions. *PLOS ONE,* 6**,** e23574.

KEIFER, O. P., HURT, R. C., RESSLER, K. J. & MARVAR, P. J. 2015. The Physiology of Fear: Reconceptualizing the Role of the Central Amygdala in Fear Learning. *Physiology,* 30**,** 389-401.

KENNAN, R. P., TAKAHASHI, K., PAN, C., SHAMOON, H. & PAN, J. W. 2005. Human cerebral blood flow and metabolism in acute insulin-induced hypoglycemia. *J Cereb Blood Flow Metab,* 25**,** 527-34.

KERMAN, I. A., BERNARD, R., ROSENTHAL, D., BEALS, J., AKIL, H. & WATSON, S. J. 2007. Distinct populations of presympathetic-premotor neurons express orexin or melanin-concentrating hormone in the rat lateral hypothalamus. *J Comp Neurol,* 505**,** 586-601.

KERMAN, I. A., ENQUIST, L. W., WATSON, S. J. & YATES, B. J. 2003. Brainstem substrates of sympatho-motor circuitry identified using trans-synaptic tracing with pseudorabies virus recombinants. *J Neurosci,* 23**,** 4657-66.

KHODAI, T., NUNN, N., WORTH, A. A., FEETHAM, C. H., BELLE, M. D. C., PIGGINS, H. D. & LUCKMAN, S. M. 2018. PACAP Neurons in the Ventromedial Hypothalamic Nucleus Are Glucose Inhibited and Their Selective Activation Induces Hyperglycaemia. *Front Endocrinol (Lausanne),* 9**,** 632.

KIM, A., KNUDSEN, J. G., MADARA, J. C., BENRICK, A., HILL, T., ABDUL KADIR, L., KELLARD, J. A., MELLANDER, L., MIRANDA, C., LIN, H., JAMES, T., SUBA, K., SPIGELMAN, A. F., WU, Y., MACDONALD, P. E., WERNSTEDT ASTERHOLM, I., MAGNUSSEN, T., CHRISTENSEN, M., VISBOLL, T., SALEM, V., KNOP, F. K., RORSMAN, P., LOWELL, B. B. & BRIANT, L. J. B. 2021. Arginine-vasopressin mediates counter-regulatory glucagon release and is diminished in type 1 diabetes. *bioRxiv***,** 2020.01.30.927426.

KIM, J., LEE, S., FANG, Y. Y., SHIN, A., PARK, S., HASHIKAWA, K., BHAT, S., KIM, D., SOHN, J. W., LIN, D. & SUH, G. S. B. 2019a. Rapid, biphasic CRF neuronal responses encode positive and negative valence. *Nat Neurosci,* 22**,** 576-585.

KIM, J. S., HAN, S. Y. & IREMONGER, K. J. 2019b. Stress experience and hormone feedback tune distinct components of hypothalamic CRH neuron activity. *Nature Communications,* 10**,** 5696.

KIM, J. S. & IREMONGER, K. J. 2019. Temporally Tuned Corticosteroid Feedback Regulation of the Stress Axis. *Trends Endocrinol Metab,* 30**,** 783-792.

KINSLEY, B. T., WEINGER, K., BAJAJ, M., LEVY, C. J., SIMONSON, D. C., QUIGLEY, M., COX, D. J. & JACOBSON, A. M. 1999. Blood glucose awareness training and epinephrine responses to hypoglycemia during intensive treatment in type 1 diabetes. *Diabetes Care,* 22**,** 1022-1028.

KINSLEY, B. T., WIDOM, B., UTZSCHNEIDER, K. & SIMONSON, D. C. 1994. Stimulus specificity of defects in counterregulatory hormone secretion in insulin-dependent diabetes mellitus: effect of glycemic control. *J Clin Endocrinol Metab,* 79**,** 1383-9.
KIROUAC, G. J. 2015. Placing the paraventricular nucleus of the thalamus within the brain circuits that control behavior. *Neurosci Biobehav Rev,* 56**,** 315-29.
KLEIBER, M. 1947. Body size and metabolic rate. *Physiological Reviews,* 27**,** 511-541.
KNIGHT, W. D., LITTLE, J. T., CARRENO, F. R., TONEY, G. M., MIFFLIN, S. W. & CUNNINGHAM, J. T. 2011. Chronic intermittent hypoxia increases blood pressure and expression of FosB/DeltaFosB in central autonomic regions. *American journal of physiology. Regulatory, integrative and comparative physiology,* 301**,** R131-R139.
KONG, D., VONG, L., PARTON, L. E., YE, C., TONG, Q., HU, X., CHOI, B., BRÜNING, J. C. & LOWELL, B. B. 2010. Glucose stimulation of hypothalamic MCH neurons involves K ATP channels, is modulated by UCP2, and regulates peripheral glucose homeostasis. *Cell metabolism,* 12**,** 545-552.
KORZON-BURAKOWSKA, A., HOPKINS, D., MATYKA, K., LOMAS, J., PERNET, A., MACDONALD, I. & AMIEL, S. 1998. Effects of glycemic control on protective responses against hypoglycemia in type 2 diabetes. *Diabetes Care,* 21**,** 283-90.
KOVÁCS, L. Á., BERTA, G., CSERNUS, V., UJVÁRI, B., FÜREDI, N. & GASZNER, B. 2019. Corticotropin-Releasing Factor-Producing Cells in the Paraventricular Nucleus of the Hypothalamus and Extended Amygdala Show Age-Dependent FOS and FOSB/DeltaFOSB Immunoreactivity in Acute and Chronic Stress Models in the Rat. *Frontiers in Aging Neuroscience,* 11.
KOWALSKI, G. M. & BRUCE, C. R. 2014. The regulation of glucose metabolism: implications and considerations for the assessment of glucose homeostasis in rodents. *American Journal of Physiology-Endocrinology and Metabolism,* 307**,** E859-E871.
KOYAMA, Y., COKER, R. H., STONE, E. E., LACY, D. B., JABBOUR, K., WILLIAMS, P. E. & WASSERMAN, D. H. 2000. Evidence that carotid bodies play an important role in glucoregulation in vivo. *Diabetes,* 49**,** 1434-42.
KROUT, K. E., BELZER, R. E. & LOEWY, A. D. 2002. Brainstem projections to midline and intralaminar thalamic nuclei of the rat. *J Comp Neurol,* 448**,** 53-101.
KUMAGAI, H., OSHIMA, N., MATSUURA, T., IIGAYA, K., IMAI, M., ONIMARU, H., SAKATA, K., OSAKA, M., ONAMI, T., TAKIMOTO, C., KAMAYACHI, T., ITOH, H. & SARUTA, T. 2012. Importance of rostral ventrolateral medulla neurons in determining efferent sympathetic nerve activity and blood pressure. *Hypertension Research,* 35**,** 132-141.
KUPERMAN, Y., WEISS, M., DINE, J., STAIKIN, K., GOLANI, O., RAMOT, A., NAHUM, T., KUHNE, C., SHEMESH, Y., WURST, W., HARMELIN, A., DEUSSING, J. M., EDER, M. & CHEN, A. 2016. CRFR1 in AgRP Neurons Modulates Sympathetic Nervous System Activity to Adapt to Cold Stress and Fasting. *Cell Metab,* 23**,** 1185-1199.
KURAMOTO, N., WILKINS, M. E., FAIRFAX, B. P., REVILLA-SANCHEZ, R., TERUNUMA, M., TAMAKI, K., IEMATA, M., WARREN, N., COUVE, A. & CALVER, A. 2007. Phospho-dependent functional modulation of GABAB receptors by the metabolic sensor AMP-dependent protein kinase. *Neuron,* 53**,** 233-247.
LABOUEBE, G., BOUTREL, B., TARUSSIO, D. & THORENS, B. 2016. Glucose-responsive neurons of the paraventricular thalamus control sucrose-seeking behavior. *Nat Neurosci,* 19**,** 999-1002.
LAMY, C. M., SANNO, H., LABOUEBE, G., PICARD, A., MAGNAN, C., CHATTON, J. Y. & THORENS, B. 2014. Hypoglycemia-activated GLUT2 neurons of the nucleus tractus solitarius stimulate vagal activity and glucagon secretion. *Cell Metab,* 19**,** 527-38.
LAWTON, J., RANKIN, D., ELLIOTT, J., HELLER, S. R., ROGERS, H. A., DE ZOYSA, N. & AMIEL, S. 2014. Experiences, views, and support needs of family

members of people with hypoglycemia unawareness: interview study. *Diabetes Care,* 37**,** 109-15.
LEDERGERBER, D. & MOSER, E. I. 2017. Memory Retrieval: Taking the Route via Subiculum. *Current Biology,* 27**,** R1225-R1227.
LEE, J. G., CHOI, I. S., PARK, E. J., CHO, J. H., LEE, M. G., CHOI, B. J. & JANG, I. S. 2007. beta(2)-Adrenoceptor-mediated facilitation of glutamatergic transmission in rat ventromedial hypothalamic neurons. *Neuroscience,* 144**,** 1255-65.
LEE, J. S., LEE, E. Y. & LEE, H. S. 2015. Hypothalamic, feeding/arousal-related peptidergic projections to the paraventricular thalamic nucleus in the rat. *Brain Res,* 1598**,** 97-113.
LEE, S. K., RYU, P. D. & LEE, S. Y. 2013. Differential distributions of neuropeptides in hypothalamic paraventricular nucleus neurons projecting to the rostral ventrolateral medulla in the rat. *Neurosci Lett,* 556**,** 160-5.
LEE, S. P., YEOH, L., HARRIS, N. D., DAVIES, C. M., ROBINSON, R. T., LEATHARD, A., NEWMAN, C., MACDONALD, I. A. & HELLER, S. R. 2004. Influence of autonomic neuropathy on QTc interval lengthening during hypoglycemia in type 1 diabetes. *Diabetes,* 53**,** 1535-1542.
LI, A.-J., WANG, Q., ELSARELLI, M. M., BROWN, R. L. & RITTER, S. 2015. Hindbrain Catecholamine Neurons Activate Orexin Neurons During Systemic Glucoprivation in Male Rats. *Endocrinology,* 156**,** 2807-2820.
LI, A.-J., WANG, Q. & RITTER, S. 2018. Selective Pharmacogenetic Activation of Catecholamine Subgroups in the Ventrolateral Medulla Elicits Key Glucoregulatory Responses. *Endocrinology,* 159**,** 341-355.
LI, C., NAVARRETE, J., LIANG-GUALLPA, J., LU, C., FUNDERBURK, S. C., CHANG, R. B., LIBERLES, S. D., OLSON, D. P. & KRASHES, M. J. 2019. Defined Paraventricular Hypothalamic Populations Exhibit Differential Responses to Food Contingent on Caloric State. *Cell Metab,* 29**,** 681-694.e5.
LI, S. & KIROUAC, G. J. 2008. Projections from the paraventricular nucleus of the thalamus to the forebrain, with special emphasis on the extended amygdala. *J Comp Neurol,* 506**,** 263-87.
LI, S. & KIROUAC, G. J. 2012. Sources of inputs to the anterior and posterior aspects of the paraventricular nucleus of the thalamus. *Brain Structure and Function,* 217**,** 257-273.
LI, W.-C., SOFFE, S. R., WOLF, E. & ROBERTS, A. 2006. Persistent Responses to Brief Stimuli: Feedback Excitation among Brainstem Neurons. *The Journal of Neuroscience,* 26**,** 4026-4035.
LI, Y., LIU, Z., GUO, Q. & LUO, M. 2019b. Long-term Fiber Photometry for Neuroscience Studies. *Neuroscience bulletin,* 35**,** 425-433.
LINGENFELSER, T., OVERKAMP, D., RENN, W., BUETTNER, U., KIMMERLE, K., SCHMALFUSS, A. & JAKOBER, B. 1996. Insulin-associated modulation of neuroendocrine counterregulation, hypoglycemia perception, and cerebral function in insulin-dependent diabetes mellitus: evidence for an intrinsic effect of insulin on the central nervous system. *J Clin Endocrinol Metab,* 81**,** 1197-205.
LINGENFELSER, T., RENN, W., SOMMERWERCK, U., JUNG, M. F., BUETTNER, U. W., ZAISER-KASCHEL, H., KASCHEL, R., EGGSTEIN, M. & JAKOBER, B. 1993. Compromised Hormonal Counterregulation, Symptom Awareness, and Neurophysiological Function After Recurrent Short-Term Episodes of Insulin-Induced Hypoglycemia in IDDM Patients. *Diabetes,* 42**,** 610-618.
LOBO, M. K., ZAMAN, S., DAMEZ-WERNO, D. M., KOO, J. W., BAGOT, R. C., DINIERI, J. A., NUGENT, A., FINKEL, E., CHAUDHURY, D., CHANDRA, R., RIBERIO, E., RABKIN, J., MOUZON, E., CACHOPE, R., CHEER, J. F., HAN, M. H., DIETZ, D. M., SELF, D. W., HURD, Y. L., VIALOU, V. & NESTLER, E. J. 2013. DeltaFosB induction in striatal medium spiny neuron subtypes in response to chronic pharmacological, emotional, and optogenetic stimuli. *J Neurosci,* 33**,** 18381-95.

LÓPEZ-BENDITO, G., STURGESS, K., ERDÉLYI, F., SZABÓ, G., MOLNÁR, Z. & PAULSEN, O. 2004. Preferential Origin and Layer Destination of GAD65-GFP Cortical Interneurons. *Cerebral Cortex,* 14**,** 1122-1133.

LUITEN, P. G., TER HORST, G. J., KARST, H. & STEFFENS, A. B. 1985. The course of paraventricular hypothalamic efferents to autonomic structures in medulla and spinal cord. *Brain Res,* 329**,** 374-8.

LUK, A. O., HO, T. S., LAU, E. S., KO, G. T., OZAKI, R., TSANG, C. C., KONG, A. P., MA, R. C., SO, W. Y., CHOW, F. C. & CHAN, J. C. 2016. Association of self-reported recurrent mild hypoglycemia with incident cardiovascular disease and all-cause mortality in patients with type 2 diabetes: Prospective analysis of the Joint Asia Diabetes Evaluation Registry. *Medicine (Baltimore),* 95**,** e5183.

LY, T. T., ANDERSON, M., MCNAMARA, K. A., DAVIS, E. A. & JONES, T. W. 2011. Neurocognitive outcomes in young adults with early-onset type 1 diabetes: a prospective follow-up study. *Diabetes Care,* 34**,** 2192-7.

MA, X. M., LEVY, A. & LIGHTMAN, S. L. 1997. Emergence of an isolated arginine vasopressin (AVP) response to stress after repeated restraint: a study of both AVP and corticotropin-releasing hormone messenger ribonucleic acid (RNA) and heteronuclear RNA. *Endocrinology,* 138**,** 4351-7.

MA, Y., WANG, Q., JOE, D., WANG, M. & WHIM, M. D. 2018. Recurrent hypoglycemia inhibits the counterregulatory response by suppressing adrenal activity. *The Journal of Clinical Investigation,* 128**,** 3866-3871.

MAGGS, D. G. & SHERWIN, R. S. 1997. Mechanisms of the Sympathoadrenal Response to Hypoglycemia. *In:* GOLDSTEIN, D. S., EISENHOFER, G. & MCCARTY, R. (eds.) *Advances in Pharmacology.* Academic Press.

MALMGREN, S. & AHRÉN, B. 2015. Deciphering the Hypoglycemic Glucagon Response: Development of a Graded Hyperinsulinemic Hypoglycemic Clamp Technique in Female Mice. *Endocrinology,* 156**,** 3866-3871.

MANDELBLAT-CERF, Y., RAMESH, R. N., BURGESS, C. R., PATELLA, P., YANG, Z., LOWELL, B. B. & ANDERMANN, M. L. 2015. Arcuate hypothalamic AgRP and putative POMC neurons show opposite changes in spiking across multiple timescales. *Elife,* 4.

MARTY, N., DALLAPORTA, M. & THORENS, B. 2007. Brain glucose sensing, counterregulation, and energy homeostasis. *Physiology (Bethesda),* 22**,** 241-51.

MCAULAY, V., DEARY, I. J. & FRIER, B. M. 2001. Symptoms of hypoglycaemia in people with diabetes. *Diabet Med,* 18**,** 690-705.

MCCRIMMON, R. J. 2017. RD Lawrence Lecture 2015 Old habits are hard to break: lessons from the study of hypoglycaemia. *Diabet Med,* 34**,** 148-155.

MCCRIMMON, R. J., EVANS, M. L., FAN, X., MCNAY, E. C., CHAN, O., DING, Y., ZHU, W., GRAM, D. X. & SHERWIN, R. S. 2005. Activation of ATP-sensitive K+ channels in the ventromedial hypothalamus amplifies counterregulatory hormone responses to hypoglycemia in normal and recurrently hypoglycemic rats. *Diabetes,* 54**,** 3169-74.

MCCRIMMON, R. J., FAN, X., CHENG, H., MCNAY, E., CHAN, O., SHAW, M., DING, Y., ZHU, W. & SHERWIN, R. S. 2006a. Activation of AMP-activated protein kinase within the ventromedial hypothalamus amplifies counterregulatory hormone responses in rats with defective counterregulation. *Diabetes,* 55**,** 1755-60.

MCCRIMMON, R. J., SHAW, M., FAN, X., CHENG, H., DING, Y., VELLA, M. C., ZHOU, L., MCNAY, E. C. & SHERWIN, R. S. 2008. Key role for AMP-activated protein kinase in the ventromedial hypothalamus in regulating counterregulatory hormone responses to acute hypoglycemia. *Diabetes,* 57**,** 444-50.

MCCRIMMON, R. J., SONG, Z., CHENG, H., MCNAY, E. C., WEIKART-YECKEL, C., FAN, X., ROUTH, V. H. & SHERWIN, R. S. 2006b. Corticotrophin-releasing factor receptors within the ventromedial hypothalamus regulate hypoglycemia-induced hormonal counterregulation. *J Clin Invest,* 116**,** 1723-30.

MCNAY, E. 2015. Recurrent Hypoglycemia Increases Anxiety and Amygdala Norepinephrine Release During Subsequent Hypoglycemia. *Frontiers in endocrinology,* 6**,** 175-175.
MCNAY, E. C., WILLIAMSON, A., MCCRIMMON, R. J. & SHERWIN, R. S. 2006. Cognitive and neural hippocampal effects of long-term moderate recurrent hypoglycemia. *Diabetes,* 55**,** 1088-95.
MCNEILLY, A. D., GALLAGHER, J. R., DINKOVA-KOSTOVA, A. T., HAYES, J. D., SHARKEY, J., ASHFORD, M. L. J. & MCCRIMMON, R. J. 2016. Nrf2-Mediated Neuroprotection Against Recurrent Hypoglycemia Is Insufficient to Prevent Cognitive Impairment in a Rodent Model of Type 1 Diabetes. *Diabetes,* 65**,** 3151-3160.
MCNEILLY, A. D., GALLAGHER, J. R., HUANG, J. T.-J., ASHFORD, M. L. J. & MCCRIMMON, R. J. 2017a. High-Intensity Exercise as a Dishabituating Stimulus Restores Counterregulatory Responses in Recurrently Hypoglycemic Rodents. *Diabetes,* 66**,** 1696-1702.
MCNEILLY, A. D. & MCCRIMMON, R. J. 2018. Impaired hypoglycaemia awareness in type 1 diabetes: lessons from the lab. *Diabetologia,* 61**,** 743-750.
MEEK, T. H., NELSON, J. T., MATSEN, M. E., DORFMAN, M. D., GUYENET, S. J., DAMIAN, V., ALLISON, M. B., SCARLETT, J. M., NGUYEN, H. T., THALER, J. P., OLSON, D. P., MYERS, M. G., JR., SCHWARTZ, M. W. & MORTON, G. J. 2016a. Functional identification of a neurocircuit regulating blood glucose. *Proceedings of the National Academy of Sciences of the United States of America,* 113**,** E2073-E2082.
MILNER, T. A., REIS, D. J., PICKEL, V. M., AICHER, S. A. & GIULIANO, R. 1993. Ultrastructural localization and afferent sources of corticotropin-releasing factor in the rat rostral ventrolateral medulla: implications for central cardiovascular regulation. *J Comp Neurol,* 333**,** 151-67.
MOGA, M. M., WEIS, R. P. & MOORE, R. Y. 1995. Efferent projections of the paraventricular thalamic nucleus in the rat. *J Comp Neurol,* 359**,** 221-38.
MOHEET, A., EMIR, U. E., TERPSTRA, M., KUMAR, A., EBERLY, L. E., SEAQUIST, E. R. & OZ, G. 2014a. Initial experience with seven tesla magnetic resonance spectroscopy of hypothalamic GABA during hyperinsulinemic euglycemia and hypoglycemia in healthy humans. *Magn Reson Med,* 71**,** 12-8.
MOHEET, A., KUMAR, A., EBERLY, L. E., KIM, J., ROBERTS, R. & SEAQUIST, E. R. 2014b. Hypoglycemia-Associated Autonomic Failure in Healthy Humans: Comparison of Two vs Three Periods of Hypoglycemia on Hypoglycemia-Induced Counterregulatory and Symptom Response 5 Days Later. *The Journal of Clinical Endocrinology & Metabolism,* 99**,** 664-670.
MOKAN, M., MITRAKOU, A., VENEMAN, T., RYAN, C., KORYTKOWSKI, M., CRYER, P. & GERICH, J. 1994. Hypoglycemia unawareness in IDDM. *Diabetes Care,* 17**,** 1397-403.
MORGAN, J. I. & CURRAN, T. 1991. Stimulus-transcription coupling in the nervous system: involvement of the inducible proto-oncogenes fos and jun. *Annu Rev Neurosci,* 14**,** 421-51.
MORILAK, D. A., FORNAL, C. A. & JACOBS, B. L. 1987. Effects of physiological manipulations on locus coeruleus neuronal activity in freely moving cats. III. Glucoregulatory challenge. *Brain Res,* 422**,** 32-9.
MUNDINGER, T. O., MEI, Q., FIGLEWICZ, D. P., LERNMARK, A. & TABORSKY, G. J., JR. 2003. Impaired glucagon response to sympathetic nerve stimulation in the BB diabetic rat: effect of early sympathetic islet neuropathy. *Am J Physiol Endocrinol Metab,* 285**,** E1047-54.
MURPHY, B. A., FAKIRA, K. A., SONG, Z., BEUVE, A. & ROUTH, V. H. 2009. AMP-activated protein kinase and nitric oxide regulate the glucose sensitivity of ventromedial hypothalamic glucose-inhibited neurons. *American Journal of Physiology-Cell Physiology,* 297**,** C750-C758.

NESTLER, E. J., BARROT, M. & SELF, D. W. 2001. ΔFosB: A sustained molecular switch for addiction. *Proceedings of the National Academy of Sciences,* 98**,** 11042-11046.
NIIMI, M., SATO, M., TAMAKI, M., WADA, Y., TAKAHARA, J. & KAWANISHI, K. 1995. Induction of Fos protein in the rat hypothalamus elicited by insulin-induced hypoglycemia. *Neurosci Res,* 23**,** 361-4.
NONOGAKI, K. 2000. New insights into sympathetic regulation of glucose and fat metabolism. *Diabetologia,* 43**,** 533-49.
NUNN, N., WOMACK, M., DART, C. & BARRETT-JOLLEY, R. 2011. Function and pharmacology of spinally-projecting sympathetic pre-autonomic neurones in the paraventricular nucleus of the hypothalamus. *Curr Neuropharmacol,* 9**,** 262-77.
NWOKOLO, M., AMIEL, S. A., O'DALY, O., BYRNE, M. L., WILSON, B. M., PERNET, A., CORDON, S. M., MACDONALD, I. A., ZELAYA, F. O. & CHOUDHARY, P. 2019a. Hypoglycemic thalamic activation in type 1 diabetes is associated with preserved symptoms despite reduced epinephrine. *J Cereb Blood Flow Metab***,** 271678x19842680.
NWOKOLO, M., AMIEL, S. A., O'DALY, O., BYRNE, M. L., WILSON, B. M., PERNET, A., CORDON, S. M., MACDONALD, I. A., ZELAYA, F. O. & CHOUDHARY, P. 2019b. Impaired Awareness of Hypoglycemia Disrupts Blood Flow to Brain Regions Involved in Arousal and Decision Making in Type 1 Diabetes. *Diabetes Care*.
OHNISHI, Y. N., OHNISHI, Y. H., HOKAMA, M., NOMARU, H., YAMAZAKI, K., TOMINAGA, Y., SAKUMI, K., NESTLER, E. J. & NAKABEPPU, Y. 2011. FosB is essential for the enhancement of stress tolerance and antagonizes locomotor sensitization by ΔFosB. *Biological psychiatry,* 70**,** 487-495.
ORBAN, B. O., ROUTH, V. H., LEVIN, B. E. & BERLIN, J. R. 2015. Direct effects of recurrent hypoglycaemia on adrenal catecholamine release. *Diab Vasc Dis Res,* 12**,** 2-12.
OSUNDIJI, M. A., HURST, P., MOORE, S. P., MARKKULA, S. P., YUEH, C. Y., SWAMY, A., HOASHI, S., SHAW, J. S., RICHES, C. H., HEISLER, L. K. & EVANS, M. L. 2011. Recurrent hypoglycemia increases hypothalamic glucose phosphorylation activity in rats. *Metabolism,* 60**,** 550-6.
OTLIVANCHIK, O., SANDERS, N. M., DUNN-MEYNELL, A. & LEVIN, B. E. 2016. Orexin signaling is necessary for hypoglycemia-induced prevention of conditioned place preference. *Am J Physiol Regul Integr Comp Physiol,* 310**,** R66-73.
OVESJO, M. L., GAMSTEDT, M., COLLIN, M. & MEISTER, B. 2001. GABAergic nature of hypothalamic leptin target neurones in the ventromedial arcuate nucleus. *J Neuroendocrinol,* 13**,** 505-16.
ÖZ, G., DINUZZO, M., KUMAR, A., MOHEET, A., KHOWAJA, A., KUBISIAK, K., EBERLY, L. E. & SEAQUIST, E. R. 2017. Cerebral glycogen in humans following acute and recurrent hypoglycemia: Implications on a role in hypoglycemia unawareness. *J Cereb Blood Flow Metab,* 37**,** 2883-2893.
PARANJAPE, S. A. & BRISKI, K. P. 2005. Recurrent insulin-induced hypoglycemia causes site-specific patterns of habituation or amplification of CNS neuronal genomic activation. *Neuroscience,* 130**,** 957-70.
PARDON, M.-C., MA, S. & MORILAK, D. A. 2003. Chronic cold stress sensitizes brain noradrenergic reactivity and noradrenergic facilitation of the HPA stress response in Wistar Kyoto rats. *Brain Research,* 971**,** 55-65.
PARK, J.-M., KIM, T.-H., JO, S.-H., KIM, M.-Y. & AHN, Y.-H. 2015. Acetylation of glucokinase regulatory protein decreases glucose metabolism by suppressing glucokinase activity. *Scientific Reports,* 5**,** 17395.
PARK, M. J., YOO, S. W., CHOE, B. S., DANTZER, R. & FREUND, G. G. 2012. Acute hypoglycemia causes depressive-like behaviors in mice. *Metabolism,* 61**,** 229-36.

PARSONS, M. P., LI, S. & KIROUAC, G. J. 2006. The paraventricular nucleus of the thalamus as an interface between the orexin and CART peptides and the shell of the nucleus accumbens. *Synapse,* 59**,** 480-90.
PAXINOS, G. & FRANKLIN, K. B. 1997. The mouse brain in stereotaxic coordinates. 2001. *Brook, New York, USA), respectively. Each experiment lasted around two and a half hours. In the end of the experiment, a,* 5.
PERROTTI, L. I., HADEISHI, Y., ULERY, P. G., BARROT, M., MONTEGGIA, L., DUMAN, R. S. & NESTLER, E. J. 2004. Induction of deltaFosB in reward-related brain structures after chronic stress. *J Neurosci,* 24**,** 10594-602.
PERSEGHIN, G., REGALIA, E., BATTEZZATI, A., VERGANI, S., PULVIRENTI, A., TERRUZZI, I., BARATTI, D., BOZZETTI, F., MAZZAFERRO, V. & LUZI, L. 1997. Regulation of glucose homeostasis in humans with denervated livers. *J Clin Invest,* 100**,** 931-41.
PEZET, S., MALCANGIO, M. & MCMAHON, S. B. 2002. BDNF: a neuromodulator in nociceptive pathways? *Brain Res Brain Res Rev,* 40**,** 240-9.
PINSKER, H., KUPFERMANN, I., CASTELLUCCI, V. & KANDEL, E. 1970. Habituation and dishabituation of the gill-withdrawal reflex in Aplysia. *Science,* 167**,** 1740-2.
POWELL, A. M., SHERWIN, R. S. & SHULMAN, G. I. 1993. Impaired hormonal responses to hypoglycemia in spontaneously diabetic and recurrently hypoglycemic rats. Reversibility and stimulus specificity of the deficits. *J Clin Invest,* 92**,** 2667-74.
PRAMMING, S., THORSTEINSSON, B., BENDTSON, I. & BINDER, C. 1991. Symptomatic hypoglycaemia in 411 type 1 diabetic patients. *Diabet Med,* 8**,** 217-22.
PUENTE, E. C., SILVERSTEIN, J., BREE, A. J., MUSIKANTOW, D. R., WOZNIAK, D. F., MALONEY, S., DAPHNA-IKEN, D. & FISHER, S. J. 2010. Recurrent moderate hypoglycemia ameliorates brain damage and cognitive dysfunction induced by severe hypoglycemia. *Diabetes,* 59**,** 1055-62.
QIN, C., LI, J. & TANG, K. 2018. The Paraventricular Nucleus of the Hypothalamus: Development, Function, and Human Diseases. *Endocrinology,* 159**,** 3458-3472.
RADLEY, J. J. & SAWCHENKO, P. E. 2011. A common substrate for prefrontal and hippocampal inhibition of the neuroendocrine stress response. *The Journal of neuroscience : the official journal of the Society for Neuroscience,* 31**,** 9683-9695.
RADLEY, J. J. & SAWCHENKO, P. E. 2015. Evidence for involvement of a limbic paraventricular hypothalamic inhibitory network in hypothalamic-pituitary-adrenal axis adaptations to repeated stress. *Journal of Comparative Neurology,* 523**,** 2769-2787.
RAMOT, A., JIANG, Z., TIAN, J. B., NAHUM, T., KUPERMAN, Y., JUSTICE, N. & CHEN, A. 2017. Hypothalamic CRFR1 is essential for HPA axis regulation following chronic stress. *Nat Neurosci,* 20**,** 385-388.
RANKIN, C. H., ABRAMS, T., BARRY, R. J., BHATNAGAR, S., CLAYTON, D. F., COLOMBO, J., COPPOLA, G., GEYER, M. A., GLANZMAN, D. L., MARSLAND, S., MCSWEENEY, F. K., WILSON, D. A., WU, C.-F. & THOMPSON, R. F. 2009. Habituation revisited: an updated and revised description of the behavioral characteristics of habituation. *Neurobiology of learning and memory,* 92**,** 135-138.
RAO, R., ENNIS, K., MITCHELL, E. P., TRAN, P. V. & GEWIRTZ, J. C. 2016. Recurrent Moderate Hypoglycemia Suppresses Brain-Derived Neurotrophic Factor Expression in the Prefrontal Cortex and Impairs Sensorimotor Gating in the Posthypoglycemic Period in Young Rats. *Dev Neurosci,* 38**,** 74-82.
RATTARASARN, C., DAGOGO-JACK, S., ZACHWIEJA, J. J. & CRYER, P. E. 1994. Hypoglycemia-induced autonomic failure in IDDM is specific for stimulus of hypoglycemia and is not attributable to prior autonomic activation. *Diabetes,* 43**,** 809-18.
REYA, T., MORRISON, S. J., CLARKE, M. F. & WEISSMAN, I. L. 2001. Stem cells, cancer, and cancer stem cells. *Nature,* 414**,** 105-11.

RITTER, S., LI, A.-J. & WANG, Q. 2019. Hindbrain glucoregulatory mechanisms: Critical role of catecholamine neurons in the ventrolateral medulla. *Physiology & behavior,* 208**,** 112568-112568.
RITTER, S., LLEWELLYN-SMITH, I. & DINH, T. T. 1998. Subgroups of hindbrain catecholamine neurons are selectively activated by 2-deoxy-D-glucose induced metabolic challenge. *Brain Res,* 805**,** 41-54.
ROOIJACKERS, H. M., WIEGERS, E. C., TACK, C. J., VAN DER GRAAF, M. & DE GALAN, B. E. 2016. Brain glucose metabolism during hypoglycemia in type 1 diabetes: insights from functional and metabolic neuroimaging studies. *Cell Mol Life Sci,* 73**,** 705-22.
ROUTH, V. H., HAO, L., SANTIAGO, A. M., SHENG, Z. & ZHOU, C. 2014. Hypothalamic glucose sensing: making ends meet. *Frontiers in Systems Neuroscience,* 8.
SABERI, M., BOHLAND, M. & DONOVAN, C. M. 2008. The locus for hypoglycemic detection shifts with the rate of fall in glycemia: the role of portal-superior mesenteric vein glucose sensing. *Diabetes,* 57**,** 1380-6.
SALEEBA, C., DEMPSEY, B., LE, S., GOODCHILD, A. & MCMULLAN, S. 2019. A Student's Guide to Neural Circuit Tracing. *Frontiers in Neuroscience,* 13.
SAMUELS, E. R. & SZABADI, E. 2008. Functional neuroanatomy of the noradrenergic locus coeruleus: its roles in the regulation of arousal and autonomic function part I: principles of functional organisation. *Current neuropharmacology,* 6**,** 235-253.
SANDERS, N. M., FIGLEWICZ, D. P., TABORSKY, G. J., JR., WILKINSON, C. W., DAUMEN, W. & LEVIN, B. E. 2006. Feeding and neuroendocrine responses after recurrent insulin-induced hypoglycemia. *Physiol Behav,* 87**,** 700-6.
SANDERS, N. M. & RITTER, S. 2000. Repeated 2-deoxy-D-glucose-induced glucoprivation attenuates Fos expression and glucoregulatory responses during subsequent glucoprivation. *Diabetes,* 49**,** 1865-74.
SANDERS, N. M., TABORSKY, G. J., JR., WILKINSON, C. W., DAUMEN, W. & FIGLEWICZ, D. P. 2007. Antecedent hindbrain glucoprivation does not impair the counterregulatory response to hypoglycemia. *Diabetes,* 56**,** 217-23.
SANDERS, N. M., WILKINSON, C. W., TABORSKY, G. J., JR., AL-NOORI, S., DAUMEN, W., ZAVOSH, A. & FIGLEWICZ, D. P. 2008. The selective serotonin reuptake inhibitor sertraline enhances counterregulatory responses to hypoglycemia. *Am J Physiol Endocrinol Metab,* 294**,** E853-60.
SANKAR, A., KHODAI, T., MCNEILLY, A. D., MCCRIMMON, R. J. & LUCKMAN, S. M. 2020. Experimental Models of Impaired Hypoglycaemia-Associated Counter-Regulation. *Trends in Endocrinology & Metabolism,* 31**,** 691-703.
SAPER, C. B. 2002. The central autonomic nervous system: conscious visceral perception and autonomic pattern generation. *Annu Rev Neurosci,* 25**,** 433-69.
SAWKA, A. M., BURGART, V. & ZIMMERMAN, D. 2001. Loss of awareness of hypoglycemia temporally associated with selective serotonin reuptake inhibitors. *Diabetes Care,* 24**,** 1845-6.
SCHOPMAN, J. E., GEDDES, J. & FRIER, B. M. 2010. Prevalence of impaired awareness of hypoglycaemia and frequency of hypoglycaemia in insulin-treated type 2 diabetes. *Diabetes Res Clin Pract,* 87**,** 64-8.
SCHWARTZ, N. S., CLUTTER, W. E., SHAH, S. D. & CRYER, P. E. 1987. Glycemic thresholds for activation of glucose counterregulatory systems are higher than the threshold for symptoms. *J Clin Invest,* 79**,** 777-81.
SEAQUIST, E. R. 2018. Beyond the brain: do peripheral mechanisms develop impaired awareness of hypoglycemia? *J Clin Invest,* 128**,** 3739-3741.
SEAQUIST, E. R., ANDERSON, J., CHILDS, B., CRYER, P., DAGOGO-JACK, S., FISH, L., HELLER, S. R., RODRIGUEZ, H., ROSENZWEIG, J. & VIGERSKY, R. 2013. Hypoglycemia and Diabetes: A Report of a Workgroup of the American Diabetes Association and The Endocrine Society. *Diabetes Care,* 36**,** 1384-1395.

SEAQUIST, E. R., MILLER, M. E., BONDS, D. E., FEINGLOS, M., GOFF, D. C., JR., PETERSON, K. & SENIOR, P. 2012. The impact of frequent and unrecognized hypoglycemia on mortality in the ACCORD study. *Diabetes Care,* 35**,** 409-14.

SENTHILKUMARAN, M., ZHOU, X. F. & BOBROVSKAYA, L. 2016. Challenges in Modelling Hypoglycaemia-Associated Autonomic Failure: A Review of Human and Animal Studies. *Int J Endocrinol,* 2016**,** 9801640.

SHAFTON, A. D., RYAN, A. & BADOER, E. 1998. Neurons in the hypothalamic paraventricular nucleus send collaterals to the spinal cord and to the rostral ventrolateral medulla in the rat. *Brain Res,* 801**,** 239-43.

SIMMONS, D. M. & SWANSON, L. W. 2008. High-resolution paraventricular nucleus serial section model constructed within a traditional rat brain atlas. *Neuroscience Letters,* 438**,** 85-89.

SIVITZ, W. I., HERLEIN, J. A., MORGAN, D. A., FINK, B. D., PHILLIPS, B. G. & HAYNES, W. G. 2001. Effect of acute and antecedent hypoglycemia on sympathetic neural activity and catecholamine responsiveness in normal rats. *Diabetes,* 50**,** 1119-25.

SKRIVARHAUG, T., BANGSTAD, H. J., STENE, L. C., SANDVIK, L., HANSSEN, K. F. & JONER, G. 2006. Long-term mortality in a nationwide cohort of childhood-onset type 1 diabetic patients in Norway. *Diabetologia,* 49**,** 298-305.

SOFIA BEAS, B., GU, X., LENG, Y., KOITA, O., RODRIGUEZ-GONZALEZ, S., KINDEL, M., MATIKAINEN-ANKNEY, B. A., LARSEN, R. S., KRAVITZ, A. V., HOON, M. A. & PENZO, M. A. 2020. A ventrolateral medulla-midline thalamic circuit for hypoglycemic feeding. *Nature Communications,* 11**,** 6218.

SOKOLOV, E. N. 1960. The neural model of the stimulus and the orienting reflex. *Voprosy Psychologii,* 4**,** 61-72.

SONG, Z. & ROUTH, V. H. 2006. Recurrent hypoglycemia reduces the glucose sensitivity of glucose-inhibited neurons in the ventromedial hypothalamus nucleus. *American Journal of Physiology-Regulatory, Integrative and Comparative Physiology,* 291**,** R1283-R1287.

SPEIGHT, J., BARENDSE, S. M., SINGH, H., LITTLE, S. A., INKSTER, B., FRIER, B. M., HELLER, S. R., RUTTER, M. K. & SHAW, J. A. 2016. Characterizing problematic hypoglycaemia: iterative design and preliminary psychometric validation of the Hypoglycaemia Awareness Questionnaire (HypoA-Q). *Diabet Med,* 33**,** 376-85.

SPRUIJT, B. M., VAN HOOFF, J. A. & GISPEN, W. H. 1992. Ethology and neurobiology of grooming behavior. *Physiol Rev,* 72**,** 825-52.

SRINIVAS, S., WATANABE, T., LIN, C. S., WILLIAM, C. M., TANABE, Y., JESSELL, T. M. & COSTANTINI, F. 2001. Cre reporter strains produced by targeted insertion of EYFP and ECFP into the ROSA26 locus. *BMC Dev Biol,* 1**,** 4.

STAHN, A., PISTROSCH, F., GANZ, X., TEIGE, M., KOEHLER, C., BORNSTEIN, S. & HANEFELD, M. 2014. Relationship between hypoglycemic episodes and ventricular arrhythmias in patients with type 2 diabetes and cardiovascular diseases: silent hypoglycemias and silent arrhythmias. *Diabetes Care,* 37**,** 516-20.

STANLEY, S., DOMINGOS, ANA I., KELLY, L., GARFIELD, A., DAMANPOUR, S., HEISLER, L. & FRIEDMAN, J. 2013. Profiling of Glucose-Sensing Neurons Reveals that GHRH Neurons Are Activated by Hypoglycemia. *Cell Metabolism,* 18**,** 596-607.

STEINBUSCH, L., LABOUEBE, G. & THORENS, B. 2015. Brain glucose sensing in homeostatic and hedonic regulation. *Trends Endocrinol Metab,* 26**,** 455-66.

STEINER, G. & BARRY, R. 2014. The mechanism of dishabituation. *Frontiers in Integrative Neuroscience,* 8.

STRACK, A. M., SAWYER, W. B., PLATT, K. B. & LOEWY, A. D. 1989. CNS cell groups regulating the sympathetic outflow to adrenal gland as revealed by transneuronal cell body labeling with pseudorabies virus. *Brain Res,* 491**,** 274-96.

STRATFORD, T. R. & WIRTSHAFTER, D. 2013. Injections of muscimol into the paraventricular thalamic nucleus, but not mediodorsal thalamic nuclei, induce feeding in rats. *Brain Res,* 1490**,** 128-33.
SWINNY, J. D., METZGER, F., J, I. J.-P., GOUNKO, N. V., GRAMSBERGEN, A. & VAN DER WANT, J. J. 2004. Corticotropin-releasing factor and urocortin differentially modulate rat Purkinje cell dendritic outgrowth and differentiation in vitro. *Eur J Neurosci,* 19**,** 1749-58.
TABORSKY, G. J., JR. & MUNDINGER, T. O. 2012. Minireview: The role of the autonomic nervous system in mediating the glucagon response to hypoglycemia. *Endocrinology,* 153**,** 1055-62.
TANIGUCHI, H., HE, M., WU, P., KIM, S., PAIK, R., SUGINO, K., KVITSANI, D., FU, Y., LU, J., LIN, Y., MIYOSHI, G., SHIMA, Y., FISHELL, G., NELSON, SACHA B. & HUANG, Z. J. 2011a. A Resource of Cre Driver Lines for Genetic Targeting of GABAergic Neurons in Cerebral Cortex. *Neuron,* 71**,** 995-1013.
TEFF, K. L. 2011. How neural mediation of anticipatory and compensatory insulin release helps us tolerate food. *Physiol Behav,* 103**,** 44-50.
TESFAYE, N., SEAQUIST, E. R. & OZ, G. 2011. Noninvasive measurement of brain glycogen by nuclear magnetic resonance spectroscopy and its application to the study of brain metabolism. *J Neurosci Res,* 89**,** 1905-12.
THOMPSON, R. F. & SPENCER, W. A. 1966. Habituation: a model phenomenon for the study of neuronal substrates of behavior. *Psychol Rev,* 73**,** 16-43.
THOMPSON, R. H. & SWANSON, L. W. 2003. Structural characterization of a hypothalamic visceromotor pattern generator network. *Brain Res Brain Res Rev,* 41**,** 153-202.
THORENS, B. 2010. Central control of glucose homeostasis: the brain--endocrine pancreas axis. *Diabetes Metab,* 36 Suppl 3**,** S45-9.
TIMOFEEVA, E. & RICHARD, D. 2001. Activation of the central nervous system in obese Zucker rats during food deprivation. *Journal of Comparative Neurology,* 441**,** 71-89.
TONG, Q., YE, C., MCCRIMMON, R. J., DHILLON, H., CHOI, B., KRAMER, M. D., YU, J., YANG, Z., CHRISTIANSEN, L. M., LEE, C. E., CHOI, C. S., ZIGMAN, J. M., SHULMAN, G. I., SHERWIN, R. S., ELMQUIST, J. K. & LOWELL, B. B. 2007. Synaptic glutamate release by ventromedial hypothalamic neurons is part of the neurocircuitry that prevents hypoglycemia. *Cell Metab,* 5**,** 383-93.
TU, E., TWIGG, S. M., DUFLOU, J. & SEMSARIAN, C. 2008. Causes of death in young Australians with type 1 diabetes: a review of coronial postmortem examinations. *Med J Aust,* 188**,** 699-702.
URBAN, D. J. & ROTH, B. L. 2015. DREADDs (designer receptors exclusively activated by designer drugs): chemogenetic tools with therapeutic utility. *Annu Rev Pharmacol Toxicol,* 55**,** 399-417.
URIBE-BAHAMONDE, Y. E., BECERRA, S. A., PONCE, F. P. & VOGEL, E. H. 2019. A Quantitative Account of the Behavioral Characteristics of Habituation: The Sometimes Opponent Processes Model of Stimulus Processing. *Frontiers in psychology,* 10**,** 504-504.
VELE, S., MILMAN, S., SHAMOON, H. & GABRIELY, I. 2011. Opioid receptor blockade improves hypoglycemia-associated autonomic failure in type 1 diabetes mellitus. *The Journal of clinical endocrinology and metabolism,* 96**,** 3424-3431.
VERBERNE, A. J. M., SABETGHADAM, A. & KORIM, W. S. 2014. Neural pathways that control the glucose counterregulatory response. *Frontiers in neuroscience,* 8**,** 38-38.
VERTES, R. P. & HOOVER, W. B. 2008. Projections of the paraventricular and paratenial nuclei of the dorsal midline thalamus in the rat. *Journal of Comparative Neurology,* 508**,** 212-237.
VIALOU, V., BAGOT, R. C., CAHILL, M. E., FERGUSON, D., ROBISON, A. J., DIETZ, D. M., FALLON, B., MAZEI-ROBISON, M., KU, S. M., HARRIGAN, E., WINSTANLEY, C. A., JOSHI, T., FENG, J., BERTON, O. & NESTLER, E. J.

2014. Prefrontal Cortical Circuit for Depression- and Anxiety-Related Behaviors Mediated by Cholecystokinin: Role of ΔFosB. *The Journal of Neuroscience,* 34**,** 3878-3887.

VIALOU, V., ROBISON, A. J., LAPLANT, Q. C., COVINGTON, H. E., DIETZ, D. M., OHNISHI, Y. N., MOUZON, E., RUSH, A. J., WATTS, E. L., WALLACE, D. L., IÑIGUEZ, S. D., OHNISHI, Y. H., STEINER, M. A., WARREN, B. L., KRISHNAN, V., BOLAÑOS, C. A., NEVE, R. L., GHOSE, S., BERTON, O., TAMMINGA, C. A. & NESTLER, E. J. 2010. ΔFosB in brain reward circuits mediates resilience to stress and antidepressant responses. *Nature Neuroscience,* 13**,** 745-752.

VICKNESON, K., BLACKBURN, J., GALLAGHER, J. R., EVANS, M. L., DE GALAN, B. E., PEDERSEN-BJERGAARD, U., THORENS, B., MCNEILLY, A. D. & MCCRIMMON, R. J. 2021. Cold-induced dishabituation in rodents exposed to recurrent hypoglycaemia. *Diabetologia,* 64**,** 1436-1441.

VONG, L., YE, C., YANG, Z., CHOI, B., CHUA, S., JR. & LOWELL, B. B. 2011. Leptin action on GABAergic neurons prevents obesity and reduces inhibitory tone to POMC neurons. *Neuron,* 71**,** 142-54.

WAMSTEEKER CUSULIN, J. I., FUZESI, T., WATTS, A. G. & BAINS, J. S. 2013. Characterization of corticotropin-releasing hormone neurons in the paraventricular nucleus of the hypothalamus of Crh-IRES-Cre mutant mice. *PLoS One,* 8**,** e64943.

WANG, L. A., NGUYEN, D. H. & MIFFLIN, S. W. 2019. Corticotropin-releasing hormone projections from the paraventricular nucleus of the hypothalamus to the nucleus of the solitary tract increase blood pressure. *Journal of Neurophysiology,* 121**,** 602-608.

WANG, R., LIU, X., HENTGES, S. T., DUNN-MEYNELL, A. A., LEVIN, B. E., WANG, W. & ROUTH, V. H. 2004. The Regulation of Glucose-Excited Neurons in the Hypothalamic Arcuate Nucleus by Glucose and Feeding-Relevant Peptides. *Diabetes,* 53**,** 1959-1965.

WANG, Y., DEMARCO, E. M., WITZEL, L. S. & KEIGHRON, J. D. 2021. A selected review of recent advances in the study of neuronal circuits using fiber photometry. *Pharmacology Biochemistry and Behavior,* 201**,** 173113.

WATTS, A. G. 2015. 60 YEARS OF NEUROENDOCRINOLOGY: The structure of the neuroendocrine hypothalamus: the neuroanatomical legacy of Geoffrey Harris. *The Journal of endocrinology,* 226**,** T25-T39.

WATTS, A. G. & DONOVAN, C. M. 2010. Sweet talk in the brain: glucosensing, neural networks, and hypoglycemic counterregulation. *Front Neuroendocrinol,* 31**,** 32-43.

WEINBERG, M. S., JOHNSON, D. C., BHATT, A. P. & SPENCER, R. L. 2010. Medial prefrontal cortex activity can disrupt the expression of stress response habituation. *Neuroscience,* 168**,** 744-756.

WHIPPLE, A. O. 1938. Thesurgical therapy of hyperinsu-linism. *J Int Chir,* 3**,** 237-276.

WILLIAMS, G. & PICKUP, J. 2004. *Hanbook of Diabetes,* Malden, Massachusetts, Blackwell Science.

WRIGHT, R. J. & FRIER, B. M. 2008. Vascular disease and diabetes: is hypoglycaemia an aggravating factor? *Diabetes Metab Res Rev,* 24**,** 353-63.

YANG, C. F., CHIANG, M. C., GRAY, D. C., PRABHAKARAN, M., ALVARADO, M., JUNTTI, S. A., UNGER, E. K., WELLS, J. A. & SHAH, N. M. 2013. Sexually Dimorphic Neurons in the Ventromedial Hypothalamus Govern Mating in Both Sexes and Aggression in Males. *Cell,* 153**,** 896-909.

YANG, X., KOW, L.-M., FUNABASHI, T. & MOBBS, C. V. 1999. Hypothalamic glucose sensor: similarities to and differences from pancreatic beta-cell mechanisms. *Diabetes,* 48**,** 1763-1772.

YUAN, Y., WU, W., CHEN, M., CAI, F., FAN, C., SHEN, W., SUN, W. & HU, J. 2019. Reward Inhibits Paraventricular CRH Neurons to Relieve Stress. *Current Biology,* 29**,** 1243-1251.e4.

ZACHARIOU, V., BOLANOS, C. A., SELLEY, D. E., THEOBALD, D., CASSIDY, M. P., KELZ, M. B., SHAW-LUTCHMAN, T., BERTON, O., SIM-SELLEY, L. J., DILEONE, R. J., KUMAR, A. & NESTLER, E. J. 2006. An essential role for ΔFosB in the nucleus accumbens in morphine action. *Nature Neuroscience,* 9**,** 205-211.

ZAMMITT, N. N., WARREN, R. E., DEARY, I. J. & FRIER, B. M. 2008. Delayed recovery of cognitive function following hypoglycemia in adults with type 1 diabetes: effect of impaired awareness of hypoglycemia. *Diabetes,* 57**,** 732-6.

ZHAO, Z., WANG, L., GAO, W., HU, F., ZHANG, J., REN, Y., LIN, R., FENG, Q., CHENG, M., JU, D., CHI, Q., WANG, D., SONG, S., LUO, M. & ZHAN, C. 2017. A Central Catecholaminergic Circuit Controls Blood Glucose Levels during Stress. *Neuron,* 95**,** 138-152.e5.

ZHENG, J. Q., SEKI, M., HAYAKAWA, T., ITO, H. & ZYO, K. 1995. Descending projections from the paraventricular hypothalamic nucleus to the spinal cord: anterograde tracing study in the rat. *Okajimas Folia Anat Jpn,* 72**,** 119-35.

ZHOU, Y., HUANG, L., ZHENG, W., AN, J., ZHAN, Z., WANG, L., CHEN, Z. & LIU, L. 2018. Recurrent nonsevere hypoglycemia exacerbates imbalance of mitochondrial homeostasis leading to synapse injury and cognitive deficit in diabetes. *Am J Physiol Endocrinol Metab,* 315**,** E973-e986.

ZIMMERMAN, C. A., LIN, Y.-C., LEIB, D. E., GUO, L., HUEY, E. L., DALY, G. E., CHEN, Y. & KNIGHT, Z. A. 2016. Thirst neurons anticipate the homeostatic consequences of eating and drinking. *Nature,* 537**,** 680-684.

ZINGG, B., PENG, B., HUANG, J., TAO, H. W. & ZHANG, L. I. 2020. Synaptic Specificity and Application of Anterograde Transsynaptic AAV for Probing Neural Circuitry. *The Journal of Neuroscience,* 40**,** 3250-3267.